University of Szeged

Faculty of Pharmacy

Institute of Pharmaceutical Technology and Regulatory Affairs

Head: *Dr. habil. Ildikó Csóka PhD*

PhD Thesis

QBD APPROACH FOR OPTIMIZATION AND CHARACTERIZATION OF ANTI-GLIOBLASTOMA DRUG EMBEDDED LIPID NANOPARTICLES FOR INTRANASAL ADMINISTRATION

By

Fakhara Sabir

Pharmacist

Supervisor:

Dr. habil. Ildikó Csóka *PhD*

SZEGED

2022

PUBLICATIONS RELATED TO THE SUBJECT OF THE THESIS

1. **Fakhara Sabir**, Ruba Ismail, and Ildikó Csóka. 2020. 'Nose-to-brain delivery of antiglioblastoma drugs embedded into lipid nanocarrier systems: status quo and outlook', *Drug discovery today*, 25: 185-94

IF: 7.352 (2020), Q1

2. **Fakhara Sabir,** Gábor Katona, Edina Pallagi, Dorina Gabriella Dobó, Hussein Akel, Dániel Berkesi, Zoltán Kónya, and Ildikó Csóka. 2021. 'Quality-by-Design-Based Development of n-Propyl-Gallate-Loaded Hyaluronic-Acid-Coated Liposomes for Intranasal Administration', Molecules (Basel, Switzerland), 26: 1429.

IF: 4.47 (2021), Q1

3. **Fakhara Sabir,** Gábor Katona, Ruba Ismail, Bence Sipos, Rita Ambrus, and Ildikó Csóka. 2021. 'Development and Characterization of n-Propyl Gallate Encapsulated Solid Lipid Nanoparticles-Loaded Hydrogel for Intranasal Delivery', Pharmaceuticals, 14: 696.

IF: 5.864 (2021), D1

4. Gábor Katona, **Fakhara Sabir,** Bence Sipos, Mohammad Naveed, Zsuzsanna Schelz, István Zupkó, & Csóka, Ildikó. 2022. 'Development of Lomustine and n-Propyl Gallate Co-Encapsulated Liposomes for Targeting Glioblastoma Multiforme via Intranasal Administration', Pharmaceutics, 2022. 14(3): p. 631.

IF: 6.072 (2022), Q1

OTHER PUBLICATIONS

1. **Sabir, Fakhara**, Mahira Zeeshan, Ushna Laraib, Mahmood Barani, Abbas Rahdar, Magali Cucchiarini, and Sadanand Pandey. 2021. 'DNA Based and Stimuli-Responsive Smart Nanocarrier for Diagnosis and Treatment of Cancer: Applications and Challenges', *Cancers*, 13: 3396.

IF: 6.639 (2021), Q1

2. **Sabir, Fakhara,** Mahmood Barani, Mahwash Mukhtar, Abbas Rahdar, Magali Cucchiarini, Muhammad Nadeem Zafar, Tapan Behl, and Simona Bungau. 2021. 'Nanodiagnosis and nanotreatment of cardiovascular diseases: An overview', *Chemosensors*, 9: 67.

IF: 3.29 (2021), Q2

PRESENTATIONS RELATED TO THE THESIS

1. **Sabir Fakhara**, Gábor Katona, Ruba Ismail, Bence Sipos, Rita Ambrus, and Ildikó Csóka. Development and Optimization of n-propyl gallate Encapsulated Hyaluronic Acid Based Hydrogel for Nose to Brain Delivery by Applying QbD Methodology, December 2020 0.3390/IECP2020-08707, Conference: The 1st International Electronic Conference on Pharmaceutics session Brain Drug.
2. **Sabir Fakhara**, Ildikó Csóka. Steps toward the treatment of glioblastoma with coated liposomes: n-propylgallate containing hyaluronic acid stabilized product developed by means of QbD methodology September 2020, Conference: EUGLOH Annual Student Research Conference Global Health Challenges: Diseases.
3. **Sabir Fakhara**, Ildikó Csóka. Significance of QbD in design and development of coated liposomes for nose to brain delivery, January 2020,10.14232/syrptbrs.2020.op39, Conference: II. Symposium of Young Researchers on Pharmaceutical Technology, Biotechnology and Regulatory Science.
4. **Sabir Fakhara**, Ildikó Csóka. Exploiting potential of intranasal delivery of lipid nano-formulation for targeting glioblastoma, January 2019, 10.14232/syrptbrs.2019.op4, Conference: I. Symposium of Young Researchers on Pharmaceutical Technology, Biotechnology and Regulatory Science.
5. **Sabir Fakhara**, Ildikó Csóka. Nose to brain delivery of n-propyl gallate loaded lipid nanoparticles for targeting glioblastoma multiforme: QbD approach, January 2021, DOI: 10.14232/syrptbrs.2021, Conference: III. Symposium of Young Researchers on Pharmaceutical Technology, Biotechnology and Regulatory Science: January 20-22nd 2021 Szeged, Hungary.
6. **Sabir Fakhara**, Ildikó Csóka**.** Nose to brain delivery of anti-glioblastoma drugs embedded into lipid nanoparticles via using QbD approach. II PhD Forum on particle engineering, nano-medicine formulation for alternative drug administration, 04 May 2021 Szeged, Hungary.
7. **Sabir Fakhara,** Gábor Katona, Ruba Ismail, Bence Sipos, Rita Ambrus and Ildikó Csóka. Development of *n*-propyl gallate encapsulated solid lipid nanoparticles loaded onto hydrogel for nose to brain delivery. 10^{th} Jubilee Interdisciplinary Doctoral Conference 12^{th}-13^{th} Nov, 2021 Pécs, Hungary.
8. **Sabir Fakhara,** Gábor Katona, Dorina Gabriella Dobó, and Ildikó Csóka. Quality by design

approach for fabrication of stabilized n-propylgallate loaded liposomes for nose to brain delivery. 10th Jubilee Interdisciplinary Doctoral Conference 12th-13th Nov, 2021 Pécs, Hungary.

ABBREVIATIONS

ANOVA	one-way analysis of variance
BBB	blood–brain barrier
CNS	central nervous system
CPPs	critical process parameters
CMA	critical materials attributes
CQA	critical quality attributes
CCD	central composite design
˚C	centigrade
EE	encapsulation efficiency
FTIR	Fourier-transformed infrared spectroscopy
HA	hyaluronic acid
HPLC	high proficiency liquid chromatography
ICH	International Conference on Harmonization
KBr	potassium bromide
kDa	kilo Dalton
LC	loading capacity
LOQ	limit of quantification
LOD	limit of detection
mV	millivolt
mm	millimol
mA	milliampere
mPa	millipascal
mg	milligram
mm^2	square millimeter
Mw	molecular weight
nm	nanometer
ppm	parts per million
PBS	phosphate buffer saline
PG	propyl gallate
PG-SLNs	PG-solid lipid nanoparticles
PDI	polydispersity index
Pas	pascal
QbD	Quality by Design
QTPP	quality target product profile
RA	risk assessment
SLNs	solid lipid nanoparticles
SEM	scanning electron microscopy
µm	micrometer
w/v	weight/volume
XRPD	X-ray powder diffractograms

Contents

1. INTRODUCTION

Glioblastoma multiforme (GBM) is the most aggressive and life-threatening type of glial brain tumor with poor diagnosis and prognosis. Its central nervous system (CNS) malignancy is classified based on an augmenting level of anaplasia, proliferation, and un-differentiation [1]. GBM has diffuse nature because these malignant cells show discrepancies in morphology and structure. Present treatment strategies for GBM include surgery, chemotherapy, and radiotherapy indicating poor therapeutic efficacy due to its very complicated and diffuse nature. The present literature survey suggested that there are few treatment therapies that could significantly increase the survival chances [2]. There is a need to design a more rational and specific strategy to treat the GBM. The nose to brain delivery is a simple and direct approach including many advantages of enhanced bioavailability, the shorter onset of action, clearance, and non-invasiveness [3]. Bypassing the blood-brain barrier (BBB) through nose-to-brain delivery can significantly increase the quantity of the API (active pharmaceutical agent) in the central nervous system (CNS) [4]. For adequate nose to brain delivery appropriate drug delivery systems (DDSs) are required with the main feature of enhancing API permeation, solubility, stability, and residence time on the nasal mucosa, resisting the mucociliary clearance [5]. The increased residence time of formulations containing anticancer drugs may result in toxicity in nasal cilia, tissue damage, and irritation [6]. Lipid-based DDSs, such as solid lipid nanoparticles (SLNs) and liposomes are advantageous carriers in this regard [7].

2. AIMS

The main aim of this study was to develop and optimize the lipid-based nanoparticle formulations-for intranasal delivery (IND) of *n*-propyl gallate (PG) and lomustine (LOM) as a potential anti-glioblastoma drugs to substitute conventional parenteral therapy. Intranasal delivery of PG and LOM can be a possible anti-glioblastoma drug combination to substitute conventional chemotherapeutics. The research work was constructed according to the following steps:

I. A detailed literature review was planned to perform the unexplored areas in the field of development of lipid nanoparticles for nose to brain delivery.

II. Application of the QbD approach to define the critical process and material parameters that impact the formulation of lipid nanoparticles (liposomes, SLNs) with desired features for optimum targeting via intranasal administration.

III. Screening and selection of suitable anti-glioblastoma drugs (PG and LOM) to develop nasal product.

IV. The physio-chemical characterization of lipid nanoparticle and *in-vitro* studies to investigate their nasal applicability under simulated nasal conditions was performed.

V. The characterization of nasal applicability of optimized liposomal and SLNs formulations.

VI. To conduct and evaluate the *in-vitro* and *ex-vivo* comparative studies for selected formulations under simulated nasal conditions

3. THEORETICAL BACKGROUND

3.1. Glioblastoma multiforme: the terminator

Malignant gliomas (MGs) are the most lethal types of primary central nervous system (CNS) malignancy, classified based on an augmenting level of undifferentiation, anaplasia and proliferation. World Health Organization (WHO) classified gliomas into four clinical grades: grade I (astrocytoma); grade II (diffuse astrocytoma, the most distinguished form); grade III (anaplastic variants of astrocytoma); and grade IV (glioblastoma). Pleomorphic glioblastoma is called GBM, because these malignant cells show variance in structure and morphology [8, 9]. The current treatment strategies for GBM include surgery, radiotherapy and chemotherapy. The focus of researchers to treat GBM is challenging because surgery and radiotherapy are not good options due to its topographically diffuse nature. Eventually, understanding the pattern of spread of individual malignant cells over long distances and into parts of the brain is essential for patient survival. A present literature survey reveals that there are just a few available therapies that could significantly improve survival chances. The circumvention of the BBB through straight intervention into insubstantial brain tissues can result in severe neurotoxicity and loss of brain key functionality. Consequently, there is a need to design a more specific and rational (non-invasive) approach to target GBM. It is also necessary to explore the potential differences in permeability between the intact and malignant brain to overcome the challenges in brain targeting [8, 10].

3.2. Strategies to bypass the BBB: bottleneck indirect targeted delivery

Many researchers and scientists have been working to develop different methods to bypass the BBB. These strategies include IND, penetration via the BBB by cellular internalization and also the opening of the BBB. The overexpression of receptors (insulin-like growth factor (IGF), transferrin receptors, low-density lipoprotein, nicotinic acetylene choline, scavenger receptors type B, and diphtheria toxin has been studied on the BBB [11]. The specific surface modification and attachment can assist in drug transport via the BBB. This sensitive and precise type of interaction between receptors and ligands stimulate receptor- mediated transport. Despite the benefits of surface-modified nanoparticles, there are limitations in their application. Firstly, their administration is invasive, during which the targeting moiety can lose its therapeutic activity. Secondly, they tend to accumulate in the liver and at other off-target sites decreasing its therapeutic efficacy. To overcome these hurdles and achieve the best therapeutic goals non-invasive delivery approaches are essential [12]. **Figure 1**. Illustrated the comparison between normal brain and in GBM.

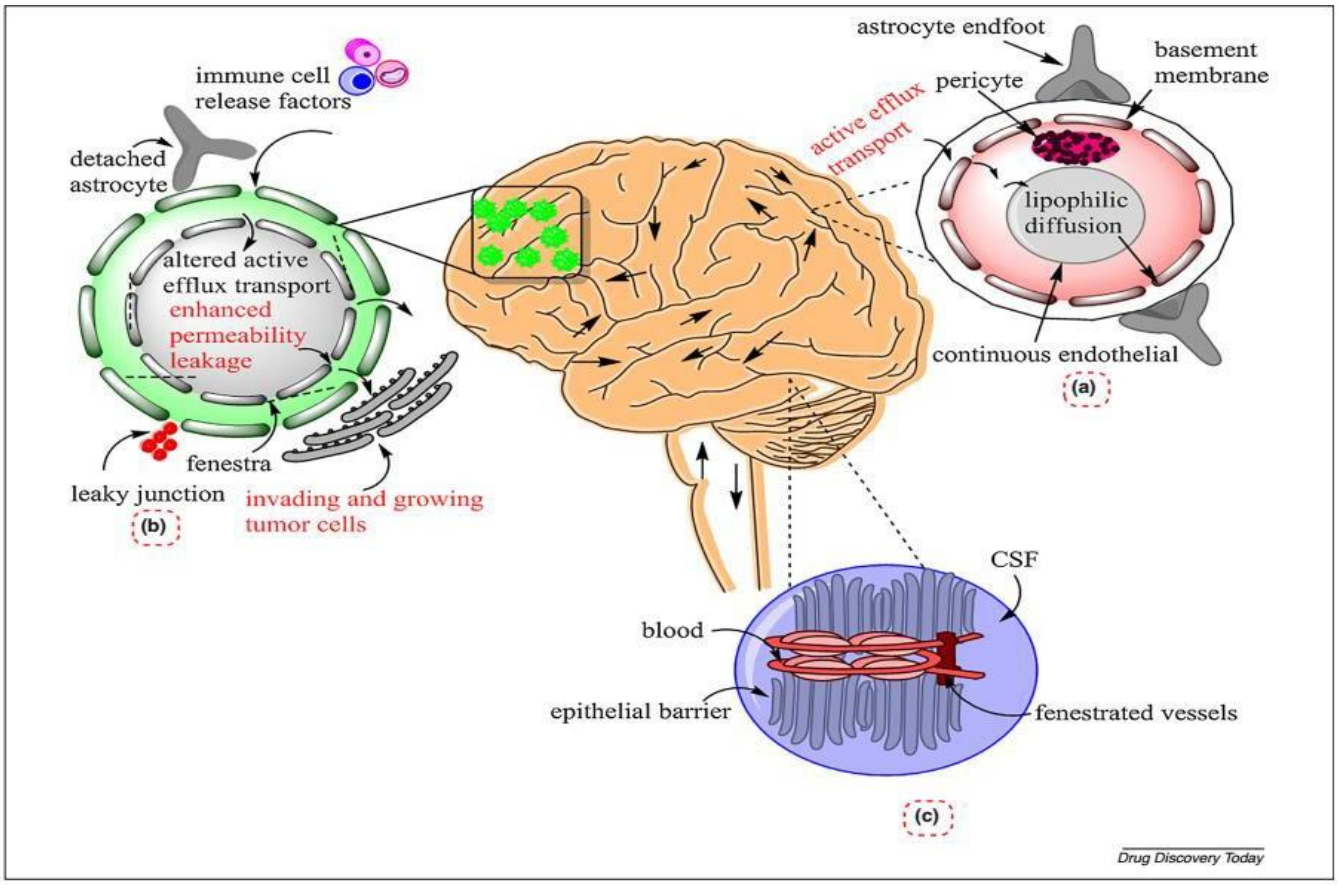

Figure 1. Challenges from blood to brain delivery in a brain tumor. The figure illustrates the comparison between barriers in normal brain and in GBM [5].

3.3. Intranasal administration: An alternative strategy to overcome BBB

Nose to brain delivery is a fascinating approach for CNS drug delivery via intranasal route. The nose to brain is a direct, non-invasive administration route, which can bypass the BBB with elimination of systemic side effects [13]. The direct delivery to the brain via indirect (olfactory and trigeminal) route can result in good pharmacokinetic/pharmacodynamic (PK/PD) profiles for CNS drugs. The drug transport from the nose through trigeminal pathway follows endocytotic or axonal transport, moreover the extra-neuronal and intra-neuronal transports are subdivision of olfactory pathway. The extra-neuronal path is the shortest route for nose to brain delivery as it just takes few minutes to reach the targeting area [14]. In contrast to that it takes hours or days for intra-neuronal pathway as it follows axonal transport to reach the target site. Moreover, the intranasal administration is a novel approach to ensure better safety profile for the deliveryof potent active agents including chemotherapeutics (when loaded them into nanoparticles) [15]. Various drugs can be transported through the intranasal route to the desired target site and circumvent the BBB andblood cerebrospinal-fluid barrier (BCSFB) [16]. There are several studies showing the better delivery of CNS components via the intranasal route in comparison to the (i.v.) administration i.e. IGF-1[17]. Numerous other studies revealed IND of the API led to more effective treatment of CNS diseases, such asautism,

depression, eating disorders, Parkinson's disease (PD) or Huntington's disease (HD) [18].

The anatomy and the physiology of the nasal cavity are significant factors, which should be taken into consideration. There are few parts of nasal mucosa that are least permeable including vibrissae of the nasal vestibule and the trans-epithelial region (the narrowest region) [19]. In comparison to that, other parts like the inferior, middle and superior turbinate of the respiratory region are more permeable, whereas, the ciliated olfactory nerve cells of the olfactory region have direct approach to the CSF. The anatomy of nasal cavity and structure variations demonstrate how the structures of the nasal cavity can affect the permeability via the intranasal route [20]. By the application of QbD approach the optimized formulation can be designed for the intranasal administration with enhanced permeation, high muco-adhesion and lowclearance [21].

3.4. Nose to brain delivery of nano-carrier system

The intranasal administration of different nano carrier systems show significant importance due to the greater ability to increase the nose to brain delivery of drugs avoiding from P-glycoprotein (P-gp) efflux transport. The carrier system can improve drug delivery in case of using bio-adhesive materials and also via opening the tight junctions of the nasal epithelial membrane [22]. Intranasal transport of nanoparticles can take place via endocytotic, olfactory or neuronal pathways. Confocal microscopic study of polystyrene nanoparticle's revealed that nanoparticles ranged from 20-200 nm follow the clathrin-coated pits; moreover, nanoparticles in the size range of 200-1000 nm can be uptake by caveolae-mediated endocytosis [23]. The transport of nanoparticles from endothelial and olfactory neurons via pinocytosis and endocytosis took place along the axon. The size of the nanoparticles intended for axonal transport should be in the size range of 100-700 nm. The IND of nanoparticles can be a suitable choice for targeting GBM. Lipid based nanoparticles like SLNs, liposomes, nano lipid carriers, lipo-plexes and lipoproteins are rational carrier system for brain targeting [24], however there are several limitations in applications e.g. toxicity issues based on their composition and site of internalization.

The formulation is usually deposited on the pseudo-stratified columnar epithelium after being delivered intra-nasally (a respiratory tract in the nasal cavity). The front portion of the nasal cavity is where the intranasal formulation whether in the form of a solution, spray, or gel (applicator), is deposited [54].

There are a few devices, however, that can help the drug formulation settle in upper region of the nasal cavity. Nanoparticles enter the nasal cavity through an intranasal route, which is deposited at the site of the nasal cavity, depending on its size, charge, and lipophilicity. The drug can enter through the nasal epithelial tissue and reach the blood, or it can be unloaded along the gastrointestinal tract (GIT) via the nasopharynx by the ciliary clearing network [55]. The system is made up of motile cilia that beat in unison, driving the viscous superior component dorsally against the nasopharynx at a faster rate of (5 mm/min). Furthermore, enzymatic activity is higher in the nasal cavity, which is deep in the olfactory region (enzymes such as cytochrome P450 dependent peptidases, mono-oxygenase, and proteases are involved in this mechanism) [56]. The nanoparticles will travel from endothelial cells to olfactory neurons by endocytosis or pinocytosis and along the axon, or via the trigeminal nerve pathways [57]. **Figure 2** shows the possible mechanism of lipid nanoparticles after intranasal administration.

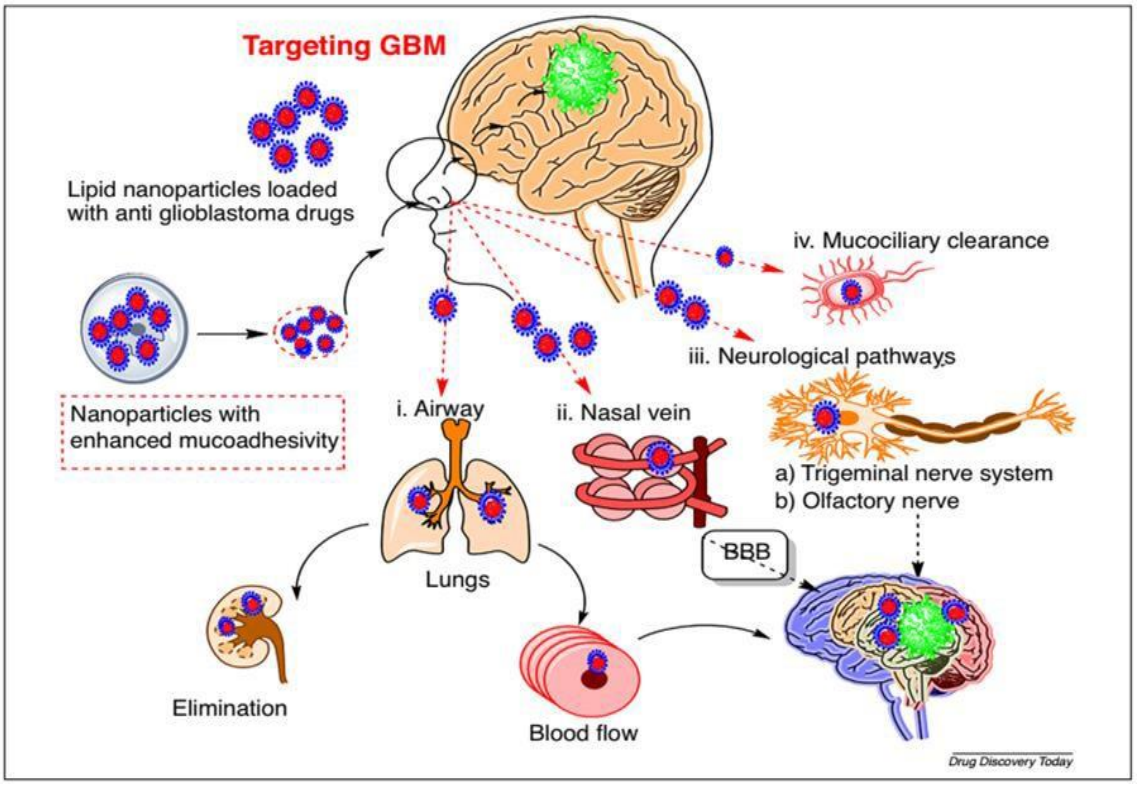

Figure 2. Possible mechanisms of lipid nanoparticles across the nasal membrane. The figure demonstrates that lipid nanoparticles with enhanced mucoadhesivity will follow four possible pathways: (i) Airway; (ii) Nasal vein; (iii) Neurological pathway; and (iv) Muco-ciliary clearance [5].

3.4.1. Lipid nanoparticles: A suitable approach for nose to brain delivery

For adequate nose to brain delivery, a colloidal delivery system is the most appropriate system that improve stability, bioavailability and drug release of the API. The increased biocompatibility of lipid nanoparticles, made them superior carriers for IND [5]. On contrary, to the lipid nanoparticles, polymeric nanoparticles have low scalability and greater cytotoxicity (e.g., 100% inhibition was detected, when cells were treated with polyester polymeric nanoparticles) along-with poor tolerability. Lipid nanoparticles are in the size range of 50-1000 nm. The greater therapeutic efficacy have been presented in GBM via lipid carriers (liposomes, SLNs) [25]. In comparison to other approaches the lipid nano-formulations of anti-neoplastic agents provide increase PK, drug stability, drug distribution and efficacy in comparison to conventional approaches [26].

3.4.2. Therapeutic efficacy of lipid nanoparticles against GBM

Various lipid nanoparticles including liposomes, lipoproteins, lipoplexes and lipid nano-carriers have been applied for treating the GBM. Liposomes are bilayer and biocompatible, spherical shaped lipid based nano-carrier system known as pioneers of lipid derived nanoparticles employed for intravenous delivery with diameter ranges from the 10-1000 nm [27]. Various liposomal factors including average hydrodynamic diameter, and uptake via the mononuclear phagocytic system (MPS) can be more significant for targeting. Despite the limitations of lipid nanoparticles, the SLNs and nanostructured lipid carriers (NLCs) seems to be the most suitable for anticancer therapy [28]. The stealth ability of lipid based nanoparticles is greater than of polymeric nanoparticles against the MPS because these systems are prepared from the biocompatible substances such as brew of natural lipids [5]. The findings of all former studies showed the decrease in tumor growth, the increase in the lifespan of the animals used and the inhibition of cell proliferation [29, 30]. The reported efficacy of lipid nanoparticles in targeting GBM also show their ability as a potential carrier for anti-cancer drugs [31]. Moreover, these lipid nanoparticles are able to prolong drug release of encapsulated API and can also enhance nasal absorption. These characteristics made lipid nanoparticles a suitable drug delivery system for intranasal administration, as they can reduce cytotoxicity of anti-neoplastic drugs at the peripheric tissues [31].

3.4.3. Novel lipid based nanoparticles for targeting GBM via intranasal route

The conventional delivery approaches for GBM have many pitfalls including invasiveness, off site targeting issue and BBB. Therefore, new delivery approaches are required in research to efficiently target brain tumors. Madane et al., developed the curcumin encapsulated NLCs (CUR-NLC) for nose to brain delivery with a particle size of 146±10 nm with PDI of 0.18±0.12 and zeta potential of 21±8 mV along with encapsulation efficiency of 90±10% [32]. Their findings revealed enhanced cytotoxicity of CUR-NLC

compared to plain CUR on U373MG glioma cell line. The bio-distribution study of the same formulation showed an enhanced drug concentration in the brain after the intranasal administration of NLCs [32]. Khan et al. developed temozolomide-loaded NLCs (TMZ-NLC) for targeting the brain through IND. TMZ-NLC showed particle size of 141-202 nm, PDI of 0.221±0.22, zeta potential of 15±3.0 mV and entrapment efficiency of 81±3.0% [29]. The findings of the in vivo experiments revealed that TMZ-NLC resulted in a significantly higher brain concentration in comparison to *i.v.* or intranasal TMZ solution. The efficacy of this direct IND of NLCs was demonstrated by the highest concentration of TMZ-NLC in the brain [29]. The intranasal administration of farnesylthiosalicylic acid (FTA)-loaded PEG-PLGA hybrid nanoparticles was found to be an equally effective method of GBM targeting in this investigation. The findings of all studies supported the use of lipid carriers to target GBM via the IND pathway [33, 34].

3.5. Application of Propylgallate (PG), Lomustine (LOM) and Hyaluronic acid (HA)

A mucoadhesive carrier system is very important for drug delivery from intranasal route. Here, we used hyaluronic acid (HA), a glycosaminoglycan, a linear polysaccharide that comprises of β-1,4-D glucoronic acid and 1,3-N-acetyl-D-glucosamine disaccharides via alternative glycosidic bonds [35, 36]. We developed muco-adhesive carrier system with HA-coating of liposomes. The muco-adhesive coating of liposomes with HA, enhanced the negative zeta potential due to the addition of the negative carboxylate residue of HA on the surface of the liposomes, therefore increasing the stability directly [37]. Our study used two API n-propylgallate (PG) and lomustine (LOM) and their combination (PG-LOM). The PG, also known as propyl 3,4,5-tri-hydroxybenzoate, an ester form of gallic acid and propanol, work as a synthetic antioxidant and preservative, that can inhibit the nucleic acid synthesis in micro-organisms, and prevent the cell growth [38]. PG can be used in the treatment of the brain tumors (GBM). In PG case alternative route is suggested as toxic effect was seen in the case of oral administration. Therefore, the intranasal route can be effective [16]. The application of PG is supported for its intranasal administration because of its low molecular weight (212.2 g/mol), pKa (7.94) and lipophilic character (logP=1.8); the result indicated the non-ionized fraction of the drug under nasal conditions (pH=5.5-6.5) can increase the nasal absorption [39]. The studies showed that PG may take part in mitochondrial impairment and inhibition of cellular respiration [40]. We also encapsulated LOM, a nitrosourea compound well established in glioma therapy and an alkylating agentwith anti-tumor activity. It is a non-specific drug affecting the cell cycle including the G1 stage, G2 stage, G2/S and M stage. In this study we encapsulated the PG and LOM into lipid nanoparticles. We formulated different lipid nano-formulation HA-coated liposomes loaded with PG, PG-SLNs [40], and LOM liposomes, PG-LOM liposomes. We studied these lipid nano-formulation and checked their suitability for intranasal administration. We compared our final product on different type of cancer cells lines and checked their anti-proliferative effects [41].

3.6. Role of the Quality by design (QbD) in the early development of a lipid carrier system for GBM targeting

Lipid-based nano-carrier systems could be a potential option based on current knowledge of barriers limiting the IND of anticancer drugs targeting the brain malignancies. The QbD idea, or the Good Manufacturing Practices (GMPs) of the twenty-first century, should be followed, however, different formulation parameters and regulatory concerns must be considered [42]. The main elements of QbD methodology are described in the relevant International Conference on Harmonization (ICH) guidelines, (i) explicitly ICH Q8 (R2), Q9, and Q10, which included characterizing the quality target product profile (QTPP); (ii) identifying the critical quality attributes (CQAs) of the targeted product; and (iii) evaluating the production method and defining the critical process parameters (DOE) [43]. The first phase in the QbD process is to gather all data from prior research that may have an impact on the target product profile. The Risk Assessment (RA) application highlighted the features having the most impact on the final lipid nano-formulation quality for IND after early understanding of space design and evaluation of QTPPs, CQAs, and CPPs [44]. The ICH recommendations exhibited the description of QbD approach in early development of a lipid carrier system for nose-to-brain administration [43, 45]. We developed lipid nanoparticles (liposomes, SLNs), there are many risk factors that should be taken into account, including particle characteristics, dissolution, structure and permeability profiles and the production method as well [46, 47]. The best feature of applying QbD approach is to eliminate the occurrence of errors at an early stage of production. The predefined set of criteria can help us to get particular feature with optimum mean diameter, zeta potential and polydispersity index (PDI) of targeted formulation [48]. The implementation of QbD ensure lipid nanoparticles with greater stability in colloidal form. We applied QbD approach on two types of lipid-based formulations (liposomes and solid lipid nanoparticles) under our study. The previous studies also suggested the optimization of lipid nanoparticles for the intranasal administration [41].

4. MATERIALS

4.1. Applied active agents

LOM was purchased from Sigma-Aldrich (Budapest, Hungary). LOM is a small molecule drug with a molecular weight of 233.6 g/mol. It has a lipophilic character (log P value of 2.16) and as a base slight high pKa value (13.3). Further properties are described in **Table 1**.

Table 1: The properties of the active agent LOM

Chemical structure	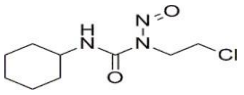
Molecular weight	233.69 g/mol
Melting point	88-90°C.
Physical Description	Pale yellow powder
Application	Chemotherapy and an alkylating agent used in treatment of brain tumor, Hodgkin's disease, other cancers

PG was purchased also from Sigma-Aldrich (Budapest, Hungary) has a low molecular weight (212.2 g/mol), both lower lipophilic character (log P = 1.8) and pKa value (7.94), than LOM. Further properties of PG are mentioned in **Table 2**.

Table 2: Properties of the active compound PG

Chemical structure	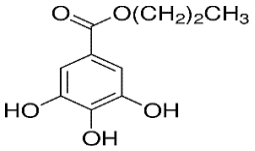
Molecular weight	212.2 g mol/mol.
Melting point	150°C.
Physical Description	white to creamy-white crystalline powder
Application	Synthetic potent Antioxidant compound

4.2. Applied excipients

Different types of excipients used for the preparation and optimization of lipid nanoparticles are listed in **Table 3**.

Table 3: Properties, role and purchase data of excipients used for preparation of lipid nano-formulation.

Excipient	Characterization	Role	Purchase data
Cholesterol	Biocompatible, inert, non-toxic	Modulating membrane fluidity, elasticity, as well as permeability.	Molar Chemicals Ltd. (Budapest, Hungary)
Transcutol-P	(Diethyl glycolmonoethyl ether) high-purity solvent and powerful solubilizer	Permeation enhancer (stabilizer)	Gattefossé (saint-Priest, France)
L-α-phosphatidylcholine (PC)from soybean	low-density lipoprotein asymmetric moleculewith glycerol backboneand occurs naturally in lecithin of egg yolk	Stabilizer, wall forming agent, increase nasal residence time, enhance nasal permeability	BASF (Ludwigshafen, Germany)
Tween 80	Polyoxyethylene sorbitan monooleate is a non-ionic surfactant.	Steric stabilizer	Fluka Chemika (Buchs, Switzerland)
Glutaraldehyde	poly(vinyl alcohol), and poly-heptapeptides	Cross-linker	Gattefossé (saint-Priest, France)
Sodium hyaluronate (HA)	Linear polysaccharide polymer. It is bio-compatible, bio-degradable, and non-immunological material.	Muco-adhesive agent	Gedeon Richter Plc. (Budapest, Hungary)
Trehalose dihydrate (TRE)	Sugar, consisting of two units of glucose, used to stabilize molecules during both freezing and drying.	Cryo-protectant	Sigma-Aldrich (New York, USA)

5. METHODS

5.1. Development and optimization of PG and LOM encapsulated lipid nanoparticles

5.1.1. QbD driven screening of influencing factors of liposomal carrier

According to the QbD methodology, the first step is always to define the target product profile, set criteria for the product and the establishment of the knowledge space development. The collection of all the influencing factors which may impact our aim. These factors should be considered from the very first steps of the formulation process, until the therapeutic response experienced by the patient. To collect these, a cause and effect (Ishikawa) diagram was set up. The Ishikawa diagram followed the traditional 4M concept, meaning the factors regarding the material characteristics, production method, product characteristics and the therapeutic expectations were taken into account. The next step is to select the factors having critical effects on the targeted product quality, the so-called Critical Quality Attributes (CQAs). As its name suggests, these factors are the critical quality indicators that promisingly influence the product quality. These are selected by prior knowledge and from the knowledge space development process. CQAs relies on the predefined goals and can hold information about the desired product's physicochemical properties, drug release profile etc. The Critical Material Attributes (CMAs) and/or the Critical Process Parameters (CPPs) should be defined as well, because they have direct or indirect influence on the CQAs. Hence, they can easily change the safety, efficacy and quality profile of the product.

5.1.2. Risk Assessment (RA) strategy of lipid-based carrier development

After determining the QTPPs and selecting the critical factors (CQAs, CPPs), the next step is to perform the RA. The RA is the evaluation of interdependence between the QTPPs elements and CQAs and between the CPPs and CQAs. The RA was implemented by using Lean QbD® software (QbDworks.com, QbDworksLLc., Fremont, CA, USA). The evaluation of connections between these screened factors was structured by using a 3-level scale. Each factor and parameter were thoroughly evaluated. The 3-grade scale reflected the impact of factor interactions with each other evaluated one by one in pairs, their interaction being low (L, green), medium (M, yellow), and high (H, red). This interdependence rating step was followed by an occurrence rating estimation of the CPPs using the same 3-grade scale. The determination of this risk occurrence is compulsory for analysis; hence it was performed using risk management protocols. As a result of the RA, the ranking of CQAs and CPPs were plotted on Pareto diagrams generated by the QbD software. The following Pareto chart ranked the impact of potential factors and highlighted the significant factors. This software application in the development of pharmaceutical formulation helps to select the items of the factorial design of experiments to obtain the optimized formulation strategy.

5.1.3. Optimization of liposomal carrier using Box-Behnken factorial Design (BBD)

Among the various methods of optimization, the BBD is the most broadly accepted and extrapolated design in the experimental phase of pharmaceutical formulation development. The significance of the BBD is based on screening and evaluating highly influential factors by applying the response surface methodology (RSM) with greater precision requiring only a few number of experimental trials [46]. The 3-level BBD was performed and exercised using TIBCO Statistica® 13.4 software (Statsoft Hungary, Budapest, Hungary). Analysis of variance (ANOVA) was applied to calculate the statistical significance of each model coefficient at a 95% confidence level. Differences were considered significant when $p < 0.05$. For the factorial design, the variables were selected based on the RA results. By exercising the response surface methodology, three different independent factors and dependent factors were assessed: the independent factors included the amount of phospholipids (X1, 12 to 36 mg), the amount of cholesterol (CHL) (X2, 8 to 24 mg), and the effect of temperature (X3, 40 to 80 °C), while the dependent factors included the average hydrodynamic diameter (Z-average) (Y1), zeta potential (Y2), and polydispersity index (PDI) (Y3). The type and ratio of the organic solvent were constant. Polynomial equations were fitted to determine the correlation among the independent and dependent variables in order to reach the optimized Z-average, PDI, and zeta potential (i.e., the highest absolute value of Z-average, the narrower PDI and the optimum zeta potential).

5.1.4. Optimization of SLNs using response surface quadratic model

Stat-Ease Design Expert® version 10 (Stat-Ease, INC.2021 East Hennepin Ave., Suite 480 software) was used to optimize the formulation process and product quality of SLNs. The amount of cholesterol (CHL) (20–60 mg), Tween 80 (10–40 mg) and temperature (20–70 ℃) were chosen as independent factors based on the RA process, while the ratio of aqueous to organic phases (acetone:ethanol) was kept constant (1:4). Central composite design was applied where SLNs were prepared for each trial, and three responses were evaluated namely, Z-average, PDI and zeta potential.

5.2. Development of lipid nanoparticles

5.2.1. Development of PG-coated liposomes

A unique direct pouring method has been used to develop liposomes. This is a straightforward bottom-up size reduction process that produces a stable formulation with an optimal lipid and drug concentration. PG (12, 20, and 40 mg), PC (12, 24, and 32 mg), and cholesterol (8, 16, and 24 mg) were dissolved in 4 mL of an ethanol: acetone (3:1) combination and then added directly to the 10 mL purified water as aqueous phase. Using a hot-plate magnetic stirrer, the organic phase was evaporated at 60°C with constant stirring (400 rpm). For further analysis, the un-entrapped drug was removed by dialysis (5-6 h) at 4°C.

The purification of liposomal formulations was conducted by centrifugation with a Hermle Z323K high performance refrigerated centrifuge (Hermle AG, Gossheim, Germany) for 1.5 h at 13,500 rpm. After centrifugation the pellet was collected and redispersed in 1 mL purified water. The HA coating solution (50 mg/mL) was performed by soaking HA on the surface of purified water and waiting for 30 min with steady stirring at 400 rpm until it swelled completely. After that, 1 mL of HA solution was added drop-wise to the liposomal solution with a syringe for 30 min at room temperature with steady stirring at 700 rpm. After that, the mixture was kept in refrigerator at 8°C for 24 h. The liposomal formulation was centrifuged again at 4°C for 10 min at 25,000 rpm to remove the excess of HA which did not participate electrostatic coating of liposomes, and the pellet was re-dispersed in 10 mL purified water. After that, 5 %w/w trehalose dihydrate was added as cryoprotectant and 1.5 mL of the coated formulation was transferred to vials and freeze-dried using a Scanvac Cool safe laboratory freeze-dryer (Labogene, Lynge,Denmark), at 40°C for 12 h under a 0.013 mbar pressure, then maintained at 25°C for 3 h for secondary drying to obtain the lyophilized powders.

5.2.2. Development of PG-SLNs by modified injection method

PG-SLNs were prepared with a modified injection method, where 10 mL of 0.2% *w*/*v* Tween 80 aqueous solution and 5 mL of the organic phase (ethanol:acetone 4:1) were added in different ratios. The PG (10 mg) and CHL (60 mg) were dissolved in a mixture of the organic phase and injected dropwise into surfactant solution under constant stirring at 700 rpm at 70 ℃. After complete evaporation of the organic phase, the formulation was purified by centrifugation for 2 h at 13,500 rpm to separate SLNs from residual solvent-containing supernatant. The collected pellets were re-dispersed in 5 mL purified water and freeze-dried with same procedure described above in presence of 5% *w*/*v* trehalose as cryoprotectant to obtain lyophilized powders. The lyophilized powder was stored at 5 ± 3 ℃ until further investigation.

5.2.3. Preparation of co-encapsulated (PG-LOM) liposomes

A novel direct pouring method (DPM) was used to develop liposomal formulations. The selection of critical quality attributes (CQAs), critical material attributes (CMAs), critical process parameters (CPPs) and quality target product profile (QTTP) was selected by the systematic and holistic QbD approach [40]. Therefore, CHL and PHC were used in different molar ratio (0.67, 1, 1.33, 1.5, 2, 2.67, 4 and 6 mol/mol for CHL). Phospholipids were dissolved in 4 mL of ethanol-acetone (3:1) mixture and directly added to 10 mL of purified water. The organic phase was evaporated at 60°C under constant stirring (400 rpm) by using a hot-plate magnetic stirrer. Drug loaded liposomes were prepared with the same procedure, both PG and LOM were added in different mass ratio (1:1,1:2,1:3,2:1,3:1,3:4 and 4:3) to the formulation to get the optimal composition, while dissolving phospholipids in organic solvent mixture. Three types of liposomes were prepared containing PG and LOM both separately and combined, namely, PG -liposomes (PG-Lipo),

LOM-liposomes (LOM-Lipo) and combined PG-LOM Liposomes (PG-LOM-Lipo) [49]. The un-encapsulated drug was removed via dialysis at 4°C by using 8 kDa MWCO dialysis membrane (Spectra/Por®, Spectrum Laboratories Inc., Rancho Dominguez, CA, USA). Dialysis bag filled with liposomal formulations were sunk into a beaker containing 500 mL physiological saline solution in order to maintain consistent osmotic pressure. After 24 h dialysis liposomes were centrifuged for 1.5 h at 13,500 rpm in two cycles, between the pellet was collected and re-dispersed in 10 mL of purified water using ultra-sonication (for 30 s). For solid-state characterization the re-dispersed pellet was freeze-dried after purification at −40 °C and 0.013 mbar for 12 h using a ScanVac CoolSafe 100–9 (LaboGene, ApS, Lynge, Denmark) laboratory apparatus. Secondary drying was carried out at 25 °C and 0.013 mbar for 6 h.

5.3. Characterization of lipid nanoparticles

5.3.1. Average hydrodynamic diameter, surface charge, and polydipersity index of lipid nanoparticles

5 mg of lyophilized liposomes were redispersed in 5 mL purified water, and the solution was sonicated for 5 min to reduce inter-particulate aggregation. A Malvern nano ZS (Malvern Instruments, Worcestershire, UK) instrument was used to measure the Z-average, zeta potential, and PDI of liposomes in folded capillary cells. The apparatus temperature and refractive index were set to 25°C and 1.445, respectively, with a total of 17 scans. All measurements were performed in triplicate data were presented as mean±SD. The Z-average, zeta potential, and PDI have defined acceptable ranges of 100-200 nm, ±30-40 (mV), and 0.0-0.03, respectively [40].

5.3.2. Gas chromatography for residual solvent determination (GC-MS) for DPM

For determination of acetone, Shimadzu GCMS-QP2010 SE (Shimadzu Europa GmbH, Duisburg, Germany) gas chromatography equipment with a 30 m long, 0.25-mm-diameter ZBWax-Plus column using He as the carrier gas was applied. The instrument was calibrated with a five-point series for acetone.

5.3.3. Drug Loading, Encapsulation Efficiency, and Percentage Yield of lipid nanoparticles

The centrifuge method was utilized to determine the encapsulation efficiency, % yield, and drug loading of PG-loaded lipid nanoparticles. Nanoparticles were initially centrifuged for 1 hour at 22,413 relative centrifuge force (RCF 16,500 rpm, 4°C). The supernatant was collected and screened using an Agilent 1260 HPLC (Agent Technologies, Santa Clara, CA, USA). The encapsulation efficiency, percent yield, and drug loading of PG and LOM loaded liposomes were all determined using the centrifuge method. The nanoparticles were initially centrifuged for 1 hour at 22,413 relative centrifugal force in a Hermle Z323 laboratory centrifuge (RCF 16,500 rpm, 4°C). ChemStationB.04.03 software (Agilent Technologies, Santa Clara, CA, USA) was used to evaluate the data. PG has a 4 min retention time. The calibration line's linear

regression was 0.998. In the instance of PG, the limit of detection (LOD) and the limit of quantification (LOQ) were 21 ppm and 63 ppm, respectively. While the quantification limit (LOQ) and detection (LOD) of LOM were 40 ppm and 13 ppm. Each formulation was tested in three different ways, the percentage of drug encapsulated was estimated as followings [47]:

$$\textbf{Encapsulation Efficiency}\ (\%) = \frac{\mathbf{w_1 - w_2}}{\mathbf{w_1}} \times \mathbf{100} \quad (1)$$

Where w_1 represents total PG/LOM in liposomes and w_2 represents free PG/LOM in the supernatant.

By weighing the lyophilized liposomes/SLNs and applying the formula below, the % yield was computed:

$$\textbf{Percentage Yield}\ (\%) = \frac{\textbf{Actual Yield}}{\textbf{Theoretical Yield}} \times \mathbf{100} \quad (2)$$

Weighing the lyophilized liposomes/SLNs was used to compute drug loading, which was then analysed using the following formula:

$$\textbf{Drug loading}\ (\%) = \frac{\mathbf{w_1 - w_2}}{\mathbf{w_{NP}}} \times \mathbf{100} \quad (3)$$

Where w_1 is the quantity of total PG/LOM in the liposomes, w_2 is the amount of free PG/LOM in the supernatant, and w_{NP} is the amount of formulation utilized for analysis,

5.3.4. Fourier Transform Infrared (FTIR) spectroscopy of lipid nanoparticles

A thermo-Nicolet AVATAR FTIR spectroscopy (Thermo-Fischer, Waltham, USA) was used to gather FTIR spectra of pure drug, cholesterol, phospholipids, and coating material in the spectral region of 4000 and 400 cm^{-1}. The spectral resolution was adjusted to 2 cm^{-1}, and 128 scans were performed in case of all samples to improve the signal-to-noise ratio. A small amount of investigated sample (m<0.01 g) was mixed with 0.15 g of KBr, thereafter homogenized and milled. The powder mixture was pressed under pressing force of 10 kN using a Specac® hydraulic press (Specac Inc. Orpington, UK), with the pressing diameter of 13 mm. The background was also measured with pure KBr and subtracted form sample spectra.

5.3.5. DSC (Differential Scanning Calorimetric) of lipid nanoparticles

To investigate the physiochemical properties and conversions, to analyze the crystallinity of solid-state products, DSC measurements were carried out. In this evaluation, drug loaded liposomes and SLNs were investigated to assess the possible intermolecular interactions between the drug, the HA-coated material, and lipids. DSC measurements were performed using a Mettler Toledo DSC 821e instrument (Mettler-Toledo GmbH, Greifensee, Switzerland). Approximately 3–5 mg of samples of physical mixtures and of components used in formulation development along with the coated material and product samples were

loaded into an aluminum pan and examined in the scanning temperature range of 25–300 ℃, with an empty Al pan used as reference. The heating rate was 20 ℃/min in the presence of argon as a carrier gas with a flow rate of 150 mL/min. Each measurement was normalized to the sample size.

5.3.6. X-ray Powder Diffraction (XRPD) of lipid nanoparticles

The XRPD method was utilized for the structural characterization of pure drug and physical mixture compared to lipid nanoparticles. A BRUKER D8 Advance X-ray powder diffractometer (Bruker AXS GmbH, Karlsruhe, Germany) was used to obtain diffractograms. All of the results were obtained using a Cu Kλ1 slit-detector source (=1.5406). All of the formulation components, as well as the formulation itself, were scanned at 40 kV and 40mA in the angular range of 3-40° 2θ with a step time of 0.1 s and a step of 0.007 at a step time of 0.1 s. The samples were measured at the ambient temperature and humidity while examined in quartz holder.

5.3.7. Morphology of lipid nanoparticles

(a) TEM

Transmission electron microscopy (TEM) (FEI Tecani G2 20 X Twin; FEI Corporate Headquarters, Hillsboro, OR, USA) was used to examine the surface properties of the liposomes formulations at a 200 kV accelerating voltage. A few microliters of liposomes dispersion were placed on a carbon-coated copper grid and superfluous drops of the sample suspension were removed with the filter paper, leaving a thin liquid layer spread over the perforations.

(b) SEM

The morphology and surface properties of PG-SLNs were investigated using scanning electron microscopy (SEM) (Hitachi S4700, Hitachi Scientific Ltd., Tokyo, Japan). At 1.3-13.1 mPa pressure, a voltage of 10 kV and a current of 10 mA was applied. The sputter-coated samples were made conductive with gold-palladium using a higher vacuum evaporator and an argon environment (BioRad SC 502, VG Microtech, Uckfield, UK). The gold-palladium coating had a thickness of about 10 nm.

5.4. *In vitro* characterization of lipid nanoparticles

5.4.1. *In vitro* release study of lipid nanoparticles

In vitro release study was performed under nasal conditions at 35°C using dialysis method under 50 rpm constant stirring. 1 mL of liposomal formulations were filled in 8 kDa dialysis bag (Spectra/Por®, Spectrum Laboratories Inc., Rancho Dominguez, CA, USA) and placed in 50 mL of simulated nasal electrolyte solution (SNES), which combined 2.98 g of KCl, 0.59 g of $CaCl_2$ anhydrous in 1000 mL of deionized water at pH 5.60. Aliquots were taken at predetermined time intervals. After filtration of withdrawn

samples, both LOM and PG contents were determined via HPLC method as described above. All of the measurements were performed in triplicate. Data was presented as mean±SD. For each sample the *in vitro* release kinetics were also assessed using a variety of mathematical models, including Zero order, First order, Higuchi, Korsmeyer-Peppas, and Hixon-Crowel [48].

5.4.2. *In vitro* permeability study of lipid nanoparticles

For *in vitro* permeation studies, a modified horizontal side-bi-side® type diffusion apparatus was employed at 35°C using a circulating thermostat (Thermo Haake C10-p5, Sigma-Aldrich Co. LLC, St. Louis, MO, USA) under 100 rpm constant stirring of both chambers. An isopropyl myristate impregnated artificial membrane (0.45 um pore size, Pall Metricel cellulose membrane) with a 0.69 cm^2 diffusion surface was used to separate the donor and receptor compartments. The donor compartment contained 9 mL of pH 5.6 SNES, whereas the acceptor compartment contained pH 7.4 PBS. After every 5 min, aliquots were withdrawn from the acceptor phase and replaced with the same volume of fresh medium. Aliquots were assayed using HPLC to determine the amount of active compound diffused to the acceptor phase. Each formulation was measured in triplicate. Data was presented as mean±SD.

5.4.3. *In vitro* scavenging assay

In 0.05 M phosphate buffer of pH 7.4 was prepared with (40 mM) hydrogen peroxide. In a hydrogen peroxide solution, PG liposomes with various drug concentrations (125, 250 and 500 ug/mL) were introduced (0.6mL, 40mM). After 10 minutes, the absorbance of hydrogen peroxide at 230 nm was measured against a blank solution of phosphate buffer without hydrogen peroxide. The following equation was used to calculate the % hydrogen-peroxide scavenging activity:

$$\boldsymbol{H_2O_2\ scavanging\ effect}\ (\%) = \boldsymbol{A_0} - \frac{\boldsymbol{A}}{\boldsymbol{A_0}} \times \mathbf{100} \qquad (4)$$

Where A0 is the absorbance of the control reaction and A is the absorbance when the initial PG-containing sample is present.

5.5. Comparative study of anti-glioblastoma drugs encapsulated liposomes

5.5.1. MTT assay, *ex vivo and* Raman chemical mapping of co-encapsulated formulations

5.5.2. *Ex vivo* raman mapping

5 µL of the formulations was instilled onto the outer surface of the nasal mucosa (physiologically open toward the nasal cavity), and after half an hour, the incision point was cut in half and inverted to the cross-sectional side and placed onto an aluminium foil-coated slide. *Ex-vivo* Raman chemical mapping was

performed via a Thermo Fisher DXR Dispersive Raman instrument (Thermo Fisher Scientific Inc., Waltham, MA, USA) equipped with a CCD camera and a diode laser operating at a wavelength of 780 nm was used. A 500 μm size surface was analysed with step size of 50 μm with an exposure time of 4s and acquisition time of 4 s, for a total of 4 scans per spectrum in the spectral range of 3500-200 cm^{-1} with cosmic ray and fluorescence corrections. The Raman spectra were normalized in order to eliminate the intensity deviation between the measured areas.

5.5.3. *Ex Vivo* nasal diffusion study on rabbit nasal mucosa

The *ex vivo* diffusion study of the formulation at nasal conditions was performed in a modified Side-bi-Side® horizontal diffusion cell. The following formulations were tested: Lom-Lipo, PG-Lipo, Lom and PG mixture solution, LOM solution and PG solution. Between the donor and the acceptor cell, rabbit nasal mucosa was placed. Both donor and acceptor cell volume were 9.0 ml for which the diffusion was investigated at 35 °C. The donor phase consisted of SNES and the acceptor phase was of pH 7.4 PBS. Sampling from the acceptor phase was performed at assigned time points (1, 3, 5, 10, 15, 30 and 60 min) and the drug concentration was measured via HPLC. The flux (J) was calculated from the quantity of the drug permeated through the membrane, divided by the surface membrane insert and the duration of experiment (μg/cm^2/h). The permeability coefficient (Kp) was determined from J and the drug concentration in the donor phase (Cd (μg/cm^3)) as follows:

$$\boldsymbol{K_p}\left[\frac{\boldsymbol{cm}}{\boldsymbol{h}}\right] = \frac{\boldsymbol{J}}{\boldsymbol{C_d}} \qquad (5)$$

5.5.4. Anti-proliferative MTT assay

Anti-proliferative effect of LOM, PG and liposome complexes were determined under in vitro study using U87 glioblastoma cells, NIH-3T3 mouse embryonic and A2780 human ovarian cancer cells by means of MTT ([3-(4,5-dimethylthiazol-2-yl)-2,5-diphenyltetrazolium bromide]) assay. Glioblastoma cells were cultivated in Dulbecco's Modified eagle's Medium supplemented with 1 mM sodium-pyruvate. NIH-3T3 and A2780 cells were cultured in Modified Eagle's Medium. Both culture media were supplemented with 10% fetal bovine serum, 1% non-essential amino acids and an antibiotic-antimycotic mixture. A limited number of human cancer cells (5000/well) were seeded onto a 96-well micro-plate and became attached to the bottom of the well overnight. On the second day of the procedure, the test substances were added in serial dilution (applied in six different concentrations). After an incubation period of 72 h, the living cells were assayed by the addition of 20 μL of 5 mg/mL MTT solution. After a 4 h incubation, the medium was removed and the precipitated formazan was dissolved in 100 μL/well of DMSO during a 60-min period of shaking. Finally, the reduced MTT was assayed at 545 nm, using a micro-plate reader. Untreated cells were

taken as the negative. All in vitro experiments were carried out on two 96-well dishes with at least five parallel wells in two independent experiments [23].

5.5.5. In vitro cellular uptake study

In vitro cellular uptake of liposomal carrier was investigated by propidium iodide (PI) labelled liposomes on U87 and a more resistant U251 glioblastoma cell line. The cells were seeded in 96-well microplates with 5000 cell/well cell number. All culture media contained 10% fetal bovine serum, antibiotic/antimycotic complex and non-essential amino acids. The plates were incubated at 37°C at 5% CO_2 tension in humidified atmosphere for an overnight period and the liposomal nanoparticles were added to the wells in order to have 100 μM PI in each well. After a 24 h incubation period the cells were stained with cell track green (CTG) in 5 μM concentration. The supernatant was removed and 100 μL medium was added to each well. The cells were examined by a Nikon Fluorescent Microscope equipped with a Digital Sight Camera System, including appropriate filters for PI.

5.6. Statistical analysis

The outcomes of this research data were statistically analysed using Microsoft® Excel (Microsoft Office Professional Plus 2013) and JMP® 13 software (SAS Institute, Cary, CA, USA). All of the findings were checked thrice and provided with a mean and standard deviation. One-way analysis of variance was used to analyse *in vitro* release and permeability data (ANOVA). A *t*-test was used for the *in vitro* scavenging assay. When the $p < 0.05$, difference was considered significant.

6. RESULTS AND DISCUSSION

6.1. Optimization of lipid nanoparticles

6.1.1. Initial knowledge space development of PG Liposomes

There are various essential aspects impacting the final quality of the coated liposomal formulation as represented in the Ishikawa diagram (**Figure 3**). It was created in response to latest scientific data on coating and nose-to-brain distribution, and it aids in the identification of the cause-and-effect relationship between the targeted product and its influencing factors. QTPPs can be selected based on the fishbone diagram. The selected parameters are listed in, along with their aims and justifications. Excipients (phospholipids, cholesterol), coating material, Z-average, zeta potential, poly-dispersity index (PDI), and aqueous phase were all examined in this investigation, depending on the established aims and therapeutic demands. All of these aspects have an impact on the product's quality [24, 31]. The process variables of novel approaches were sonication time (for mixing lipids into the organic phase), temperature (for evaporation), and stirring time (rpm).

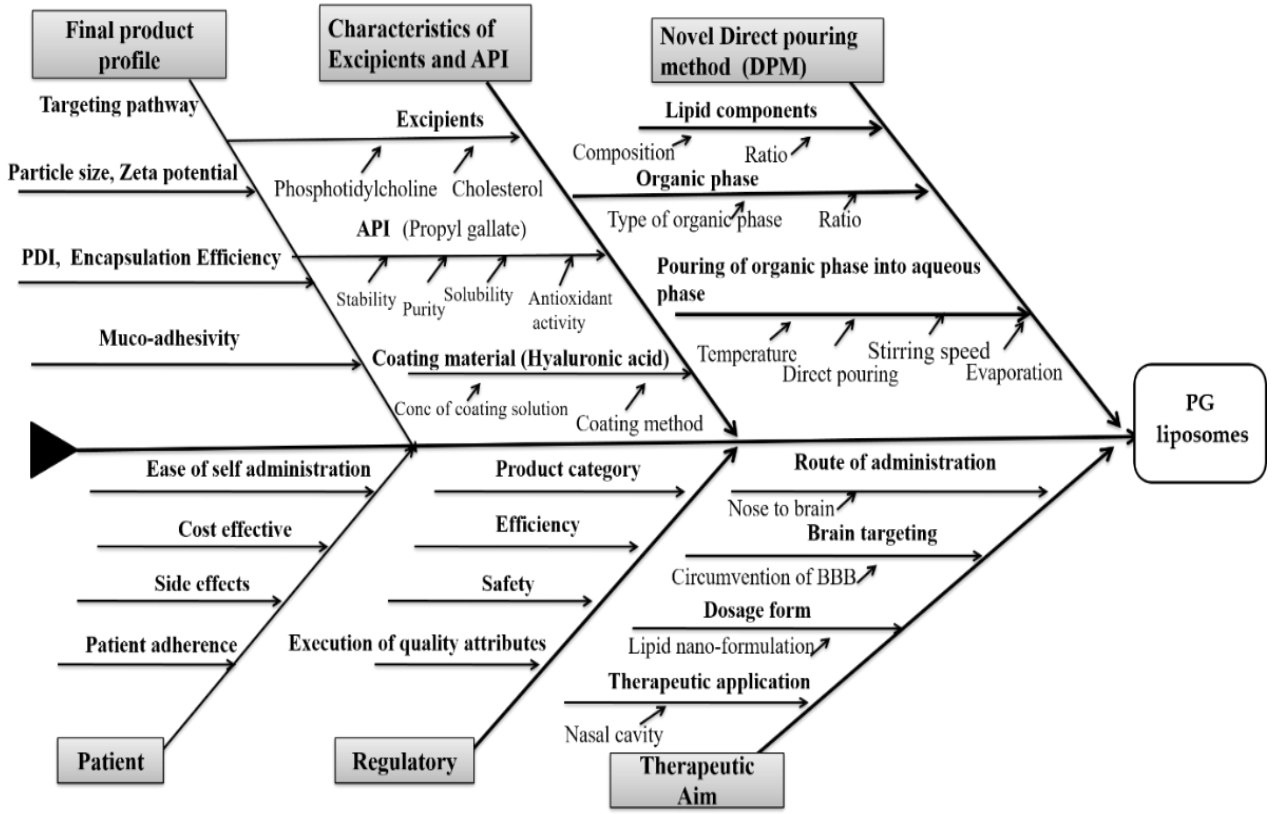

Figure 3. Ishikawa showing the cause-and-effect relationships between influencing factors of hyaluronic acid (HA)-coated, n-propyl gallate (PG)-loaded liposomes for nose-to-brain drug delivery.

6.1.2. The risk assessment evaluation of PG-Liposomes

RA was used to follow the QbD-based formulation design and development after determining the impact (H, M, L) of the QTPPs and evaluating the CPPs and CQAs. For RA, a preliminary assessment of the dependency between QTPP elements and CQAs, as well as between CQAs and critical material attributes (CMAs/CPPs), was made using the previously mentioned 3-grade scale, as their impact on one another is high, medium, or low. The level of influence is determined by scientific understanding in the literature as well as in experiments. The frequency of CPPs was also calculated. The severity or impact score for each element affecting the final liposomal product was determined based on the observations. The severity scores and their order are displayed in the software-generated Pareto charts. In this scenario, the scores for each CQAs and CPPs are displayed in **Figure 4** as Pareto charts. The Pareto chart concept, sometimes known as the 80/20 rule, states that for many occurrences, 20% of the causes create 80% of the effects. In the drug development process, these 20% of crucial components necessitate 80% of concentrated assessment.

The rankings in **Figure 4** aid in the construction of a priority list based on the factors that have a crucial impact on the desired end product and describe the influencing features of each aspect. The CQAs are listed in sequence (**Figure 4a**); the amount of phospholipids, cholesterol, and active pharmaceutical ingredients (APIs) all have the same and highest critical effect on the final product's quality. The remaining components in the diagram, the coating material, zeta potential, and aqueous phase, have a less impact on product quality. The ranks of the CPPs relevant to the current liposome formation process are shown in **Figure 4b**. It is clear that the DPM's temperature has the largest impact on the final result. Besides temperature, rotation speed for both mixing and evaporation has been shown to have nearly comparable effects on product quality, whereas mixing sonication duration has the lowest severity score. The results from evaluation indicate that this factor has the least impact on the end product's ultimate quality. The studied components of Box–Behnken design (BBD) could be chosen based on the results of the previously reported RA.

6.1.3. Design of Experiments: Box–Behnken design for PG-liposomes

The RA results aided in the design of the experiment. To screen the effects of the formulation parameters on the quality of the final coated liposomal formulation, the critical factors with the greatest severity ratings were chosen. The quantity of phospholipids PC (mg) and cholesterol (mg) selected from the CQAs, as well as the temperature (°C) of evaporation screened out from the CPPs, were the variables X_1 and X_2. The Z-average, PDI, and zeta potential were chosen as dependent factors according to our design strategy. After applying QbD, the highly relevant parameters were chosen and incorporated to screen against the optimized

formula for all researched variables within acceptable ranges. The ANOVA table produced from the design of experiments (DOE) and the results was used to validate BBD screening for each factor.

CQA \ QTPP	Therapeutic Effect	Route of Administration	Dosage form	Coated Liposomes	Targeting Pathway
Coating material 12 %	High	Medium	Low	High	Medium
Phospholipids 18 %	Low	High	Low	High	High
Cholesterol 9 %	Low	Low	Low	High	Low
API 13 %	High	High	Medium	Low	Medium
Zeta potential 14 %	High	Medium	Medium	High	Medium
Aqueous phase 4 %	Low	Low	Low	Medium	Low
Particle Size 20 %	High	High	Low	High	High
PDI 9 %	Low	Low	Low	High	Low

Process		Organic phase preparation	Mixing of organic and aqueous phase	Evaporation	
CQA \ CPP		Sonication time 21 %	Stirring speed 22%	Stirring speed 23%	Temperature 34%
Coating material	12 %	Low	Medium	Low	Medium
Phospholipids	18 %	Medium	Medium	Medium	High
Cholesterol	9 %	Medium	High	Medium	High
API	13 %	Medium	Low	Low	Medium
Zeta potential	14 %	High	High	High	High
Aqueous phase	4 %	Low	High	High	High
Particle Size	20 %	High	Medium	High	High
PDI	9 %	High	Medium	High	High

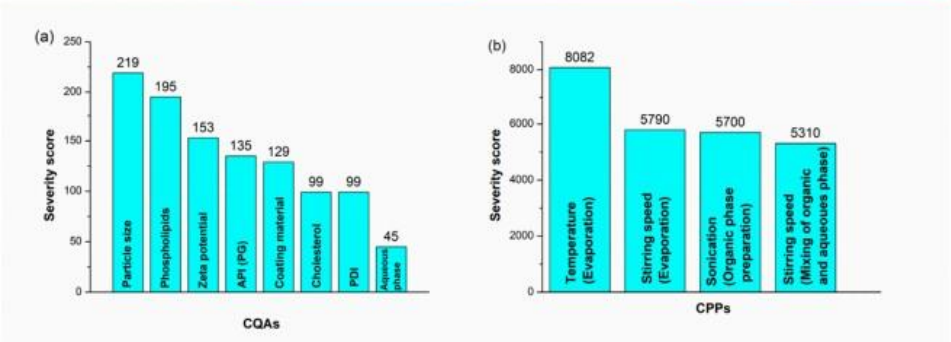

Figure 4. Interdependence rating and estimation of QTPPs elements and critical quality attributes (CQAs) and critical process parameters (CPPs), and Pareto charts showing the severity/impact among selected (a) CQAs and (b) CPPs

6.1.4. Influence of investigated parameters on the Z-Average, PDI, and Zeta Potential

The interdependence between the studied independent and dependent responses was explained by the significance of effects for each variable (**Table 4**). The Z-average is closely related to particle size in colloidal drug delivery systems, therefore changes in it can signal changes in the primary particle size as well.

Table 4. Z-average, polydispersity index (PDI), and zeta potential of 15 runs on the design of experiments

Number of Runs	Temperature (°C)	Amount of Phospholipids (mg)	Amount of Cholesterol (mg)	Z-Average (nm)	PDI	Zeta Potential (mV)*
1	50	16	16	150±10	0.27±0.01	-22±8.4
2	70	16	16	155±5.5	0.28±0.02	-18±6.5
3	50	32	16	145±4.5	0.29±0.02	-23±8.4
4	70	32	16	140±5.5	0.28±0.05	-24±8.4
5	50	24	8	125±6.6	0.25±0.07	-27±7.5
6	70	24	8	125±7.8	0.22±0.01	-28±8.5
7	50	24	24	400±22	0.40±0.08	-8±10.2
8	70	24	24	450±23	0.45±0.08	-7±12
9	60	16	8	121±24	0.24±0.09	-33±5.5
10	70	32	8	123±40	0.25±0.08	-28±6.5
11	60	16	24	430±20	0.55±0.05	-6±10
12	60	32	24	420±12	0.49±0.01	-8±10.2
13	60	24	16	130±10	0.21±0.02	-29±3.3
14	80	24	16	135±10	0.22±0.02	-26±5.5
15	70	24	16	142±8	0.27±0.01	-25±6.2

***Data are the mean±SD (n=3 independent formulations)**

The BBD results were used to create an improved colloidal stable system. A greater Z-average was achieved at a smaller concentration of PC, but as the concentration of phospholipids was increased to a significant extent, the Z-average reduced to 130 nm. All trials show an increase in the amount of phospholipids resulted in the development of large size particles. Phospholipids function as a surfactant, increasing solubility at the interface between two phases and lowering the Z-average. The Z-average increased as the concentration of phospholipids increased due to increasing viscosity. Temperature had a similar effect; a higher Z-average was observed at a lower temperature, but its size reduced as the temperature increased during the process.

The effects of phospholipids, cholesterol, and temperature on the PDI were also studied in (**Figure 5b**). The PDI value was within the ideal range at medium or moderate values of these three parameters, while it was high at the two ends. Only cholesterol had a substantial effect on the variation in the PDI, according to the following findings. The influence of phospholipids, cholesterol, and temperature on the

zeta potential was also investigated, as shown by the DOE's corresponding coefficient (Figure 5c). When compared to the content of phospholipids, the coefficient revealed that temperature and cholesterol had a substantial effect on liposome stability.

The zeta potential of the formulation is largely influenced by the amount of phospholipids used and the process temperature, as illustrated by the surface plot. Liposomes with a low cholesterol concentration were formulated at 60°C, resulting in a stable lowest surface charge and, as a result, increased stability. The zeta potential of the formulation is strongly influenced by the amount of phospholipids used and the temperature (°C), as seen by the surface plot. Liposomes formulated with a low cholesterol concentration and developed at 60°C had the lowest surface charge and increased stability.

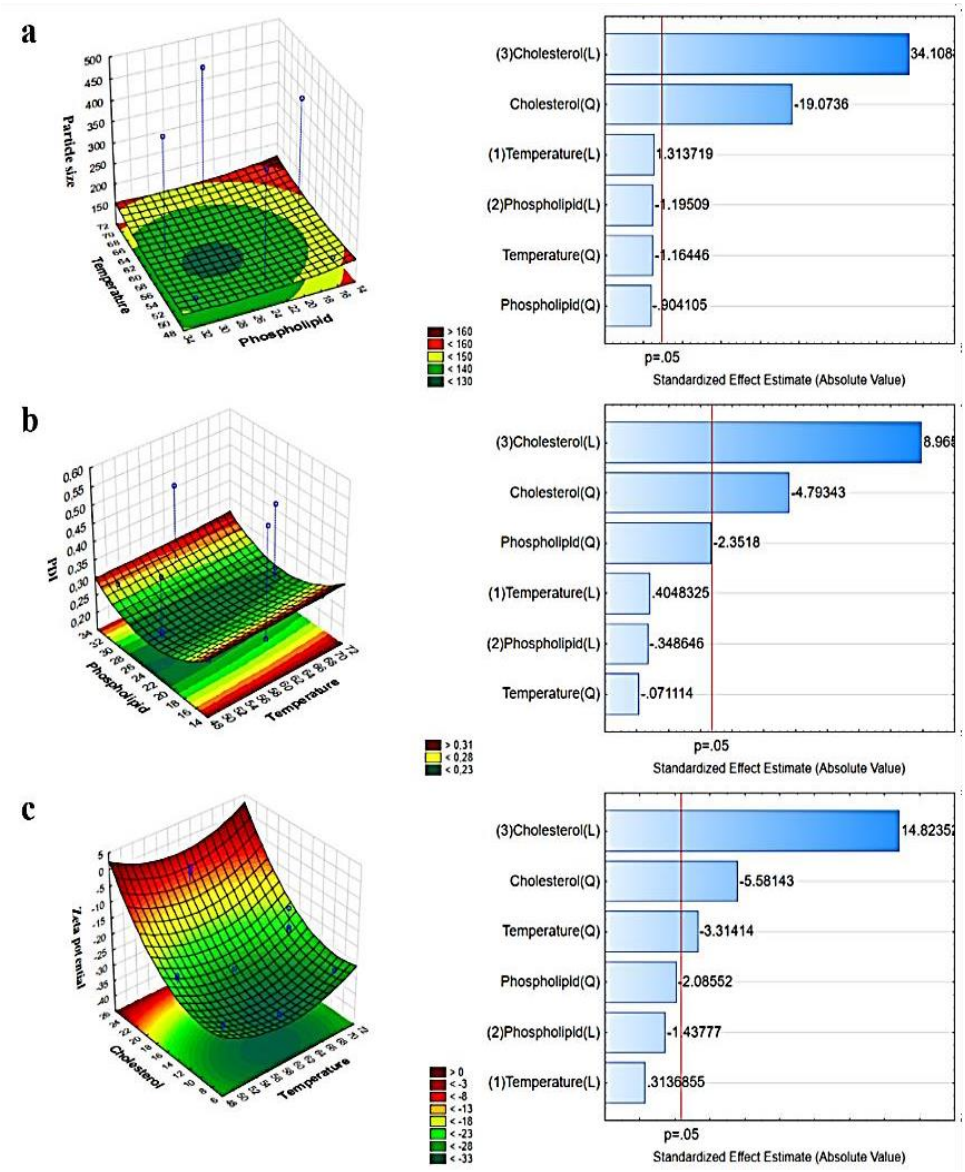

Figure 5. Three-dimensional surface plot and Pareto chart showing the combined impact of phospholipids and temperature on the Z-average (**a**), on the PDI (**b**), and on the zeta potential (**c**)

6.1.5. Quality by design approach and risk assessment (RA) of PG-SLNs

The particle properties of the nano-formulation were thoroughly evaluated during the RA process, as these are critical aspects for IND. Quantification of these findings were done based on the interdependence rating. The interdependence rating assigned mostly high-grade scores when it came to particle characteristics (Z-average, PDI, and zeta potential), which is supported by the higher severity scores in Figure 6a when compared to the applicability affecting risk factors like muco-adhesivity, viscosity, and swelling properties. The basis for proper particle size and distribution are critical in QbD-driven nanoparticle formulation, since these are the fundamental factors that can impact the dissolution and permeability profiles that are the crucial steps in nasal administration in the nasal cavity and across the nasal mucosa. According to the calculations, material attributes such as Tween 80 and cholesterol concentrations have the highest risk severity, followed by the temperature at dissolution phase when compared to the sub-processes, as shown in **Figure 6**.

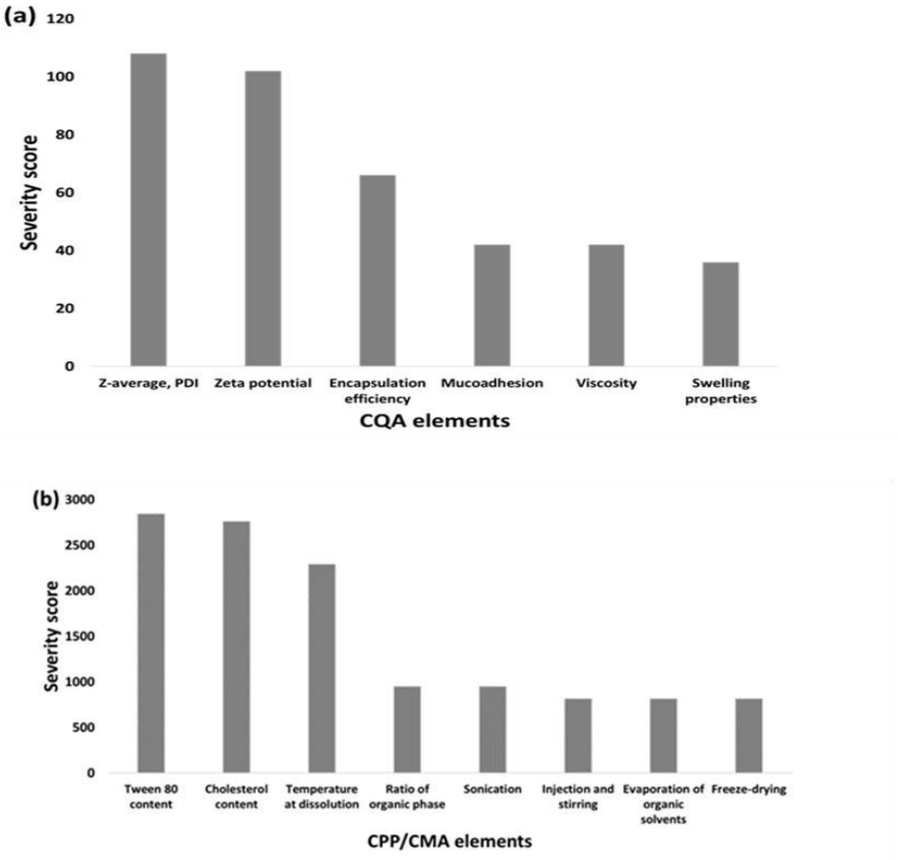

Figure 6. Probability rating of CQA (**a**) and CPP/CMA (**b**) elements. The Pareto charts are presented as the calculated severity scores assigned to the elements

6.1.6. Central composite design (CCD) for PG-SLNs

SLNs were optimized in a 15-formulation experiment series, where the effect of the factors with the greatest

severity score, notably cholesterol content (A), Tween 80 content (B), and temperature (°C), on the independent factors: Z-average, PDI, and zeta potential, was studied. After adding the experimental data into the software, it calculated the optimal composition, which can resulting in lowest particle size, PDI, and the characteristic with the most negative zeta potential. Based on the lowest Z-average, PDI, and greater negative zeta potential, the software screened the optimal trial with desirability of 0.99. Tween 80 and cholesterol in a 1:6 ratio were used in the improved PG-SLNs. The polynomial equations (Eq. 6, 7and 8) obtained for the fitted full model demonstrating the effect of formulation variables on the particle size, Zeta potential and PDI.

$$Particlesize=160.57-23.74A+144.53B-60.62C+16.88AB-17.97AC-50.11BC+26.74A^2+176.21B^2-16.67C^2 \quad (6)$$

$$ZetaPotential=-27.42-0.8A+11.08B+3.45C+8.7AB-0.67AC+2.8BC+4.78A^2+8.2B2-0.73C^2 \quad (7)$$

$$PDI=0.24-0.01A+0.0988B+0.028C+0.042AB-0.057AC+0.026BC-0.012A^2+0.075B^2+0.019C^2 \quad (8)$$

The Z-average was lower with surfactant addition at low cholesterol concentrations due to decreased lipid aggregation because of Tween 80 inclusion. Despite the fact that greater temperature resulted in smaller particle sizes, the temperature effect was not statistically significant.

6.2. Characterization of lipid nanoparticles

6.2.1. Analysis of Z-Average, PDI, and Zeta Potential

The Z-average, PDI, and zeta potential were measured both for optimized PG-loaded uncoated and HA-coated liposomes. (**Table 5**) illustrated the analysis of Z-average (nm), PDI and ZP (mV) of coated and uncoated nanoparticles. All the results met the standard set criteria, as mentioned above. The Z-average range was between 123 ± 2.5 nm and 300 ± 3.3 nm. The particle size of uncoated liposomes was lower, as mentioned in the previous section, than that of coated ones, which showed that the HA coating of liposomes was successful. The PDI was lower for optimized liposomes, which indicated a more uniform vesicle size for the final formulation. The zeta potential of coated liposomes was higher than that of uncoated liposomes, which showed increased stability of coated liposomes.

Table 5. Analysis of particle size, PDI, and zeta potential of uncoated and coated liposomes

Formulations	**Z-Average *(nm)**	**PDI***	**Zeta Potential *(mV)**
Uncoated PG-liposomes	135.2±5.2	0.094±0.001	-29.9±5.8
Coated PG-liposomes	167.9±3.5	0.129±0.002	-33.6±4.5
PG-SLNs	103±46	0.16 ±0.001	-36 ±4.78

6.2.2. Determination of acetone residual in liposomal formulations fabricated via DPM

Since, acetone is a Class 3 solvent, its residual content in the daily dose of the final product should be less than 5000 ppm, according to the ICH Q3C (R5) guideline for residual solvents. Gas chromatography was used to determine the residual acetone content in both coated and uncoated formulations shown in **Table 6**.

Table 6. Concentration of residual organic solvent in the optimized formulations.

Formulations	**Acetone**	**Maximum ResidualLevel* (ppm)**
Uncoated PG-liposomes	442 ppm	5000
Coated PG-liposomes	47 ppm	

*Based on the International Conference for Harmonisation (ICH) Q3C (R5)

Both results were acceptable under the established criteria of maximum allowable residual level, indicating that the DPM can be used to prepare liposomes.

6.2.3. Encapsulation Efficiency, Percentage Yield, and Drug-Loading

The encapsulation efficiency of PG-loaded liposomes was determined to be 90.6±0.47%. The percentage yield was 71.3±1.52%, indicating that the results of PG-loaded liposomes were in accordance with the desired parameters. The liposomes' drug-loading capacity was 61±0.2 %, which could be due to a higher amount of lipid used as the wall-forming agent **(Table 7).** The measured encapsulation efficiency of the optimized formulation was higher, with the objective of having a large amount of the drug at the site of action [32]. Optimized PG-SLNs had an EE of 84±47% and an LC of 60±03 %. The PG-SLNs had a yield of up to 80 ±0.1%.

Table 7. Measurement of Encapsulation Efficiency (%) Loading capacity (%) and % yield

Formulations	**Encapsulation Efficiency (%EE)**	**Loading capacity (%)**	**% yield**
PG-liposomes	81.39±2.6	61±0.2	71.3±1.52
PG-SLNs	84±47	60±0.3	80 ±0.1

6.2.4. Fourier-Transform Infrared Spectroscopy (FTIR)

The FTIR spectra of the components of coated and uncoated liposomes are presented in **Figure 7a**. Compatibility study results showed that there was no interaction between the formulation components. The spectra of coated liposomes showed peaks at ~1650 cm^{-1} (amide I of the α-helical region) and 1050 cm^{-1} (C-O-C stretching vibrations of the α-glucopyranose structure), that could not be observed in the spectra of uncoated liposomes, suggesting that the HA coating was successfully performed. **Figure 7b** shows the FTIR spectrum of PG-SLNs and its constituents.

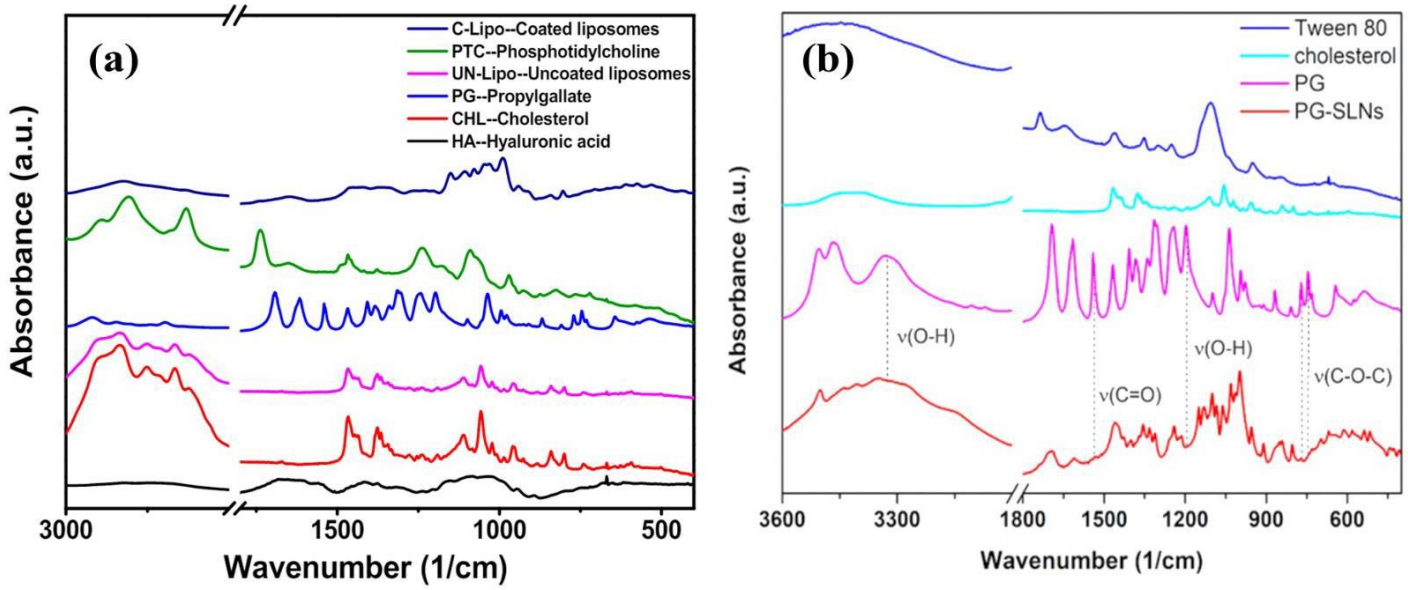

Figure 7. Fourier-transform infrared spectroscopy (FTIR) spectra (a) coated liposomes and components of liposomes (b) PG-SLNs and components of SLNs

6.2.5. Differential Scanning Calorimetry (DSC) analysis results

The thermal behaviour of PG, cholesterol, PC, HA, and liposomes coated and uncoated with HA was investigated with DSC **(Figure 7b**). The endothermic peaks at 150℃ on the DSC curves of PG and cholesterol correspond to their melting points. PC and HA did not exhibit any distinct melting event, possibly due to their non-crystalline nature, while an endothermic peak at 223℃ (PC) and an exothermic peak at 240℃ (HA) was observed due to their degradation pattern. The decomposition of HA can also be observed on the DSC curves of liposomes at 255℃ (uncoated) and 265℃ (coated), but the decomposition of PC as a wall-forming agent was only detected in the case of uncoated liposomes at 213 ℃. HA coating increased the thermal stability of liposomes and prevented them from degradation until 265℃. Since the thermograms of PG-loaded liposomes did not display any endothermic peaks at 150 ℃ compared to the pure PG thermogram, the encapsulation of PG in the liposomes was indicated. And the endothermic peak (**Figure 8b**) at 141°C. (PG-Lipo) and 140 ℃ (PG-LOM-Lipo) can be related to the melting point of PG, while at 88 ℃ (PG-Lipo) and 89 ℃ (PG-LOM-Lipo), related to the melting point of LOM. A slight shift in the melting points to lower temperatures can be observed in comparison to initial substances,

which might be the effect of the lipids.

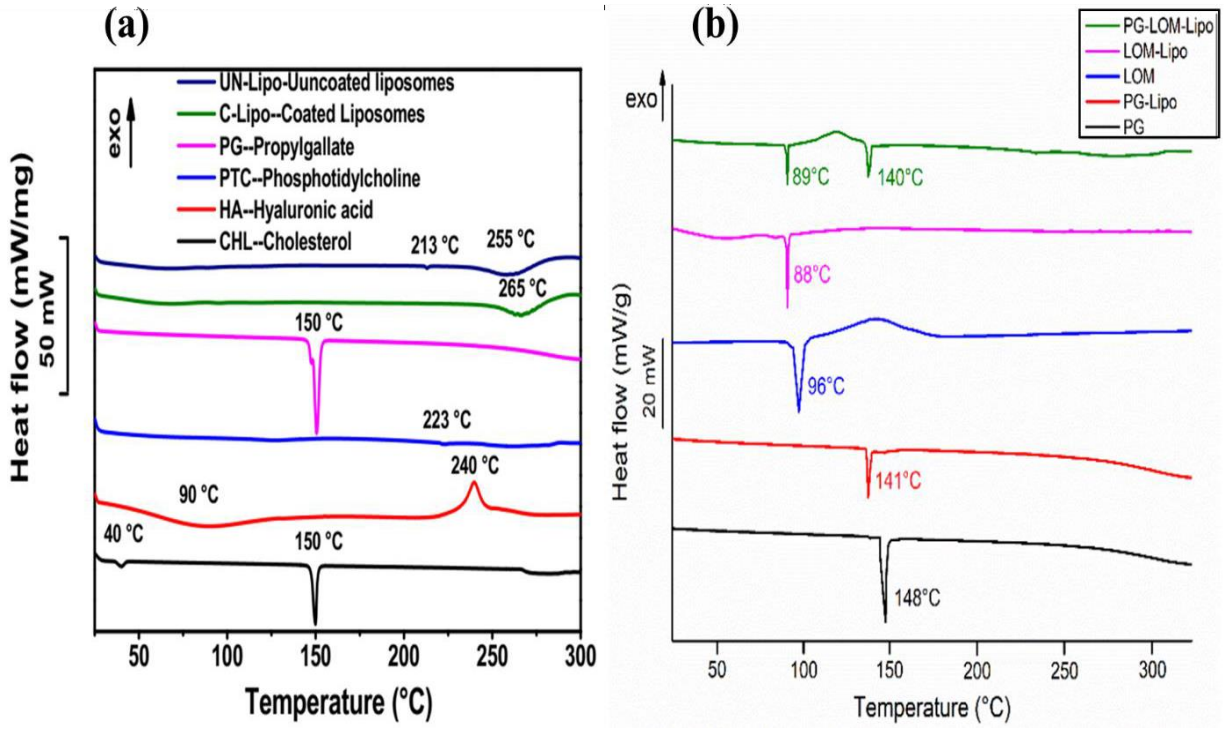

Figure 8. (a) DSC thermogram of coated liposomes and its constituents (b) DSC thermogram of formulations (PG-Lipo, LOM-Lipo and PG-LOM-Lipo) and initial active ingredients (PG and LOM).

6.2.6. X-ray Powder Diffraction (XRPD) analysis results of PG-Lipo and PG-SLNs

XRPD studies showed the crystalline nature of PG and cholesterol and the amorphous nature of PC and HA as coating materials in accordance with the DSC results, as shown in **Figure 5**. In the diffractograms of uncoated and coated liposomes, the characteristic peaks of cholesterol (at 5.18, 13.8, 15.34, 16.6, 17, and 17.6 2θ) as a wall-forming agent can be observed, but in the case of coated liposomes, these peaks disappeared. The characteristic peaks of PG could be detected in the liposomal formulations, which shows that the drug was encapsulated. (**Figure 9a**) results show that the characteristic peaks of PG (4.1, 6.2, 25.8, and 26.4 2 θ) could not be seen in the diffractogram of PG-SLNs, indicating that the crystalline structure of PG has been transformed to amorphous form. XRPD analysis was carried out to support DSC results. The XRPD diffractograms of liposomal formulations and initial compounds are presented in **Figure 9b**. XRPD diffractograms of liposomal pellets supported DSC results. Characteristic peaks related to PG and LOM were present in the liposomal formulations, which supported the crystalline existence of both drugs in the liposomal formulation.

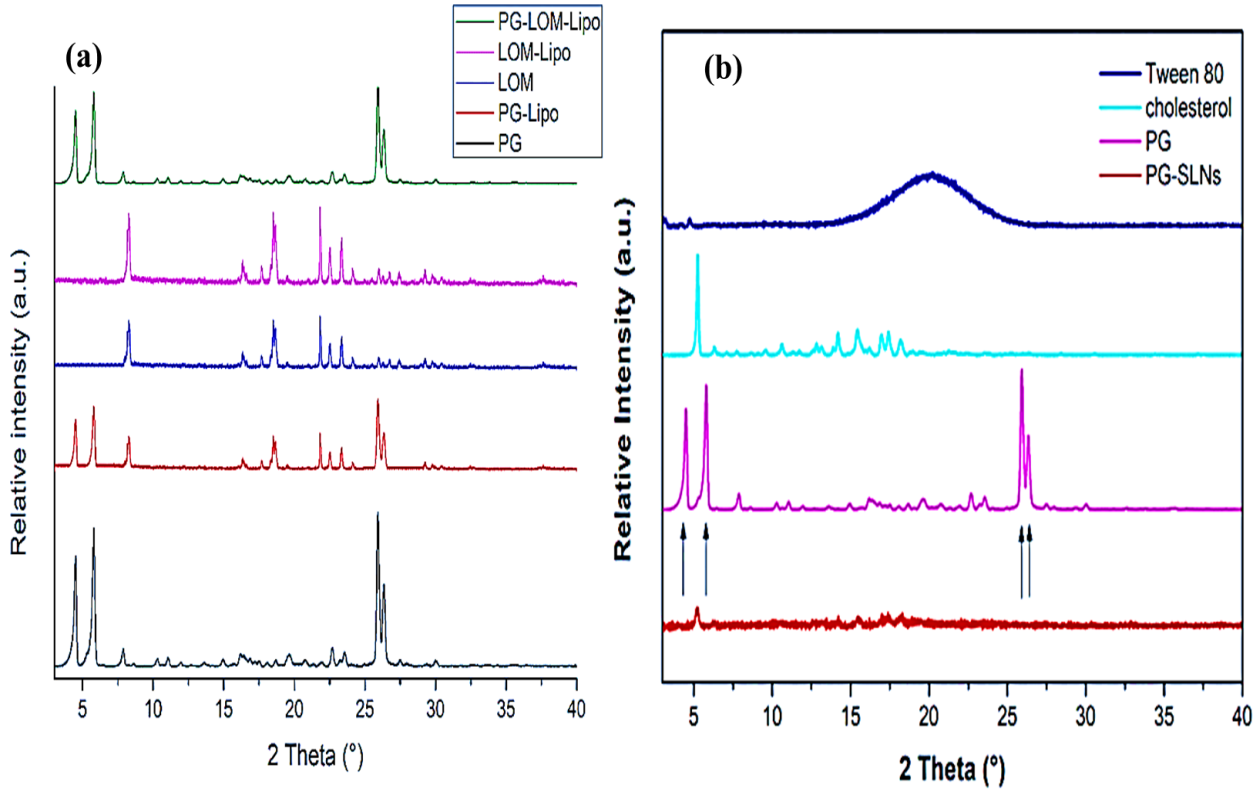

Figure 9. XRPD diffractogram (**a**) XRPD diffractograms of liposomal formulations and its constituents (**b**) XRPD diffractograms of PG-SLNs formulation and its constituents

6.2.7. Morphology of liposomes and PG-SLNs

The transmission electron microscopy (TEM) images of PG-loaded liposomes with coating and without coating showed the spherical shape and uniform distribution of liposomes, as shown in **Figure 10**, showing a mono-disperse distribution without any aggregation. The TEM images revealed that particle sizes were ~100–120 nm. The results of TEM images were comparable with the dynamic light scattering (DLS) results and were within the nano-range.

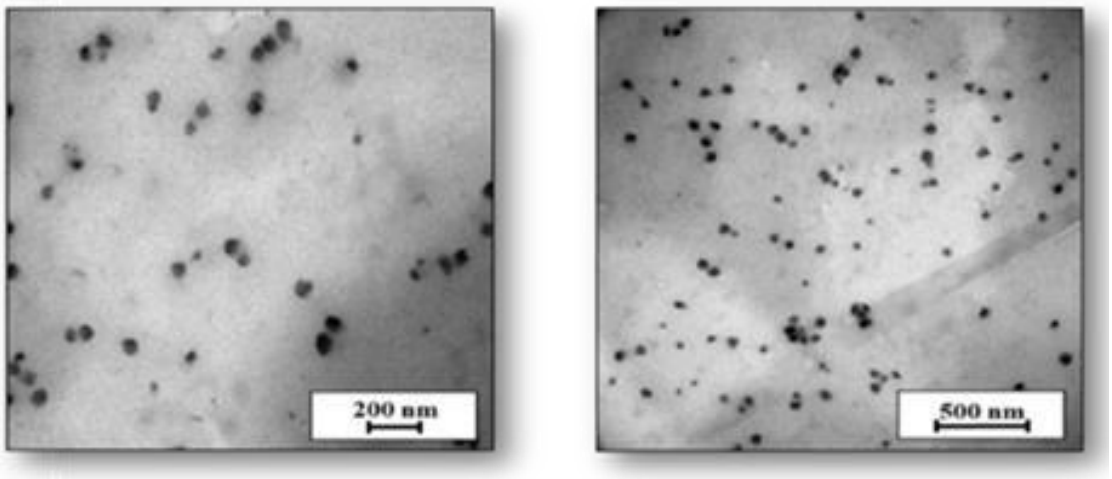

Figure 10. Transmission electron microscopy (TEM) images of liposomes at different resolution scales

SEM images of lyophilized PG-SLNs, shown in **Figure 11**, also proves that the nanoparticles have spherical morphology and are homogenous distribution.

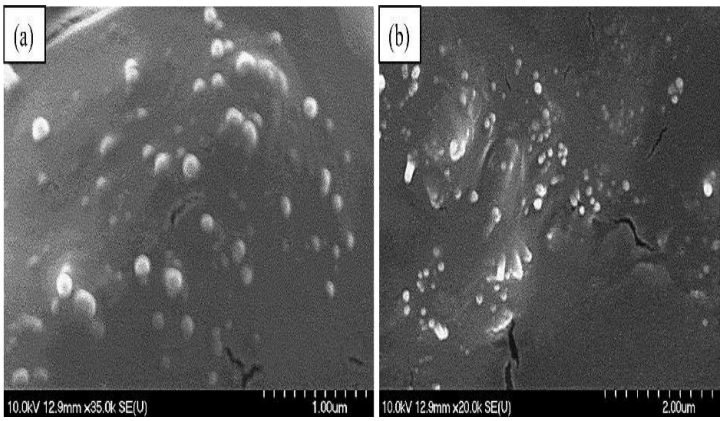

Figure 11. SEM images of optimized lyophilized PG-SLNs (a,b)

6.3. Results of *In Vitro* characterizations of PG-Lipo and PG-SLNs

6.3.1. *In Vitro* release study of PG-Lipo

In vitro release study of uncoated and HA-coated liposomes showed 75% and 60% drug release within 24 h, respectively, in simulated nasal electrolyte solution (SNES) (pH 5.6), as shown in Figure 12a, while80% of the drug was released within 48 h from coated liposomes. The release of PG from solution was significantly lower (10% within 24 h) in comparison to other liposomal formulations. Drug release kinetics was determined by fitting kinetic models, and data were evaluated by the correlation coefficient (R^2). In the case of uncoated and HA-coated liposomes, the R^2 obtained for fitting the release data of PG to the Higuchi model indicated that drug release from the liposomes was diffusion controlled, as shown in Table 7. *In vitro* release study results have shown that the slower release from coated liposomes is due to the restriction of water diffusion into the carrier matrix, which subsequently slows down the drug release rate. Another possible reason is that coating adds a barrier against drug diffusion with regard to the electrostatic interaction between the positively charged PC and the negatively charged HA [33].

Table 7. R^2 values of drug release from uncoated and HA-coated liposomes

Kinetic Model	Zero Order	First Order	Korsmeyer-Peppas	Higuchi	Hixon-Crowel
R^2 Value of uncoated liposomes	0.7211	0.8922	0.8656	0.9238	0.8691
R^2 value of coated liposomes	0.745	0.8935	0.8662	0.9073	0.8448

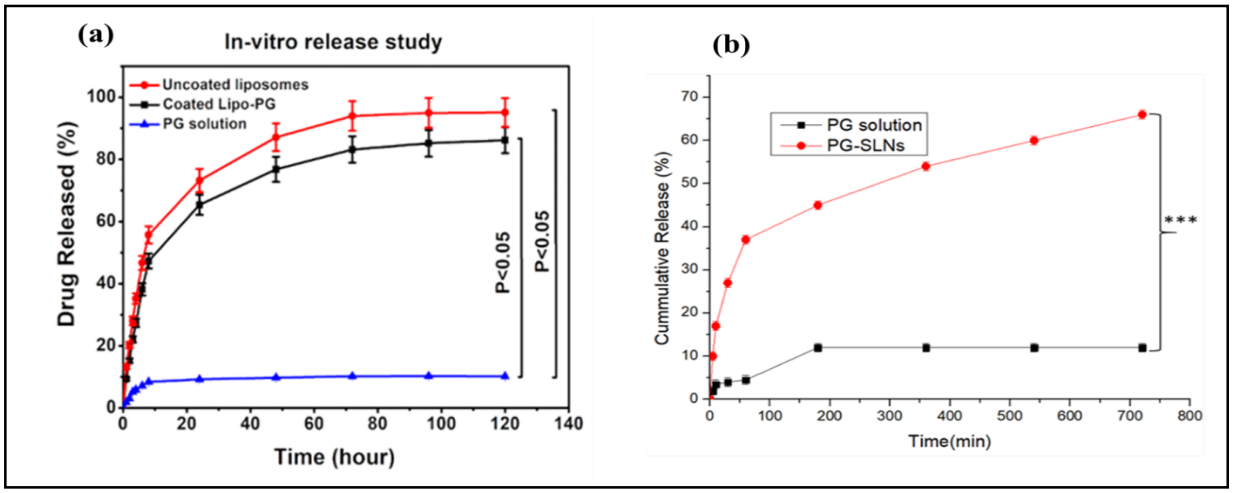

Figure 12. *In vitro* release study of PG in phosphate buffer (pH 5.6) (**a**) and *in vitro* release studies of uncoated liposomes, coated liposomes, and PG solution (**b**) PG-SLNs and PG solution

7.1.1. *In Vitro* release study of PG-SLNs

At pH 5.6, *in vitro* release experiments of PG-SLNs revealed burst drug release (40 % of drug) in the first 60 min. Following that, the drug release rate decreased as a result of a constant release rate as shown in Figure 12b. PG-SLNs drug release followed Higuchi kinetics (R^2 = 0.96), which can be attributed to the lipid matrix's drug release controlling mechanism in the simulated nasal media [39].

7.1.2. *In Vitro* permeability study of PG-Lipo

The modified side-bi-side apparatus was used for the *in vitro* nasal permeation study of uncoated and coated PG-loaded liposomes and the PG solution. **Figure 13a** shows the rate of PG permeation from the donor to the acceptor phase. The maximum permeation of PG from coated liposomes was 420 µg/cm^2 after 60 min. The PG-containing uncoated liposomes provided faster diffusion and higher drug concentration (>500 µg/cm^2 after 60 min) in comparison to the PG solution. In case of the PG solution, permeation was negligible, about 5 µg/cm^2. However, when compared with coated liposomes, there was a difference of 80 µg/cm^2 among the permeation values. A slightly lower permeation rate of coated liposomes was observed due to the muco-adhesive nature of HA, which helps to increase the residence time of the coated formulation on the mucosa and protect it from premature muco-cililary clearance. The *in vitro* permeation of the PG-containing coated liposomes provided faster diffusion and higher drug concentration comparatively.

7.1.3. *In Vitro* permeation of PG-SLNs

The *in vitro* nasal permeation investigation used a modified Side-bi-Side® equipment to examine the diffusion of PG solution, PG-SLNs [31, 36–38]. **Figure 13b** illustrates the cumulative PG penetration from the donor to acceptor phase through an isopropyl myristate-impregnated synthetic cellulose membrane. After 60 min, the cumulative permeation of PG from PG-SLNs was 190 µg/cm^2.

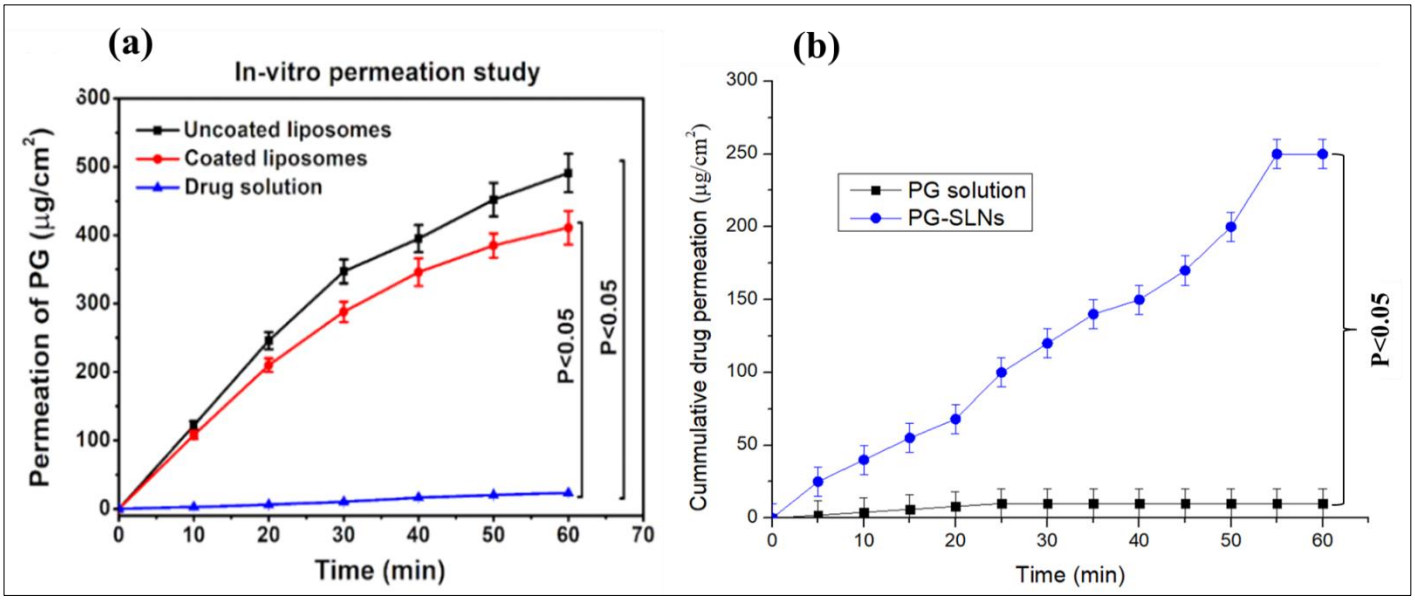

Figure 13. (**a**) *In vitro* permeation of pure PG solution, uncoated liposomes, coated liposomes (**b**). PG solution, PG-SLNs Data are means ± SD (*n* = 3 independent measurements).

7.1.4. Anti-Oxidant activity measurement with Hydrogen peroxide (H_2O_2)

Coated and uncoated liposomes containing PG in different concentrations were screened for *in vitro* scavenging activity using hydrogen peroxide. The scavenging activity of the formulations and the initial PG solution (as a control) are presented in (**Figure 14a**). It was revealed that the liposomal formulations preserved the antioxidant activity of PG based on the scavenging activity measurement against H_2O_2. The hydrogen-donating activity, was measured using hydrogen peroxide radicals as the hydrogen acceptor, demonstrated a strong association between the concentration of PG and the rate of inhibition. With increase in concentration of PG the inhibition was enhanced. At a low concentration of 125 µg/mL, no significant difference in the antioxidant activity was observed for both PG liposomes and the initial PG solution. In case of higher PG concentrations (250 and 500 µg/mL), a significantly improved antioxidant activity of both coated and uncoated liposomes was reached, which can be explained by the stabilizing effect of the liposome carrier at a 95% confidence interval. The scavenging capacity of PG-SLNs and PG solution was also studied. (**Figure 14b**). The antioxidant activity of PG against H_2O_2 was increased by increasing the PG concentration.

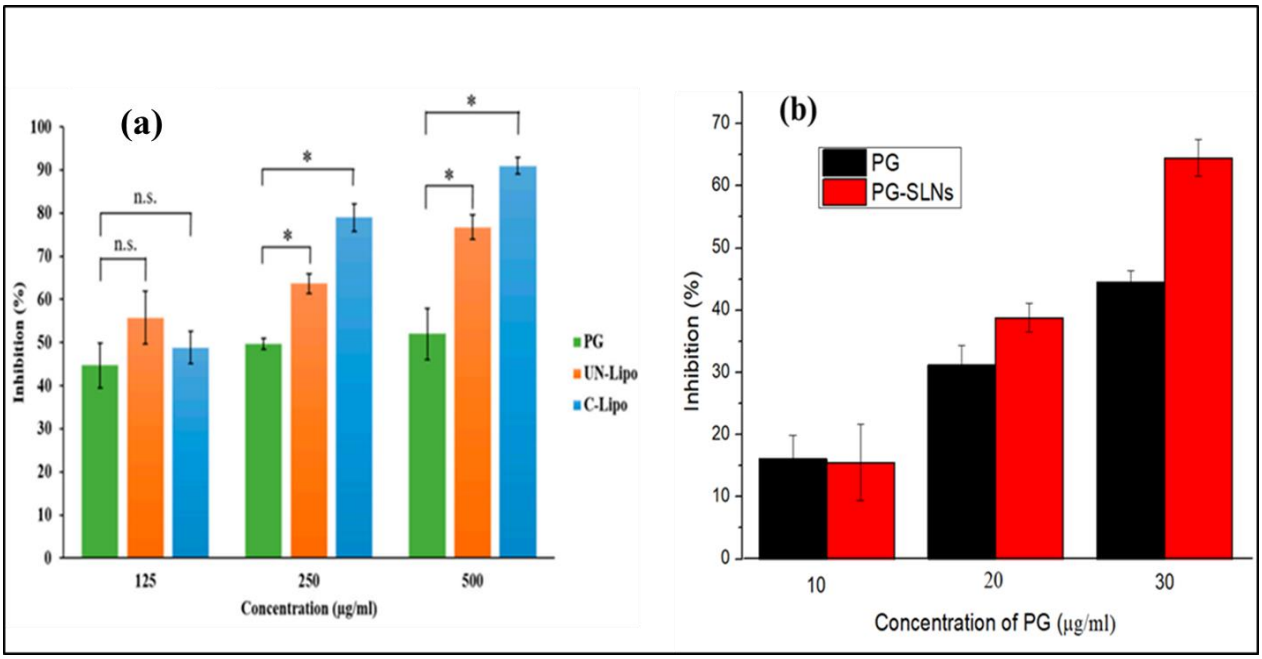

Figure 14. (a) Percentage inhibition of hydrogen-peroxide-scavenging activity of different concentrations of PG-containing coated and uncoated liposomes. **(b)** Percentage inhibition of the hydrogen-peroxide-scavenging activity of different concentrations of PG-containing SLNs Statistical analysis: t-test. *p<0.05; n.s. means not significant compared to the PG control.

6.4. Optimization and characterization of stable co-encapsulated lipid nano-formulation

Based on the preliminary study results the liposomal formulation was selected and screened for further characterization studies because of its greater stability in comparison to SLNs when co-encapsulated with PG and LOM.

6.4.1. Optimization of PG-LOM liposomes

The effect of different weight ratio of CHL and PHC were investigated on Z-average, PDI and zeta potential (ZP) as shown in **Figure 15**. The particle size of intranasal administered nanoparticles is required to be reduced as low as possible, to ensure adequate absorption of the encapsulated drug. The Z-average of CHL: PCL 1.33 was found significantly lower in comparison to other investigated compositions, the only exception was detected in case of CHL: PCL 6. From this point of view these two composition seemed to be optimal. However, while investigating the PDI it is clearly shown CHL: PCL 6 has significantly higher PDI, which predicts hetero-disperse particle size distribution, therefore uncertain absorption properties and physical stability. The third important parameter for defining the optimal composition was the ZP. From stability point of view the higher the absolute value of ZP, higher the chance to avoid aggregation of nanoparticles as a result of repulsion forces. However, as the mucosal membrane is also negatively charged, the absorption of highly negatively charged nanoparticles may be hindered. This fact also supports the selection of CHL: PCL 1.33 as optimal composition, showing the least negative surface charge (-31 ± 2.9

mV), which indicates minimal electrostatic repulsion with mucosal membrane, therefore improved nasal absorption. CHL: PCL 1.33 also resulted in one of the lowest Z-average (118 ± 6.3 nm) and narrow PDI (0.13 ± 0.014).

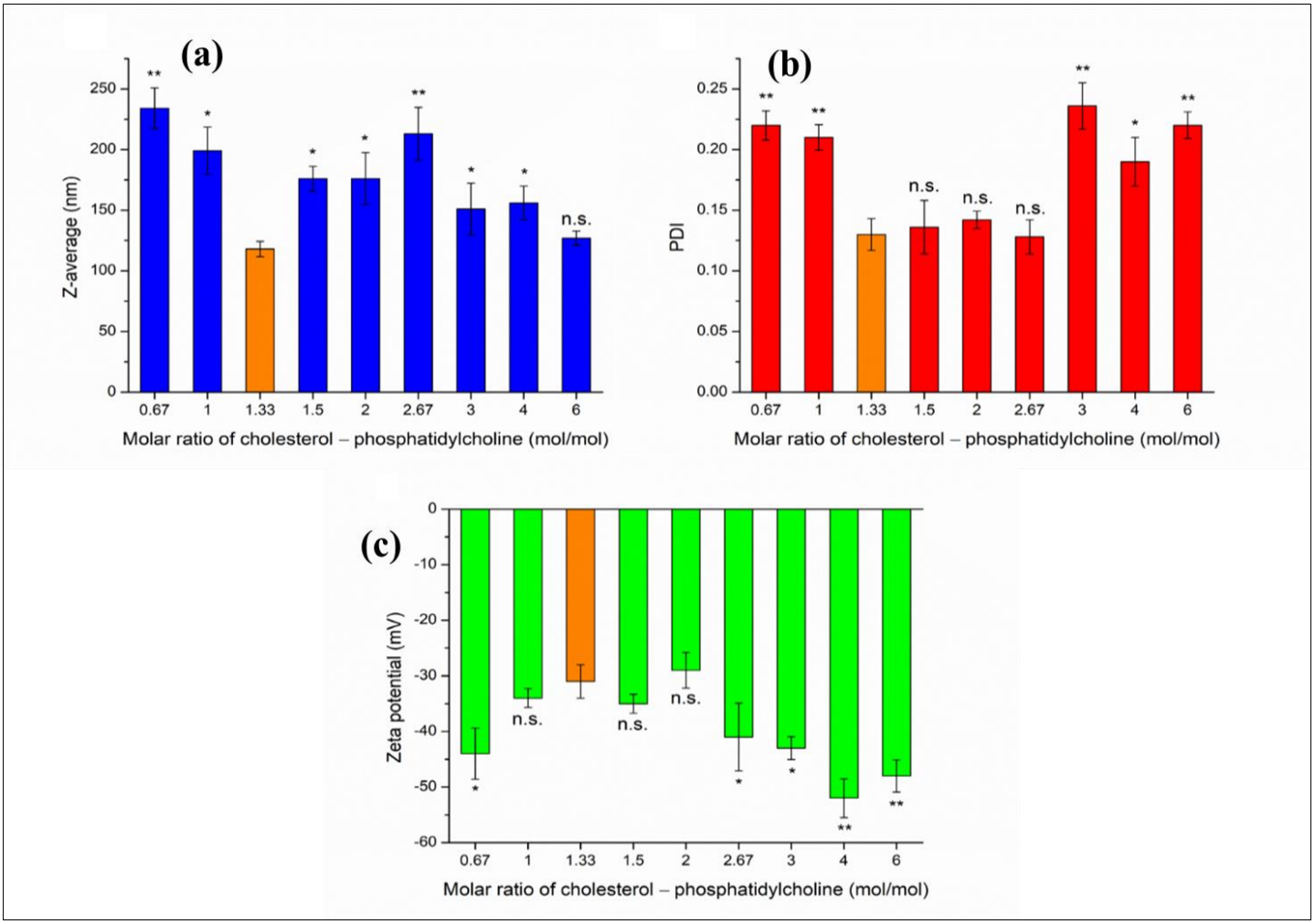

Figure 15. Effect of different molar ratio of cholesterol and phosphatidylcholine (CHL: PCL) for cholesterol on Z-average (A), polydispersity index (B) and zeta potential (C). ANOVA test was performed to check the significance of the differences between CHL: PCL 1.3 and other compositions, * $p < 0.05$; ** $p < 0.01$; n.s. indicates no significant differences. Measurements were carried out in triplicate (n = 3 independent formulations), and data are represented as means ± SD.

After selecting the optimal phospholipid composition of liposomal carrier (CHL: PCL 1.33) drug-loading in different mass ratio was performed. To reach out the optimal PG-LOM composition, the effect of different drug ratio on nano-particulate characteristics, as Z-average, PDI, zeta potential and EE was evaluated (**Figure 16**).

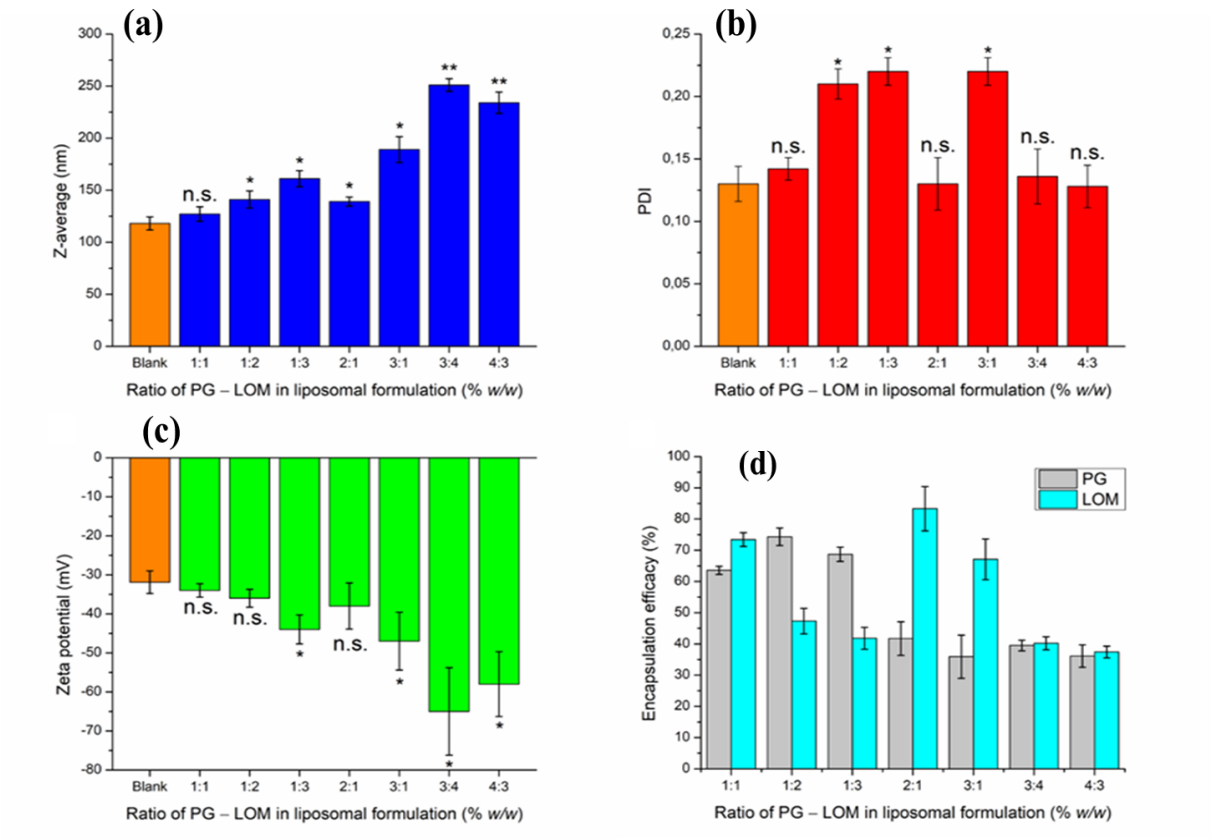

Figure 16. Effect of different PG-LOM ratio on Z-average (A), polydispersity index (B), zeta potential (C) and encapsulation efficacy (D) of optimized liposomal carrier. ANOVA test was performed to check the significance of the differences between optimized blank liposome and drug-loaded formulation. * $p < 0.05$; ** $p < 0.01$; n.s. indicates no significant differences. Measurements were carried out in triplicate (n = 3 independent formulations), and data are represented as means ± SD.

Both PG and LOM tends to encapsulate both inside the phospholipid bilayer and in crystalline form in the vesicle of liposome, because of their lipophilic nature, this fact is also supported with the slight increase in Z-average, while increasing the amount of drugs in the formulation. Based on the Z-average values, the applied drug concentrations should be minimized to avoid significant deviation in vesicle size of liposomal formulation. The PDI values showed no significant difference, at higher drug concentrations similarly narrow PDI was observed as in case of blank carrier. The ZP values were proportional with the increase of drug concentrations, indicating inhibition of aggregation due to electrostatic repulsion. However, increased ZP has negative effect on the absorption ability through the electrostatic interaction with negatively charged mucosal membrane. The EE data showed appropriate results in case of PG-LOM 1:1 ratio, in case of other compositions the EE of one of the drug component was not optimum. All in all, it has been revealed the application of PG-LOM in 1:1 ratio showed no significant effect on nanoparticle characteristics in comparison to blank liposomal carrier, therefore this mass ratio was selected for further characterization.

The obtained Z-average (127 ± 6.9 nm), PDI (0.142 ± 0.009) ZP (-34 ± 1.7 mV), and high EE (59.87 ± 0.9% of PG and 71.78 ± 1.5% of LOM, respectively) in case of both drugs were suitable for acceptance criteria of nose-to-brain transport. Based on these results, the optimized co-encapsulated formulation (PG-LOM-Lipo) contained both PG and LOM in 2-2 mg/mL after re-dispersion the pellet in 10 mL purified water, which was appliedfor further characterizations. As comparison single drug-loaded liposomes, PG-Lipo and LOM-Lipo (containing 2-2 mg/mL of PG and LOM, respectively) were also prepared and characterized. The EE, LC and DC of the optimized and control formulations were determined and compared to each other (**Table 8**). Each composition resulted in high EE, LC and DC, which estimates encapsulated drug can be found both in the membrane and vesicle of liposome, indicating controlled drug release from the liposomes mediated by small lipid-drug aggregates or assemblies formed due to the lipophilic nature of drugs. The combined formulation (PG-LOM-Lipo) showed reduced EE and LC in comparison to corresponding single component-loaded liposomes, which can be claimed with the stearic hindrance caused by the presence of two drug molecules. However, the relative value of EE and LC of both PG and LOM in PG-LOM-Lipo is quite similar, this effect can probably be explained primarily by the almost same molecular weight of two compounds.

Table 8. Effect of drug components on encapsulation efficacy (EE), loading capacity (LC) and drug content (DC)

Liposomal formulation	EE_{PG} (%)	EE_{LOM} (%)	LC_{PG} (%)	LC_{LOM} (%)	DC_{PG} (%)	DC_{LOM} (%)
PG-Lipo	81.39 ± 2.6	—	19.46 ± 1.1	—	98.56±0.5	—
LOM-Lipo	—	87.22 ± 3.1	—	28.65 ± 1.9	—	97.47±1.6
PG-LOM-Lipo	59.87 ± 0.9	71.78 ± 1.5	12.91 ± 1.8	17.11 ± 2.1	96.24±2.2	96.71±2.9

* Data is presented as mean ± SD (n = 3 independent formulations)

6.5. Comparative *In Vitro* and *Ex Vivo* studies of stable co-encapsulated liposomal formulations

6.5.1. *In Vitro* release study of compared formulation (LOM-Lipo, PG-Lipo, LOM-PG Lipo)

Drug release kinetic of liposomal formulations is a crucial part of the rational design, predicting the subsequent characteristics of drug delivery system after administration. The *in vitro* release profile reveals important information on the structure and behaviour of the formulation, possible interactions between the drug and lipid composition, and their influence on the rate and mechanism of drug release. The dialysis-based release method is a well-established and useful technique to study *in vitro* release from nano-

particulate delivery systems. Applying a dialysis bag with 8 kDa cutoff ensures the physical separation of liposomal formulation and suspended particles of initial suspension from the release medium and allows only the passive diffusion of free LOM and PG. The time-dependent in vitro release profiles of LOM- and PG-loaded liposomes were determined with HPLC (**Figure17**) [39].

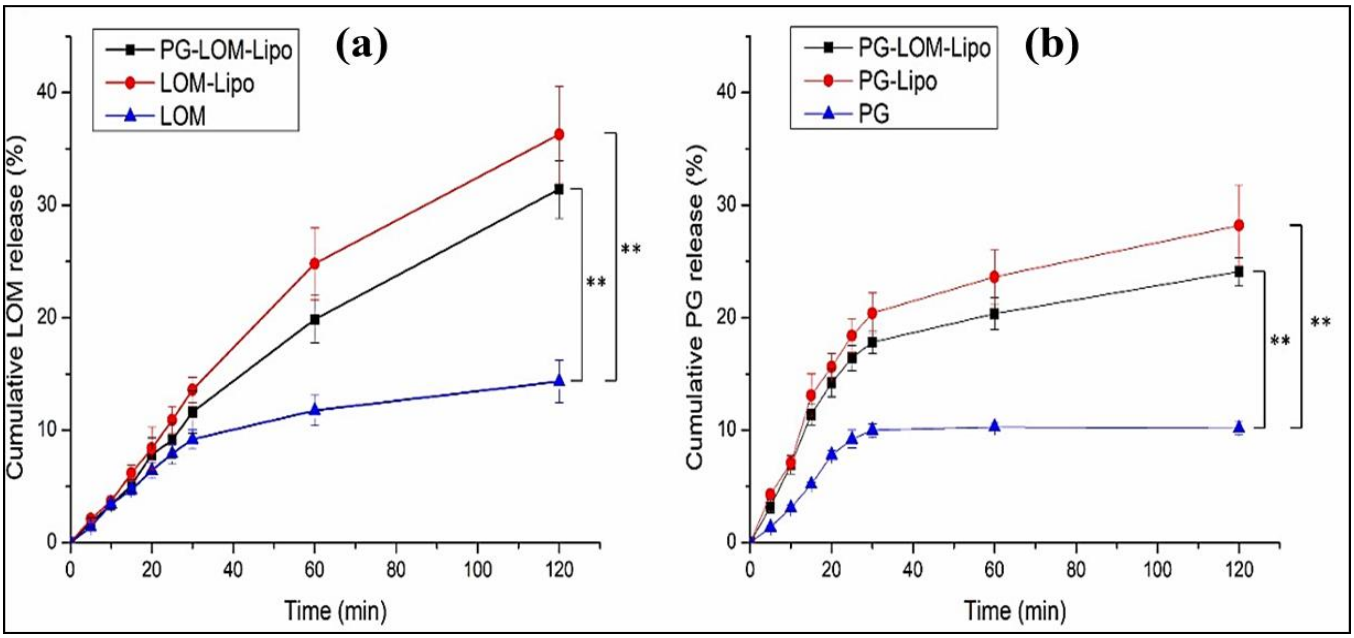

Figure 17. Cumulative drug release of LOM- (A) and PG-containing (B) formulations (A) in comparison to initial LOM and PG suspension. ANOVA test was performed to check the significance of the differences between liposomal formulations and initial drug suspension,** $p < 0.01$. Measurements were performed in triplicate (n = 3 independent formulations), and data are represented as means ± SD.

The drug release profile of reference LOM and PG suspension shows only a slight increase, however in case of liposomal formulations significantly increased (~3-fold) drug release was observed compared to both LOM and PG (**, p <0.01), which can be claimed with the nano size and increased specific surface area of liposomal carrier.

LOM release from PG-LOM-Lipo (R^2 =0.9971) and LOM-Lipo (R^2 =0.9968) followed Hixson-Crowell kinetic, as well as PG release from PG-LOM-Lipo (R^2 =0.994) and PG-Lipo (R^2 =0.9947), which is presumably the result of specific surface area and Z-average decrease due to the effect of ion strength in SNES and drug diffusion from liposomes.

6.5.2. *Ex Vivo* permeation studies

Modified Side-bi-Side® diffusion cell was used for the *in vitro* nasal permeation study, whereas the diffusion of PG-Lipo, LOM-Lipo, PG-LOM-Lipo, PG solution and LOM solution through rabbit nasal mucosa was compared. **Figure 18A** shows the cumulative LOM permeation, while **Figure 18B** the cumulative PG permeation from donor to acceptor phase through the isolated nasal mucosa. Both in case of LOM and PG loaded liposomes the permeation was significantly higher in comparison to solutions. Comparing the liposomal carriers, no significant difference of cumulative permeation of LOM was

achieved between LOM-Lipo and LOM-PG Lipo, however in case of PG the permeation was significantly lower from co-encapsulated liposome, which can be claimed with the increase vesicle size.

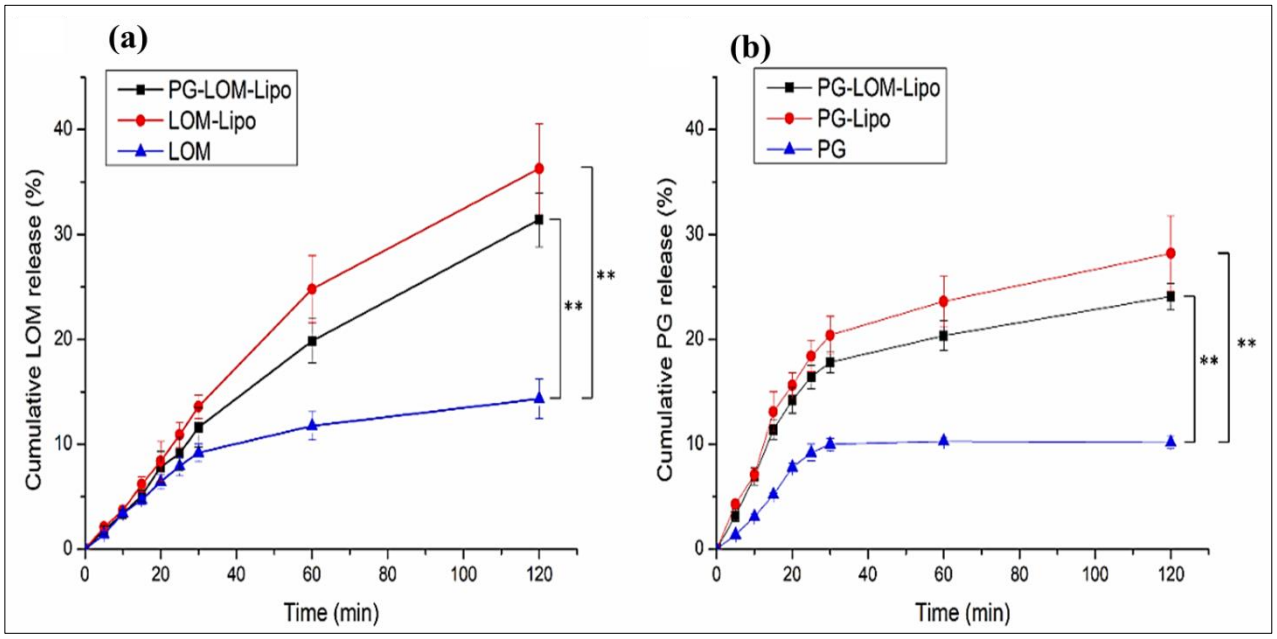

Figure 18. *Ex vivo* nasal permeability study of LOM-containing (A) and PG-containing (B) liposomal formulations in comparison to solutions.

6.5.3. *In Vitro* cell line studies (anti-proliferative assay results)

IC_{50} values of the tested formulations and their 95% confidence intervals (CI) was calculated. LOM Lipo, PG Lipo, LOM-PG Lipo formulations were tested on murine fibroblast cells and human glioblastoma cell lines (U87) for the anti-proliferative effects with MTT assay (**Table 9**). The cells were examined in 96-well plates in water-based culture media. LOM showed the highest anti-proliferative activity in DMSO solvent, however the liposome incorporated anticancer drug did not show significant anti-proliferative effect alone.

Table 9. IC50 values of the tested formulations LOM, PG, PG-LOM (DMSO), LOMLipo, PG Lipo, LOM-PG Lipo

Compounds	**IC50 values (µM) [95% CI]**		
	NIH	**U87**	**A2780**
LOM (DMSO)	264.80 [220.3-318.3]	35.09 [31.02-39.69]	41.88 [35.74-49.09]
PG (DMSO)	29.14 [25.10-33.83]	59.42 [51.67-68.32]	14.64 [12.97-16.53]
LOM (Liposomes 10 mg/5 ml)	>500	>500	>100

LOM (Liposomes 10 mg/10 ml)	>500	>500	>100
PG (Liposome)	62.93 [56.83]	275.3 [246.8-307.2]	49.00 [44.24-54.27]
LOM-PG-Liposome	140.20 [125.30-156.80]	217.60 [190.60-248.40]	70.45 [63.55-78.10]

The anti-oxidant PG can contribute to the anti-cancer effects of the cytotoxic agent by exerting anti-proliferative action in itself. It is a potent cytotoxic and anti-cancer compound. In the given experimental environment, PG-liposomes show IC50 value at greater concentration on NIH-3T3 in comparison to PG DMSO solution. Therefore, the PG is more cytotoxic in pure form instead when encapsulated into liposomes. Similarly, the LOM-PG Lipo showed cytotoxic effect at higher concentration in comparison to LOM, PG solution. The PG-LOM Lipo and PG Lipo showed highest anti-proliferative effect in U87 glioma lines. PG-loaded liposomes showed highest anti-proliferative effect in comparison to other liposomesloaded formulations. In anti-proliferative assay of PG-LOM Lipo showed potent anti-proliferative activity in comparison to other formulations on U87 glioma cell lines. As the, dose of PG and LOM was half when use in combination in comparison to PG-Lipo and LOM-Lipo alone. The Table 13 shows IC50 values of the tested formulation.

6.5.4. *Ex Vivo* Raman mapping

In order to investigate the passive trans-mucosal uptake of liposomal formulations Raman mapping was applied. Isolated rabbit mucosa was treated with PG-Lipo, LOM-Lipo, PG-LOM-Lipo, PG solution and LOM solution, and the penetration depth was analysed and compared with non-treated nasal mucosa specimen using Raman correlation mapping (**Figure 19**).

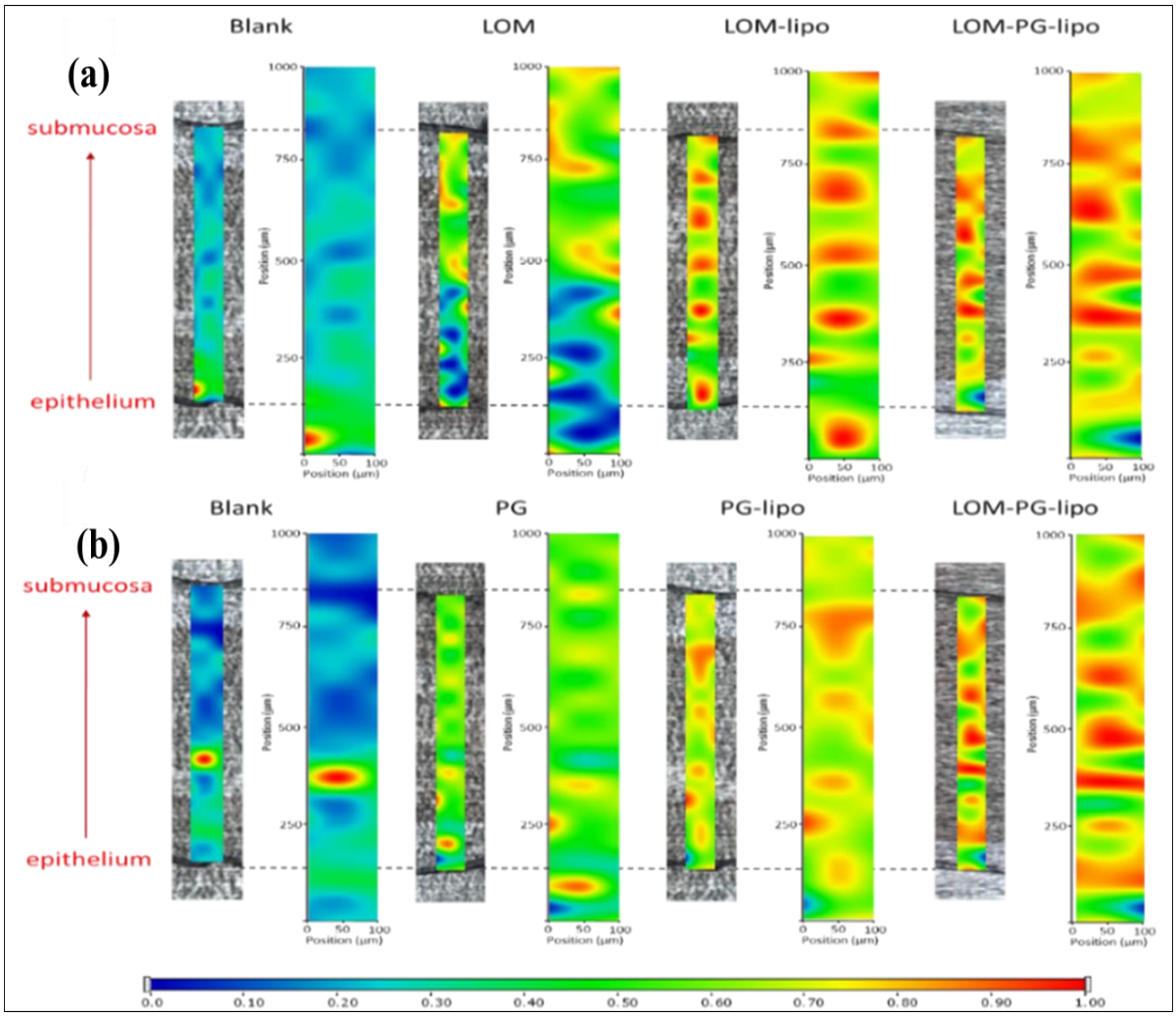

Figure 19. Raman correlation maps of the distribution of LOM (A) and PG (B) in the rabbit nasal mucosa compared to the non-treated nasal mucosa specimen.

The mucosal distribution correlation maps show a remarkable Raman intensity on the top of the nasal mucosa specimens in both cases (non-treated, treated), which can correspond to the high protein content of the epithelial layer. **Figure 19** shows the Raman maps of treated and non-treated mucosa profiling the individual spectrum of both LOM (**Figure 19A**) and PG (**Figure 19B**). The intensity changes of Raman maps clearly indicate that both LOM and PG can penetrate from solution through the nasal mucosa but with less extent in comparison to encapsulated liposomes. Results were consistent with the *ex vivo* diffusion studies. Based on these results, the improved penetration of both LOM and PG through the nasal mucosa can be increased by using liposomal carrier.

6.5.5. Cellular uptake of propidium-iodide labelled liposomes

As PI is not membrane permeable, therefore it is a good marker for investigating cellular uptake. By loading PI as cargo in the liposomal carrier the endocytosis of liposomes can be visualized. **Figure 20** shows the fluorescent microscopic results of U87 and U251 cells treated with PI-loaded liposomes (PI-Lipo) for 24 h.

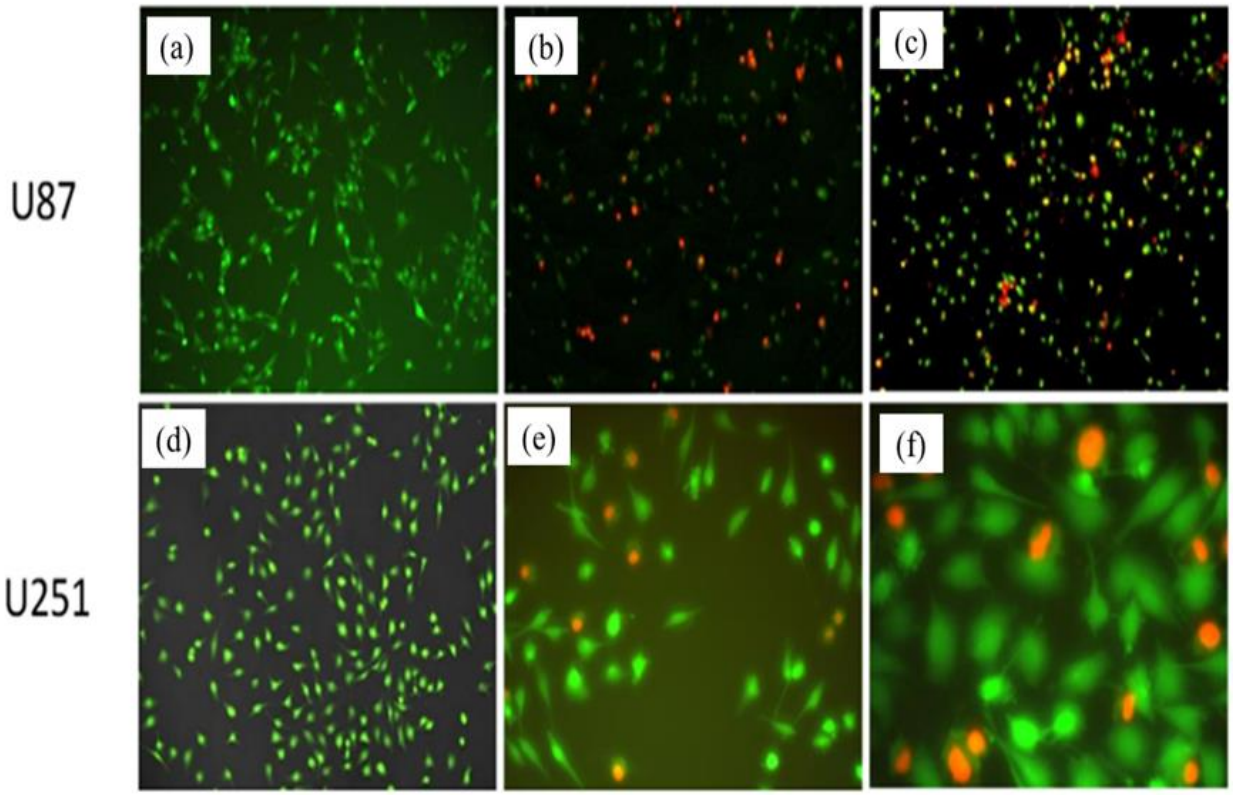

Figure 20. Fluorescence imaging of PI-Lipo cellular uptake on U87 (b and c) at 10×magnification and U251 cell line at 20× (e) and at 40×magnification (f) compared to control group of U87 (a) and U251 (b) after 24 h incubation.

On both U87 and the more resistant U251 cell lines successful uptake of liposomes can be detected, as indicating the red fluorescence inside the cells. These results support the evidence that the drug tends to enter the tumor cells and its release takes place within the cell.

7. CONCLUSIONS

The DPM as a novel liposome preparation method has not been previously applied for the preparation of liposomes. As a gentle formulation method, it is suitable for loading anti-oxidants into liposomes, preserving their stability. Regulatory authorities suggested the application of the QbD approach for designing an optimized product suitable for intranasal delivery. The study helped in the preparation of coated liposomes, and PG was used as the model compound that has proven anti-cancer efficacy. PG-SLNs were successfully prepared using a modified injection method. Following the QbD approach for the optimization of formulation and process parameters affecting the quality of the nano-system, the initial risk assessment study and the design of experiment were applied. Our optimized platform provided in vitro proof of the potential of combining the advantages of lipid-based NPs with PG as a promising intranasal delivery system. The stability of liposomal formulation was greater than the stability of PG-SLNs. Therefore, the liposomal formulation was further applied for combination therapy. Moreover, there was no significant differences was measured in the efficacy and stability of HA-coated and uncoated liposomes. Therefore, we only applied uncoated liposomes for further ex-vivo and in vitro cell line investigation. PG and LOM co-encapsulated liposomes were compared against PG-Lipo, LOM-Lipo. The optimized formulation of PG-LOM Lipo has Z-average of (172±2.5 nm), PDI (0.149±0.002), ZP (-36.6±4.5 mV). The physicochemical characterization studies showed no interaction between the components of formulation and the final formulation. The *in vitro* cell line study show highest efficacy of formulation loaded with PG-LOM Lipo on U87 glioma cells. *Ex vivo* permeation studies showed good results and greater permeation on rabbit nasal mucosa cells for all three compared formulations. The PG-LOM combination showed greater permeation via nasal mucosa cell. The Raman mapping indicated that both components of formulation can penetrate via the nasal mucosa. The both *ex vivo* and permeation study results are consistent with each other These all study findings justify the application of co-encapsulated PG-LOM liposomes as a potential carrier system to deliver anti-glioblastoma drugs via intranasal route. Uptake study results supports that liposomes carrier system is suitable to enter the tumor cells via endocytosis and the drug will be released inside the tumor cells (U251, U87).

8. NOVELTY of STUDY

The conventional techniques for liposome development and size reduction are convenient to use with sophisticated equipment. However, problems related to scale-up and scale-down applications have encouraged improvements to conventional processes that led to the development of novel methods for liposome development. Applying the novel DPM avoids the use of any additional size reduction or extrusion technique, which makes the preparation process more feasible and precise and less time consuming. Moreover, this method also provides a greater percentage yield of liposomes. The authors recommend this technique for industrial scale-up for more optimum preparation of liposomes. There is no data regarding the encapsulation of PG into nanoparticles. As PG is a water-insoluble compound, loading it into a nano-carrier can enhance its water solubility and drug release profile via different administration routes. The present study also focused on the formulation of PG-SLNs. The novelty of our work lies in the fact that our research team explored the first-time application of the PG-lipid nanoparticles for intranasal delivery route. The combination therapy of LOM is very much in use due to its dose related toxicity issues. We used the novel combination of PG-LOM that was not prescribed before in literature to treat glioma. The applicability of a LOM and PG in a nasal formulation is a novel approach in pharmaceutical technology, therefore limited data for such systems are available up until now. This novel combination of PG and LOM, should take advantage of each compound's strengths and limitations to improve efficacy, and overcome drug resistance. Through our study we provide the documented prove of increase efficacy and anti-proliferative efficacy of LOM-PG combination on cancer cell lines. Our cell line study results of LOM-PG showed increased efficacy in ovarian-carcinoma cell lines. This potent combination can prove very useful in near future to treat several type of cancers. As we found enhanced anti-proliferative efficacy of LOM-PG at very low concentration. Based on our preliminary study results at various type of cancer cell lines we suggested this novel combination for cancer targeting in future along-with other chemotherapeutics.

ACKNOWLEDGEMENTS

I would like to express my deepest gratitude to the head of the department and to my supervisor **Professor Dr. Ildikó Csóka** for her support and advice during the preparation of this project. And also for giving me an opportunity to pursue my Ph.D under her supervision. I would like to acknowledge **Dr. Rita Ambrus, Professor Dr. Piroska Szabó-Révész** and my colleagues **Dr. Gábor Katona, Dr. Ruba Ismail** for helping me and guiding me throughout my Ph.D project. I would like to thank **Professor Dr. István Zupkó** and **Dr. Zsuzsanna Schelz** for sharing their knowledge regarding cancer cell line study, and for the successful collaboration, and guidance. I would also like to thank the laboratory technicians, particularly, **Piroska Lakatosné** and **Erika Feczkóné** for their care and help that made the hard things easier. Then I would like to thank all my colleagues **(Dr. Dorina G. Dobó, Dr. Edina Pallagi)** and friends (especially **Dr. Yousif Ibrahim, Dr. Bence Sipos and Dr. Abbas Rahdar, Dr. Maimoona Qindeel, Dr. Tamás Kiss)** for their scientific support. My last words are dedicated to my family. Thanks for your support and encouragement during these years. I know how hard it was to be away, but you have been with me during all the moments of sadness and joy.

FINANCIAL SUPPORT

I would to acknowledge the financial support of the Stipendium Hungaricum Programme, Ministry of Human Capacities, and Hungary, grant number **(Grant TKP-2020)** by the National Research, Development and Innovation Office, **Hungary GINOP-2.3.2-15-2016-00060**.

REFERENCES

1. Hanif, F., et al., *Glioblastoma Multiforme: A Review of its Epidemiology and Pathogenesis through Clinical Presentation and Treatment.* Asian Pacific journal of cancer prevention : APJCP, 2017. **18**(1): p. 3-9.
2. De Vleeschouwer, S. and G. Bergers, *Glioblastoma: to target the tumor cell or the microenvironment?* Exon Publications, 2017: p. 315-340.
3. Musalea, S. and P. Girama, *NOSE TO BRAIN DELIVERY: ROLE OF VIRAL AND NON-VIRAL VECTORS FOR NEUROLOGICAL DISORDER.* INDIAN DRUGS, 2021. **58**(05): p. 05.
4. Salade, L., et al., *How to characterize a nasal product. The state of the art of in vitro and ex vivo specific methods.* International journal of pharmaceutics, 2019. **561**: p. 47-65.
5. Sabir, F., R. Ismail, and I. Csoka, *Nose-to-brain delivery of antiglioblastoma drugs embedded into lipid nanocarrier systems: status quo and outlook.* Drug discovery today, 2020. **25**(1): p. 185-194.
6. Emami, A., et al., *Toxicology Evaluation of Drugs Administered via Uncommon Routes: Intranasal, Intraocular, Intrathecal/Intraspinal, and Intra-Articular.* International journal of toxicology, 2018. **37**(1): p. 4-27.
7. García-Pinel, B., et al., *Lipid-Based Nanoparticles: Application and Recent Advances in Cancer Treatment.* Nanomaterials (Basel, Switzerland), 2019. **9**(4): p. 638.
8. Mughal, A.A., et al., *Patterns of Invasive Growth in Malignant Gliomas—The Hippocampus Emerges as an Invasion-Spared Brain Region.* Neoplasia, 2018. **20**(7): p. 643-656.
9. van Schaijik, B., et al., *Circulating tumor stem cells and glioblastoma: A review.* Journal of Clinical Neuroscience, 2019. **61**: p. 5-9.
10. Zhang, Q., et al., *Current status and potential challenges of mesenchymal stem cell-based therapy for malignant gliomas.* Stem Cell Research & Therapy, 2018. **9**(1): p. 1-9.
11. Gao, H., *Progress and perspectives on targeting nanoparticles for brain drug delivery.* Acta pharmaceutica Sinica. B, 2016. **6**(4): p. 268-286.
12. Wang, S., et al., *Receptor-Mediated Drug Delivery Systems Targeting to Glioma.* Nanomaterials (Basel, Switzerland), 2015. **6**(1): p. 3.
13. Giunchedi, P., E. Gavini, and M.C. Bonferoni, *Nose-to-Brain Delivery.* Pharmaceutics, 2020. **12**(2): p. 138.
14. Pardeshi, C.V. and V.S. Belgamwar, *Direct nose to brain drug delivery via integrated nerve pathways bypassing the blood-brain barrier: an excellent platform for brain targeting.* Expert Opin Drug Deliv, 2013. **10**(7): p. 957-72.
15. Lee, D. and T. Minko, *Nanotherapeutics for Nose-to-Brain Drug Delivery: An Approach to Bypass the Blood Brain Barrier.* Pharmaceutics, 2021. **13**(12): p. 2049.
16. Bruinsmann, F.A., et al., *Nasal Drug Delivery of Anticancer Drugs for the Treatment of Glioblastoma: Preclinical and Clinical Trials.* Molecules (Basel, Switzerland), 2019. **24**(23): p. 4312.
17. Thorne, R.G. and W.H. Frey, *Delivery of neurotrophic factors to the central nervous system.* Clinical pharmacokinetics, 2001. **40**(12): p. 907-946.
18. Erdő, F., et al., *Evaluation of intranasal delivery route of drug administration for brain targeting.* Brain Research Bulletin, 2018. **143**: p. 155-170.
19. Costa, C.P., et al., *Intranasal delivery of nanostructured lipid carriers, solid lipid nanoparticles and nanoemulsions: A current overview of in vivo studies.* Acta pharmaceutica Sinica. B, 2021. **11**(4): p. 925-940.
20. Ugwoke, M.I., N. Verbeke, and R. Kinget, *The biopharmaceutical aspects of nasal mucoadhesive drug delivery.* Journal of pharmacy and pharmacology, 2001. **53**(1): p. 3-22.
21. Katona, G., et al., *Development of In Situ Gelling Meloxicam-Human Serum Albumin Nanoparticle Formulation for Nose-to-Brain Application.* Pharmaceutics, 2021. **13**(5): p. 646.
22. Bahadur, S., et al., *Intranasal Nanoemulsions for Direct Nose-to-Brain Delivery of Actives for CNS Disorders.* Pharmaceutics, 2020. **12**(12): p. 1230.
23. Mistry, A., S. Stolnik, and L. Illum, *Nose-to-Brain Delivery: Investigation of the Transport of Nanoparticles with Different Surface Characteristics and Sizes in Excised Porcine Olfactory Epithelium.* Mol Pharm, 2015. **12**(8): p. 2755-66.
24. Battaglia, L., et al., *Lipid nanoparticles for intranasal administration: application to nose-to-brain delivery.* Expert opinion on drug delivery, 2018. **15**(4): p. 369-378.
25. Nieto González, N., et al., *Polymeric and Lipid Nanoparticles: Which Applications in Pediatrics?*

Pharmaceutics, 2021. **13**(5): p. 670.
26. Musthaba, S., et al., *Nano approaches to enhance pharmacokinetic and pharmacodynamic activity of plant origin drugs.* Current Nanoscience, 2009. **5**(3): p. 344-352.
27. Chitkara, D., S. Singh, and A. Mittal, *Nanocarrier-based co-delivery of small molecules and siRNA/miRNA for treatment of cancer.* Therapeutic Delivery, 2016. **7**(4): p. 245-255.
28. Tenchov, R., et al., *Lipid Nanoparticles—From Liposomes to mRNA Vaccine Delivery, a Landscape of Research Diversity and Advancement.* ACS Nano, 2021.
29. Khan, A., et al., *Brain targeting of temozolomide via the intranasal route using lipid-based nanoparticles: brain pharmacokinetic and scintigraphic analyses.* Molecular pharmaceutics, 2016. **13**(11): p. 3773-3782.
30. Sandoval, M.A., et al., *EGFR-targeted stearoyl gemcitabine nanoparticles show enhanced anti-tumor activity.* Journal of controlled release, 2012. **157**(2): p. 287-296.
31. Seluanov, A., et al., *Mechanisms of cancer resistance in long-lived mammals.* Nature reviews. Cancer, 2018. **18**(7): p. 433-441.
32. Madane, R.G. and H.S. Mahajan, *Curcumin-loaded nanostructured lipid carriers (NLCs) for nasal administration: design, characterization, and in vivo study.* Drug Deliv, 2016. **23**(4): p. 1326-34.
33. Ong, W.Y., S.M. Shalini, and L. Costantino, *Nose-to-brain drug delivery by nanoparticles in the treatment of neurological disorders.* Curr Med Chem, 2014. **21**(37): p. 4247-56.
34. Sekerdag, E., et al., *A potential non-invasive glioblastoma treatment: Nose-to-brain delivery of farnesylthiosalicylic acid incorporated hybrid nanoparticles.* Journal of Controlled Release, 2017. **261**: p. 187-198.
35. Sabir, F., et al., *Development and Characterization of n-Propyl Gallate Encapsulated Solid Lipid Nanoparticles-Loaded Hydrogel for Intranasal Delivery.* Pharmaceuticals, 2021. **14**(7): p. 696.
36. Tripodo, G., et al., *Hyaluronic acid and its derivatives in drug delivery and imaging: recent advances and challenges.* European Journal of Pharmaceutics and Biopharmaceutics, 2015. **97**: p. 400-416.
37. Griesser, J., G. Hetényi, and A. Bernkop-Schnürch, *Thiolated hyaluronic acid as versatile Mucoadhesive polymer: from the chemistry behind to product developments—what are the capabilities?* Polymers, 2018. **10**(3): p. 243.
38. Meure, L.A., N.R. Foster, and F. Dehghani, *Conventional and dense gas techniques for the production of liposomes: a review.* Aaps Pharmscitech, 2008. **9**(3): p. 798-809.
39. Sabir, F., et al., *Quality-by-Design-Based Development of n-Propyl-Gallate-Loaded Hyaluronic-Acid-Coated Liposomes for Intranasal Administration.* Molecules (Basel, Switzerland), 2021. **26**(5): p. 1429.
40. Sabir, F., et al., *Quality-by-Design-Based Development of n-Propyl-Gallate-Loaded Hyaluronic-Acid-Coated Liposomes for Intranasal Administration.* Molecules, 2021. **26**(5): p. 1429.
41. Gurumukhi, V.C. and S.B. Bari, *Fabrication of efavirenz loaded nano-formulation using quality by design (QbD) based approach: exploring characterizations and in vivo safety.* Journal of Drug Delivery Science and Technology, 2020. **56**: p. 101545.
42. Agrahari, V. and V. Agrahari, *Facilitating the translation of nanomedicines to a clinical product: challenges and opportunities.* Drug discovery today, 2018. **23**(5): p. 974-991.
43. Yu, L.X., et al., *Understanding pharmaceutical quality by design.* The AAPS journal, 2014. **16**(4): p. 771-783.
44. Pallagi, E., et al., *Initial risk assessment as part of the quality by design in peptide drug containing formulation development.* European Journal of Pharmaceutical Sciences, 2018. **122**: p. 160-169.
45. Rathore, A.S., *Quality by design (QbD)-based process development for purification of a biotherapeutic.* Trends in biotechnology, 2016. **34**(5): p. 358-370.
46. Martins, S., et al., *Lipid-based colloidal carriers for peptide and protein delivery–liposomes versus lipid nanoparticles.* International journal of nanomedicine, 2007. **2**(4): p. 595.
47. Seyfoddin, A., J. Shaw, and R. Al-Kassas, *Solid lipid nanoparticles for ocular drug delivery.* Drug delivery, 2010. **17**(7): p. 467-489.
48. Porfire, A., et al., *Pharmaceutical development of liposomes using the QbD approach.* Liposomes Adv. Perspect, 2019. **2019**: p. 1-20.
49. Katona, G., et al., *Development of Lomustine and n-Propyl Gallate Co-Encapsulated Liposomes for Targeting Glioblastoma Multiforme via Intranasal Administration.* Pharmaceutics, 2022. **14**(3): p. 631.

ANNEX-I

ELSEVIER

Nose-to-brain delivery of antiglioblastoma drugs embedded into lipid nanocarrier systems: status quo and outlook

Fakhara Sabir, Ruba Ismail and Ildiko Csoka

University of Szeged, Faculty of Pharmacy, Institute of Pharmaceutical Technology and Regulatory Affairs, H-6720 Szeged, Eötvös u. 6, Hungary

Glioblastoma multiforme (GBM) is one of the most devastating and deadly types of tumor. Among all the present treatment strategies, the utmost prerequisite is prolonged intervention at the malignant site. The blood–brain barrier (BBB) is the bottleneck in the delivery of anti-GBM drugs and invasive treatment comes with many pitfalls. This review will discuss the potential of embedding antitumor drugs into nanocarriers for intranasal delivery. Additionally, it emphasizes the significance of applying quality by design (QbD) methodology from the early development stages to ensure the high quality, safety and efficacy of the developed carrier system.

Introduction

Malignant gliomas (MGs) are the most lethal forms of primary central nervous system (CNS) malignancy, classified based on an augmenting level of undifferentiation, anaplasia and proliferation. WHO classified gliomas into four clinical grades: grade I (astrocytoma); grade II (diffuse astrocytoma, the most distinguished form); grade III (anaplastic variants of astrocytoma); and grade IV (glioblastoma) [1]. Pleomorphic glioblastoma is called glioblastoma multiforme (GBM) because these malignant cells show a discrepancy in structure and morphology [2]. The current treatment strategies for GBM include surgery, radiotherapy and chemotherapy. The focus of researchers to treat GBM is challenging because surgery and radiotherapy are not good options because of its topographically diffuse nature [3]. Eventually, understanding the pattern of spread of individual malignant cells over long distances and into parts of the brain is essential for patient survival. A present literature survey reveals that there are just a few available therapies that could significantly improve survival chances [4]. The circumvention of the blood–brain barrier (BBB) through straight intervention into insubstantial brain tissues can result in severe neurotoxicity and loss of brain key functionality. Consequently, there is a need to design a more specific and rational (noninvasive) approach to target GBM. It is also necessary to explore the potential differences in permeability between the intact and malignant brain to overcome the challenges in brain targeting [5]. Figure 1 demonstrates the differences between barriers in the intact brain and in GBM.

The intranasal route is a direct and simple approach, including many advantages of higher bioavailability, shorter onset of action, circumvention of systemic toxicity, noninvasiveness and clearance. Additionally, avoiding the BBB could significantly increase the concentration of the active pharmaceutical agent in the central nervous system (CNS). According to data present in the literature, pharmacological active agents can be delivered through the nasal cavity via the trigeminal and olfactory nerves. Drug permeation is basically dependent upon the key characteristics of an active agent or carrier, like its metabolic stability, solubility, residence time in the mucous layer and rate of mucociliary clearance [6].

The safety and toxicological evaluation of products delivered intranasally is of great importance. The prolonged contact of formulations containing cytotoxic materials can cause ciliotoxicity, tissue damage and irritation [7]. Therefore, regardless of the presence of carrier-free approaches for intranasal delivery, a carrier system could be useful to deliver chemotherapeutics via the intranasal route; among all delivery systems, nanoparticle-based carriers have been intensely studied for research imaging, treatment and diagnosis of brain tumors. Lipid-based colloidal systems, for example liposomes and solid lipid nanoparticles (SLNs), increased drug transfer to the brain through the intranasal route [8]. For instance, *in vitro* hemolysis and cytotoxicity studies of doxorubicin

Corresponding author: Csoka, I. (csoka@pharm.u-szeged.hu)

https://doi.org/10.1016/j.drudis.2019.10.005

Please cite this article in press as: Sabir, F. et al. Nose-to-brain delivery of antiglioblastoma drugs embedded into lipid nanocarrier systems: status quo and outlook, Drug Discov Today (2019), https://doi.org/10.1016/j.drudis.2019.10.005

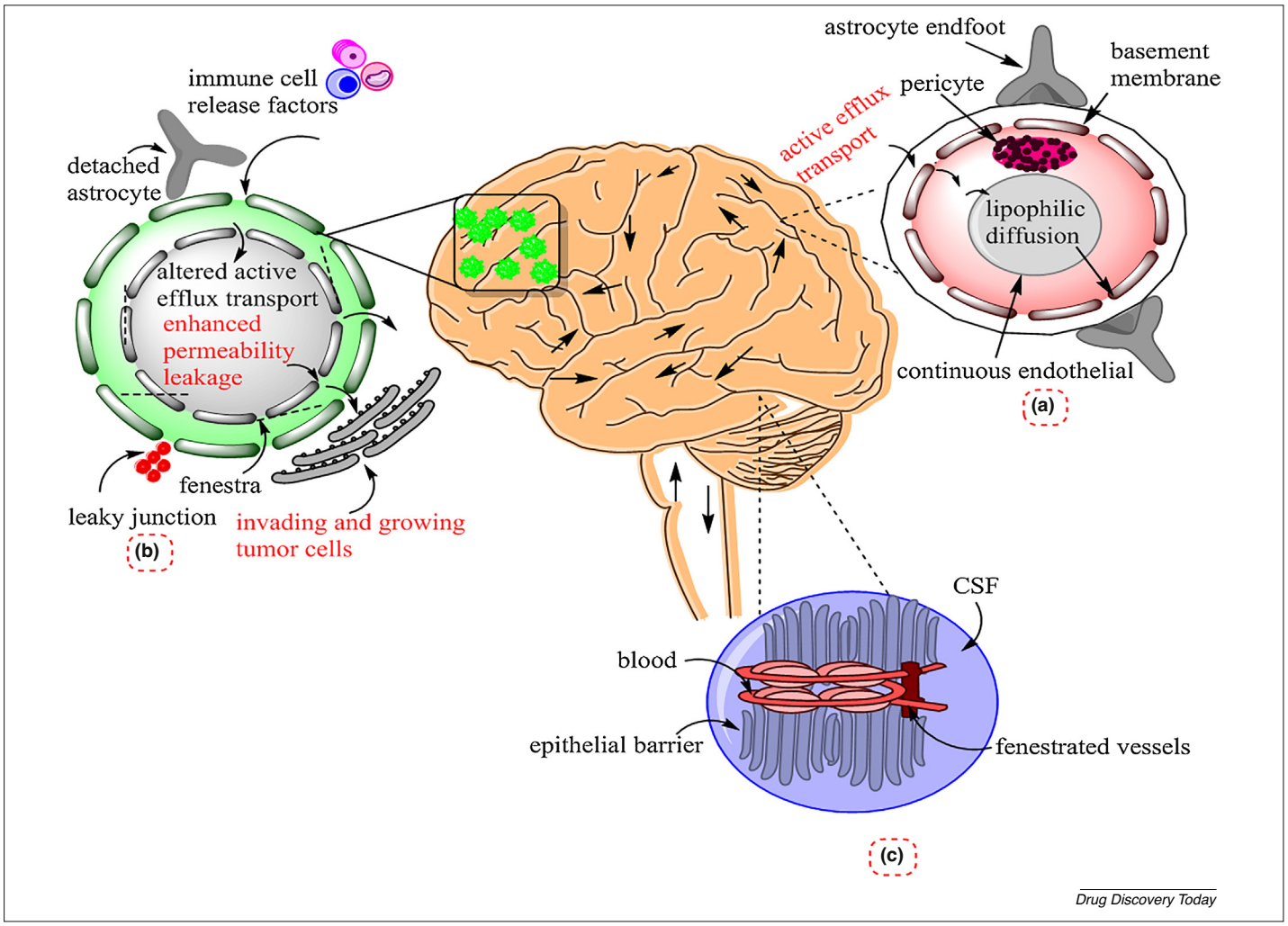

FIGURE 1

Challenges in blood to brain delivery in a brain tumor. The figure illustrates the comparison between barriers in normal brain and in GBM. **(a)** Normal blood–brain barrier (BBB) composed of: astrocyte (role in morphology), pericyte, endothelial cells (role in tight junction structure and vasoregulation). **(b)** Blood–tumor barrier **(**deatched astrocyte, fenestra, leaky juctions – blood vessels that supply the tumor are leaky and incompletely formed but the healthy brain components are still present in the main region of GBM). **(c)** Blood–cerebrospinal-fluid (CSF) barrier (composed of a choroid plexus having epithelial cells and tight junctions, increased level of albumin in the CSF in GBM which might cause disturbance of the BBB or release from tumor).

(DOX)-loaded liposomal nanoparticles were performed, which resulted in specificity and enhanced levels of drug accumulation in gliomas [9,10]. Colloidal nanocarrier systems [liposomes, SLNs, lipoproteins, lipoplexes, etc.] have shown clear amassing in gliomas but the shortening of noninvasive accumulation and retention evaluation tools could hinder monitoring the exact duration and location of nanoparticles within the brain [11]. This review will focus on the potential of lipid nanocarrier systems to deliver anticancer drugs via the intranasal route, as well as the significance of applying quality by design (QbD) software for the targeted delivery of cytotoxic materials via the intranasal route to maintain the safety and product profile.

Strategies to circumvent the BBB: bottleneck in targeting glioblastoma

Scientists have been working to develop versatile methods to circumvent the BBB, which include the opening of the BBB, intranasal delivery and penetration via the BBB by cellular internalization. The overexpression of receptors (like low-density lipoprotein, nicotinic acetylene choline, insulin-like growth factor (IGF), transferrin receptors, diphtheria toxin, leptin and scavenger receptor type B) has been reported on the BBB. The specific ligand functionalization and attachment can intervene in drug transport via the BBB. This precise and sensitive type of interaction between ligands and receptors governs receptor-mediated transport [12–14]. However, there are limitations in implementation of a functionalized or specific ligand attached moiety. First, it can lose its therapeutic activity; second, all present strategies are invasive and accumulation of drug cargos in the liver and other off-target sites governs its therapeutic efficacy [7]. Therefore, there is a need for noninvasive delivery approaches to achieve the best therapeutic goals.

An alternative route of administration

An alternative route of administration to CNS drug delivery is intranasal administration. The intranasal delivery (IND) route

Please cite this article in press as: Sabir, F. et al. Nose-to-brain delivery of antiglioblastoma drugs embedded into lipid nanocarrier systems: status quo and outlook, Drug Discov Today (2019), https://doi.org/10.1016/j.drudis.2019.10.005

is a noninvasive, direct and more effective route of administration than intravenous (i.v.) delivery and can avoid the BBB together with systemic side effects. The IND pathways (trigeminal and olfactory pathways) in the nasal cavity are reasons for direct delivery to the brain and result in good pharmacokinetic/pharmacodynamic (PK/PD) profiles for CNS drugs. Drug delivery from the nose via the trigeminal pathway follows either axonal or endocytotic transport, whereas the olfactory pathway is further divided into intraneuronal and extraneuronal pathways. The intraneuronal pathway follows axonal transport and it takes hours or days for the active pharmaceutical ingredient (API) to reach the target site, whereas the extraneuronal path follows the perineural route and it just takes a few minutes to reach the target site [15,16]. Furthermore, this delivery route is a new approach for the delivery of potent active agents and for antineoplastic agents that can be loaded into nanocarriers to ensure a better safety profile. By using this route, nanoparticles can carry drugs easily to the target site, and can bypass the main barriers: the BBB and the blood–cerebrospinal-fluid barrier (BCSFB). There are many studies revealing better target delivery of CNS drugs via the intranasal route in contrast to i.v. administration. Schioth *et al.* reported that IGF-1, when given intranasally, had greater CNS efficacy when compared with i.v. intervention. Many other studies also showed that the intranasal delivery of the API led to better cure rates of CNS diseases, such as depression, autism, eating disorders, Parkinson's disease (PD) and Huntington's disease (HD), as well as various other diseases yet to be treated. Besides these advantages, there is a long list of factors that can limit the permeability of drug carriers via the intranasal route. Therefore, while designing intranasal formulations, the factors regarding the anatomy and the physiology of the nasal cavity should be considered. The vibrissae of the nasal vestibule and the transepithelial region of the atrium (narrowest region) are the parts that are the least permeable. By contrast, other parts like the superior, middle and inferior turbinate of the respiratory region are more permeable, whereas the specialized ciliated olfactory nerve cells of the olfactory region have direct access to the CSF. Table 1 explains how the structures of the nasal cavity affect permeability via the intranasal route [16,17]. By considering the crucial factors affecting drug delivery via the nasal cavity, a formulation can be designed for nose-to-brain delivery with increased permeation, low clearance and high mucoadhesion by the application of the QbD [18].

Nanocarrier systems for nose-to-brain delivery

The safety data for intranasal formulations are of great importance. Nanoparticles have the potential to improve nose-to-brain delivery because they have can avoid enzymatic degradation and transport from P-glycoprotein (P-gp) efflux proteins. These carrier systems can enhance therapeutic brain delivery by using bioadhesive materials and also by opening the closed junctions of the nasal epithelial membrane. The transport of nanoparticles through the intranasal route takes place via olfactory neurons by endocytotic or neuronal pathways. The confocal microscopy study of polystyrene nanoparticles reported that nanocarriers within the range 20–200 nm can follow clathrin-coated pits; however, nanoparticles in the size range 200–1000 nm can be transported via caveolae-mediated endocytosis [7,15].

Nanoparticles can also follow the transport from endothelial cells to olfactory neurons via endocytosis or pinocytosis and move along the axon. For this transport pathway, the size of nanoparticles should be within the diameter of the axon, which is up to 100–700 nm. Therefore, the intranasal delivery of nanoparticles could be a promising choice for targeting life-threatening diseases like GBM. Regarding the carrier systems, the essential classes of nanoparticles that are at the center of focus for brain targeting include polymeric nanoparticles such as micelles, iron oxide nanoparticles, gold nanoparticles, quantum dots and lipid-based nanoparticles like nano lipid carriers (NLCs), SLNs, liposomes, lipoplexes and lipoproteins [19]. In general, nanoparticles can induce toxicity depending upon their internalization site and composition. It is also reported that nanoparticles can induce inflammation, DNA damage and oxidative stress. The IND of metal nanoparticles into brain is relatively well known for harmful neurological effects. The extensive exposure of metal nanoparticles can cause serious damage and even can lead to diseases such as Alzheimer's disease (AD) and PD. The present study is relevant to lipid nanoparticles that are most biocompatible and least toxic in nature. Clearance of nanoparticles from the brain occurs via the mononuclear phagocytes system (MPS). The aspects of toxicity and clearance via macrophages are not accurate and might be caused by variations in nanoparticles properties (like charge, shape, size, coating) and use of different quantification methods [20]. Figure 2 explains the nanoparticle attributes influencing drug delivery via the intranasal route.

TABLE 1

Impact of various structural characteristics of nasal cavity on permeation

Structural parts/region of the nasal cavity	Effect on permeation	Refs
Nasal hairs (vibrissae) of the nasal vestibule (sebaceous glands)	Least permeable owing to the presence of keratinized cells	[17]
Transepithelial region of the atrium (narrowest region)	Less permeable because it has a small surface area and stratified cells are present anteriorly	[35]
Superior, middle and inferior turbinate of the respiratory region	Most permeable region due to greater surface area and increased blood supply	[36]
Specialized ciliated olfactory nerve cells of the olfactory region	Direct pathway to cerebrospinal fluid (CSF)	[35]
Ciliated cells and squamous epithelial cells of the nasopharynx	Nasal cavity drainage receiver	[17]

Please cite this article in press as: Sabir, F. et al. Nose-to-brain delivery of antiglioblastoma drugs embedded into lipid nanocarrier systems: status quo and outlook, Drug Discov Today (2019), https://doi.org/10.1016/j.drudis.2019.10.005

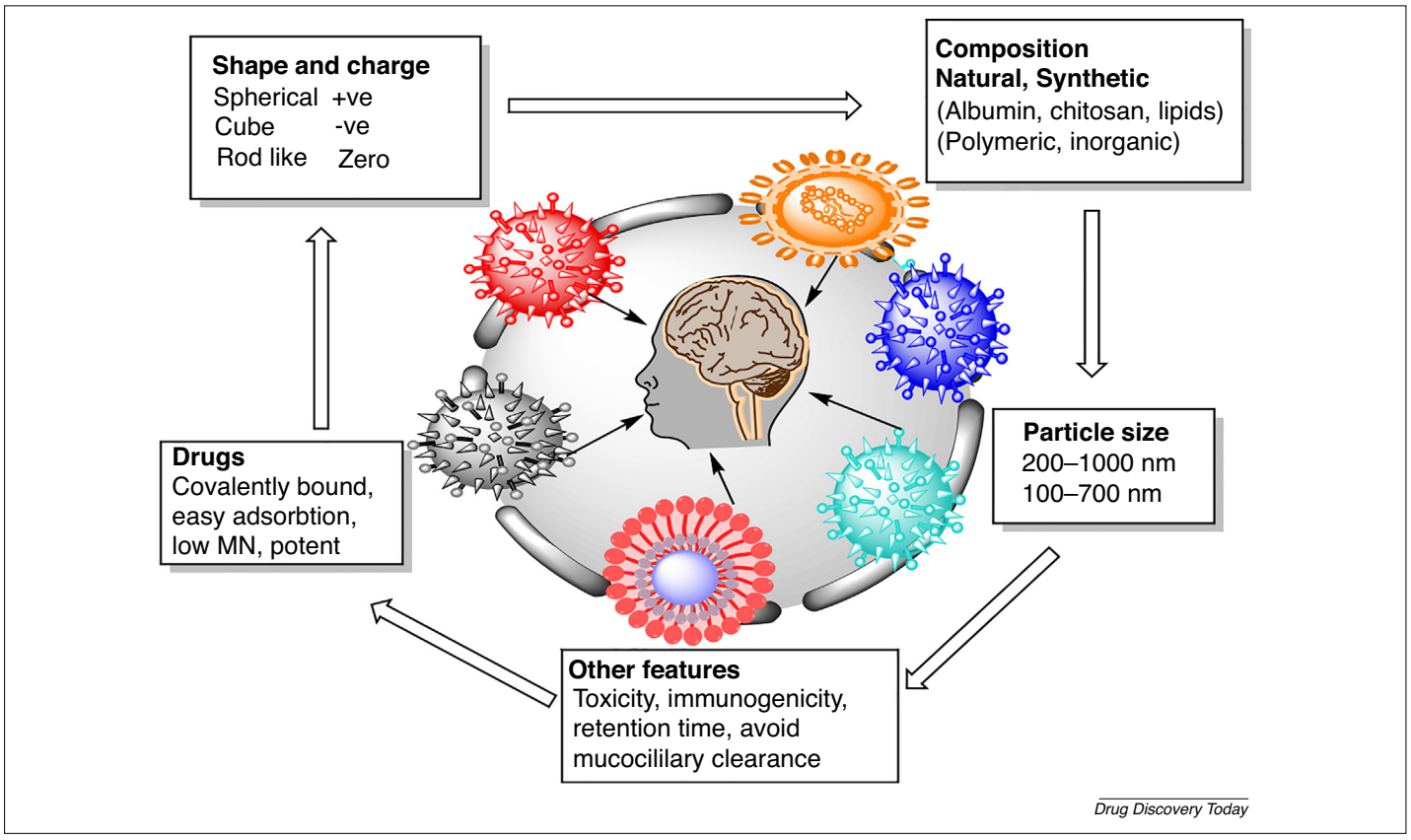

FIGURE 2

Nanoparticle attributes influencing the delivery of active pharmaceutical ingredient (API) via the intranasal route. The figure illustrates the significant features of nanoparticles for intranasal delivery like pysiochemical properties (size, charge, composition) and other significant features such as low immunogenicity, low toxicity, avoiding mucociliary clearance and increased retention time (high mucoadhesivity).

Lipid nanocarriers: a promising approach for intranasal delivery

For significant nose-to-brain delivery, a colloidal drug delivery system is the most suitable system that refers to increased bioavailability and sustained release and high stability of the API. The enhanced biocompatibility, high scalability, safety and efficacy of lipid nanoparticles made them superior carriers for nose-to-brain delivery. In contrast to lipid nanoparticles, polymeric nanoparticles have low scalability, high cytotoxicity (e.g., 100% mortality was reported when cells were treated with polyester polymer nanoparticles) and poor tolerability. Most lipid nanoparticles have a particle size within the range 50–1000 nm. As described in the previous section, a particle size between 50 and 700 nm is the most favorable for intranasal delivery via neuronal transport [15]. Among these lipid carriers, liposomes and SLNs discussed in the following section have shown greater therapeutic efficacy in GBM. The lipid nanoformulations of anticancer agents provide enhanced drug stability, PK, drug distribution and efficacy compared with other approaches [7].

Therapeutic efficacy of lipid nanoparticles in targeting glioblastoma

Liposomes, SLNs, lipoproteins, lipoplexes and nanostructured lipid carriers have been widely used for targeting GBM. Liposomes are bilayer spherical biocompatible carriers and these lipid-based nanostructures are actually the pioneers of lipid-based particles employed for parenteral delivery with diameter ranges from 10 to 1000 nm and are precursors of nanostructured lipid carriers (NLCs) and SLNs [21]. Table 2 summarizes the use of liposomes in the management of MGs via different delivery routes. The results of all these studies revealed an increase in survival time along with the inhibition of proliferation [22]. It should be considered that various liposomal factors like the size, particle diameter and uptake by the MPS can be crucial for targeting [23].

Lipid nanoparticles including SLNs and NLCs are the most suitable among all other lipid nanoparticles, without being constrained by their limitations. The stealth ability of lipid nanoparticles is higher than other polymeric nanoparticles against the MPS because they are fabricated from biocompatible substances such as a brew of natural lipids [24]. Table 3 demonstrates the therapeutic efficacy of SLNs and NLCs in targeting GBM. The results of all previous studies revealed the decrease in tumor growth, the increase in the lifespan of the animals used and the inhibition of cell proliferation.

The proven efficacy (from studies mentioned in Tables 2 and 3) of lipid nanoparticles in targeting GBM has shown their potential to encapsulate anticancer drugs. Furthermore, these lipid nanoparticles have a good ability to protect the loaded API and, because

Please cite this article in press as: Sabir, F. et al. Nose-to-brain delivery of antiglioblastoma drugs embedded into lipid nanocarrier systems: status quo and outlook, Drug Discov Today (2019), https://doi.org/10.1016/j.drudis.2019.10.005

TABLE 2

Applications of liposomes in the management of GBM

Encapsulated substance	Model of study	Type of liposomes	Central nervous system (CNS) action/effects on GBM	Refs
Doxorubicin (DOX)	Clinical study	PEG-liposomes	Enhanced efficacy Inhibition of tumor growth Enhanced survival time	[37]
Interferon (IFN)-β Plasmid	Clinical study	Cationic liposomes	Antiproliferative Reduction of tumor size	[38]
Recombinent herpes simplex virus thymidines kinase (adeno viral carrier)	Glioma model in mouse	Cationic liposomes	Reduced immunogenicity Antiproliferative	[39]
Antisense growth factor	Human malignant glioma cell lines	Cationic liposomes	Inhibition of tumor growth	[40]
Lomustine	Rabit glioma model	Temperature-sensitive liposomes (TSL)	Thermo targeting with inhibition of tumor growth	[41]
Epirubicin (EPI) plus celecoxib	Mice	PTD peptide attached liposomes	Destruction of glioma vasculogenic mimicry channels	[42]
Paclitaxel (PTX)	Mice	Dual targeting, cell penetrating peptid attached liposomes	Selective targeting Inhibition of tumor growth	[43]
Small interfering RNA (siRNA)	Mice	Ligand-targeted liposomes (CTX)	Enhance the efficacy and internalization into glioma cells	[40]
Daunorubicin (DNR) and quinacrine	Mice	Ligand-targeted liposomes (WGA and TAM)	Killing of glioblastoma cells and dimishing brain gliomas	[44]
DOX and iron oxide	Mice	Ligand-targeted liposomes (RGD)	Enhance targeting ability and site-specific delivery	[45]
Irinotecan	Rats	Ligand-targeted liposomes	Inhibit tumor growth increase lifespan of rats	[46]
DOX	Rats	Lactoferrin liposomes	Destruction of tumor cells and significant enhanced survival rate in tumor-bearing rats	[47]

TABLE 3

Summary of applications of SLNs/NLCs in targeting GBM

Encapsulated substance	Model of study	Type of SLN/NLCs	Central nervous system (CNS) action/ effects on GBM	Refs
Carmustine	U87 cell line (*In vitro* human brain model)	Cationic solid lipid nanoparticles (CASLNs)	Antiproliferative effect Decrease expression of tumor necrosis factor (TNF)-α	[48]
DOX and etoposide	U87 cell lines, HBMEC, human astrocytes	CASLNs	Significant reduction in tumor growth	[49]
Edelfosine (EDF)	Glioma cell line C6 *in vivo* C6 glioma xenograft tumor	SLNs (composed of compritolor)	The antimalignant effect, inhibition of tumor growth	[50]
Cytarabine (CRB)	EL-4 cell lines	NLCs	Cytotoxic effect on tumor cell line	[51]
siRNAs	U87MG cell lines and tumor xenograft for *in vivo* study	Low-density lipoprtoein (LDL) and polyethylene glycol (PEG) SLNs	The decrease in tumor cell proliferation	[52]
Camptothecin (CPT)	BCEC Porcine brain capillary endothelial cells compared with (RAW264.7)	CA-SLNs	Higher cytotoxicity in brain cells enhance antitumor efficacy	[53]
Etoposide	K562 cell line, MTT assay and flow cytometry	NLCS with transferrin	Enhanced cellular uptake and antiproliferative effect	[54]
Locked nucleic acid (LNA) (antioncogenic miR-21)	U87 MG (malignant glioma cell line)	Lipid nanocapsule (LNCs) with L-1 peptide	Reduction of miR-21 expression and antiproliferative	[55]
Curcumin	U251MG cell line, rats bearing C6 gliomas	CA-LNCs	The decrease in tumor size and malignancy	[56]
Resveratrol (RVR)	U87 cell line	Functionalized SLNs	Enhance cytotoxicity	[57]
DOX	BBB model (hcmec/D3 cell)	CA-SLNs	Increased toxicity for glioblastoma cells	[58]
Polo-like kinase 1(PLK1) siRNAs (siPLK1)	Rats bearing orthotopic xenograft model	HA-LNPs (hyaluronic acid)	Increased cell death (by reducing expression of PLK1)	[59]
Temozolomide (TMZ)	U87MG *in vitro* cells lines	NLCs	Very much enhanced antitumor activity	[60]
Vincristine (VCR) and TMZ	U87MG *in vitro* cell line and mice induced with malignant glioma model	SLNs and NLCs	NLCS show better antitumor activity than SLNs	[61]

of their occlusive nature, they can also increase nasal retention time. These features make lipid nanoparticles a significant carrier for nose-to-brain delivery because they can avoid the cytotoxicity issues of antineoplastic drugs [7,25].

Novel lipid nanoparticle formulation for targeting glioblastoma via IND

New delivery approaches are required in research to efficiently target brain tumors. Curcumin-loaded NLCs (CUR-NLC) for

Please cite this article in press as: Sabir, F. et al. Nose-to-brain delivery of antiglioblastoma drugs embedded into lipid nanocarrier systems: status quo and outlook, Drug Discov Today (2019), https://doi.org/10.1016/j.drudis.2019.10.005

intranasal administration were developed with a particle diameter of 146 nm, encapsulation efficiency (EE) of 90%, a charge of 21 mV and polydispersity index (PDI) rating of 0.18. The results of the following investigation reveal the increased cytotoxicity of CUR-NLC compared with that of free CUR in the glioma cell line U373MG. The biodistribution study for the same formulation showed an increased drug concentration in the brain after the intranasal application of NLCs. The results of this study led to the conclusion that CUR-NLC is an efficient delivery system for targeting GBM [23]. Temozolomide-loaded NLCs (TMZ-NLC) were prepared to ensure brain targeting via the intranasal route. The optimized formulation showed a particle size within the nano range, zeta potential of 15 mV, entrapment efficiency of 81% and PDI of 0.2. The results of the *in vivo* studies indicated the significant enhanced brain concentration of TMZ-NLC in comparison with TMZ dispersion (i.v., intranasal). The highest concentration of TMZ-NLC in the brain proved the efficacy of this direct intranasal administration of NLCs. The following study described that the intranasal administration of NLCs increased residence time and resulted in higher bioavailability in the brain at lower doses, denoting this delivery route the most suitable for targeting glioma [26].

Novel farnesyl thio salicylic acid (FTA)-loaded lipid cationic hybrid nanoparticles (HNPs) were formulated and evaluated for antitumor activity via the intranasal route. Glioma 2 (RG2) cells were placed into Wistar rats. The tumor-bearing rats were treated with FTA-encapsulated HNPs by intranasal and i.v. administration. The evaluation of tumor sizes with FTA-encapsulated HNPs resulted in a clear decrease (~55%) in tumor size. This study proved that the intranasal intervention of FTA-loaded HNPs is an equally effective approach in GBM targeting. The results of all studies support the use of the IND route for targeting GBM by using lipid carriers [27].

Mechanism of nanoparticle drug delivery via the intranasal route

The intranasally administered formulation will deposit on the pseudostratified columnar epithelium (a respiratory tract in the nasal cavity). The site of deposition of the intranasal formulation administered in the form of solution, spray or gel (via applicator) is the front region of the nasal cavity. However, there are a few devices that can settle the drug formulation in a higher region of the nasal cavity. The nanoparticles intervene via intranasal passage deposited at the site of the nasal cavity depending on its properties like size, charge and lipophilicity. There are four options for the drug, either to enter via the nasal epithelial tissue and arrive at the circulation or be unloaded along the gastrointestinal tract (GIT) through the nasopharynx by the ciliary clearance network. The system is made up of cilia, which are motile and beat in a synchronized manner, thereby propelling the viscous superior part dorsally against the nasopharynx quickly (5 mm/min). In addition, enzymatic activity is also higher in the nasal cavity deep in the olfactory region (enzymes like cytochrome P450 dependent peptidases, monooxygenase and proteases are involved in that procedure) [28]. The nose-to-brain delivery of the nanoparticles will follow the transport from endothelial cells to the olfactory neurons via endocytosis or pinocytosis and move along the axon or it will follow the trigeminal nerve pathway. For this transport pathway, the size of nanoparticles should be within the diameter of the axon: 100–700 nm [29]. Figure 3 explains all the possible mechanisms and pathways involved in the transport of lipid nanoparticles.

In vitro/*in vivo*/*ex vivo* models for testing nose-to-brain delivery

For an exploration of the mechanism behind the transport of drugs via the intranasal route, different types of *in vitro*, *in vivo* and *ex vivo* models are used. These diverse types of models are applied for different studies: *in vitro* models for permeation and diffusion studies; *in vivo* models for the determination of absorption and PK profile of the API; and *ex vivo* models for perfusion studies in the nasal cavity. The selection of *in vivo* models should be adequate for studying the anatomy of the nasal cavity. The first animal model used for intranasal study was the rat and, later, with the development in absorption data, other animal models like sheep, monkey, mouse and rabbit were also used. For adequate PK studies rabbit, dog, sheep and monkey models are commonly suggested, whereas mouse and rat models are used for preliminary absorption studies [30].

Besides the significance of *in vivo* models, the transport mechanism of drug absorption from the nasal route had to be explored. *In vitro* models were fabricated to replace the *in vivo* and *ex vivo* models. Furthermore, it is difficult to extrapolate the data of the absorption and kinetics studies obtained from the animal models to humans (owing to the difference of species). It is necessary to select adequate cell lines that can reproduce results at significantly low costs. There are a number of *in vitro* cell culture models like NAS2BL (originating from rat nasal squamous carcinoma), BT (originating from bovine turbinates), CaCo-2 cell lines (from human colon carcinoma), Calu-3 (originating from human lung adenocarcinoma), RPMI 2650 (from human nasal epithelial tissues) and 16HBE14o- (from human normal bronchial epithelium of male heart lung transplant patient) [30]. Among these models, CaCo-2 and RPMI 2650 are used to evaluate permeability and absorption via the nasal route. However, there are some disadvantages of cell lines, for example RPMI 2650 are undifferentiated cells that encounter the limited expression of ciliated and goblet cells. The absence of a developed monolayer makes this cell line impractical to use for a transport study. By contrast, Calu-3 cells can develop monolayers and are suitable for transport study but the origin of this cell line is not the normal epithelial cells of the nasal cavity. The 16HBE14o- cell line possesses high transepithelial electrical resistance (TEER) making it suitable for transportation study but this cell line originates from normal bronchial epithelium of a male heart and lung transplant patient. For the determination of drug delivery and the development of formulations via the intranasal route, it is important to use reliable *ex vivo* models. The excised tissue is usually from the nasal mucosa of slaughtered or experimental animals (rats, rabbits, dogs, monkeys, sheep) or from humans as well. The *ex vivo* study is very important to obtain all the information regarding the toxicity, efflux, metabolism and permeation of the developed formulation. Besides the many advantages of *ex vivo* models, there are a few limitations,

Please cite this article in press as: Sabir, F. et al. Nose-to-brain delivery of antiglioblastoma drugs embedded into lipid nanocarrier systems: status quo and outlook, Drug Discov Today (2019), https://doi.org/10.1016/j.drudis.2019.10.005

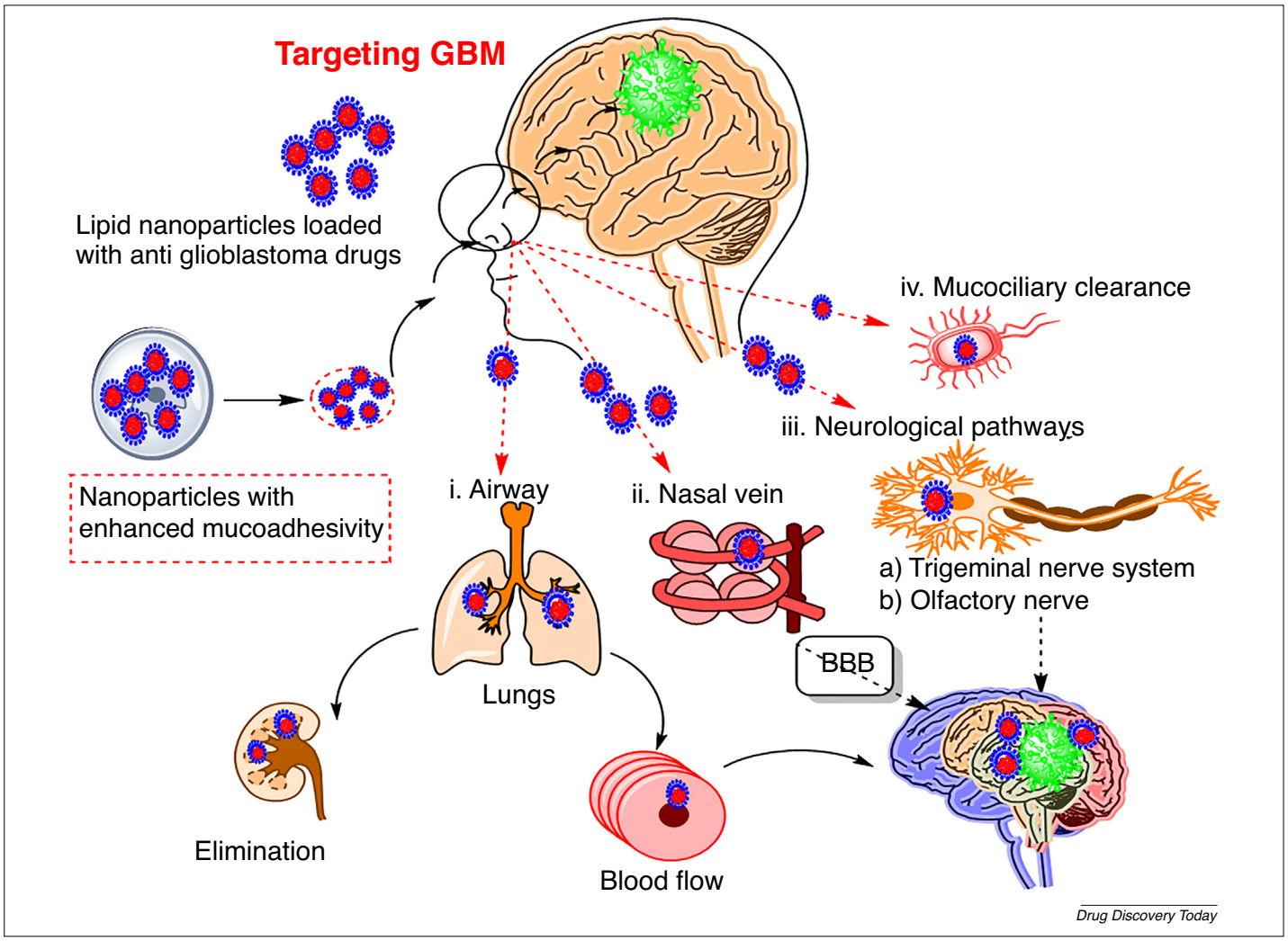

FIGURE 3

Possible mechanisms of lipid nanoparticles across the nasal membrane. The figure demonstrates that lipid nanoparticles with enhanced mucoadhesivity will follow four possible pathways: (i) airway; (ii) nasal vein; (iii) neurological pathway; and (iv) mucociliary clearance. The nanoparticles will follow the transport from endothelial cells to olfactory neurons via endocytosis or pinocytosis and move along the axon or follow the trigeminal nerve pathway.

such as the lack of interstitial flow rate determination and the thickness of nasal epithelial tissues of the excised mucosa. The Ussing chamber is the *ex vivo* nasal model for permeability studies [31].

Significance of QbD in the early development of a lipid carrier system for targeting glioblastoma

Depending on up-to-date knowledge about barriers limiting the IND of anticancer drugs targeting brain tumors, lipid-based nanocarrier systems could offer a promising strategy. However, because many formulation parameters and regulatory aspects should be considered, the QbD concept or the GMP of the 21st century should be followed. The main elements of QbD methodology are described in the relevant guidelines of the International Council on Harmonization (ICH), specifically ICH Q8 (R2), Q9 and Q10; and these include: (i) defining the quality target product profile (QTPP); (ii) selecting the critical quality attributes (CQAs) of the targeted product; (iii) selecting the production method and defining the critical process parameters (CPPs) that can highly affect the CQAs; and (iv) analysis of the initial risk assessment (RA), which is followed by optimizing the level of the risky factors by applying a suitable design of experiment (DOE) [32]. The very first step of QbD is to collect all the data from previous studies that could affect the target product profile. After early knowledge of space design and evaluation of QTPPS, CQAs and CPPs, the RA application revealed the attributes having the highest impact on the final lipid nanoformulation quality for IND. Figure 4 demonstrated the description of QbD methodology in early development of a lipid carrier system for nose-to-brain delivery based on the relevant ICH guidelines [33,34].

Concluding remarks and future directions

This review summarizes the importance of nose-to-brain delivery in targeting GBM. Nanoformulations are considered as one of the most important targeting carriers. Besides many advantages, nanoformulations loaded with cytotoxic material can still accumulate in other parts and tissues of the body, for instance in the liver, spleen and kidney. Therefore, it is necessary to design and fabricate a method that can overcome the shortcomings of previously used carriers and delivery routes. The alternative route and the lipid

Please cite this article in press as: Sabir, F. et al. Nose-to-brain delivery of antiglioblastoma drugs embedded into lipid nanocarrier systems: status quo and outlook, Drug Discov Today (2019), https://doi.org/10.1016/j.drudis.2019.10.005

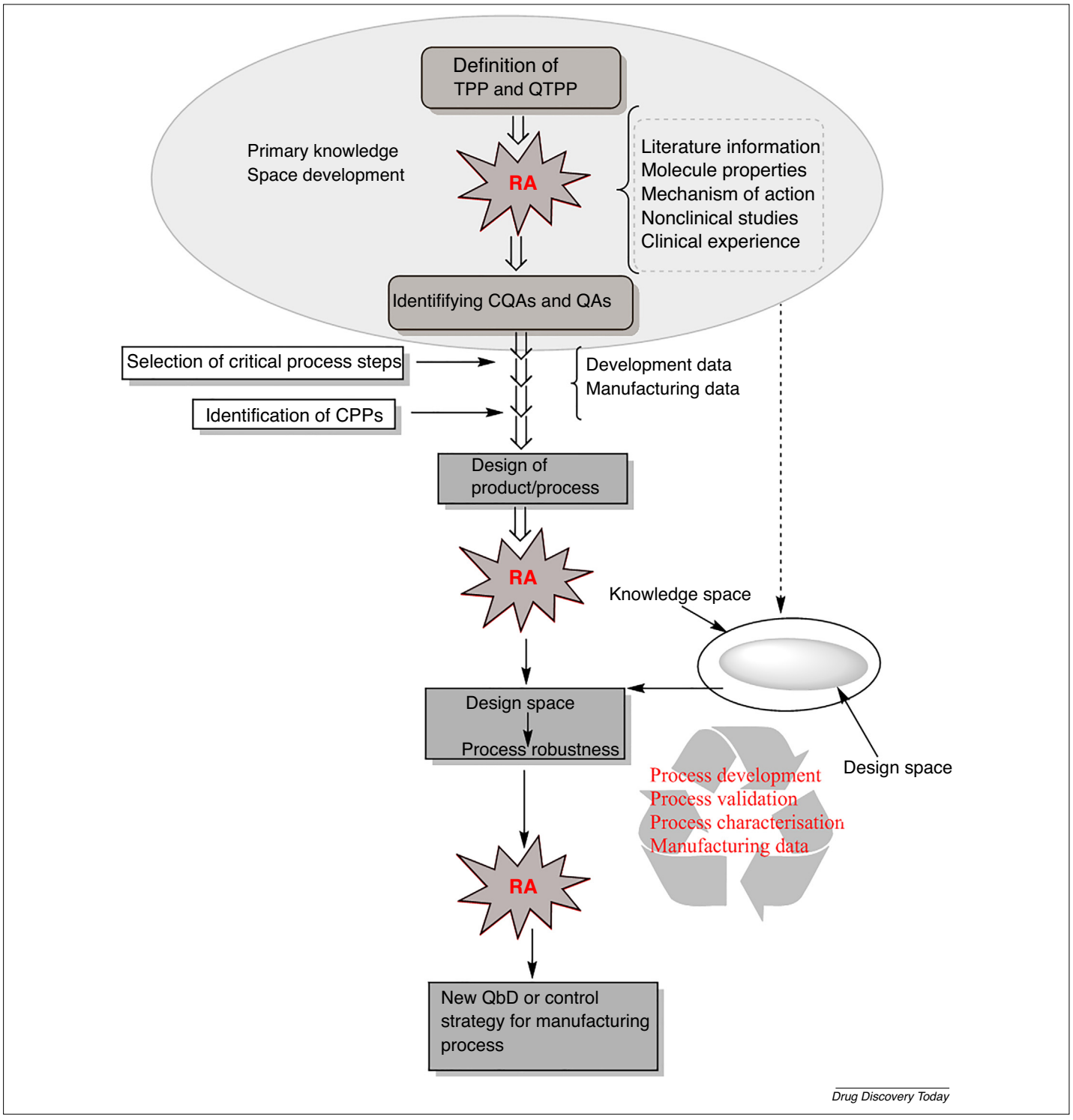

FIGURE 4

Steps and elements of quality by design (QbD) methodology that will help to design and validate the process for development of intranasal formulation. Step 1: identification of target product profile (TPP) and quality target product profile (QTPP), which comprises therapeutic and other quality requirements. Step 2: identification of critical quality attributes (CQAs), which are associated with in-process materials, and critical process parameters (CPPs) having an effect on CQAs. Step 3: risk assessment (RA) is a process of collecting information to support risk decision and it is also a main activity of QbD methodology that can be performed at initial and final phases of development.

nanocarrier provide chances to deliver anticancer drugs (with potential efficacy) against GBM, and this will be a new and expedient approach to GBM treatment strategies. Furthermore, for successful IND of anticancer drugs, risk assessment is the main component of QbD which should be applied using special software to calculate the risk severity of CQAs and CPPs regarding the encapsulation of potential API into lipid-based carrier systems. Thus, the application of the QbD concept can save time and effort by directing the focus toward structuring the quality in each step of formulation design.

Please cite this article in press as: Sabir, F. et al. Nose-to-brain delivery of antiglioblastoma drugs embedded into lipid nanocarrier systems: status quo and outlook, Drug Discov Today (2019), https://doi.org/10.1016/j.drudis.2019.10.005

Conflicts of interest

The authors declare no conflicts of interest, financial or otherwise.

Acknowledgments

F.S. made substantial contributions to writing the manuscript and designing the figures and tables. Additionally did the major contribution in revising the manuscript. R.I. contributed to evaluating the manuscript, writing the QbD and general opinion sections, in addition to making critical revision of the whole manuscript. I.C. contributed to the conception of the manuscript, planning and supervising the work at each step and giving the final approval.

References

1 Hombach-Klonisch, S. *et al.* (2018) Glioblastoma and chemoresistance to alkylating agents: involvement of apoptosis, autophagy, and unfolded protein response. *Pharmacol. Ther.* 184, 13–41
2 van Schaijik, B. *et al.* (2019) Circulating tumor stem cells and glioblastoma: a review. *J. Clin. Neurosci.* 61, 5–9
3 Zhang, Q. *et al.* (2018) Current status and potential challenges of mesenchymal stem cell-based therapy for malignant gliomas. *Stem Cell Res. Ther.* 9, 1–9
4 Mughal, A.A. *et al.* (2018) Patterns of invasive growth in malignant gliomas – the hippocampus emerges as an invasion-spared brain region. *Neoplasia* 20, 643–656
5 Sekerdag, E. *et al.* (2017) Nose-to-brain delivery of farnesylthiosalicylic acid loaded hybrid nanoparticles in the treatment of glioblastoma. *J. Neurol. Sci.* 381, 171–172
6 Tucker, C. *et al.* (2018) The intranasal route as an alternative method of medication administration. *Crit. Care Nurse* 38, 26–31
7 Battaglia, L. *et al.* (2018) Lipid nanoparticles for intranasal administration: application to nose-to-brain delivery. *Expert Opin. Drug Deliv.* 15, 369–378
8 Shankar, R. *et al.* (2018) Lipid nanoparticles: a novel approach for brain targeting. *Pharm. Nanotechnol.* 6, 81–93
9 Lakkadwala, S. and Singh, J. (2019) Co-delivery of doxorubicin and erlotinib through liposomal nanoparticles for glioblastoma tumor regression using an *in vitro* brain tumor model. *Colloids Surf. B Biointerfaces* 173, 27–35
10 Shah, M.K. *et al.* (2019) Lipid nanocarriers: preparation, characterization and absorption mechanism and applications to improve oral bioavailability of poorly water-soluble drugs. *Biomed. Appl. Nanoparticles* 2019, 117–147
11 Glaser, T. *et al.* (2017) Targeted nanotechnology in glioblastoma multiforme. *Front. Pharmacol.* 8, 166
12 He, Q. *et al.* (2018) Towards improvements for penetrating the blood–brain barrier — recent progress from a material and pharmaceutical perspective. *Cells* 7, 24
13 Pires, P.C. and Santos, A.O. (2018) Nanosystems in nose-to-brain drug delivery: a review of non-clinical brain targeting studies. *J. Control. Release* 270, 89–100
14 Md, S. *et al.* (2018) Nano-carrier enabled drug delivery systems for nose to brain targeting for the treatment of neurodegenerative disorders. *J. Drug Deliv. Sci. Technol.* 43, 295–310
15 Selvaraj, K. *et al.* (2018) Nose to brain transport pathways an overview: potential of nanostructured lipid carriers in nose to brain targeting. *Artif. Cells Nanomed. Biotechnol.* 46, 2088–2095
16 Mistry, A. *et al.* (2009) Effect of physicochemical properties on intranasal nanoparticle transit into murine olfactory epithelium. *J. Drug Target* 17, 543–552
17 Schwarz, B. and Merkel, O.M. (2019) Nose-to-brain delivery of biologics. *Future Sci.* 10, 207–210. http://dx.doi.org/10.4155/tde-2019-0013
18 Agrawal, M. *et al.* (2018) Nose-to-brain drug delivery: an update on clinical challenges and progress towards approval of anti-Alzheimer drugs. *J. Control. Release* 281, 139–177
19 Qindeel, M. *et al.* (2019) Development of novel pH-sensitive nanoparticles loaded hydrogel for transdermal drug delivery. *Drug Dev. Ind. Pharm.* 45, 1–29
20 Rizvi, S.A. and Saleh, A.M. (2018) Applications of nanoparticle systems in drug delivery technology. *Saudi Pharm. J.* 26, 64–70
21 Liao, W. *et al.* (2018) Recent advances on glioblastoma multiforme and nano-drug carriers: a review. *Curr. Med. Chem.* 25, 1–11. http://dx.doi.org/10.2174/0929867325666180514113136
22 Riaz, M. *et al.* (2018) Surface functionalization and targeting strategies of liposomes in solid tumor therapy: a review. *Int. J. Mol. Sci.* 19, 195
23 Madane, R.G. and Mahajan, H.S. (2016) Curcumin-loaded nanostructured lipid carriers (NLCs) for nasal administration: design, characterization, and *in vivo* study. *Drug Deliv.* 23, 1326–1334
24 Anand, A. *et al.* (2019) Brain targeted delivery of anticancer drugs: prospective approach using solid lipid nanoparticles. *IET Nanobiotechnol.* 13, 353–362
25 Sandoval, M.A. *et al.* (2012) EGFR-targeted stearoyl gemcitabine nanoparticles show enhanced anti-tumor activity. *J. Control. Release* 157, 287–296
26 Khan, A. *et al.* (2016) Brain targeting of temozolomide via the intranasal route using lipid-based nanoparticles: brain pharmacokinetic and scintigraphic analyses. *Mol. Pharm.* 13, 3773–3782
27 Sekerdag, E. *et al.* (2017) A potential non-invasive glioblastoma treatment: nose-to-brain delivery of farnesylthiosalicylic acid incorporated hybrid nanoparticles. *J. Control. Release* 261, 187–198
28 Crowe, T.P. *et al.* (2018) Mechanism of intranasal drug delivery directly to the brain. *Life Sci.* 195, 44–52
29 Samaridou, E. and Alonso, M.J. (2018) Nose-to-brain peptide delivery – the potential of nanotechnology. *Bioorg. Med. Chem.* 26, 2888–2905
30 Sousa, F. and Castro, P. (2016) Cell-based *in vitro* models for nasal permeability studies. In *Concepts and Models for Drug Permeability Studies* (Sarmento, B., ed.), pp. 83–100, Elsevier
31 Erdő, F. *et al.* (2018) Evaluation of intranasal delivery route of drug administration for brain targeting. *Brain Res. Bull.* 143, 155–170
32 Nayak, A.K. *et al.* (2019) Application of quality by design for the development of biopharmaceuticals. In *Pharmaceutical Quality by Design*. pp. 399–411, Elsevier
33 Csóka, I. *et al.* (2018) Extension of quality-by-design concept to the early development phase of pharmaceutical R&D processes. *Drug Discov. Today* 23, 1340–1343
34 Pallagi, E. *et al.* (2018) Initial risk assessment as part of the quality by design in peptide drug containing formulation development. *Eur. J. Pharm. Sci.* 122, 160–169
35 Saudagar, R. and Kulkarni, M.M. (2017) Review on *in-situ* nasal gel drug delivery system. *Res. J. Pharm. Technol.* 10, 1870
36 Palhal, A.P. *et al.* (2017) *In-situ* nasal gel: modernistic advancement in drug delivery. *World J. Pharm. Res.* 6, 566–577
37 Beier, C.P. *et al.* (2009) RNOP-09: pegylated liposomal doxorubicine and prolonged temozolomide in addition to radiotherapy in newly diagnosed glioblastoma – a Phase II study. *BMC Cancer* 9, 308
38 Yoshida, J. *et al.* (2004) Human gene therapy for malignant gliomas (glioblastoma multiforme and anaplastic astrocytoma) by *in vivo* transduction with human interferon β gene using cationic liposomes. *Human Gene Ther.* 15, 77–86
39 Jahangiri, A. *et al.* (2017) Convection-enhanced delivery in glioblastoma: a review of preclinical and clinical studies. *J. Neurosurg.* 126, 191–200
40 Aigner, A. and Kögel, D. (2018) Nanoparticle/siRNA-based therapy strategies in glioma: which nanoparticles, which siRNAs? *Nanomedicine* 13, 89–103
41 Song, J. *et al.* (2018) Effectiveness of lomustine and bevacizumab in progressive glioblastoma: a meta-analysis. *OncoTarget. Ther.* 11, 3435
42 Ju, R.-J. *et al.* (2016) Destruction of vasculogenic mimicry channels by targeting epirubicin plus celecoxib liposomes in treatment of brain glioma. *Int. J. Nanomed.* 11, 1131
43 Liu, Y. *et al.* (2016) Dual receptor recognizing cell penetrating peptide modified liposomes for anti-glioma therapy. *Nanomed. Nanotechnol. Biol. Med.* 2, 500
44 Li, X.-T. *et al.* (2014) Multifunctional targeting daunorubicin plus quinacrine liposomes, modified by wheat germ agglutinin and tamoxifen, for treating brain glioma and glioma stem cells. *Oncotarget* 5, 6497
45 Pacheco-Torres, J. *et al.* (2015) Image guided drug release from pH-sensitive ion channel-functionalized stealth liposomes into an *in vivo* glioblastoma model. *Nanomed. Nanotechnol. Biol. Med.* 11, 1345–1354
46 Chen, P.-Y. *et al.* (2012) Comparing routes of delivery for nanoliposomal irinotecan shows superior anti-tumor activity of local administration in treating intracranial glioblastoma xenografts. *Neuro Oncol.* 15, 189–197
47 Chen, H. *et al.* (2011) Lactoferrin modified doxorubicin-loaded procationic liposomes for the treatment of gliomas. *Eur. J. Pharm. Sci.* 44, 164–173
48 Kuo, Y.-C. and Liang, C.-T. (2011) Inhibition of human brain malignant glioblastoma cells using carmustine-loaded catanionic solid lipid nanoparticles with surface anti-epithelial growth factor receptor. *Biomaterials* 32, 3340–3350
49 Kuo, Y.-C. and Lee, C.-H. (2015) Inhibition against growth of glioblastoma multiforme *in vitro* using etoposide-loaded solid lipid nanoparticles with ρ-aminophenyl-α-D-manno-pyranoside and folic acid. *J. Pharm. Sci.* 104, 1804–1814
50 Kuo, Y.-C. and Wang, C.-C. (2015) Carmustine-loaded catanionic solid lipid nanoparticles with serotonergic 1B receptor subtype antagonist for *in vitro* targeted delivery to inhibit brain cancer growth. *J. Taiwan Inst. Chem. Eng.* 46, 1–14
51 Sharma, P. *et al.* (2011) Development and evaluation of nanostructured lipid carriers of cytarabine for treatment of meningeal leukemia. *J. Nanosci. Nanotechnol.* 11, 6676–6682

Please cite this article in press as: Sabir, F. et al. Nose-to-brain delivery of antiglioblastoma drugs embedded into lipid nanocarrier systems: status quo and outlook, Drug Discov Today (2019), https://doi.org/10.1016/j.drudis.2019.10.005

52 Jin, J. *et al.* (2011) *In vivo* specific delivery of c-Met siRNA to glioblastoma using cationic solid lipid nanoparticles. *Bioconj. Chem.* 22, 2568–2572
53 Martins, S.M. *et al.* (2013) Brain targeting effect of camptothecin-loaded solid lipid nanoparticles in rat after intravenous administration. *Eur. J. Pharm. Biopharm.* 85, 488–502
54 Khajavinia, A. *et al.* (2012) Targeting etoposide to acute myelogenous leukaemia cells using nanostructured lipid carriers coated with transferrin. *Nanotechnology* 23, 405101
55 Griveau, A. *et al.* (2013) Silencing of miR-21 by locked nucleic acid–lipid nanocapsule complexes sensitize human glioblastoma cells to radiation-induced cell death. *Int. J. Pharm.* 454, 765–774
56 Chen, Y. *et al.* (2016) Nanostructured lipid carriers enhance the bioavailability and brain cancer inhibitory efficacy of curcumin both *in vitro* and *in vivo*. *Drug Deliv.* 23, 1383–1392
57 Jose, S. *et al.* (2014) *In vivo* pharmacokinetics and biodistribution of resveratrol-loaded solid lipid nanoparticles for brain delivery. *Int. J. Pharm.* 474, 6–13
58 Chirio, D. *et al.* (2014) Positive-charged solid lipid nanoparticles as paclitaxel drug delivery system in glioblastoma treatment. *Eur. J. Pharm. Biopharm.* 88, 746–758
59 Cohen, Z.R. *et al.* (2015) Localized RNAi therapeutics of chemoresistant grade IV glioma using hyaluronan-grafted lipid-based nanoparticles. *ACS Nano* 9, 1581–1591
60 Song, S. *et al.* (2016) Novel RGD containing, temozolomide-loading nanostructured lipid carriers for glioblastoma multiforme chemotherapy. *Drug Deliv.* 23, 1404–1408
61 Wu, M. *et al.* (2016) Vincristine and temozolomide combined chemotherapy for the treatment of glioma: a comparison of solid lipid nanoparticles and nanostructured lipid carriers for dual drugs delivery. *Drug Deliv.* 23, 2720–2725

Please cite this article in press as: Sabir, F. et al. Nose-to-brain delivery of antiglioblastoma drugs embedded into lipid nanocarrier systems: status quo and outlook, Drug Discov Today (2019), https://doi.org/10.1016/j.drudis.2019.10.005

ANNEX-II

molecules

MDPI

Article

Quality-by-Design-Based Development of n-Propyl-Gallate-Loaded Hyaluronic-Acid-Coated Liposomes for Intranasal Administration

Fakhara Sabir [1], Gábor Katona [1], Edina Pallagi [1], Dorina Gabriella Dobó [1], Hussein Akel [1], Dániel Berkesi [2], Zoltán Kónya [2] and Ildikó Csóka [1,*]

[1] Faculty of Pharmacy, Institute of Pharmaceutical Technology and Regulatory Affairs, University of Szeged, H-6720 Szeged, Hungary; fakhra.sabir@gmail.com (F.S.); katona.gabor@szte.hu (G.K.); edina.pallagi@pharm.u-szeged.hu (E.P.); dobo.dorina@pharm.u-szeged.hu (D.G.D.); hussein.akel@hotmail.com (H.A.)

[2] Faculty of Science and Informatics, Department of Applied & Environmental Chemistry, University of Szeged, H-6720 Szeged, Hungary; daniel.berkesi@chem.u-szeged.hu (D.B.); konya@chem.u-szeged.hu (Z.K.)

* Correspondence: csoka.ildiko@szte.hu; Tel.: +36-62-546-116

Abstract: The present study aimed to develop n-propyl gallate (PG)-encapsulated liposomes through a novel direct pouring method using the quality-by-design (QbD) approach. A further aim was to coat liposomes with hyaluronic acid (HA) to improve the stability of the formulation in nasal mucosa. The QbD method was used for the determination of critical quality attributes in the formulation of PG-loaded liposomes coated with HA. The optimized formulation was determined by applying the Box–Behnken design to investigate the effect of composition and process variables on particle size, polydispersity index (PDI), and zeta potential. Physiochemical characterization, in vitro release, and permeability tests, as well as accelerated stability studies, were performed with the optimized liposomal formulation. The optimized formulation resulted in 90 ± 3.6% encapsulation efficiency, 167.9 ± 3.5 nm average hydrodynamic diameter, 0.129 ± 0.002 PDI, and −33.9 ± 4.5 zeta potential. Coated liposomes showed significantly improved properties in 24 h in an in vitro release test (>60%), in vitro permeability measurement (420 μg/cm^2) within 60 min, and also in accelerated stability studies compared to uncoated liposomes. A hydrogen-peroxide-scavenging assay showed improved stability of PG-containing liposomes. It can be concluded that the optimization of PG-encapsulated liposomes coated with HA has great potential for targeting several brain diseases.

Keywords: intranasal delivery; hyaluronic acid; scavenging assay; risk assessment; in vitro release study

Citation: Sabir, F.; Katona, G.; Pallagi, E.; Dobó, D.G.; Akel, H.; Berkesi, D.; Kónya, Z.; Csóka, I. Quality-by-Design-Based Development of n-Propyl-Gallate-Loaded Hyaluronic-Acid-Coated Liposomes for Intranasal Administration. *Molecules* **2021**, *26*, 1429. https://doi.org/10.3390/molecules26051429

Academic Editor: Abdelwahab Omri

Received: 1 February 2021
Accepted: 2 March 2021
Published: 6 March 2021

1. Introduction

Intranasal delivery has been considered as one of most suitable alternative drug delivery routes to directly access the brain, bypassing the blood–brain barrier (BBB) [1–3]. This route of administration has the potential to deliver active pharmaceutical agents in higher concentrations in several brain diseases, including tumor and neurodegenerative diseases as Alzheimer's and Parkinson's diseases. In overcoming the difficulties of brain targeting arising from the physiological defense mechanism of the BBB, the quality-by-design (QbD) methodology offers a suitable tool to develop more appropriate and efficient carrier systems [2,4]. For that purpose, liposomes are considered as the most suitable carrier due to their increased bioavailability, scalability, and high stability [5,6]. The lipid carrier system is well tolerated through intranasal administration, and it can minimize cytotoxicity compared to other nanoparticles. Lipid nanoparticles have a wide range of particle sizes, from 50 to 1000 nm [7]. However, for nose-to-brain delivery via axonal transport, the particle size range between 50 and 700 nm is the most suitable [8].

Hyaluronic acid (HA) is a naturally occurring biopolymer in living organisms. Its advantageous properties, including muco-adhesion, biocompatibility, and targetability to HA receptors (CD44), which are highly expressed in various tumor and stem cells, support intranasal application. The coating of liposomes with HA increases their negative zeta potential due to the addition of the negative carboxylate residue of HA on the surface of the liposomes, thereby increasing directly their stability [9]. A novel bottom-up method of preparation called the direct pouring method (DPM) is a modified form of the solvent injection and emulsification method but quite feasible as it avoids the use of extra size reduction, extrusion, or filtration techniques. DPM involves two simple steps, the solubilization of lipids into the organic phase and the direct pouring of the organic phase into the aqueous phase along with the evaporation of the organic solvents, as shown in Figure 1.

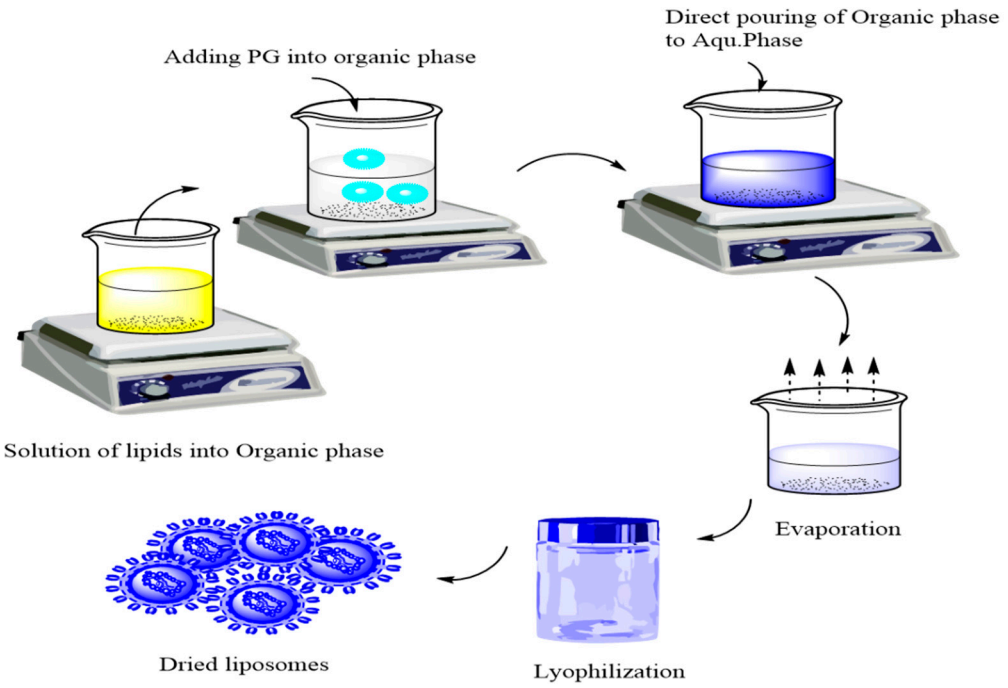

Figure 1. Direct pouring method for preparation of liposomes.

n-Propyl gallate (PG), also known as propyl 3,4,5-tri-hydroxybenzoate, an ester form of gallic acid and propanol, functions as a synthetic antioxidant and preservative, can inhibit nucleic acid synthesis in micro-organisms, and prevent their growth [10]. PG can be promising in the treatment of brain tumors, e.g., glioblastoma multiforme, as long as it can reach the brain. Alternative administration routes are preferred as previously a slight toxic effect was reported in the case of oral administration [11]. For that purpose, the intranasal route can be effective. PG's nose-to-brain applicability is supported by its low molecular weight (212.2 g/mol), lipophilic character (logP = 1.8), and pKa (7.94); as a result, the non-ionized fraction of the drug dominates in nasal conditions (pH = 5.5–6.5), enhancing absorption. However, PG is particularly insoluble in water, and it is sensitive to the nasal environment because of its hydrogen donor nature. Therefore, suitable carriers, such as liposomes, are required to enhance its stability in and affinity for biological membranes and, moreover, to increase its concentration at the target site, eliminating local irritation [12]. Previous studies showed that PG may contribute to mitochondrial impairment and the inhibition of cellular respiration. PG has proven efficacy and has vital anti-cancer effects on various cancer cells that may lead to DNA genotoxicity, cytotoxicity, and fragmentation [13]. It also has been revealed that PG used with other antitumor agents in various in vivo studies exhibited significant efficacy in gastrointestinal tract cancer. The anti-cancer mechanism of

PG is based on inhibition of the cell growth cycle via the production of reactive oxygen species and the stimulation of the autophagy of malignant cells [10,14].

The QbD concept as a risk-and-knowledge-based quality management method aims to achieve the desired product quality and fulfill the therapeutic need. The data from previous studies have revealed that this approach can be applied during all formulation development stages [15–17]. The QbD-based formulation strategy involves the following stages: (1) defining and identifying the quality target product profile (QTPP) based on the past literature and appropriate bioinformatics relevance, (2) defining the product design and development process according to a predefined product profile, (3) identifying potential critical quality attributes (CQAs) and critical process parameters (CPPs) and performing a risk assessment (RA), (4) setting up with the help of RA results practical development (the design-of-experiments step of the method) and implementing it in accordance with the most relevant factors (CPPs, CQAs) selected by RA to define the design space, (5) developing a process control strategy to ensure persistent product quality, and (6) managing the product quality during its shelf life [18,19].

As stated by International Conference for Harmonisation (ICH) guidelines, the development of novel drug delivery systems should be supervised heavily under quality control methods, for which QbD provides a suitable tool [20–22]. In the case of liposomal formulations, there are many risk factors that should be taken into account, including particle characteristics, structure, dissolution and permeability profiles, and the production procedure as well. With the help of QbD, the product can meet the criteria of liposomal formulations, the nose-to-brain delivery pathway, and the enhanced therapeutic effect. The main advantage of using QbD lies in the fact that it is a continuous feedback system that could eliminate the possibility of errors at an early stage of production. With early set criteria, proper particle characteristics with optimized size and size distribution along with a zeta potential value of PG-loaded liposomes can be ensured, representing high stability in colloidal solution form. Besides, the structure of the final product in solid form is also crucial in connection with solubility, particularly its dissolution and absorption profile. Qbd-driven optimization of liposomes for the nasal administration route has already been successfully applied in a previous study [23].

This study focused on the QbD-based development of PG-loaded liposomes coated with HA for intranasal delivery. The coating of liposomes with hyaluronic acid can improve their stability by reducing macrophage uptake after absorption from the nasal mucosa. Moreover, it can enhance the targetability of the nanocarrier. In addition, the use of QbD strengthens the validation of the novel method (DPM) for the development of HA-coated liposomes [18,24,25].

2. Results

2.1. Initial Knowledge Space Development

Several different factors could have a significant impact on the quality of a PG-containing liposomal formulation for nasal administration (Figure 2).

The collected factors presented in the Ishikawa diagram include all the possible critical factors affecting the final quality of the coated liposomal formulation. It was developed following the recent scientific data regarding coating and nose-to-brain delivery and helps in recognizing the cause-and-effect relationship between the aimed product and its influencing factors. Based on the fishbone diagram, QTPPs can be selected. These selected parameters with their targets and their justification are listed in Table 1.

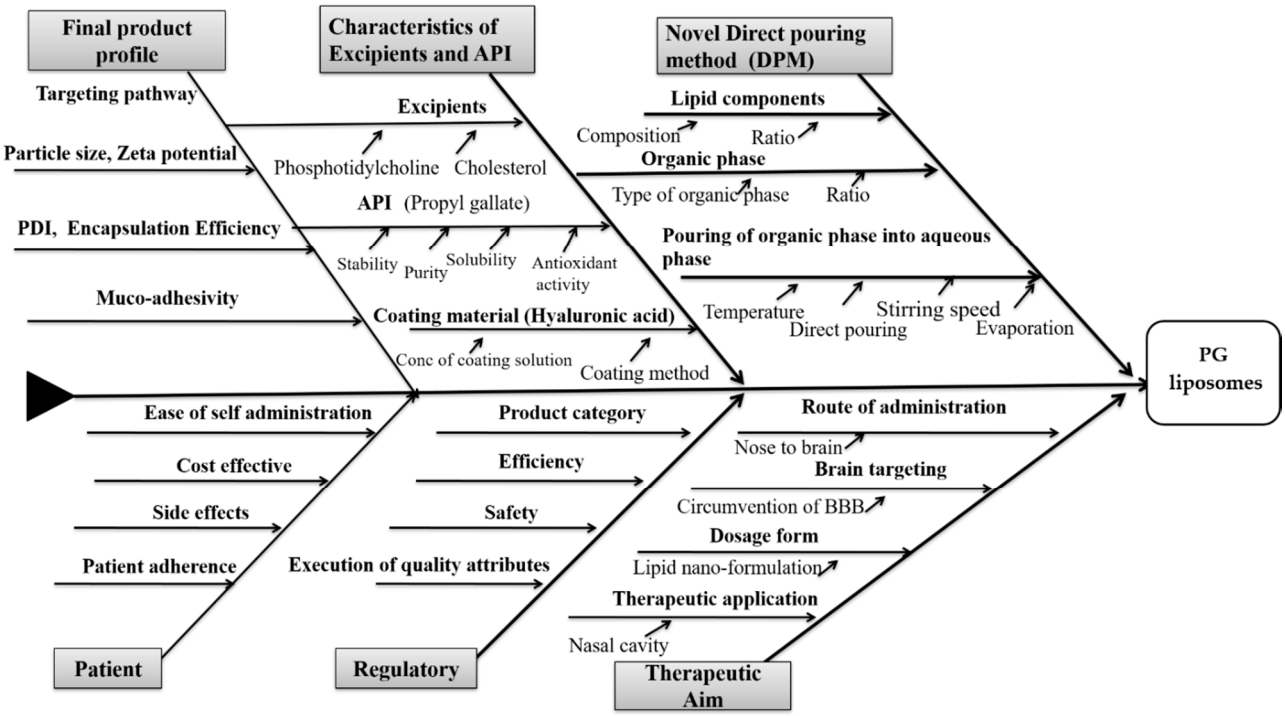

Figure 2. Ishikawa diagram showing the cause-and-effect relationships between influencing factors of hyaluronic acid (HA)-coated, n-propyl gallate (PG)-loaded liposomes for nose-to-brain drug delivery.

Table 1. Selection of quality target product profiles (QTPPs) of PG-loaded liposomes for nose-to-brain delivery, along with respective target and justification.

QTPP	Target	Justification
Therapeutic effect	The CNS (the model API is PG)	Circumvention of the blood–brain barrier (BBB). PG has antioxidant and anti-inflammatory activity that are essential in the treatment of cancer [26].
Administration route	Nasal administration (nose-to-brain delivery)	Non-invasive, direct, and more effective route of administration than other invasive routes. Nanoparticles are transported from endothelial cells to the olfactory neurons via endocytosis or pinocytosis and move along the axon or follow the trigeminal nerve pathway [27,28].
Dosage form	Liquid nano-formulation	Enhanced biocompatibility, high scalability, safety, and efficacy of lipid nanoparticles. A liquid formulation is more feasible for nose-to-brain administration [29].
Coated lipid nanoparticles	Enhanced stability	The hyaluronic acid (HA) coating will enhance the stay time within the nasal mucosa. Active target delivery at the CD44 receptor is possible via coating with HA. Additionally, it will synergize stability [30].
Targeting pathway	Preferred particle size range 100–700 nm	Nanoparticles within the range of 20–200 nm can follow clathrin-coated pits, and nanoparticles in the size range of 200–1000 nm can be transported via caveolae-mediated endocytosis.

The present study considered the following CQAs, depending upon the predefined goals and therapeutic needs: excipients (phospholipids, cholesterol as its quality may affect the end product profile), coating material, Z-average, zeta potential, polydispersity index (PDI), and aqueous phase. All these factors are relevant to the quality of the product [24,31]. The process variables of the following new approach included the sonication time (for mixing lipids into the organic phase), temperature (for evaporation), and rotations per minute (rpm) of the hot plate (speed of rotation for evaporation).

2.2. Results of Risk Assessment

After determination of the impact (H, M, L) of the QTPPs and evaluation of the CPPs and CQAs, RA was applied in order to follow the QbD-based formulation design and development. For RA, an estimation of the interdependence between the QTPP elements and CQAs and between the CQAs and critical material attributes (CMAs/CPPs) was made first by using the previously mentioned 3-grade scale, as their impact on each other is high, medium, or low. The assessment of the level of effect depends on the scientific knowledge in the literature and experimental experience. The occurrence of the CPPs was also estimated. Based on the observations, the severity or impact score for each factor determining the final liposomal product was calculated. The severity scores and their order are shown in Pareto charts generated by the software. In this case, these scores for every CQA and CPP are shown in Pareto charts in Figure 3. The Pareto chart principle known as the 80/20 rule describes that for many events, 80% of the effects come from 20% of the causes. These 20% of critical factors require 80% of focused measurement in the drug development process. The rankings presented in the charts of Figure 3 helps to create a priority list by the factors' having critical effect on the aimed end product and describe the influencing properties of each factor. The order of the CQAs is shown (Figure 3a); the quantity of phospholipids, cholesterol, and active pharmaceutical ingredients (APIs) has the same and highest critical effect on the required quality of the final product. A lower critical effect is exerted on product quality by the rest of the factors in the diagram: the coating material, zeta potential, and aqueous phase. Figure 3b shows the rankings of the CPPs related to the present liposome development process. It shows that the temperature of the DPM has the greatest critical effect on the final product. After temperature, the rotation speed for both mixing and evaporation has been shown as having an almost equal effect on product quality, while the severity score is the lowest for mixing sonication time, indicating that this factor has the least effect on the final quality of the end product. Depending on the result of the previously presented initial RA, the factors for the Box–Behnken design (BBD) of the experiment could be selected.

2.3. Design of Experiments: Box–Behnken Design

The RA results helped to align the experimental design. The critical factors with the highest severity scores were selected to screen the effects of the formulation parameters on the quality of the final coated liposomal formulation. These were the following: the quantity of phospholipids (L-α-phosphatidylcholine (PC)) and the quantity of cholesterol (mg) selected from the CQAs, and the temperature (°C) of evaporation taken from the CPPs as variable X_2. According to our selection methodology, the Z-average, PDI, and zeta potential were selected as dependent factors. The highly significant parameters were selected after applying QbD and subjected to screening with respect to the obtained optimized formula for all studied variables within accepted ranges. BBD screening was validated by ANOVA for each factor (ANOVA table obtained from the design of experiments (DOE) results). Table 2 shows all the values of responses for 15 runs of BBD.

CQA \ QTPP	Therapeutic Effect	Route of Administration	Dosage form	Coated Liposomes	Targeting Pathway
Coating material 12 %	High	Medium	Low	High	Medium
Phospholipids 18 %	Low	High	Low	High	High
Cholesterol 9 %	Low	Low	Low	High	Low
API 13 %	High	High	Medium	Low	Medium
Zeta potential 14 %	High	Medium	Medium	High	Medium
Aqueous phase 4 %	Low	Low	Low	Medium	Low
Particle Size 20 %	High	High	Low	High	High
PDI 9 %	Low	Low	Low	High	Low

Process		Organic phase preparation	Mixing of organic and aqueous phase	Evaporation	
CQA \ CPP		Sonication time	Stirring speed	Stirring speed	Temperature
		21 %	22%	23%	34%
Coating material	12 %	Low	Medium	Low	Medium
Phospholipids	18 %	Medium	Medium	Medium	High
Cholesterol	9 %	Medium	High	Medium	High
API	13 %	Medium	Low	Low	Medium
Zeta potential	14 %	High	High	High	High
Aqueous phase	4 %	Low	High	High	High
Particle Size	20 %	High	Medium	High	High
PDI	9 %	High	Medium	High	High

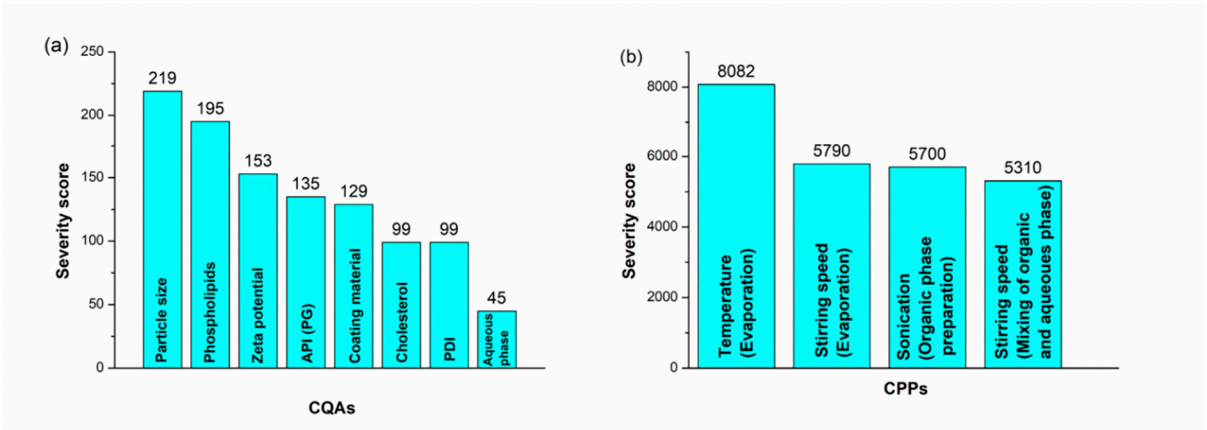

Figure 3. Interdependence rating and estimation of QTPP elements and critical quality attributes (CQAs) and of CQAs and critical process parameters (CPPs), and Pareto charts showing the severity/impact among selected (**a**) CQAs and (**b**) CPPs.

Table 2. Z-average, polydispersity index (PDI), and zeta potential of 15 runs on the design of experiments.

Number of Runs	Temperature (°C)	Amount of Phospholipids (mg)	Amount of Cholesterol (mg)	Z-Average (nm) *	PDI *	Zeta Potential (mV) *
1	50	16	16	150 ± 10	0.27 ± 0.01	−22 ± 8.4
2	70	16	16	155 ± 5.5	0.28 ± 0.02	−18 ± 6.5
3	50	32	16	145 ± 4.5	0.29 ± 0.02	−23 ± 8.4
4	70	32	16	140 ± 5.5	0.28 ± 0.05	−24 ± 8.4
5	50	24	8	125 ± 6.6	0.25 ± 0.07	−27 ± 7.5
6	70	24	8	125 ± 7.8	0.22 ± 0.01	−28 ± 8.5
7	50	24	24	400 ± 8.8	0.40 ± 0.08	−8 ± 10.2
8	70	24	24	450 ± 22	0.45 ± 0.09	−7 ± 12
9	60	16	8	121 ± 2.3	0.24 ± 0.08	−33 ± 5.5
10	70	32	8	123 ± 2.4	0.25 ± 0.06	−28 ± 6.5
11	60	16	24	430 ± 40	0.55 ± 0.08	−6 ± 10
12	60	32	24	420 ± 20	0.49 ± 0.05	−8 ± 10.2
13	60	24	16	130 ± 12	0.21 ± 0.01	−29 ± 3.3
14	80	24	16	135 ± 10	0.22 ± 0.02	−26 ± 5.5
15	70	24	16	142 ± 8	0.27 ± 0.02	−25 ± 6.2

* Data are the mean ± SD (n = 3 independent formulations).

2.4. Influence of Investigated Parameters on the Z-Average, PDI, and Zeta Potential

The result of the significance of effects for each variable explained the interdependence between the studied independent and dependent responses. In colloidal drug delivery systems, the Z-average is closely related to the particle size; therefore, a change in it can indicate changes in the primary particle size as well. Based on the BBD results, an optimized colloidal stable system was obtained. At a lower concentration of PC, a higher Z-average was obtained, but as the concentration of the phospholipids was increased up to a significant amount, the Z-average decreased to 130 nm. A further increase in the amount of phospholipids led to the formation of particles of large sizes, as shown in Figure 4a. Phospholipids act as a surfactant and result in higher solubility at the interface of two phases, leading to a reduced Z-average. However, as the concentration of phospholipids increased, due to higher viscosity, the Z-average increased. The effect of temperature was similar; at a lower temperature, a larger Z-average was observed, but its size decreased with an increase in temperature during the process. The surface polynomial (Equation (1)) obtained for the fitted full model explaining the effect of formulation and process variables on the mean Z-average is:

$$Z - average = 231.82 + 11.9x_1 - 7.239x_2 + 301.73x_3 - 4.88x_1x_2 + 24.88x_1x_3 - 5.52x_2x_3 - 9.87x_1^2 - 8.7x_2^2 - 136.2x_3^2 \quad (1)$$

with R^2 = 0.998, adjusted R^2 = 0.996, and mean square (MS) = 85.858.

The influence of phospholipids, cholesterol, and temperature on the PDI was also investigated (Figure 4b).

At average or moderate values of these three factors, the PDI value fell within the optimum range, while at the two extremities, the PDI value was high. According to the following results, only cholesterol had a significant effect on the variation in the PDI.

The polynomial equation (Equation (2)) obtained for the fitted full model demonstrating the effect of formulation variables on the PDI is:

$$PDI = 0.334 + 0.0089x_1 + 0.0015x_2 + 0.2233x_3 - 0.0194x_1x_2 + 0.049x_1x_3 - 0.0531x_2x_3 + 0.0089x_1^2 - 0.0513x_2^2 - 0.1013x_3^2t \quad (2)$$

with R^2 = 0.969, adjusted R^2 = 0.901, and MS = 0.001.

The effect of phospholipids, cholesterol, and temperature on the zeta potential was also studied and is shown in the corresponding coefficient obtained from the DOE (Figure 4c). The

coefficient showed that temperature and cholesterol had a significant effect on the stability of liposomes as compared to the concentration of phospholipids.

The polynomial equation (Equation (3)) obtained for the fitted full model demonstrating the influence of formulation variables on the zeta potential is:

$$Zeta\ potential = 19.6 + 0.491x_1 - 1.67x_2 + 22.42x_3 - 2.71x_1x_2 + 1.216x_1x_3 - 2.141x_2x_3 - 4.43x_1^2 - 2.76x_2^2 - 7.016x_3^2 \quad (3)$$

with R^2 = 0.972, adjusted R^2 = 0.948, and MS = 4.508.

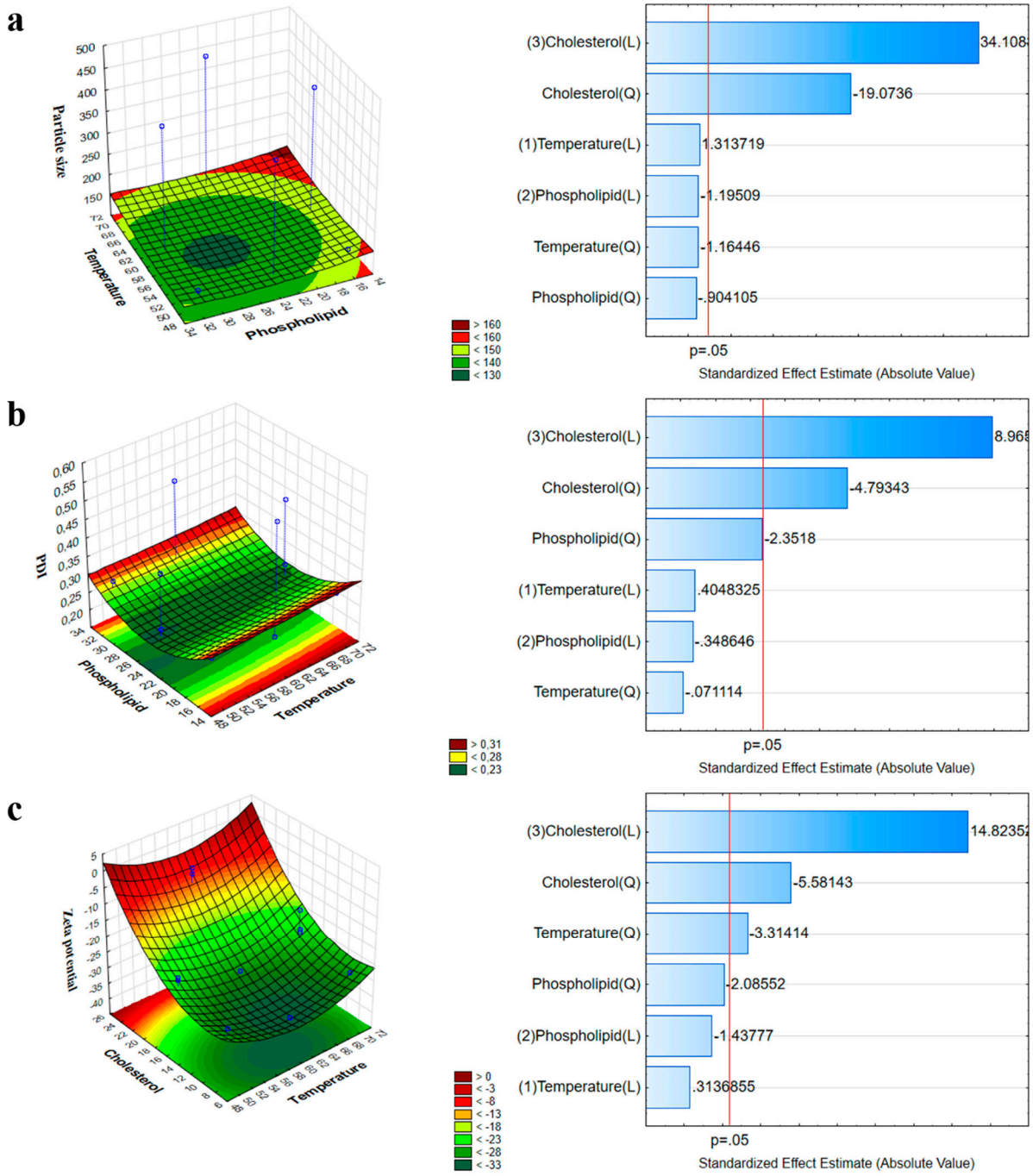

Figure 4. Three-dimensional surface plot and Pareto chart showing the combined impact of phospholipids and temperature on the Z-average (**a**), on the PDI (**b**), and on the zeta potential (**c**).

The surface plot shows that the zeta potential of the formulation is significantly dependent on the applied amount of phospholipids and the process temperature. The formulation of liposomes with a low concentration of cholesterol at 60 °C resulted in a stable lowest surface charge and, therefore, increased stability.

2.5. Characterization of Z-Average, PDI, and Zeta Potential and Analysis of Coated and Uncoated Liposomes

The Z-average, PDI, and zeta potential were measured both for optimized PG-loaded uncoated and HA-coated liposomes. The Z-average of uncoated liposomes was reported as 135.2 ± 5.2 nm, with a PDI of 0.094 ± 0.001 and a zeta potential of −29.9 ± 5.8 mV, and of coated liposomes was found to be 167.9 ± 3.5 nm, with a PDI of 0.129 ± 0.002 and a zeta potential of −33.6 ± 4.5 mV (Table 3.). All the results met the standard set criteria, as mentioned above. The Z-average range was between 123 ± 2.5 nm and 300 ± 3.3 nm. The particle size of uncoated liposomes was lower, as mentioned in the previous section, than that of coated ones, which showed that the HA coating of liposomes was successful. The PDI was lower for optimized liposomes, which indicated a more uniform vesicle size for the final formulation. The zeta potential of coated liposomes was higher than that of uncoated liposomes, which showed increased stability of coated liposomes.

Table 3. Analysis of particle size, PDI, and zeta potential of uncoated and coated liposomes.

Formulation	Z-Average * (nm)	PDI *	Zeta Potential * (mV)
Uncoated liposomes	135.2 ± 5.2	0.094 ± 0.001	−29.9 ± 5.8
Coated liposomes	167.9 ± 3.5	0.129 ± 0.002	−33.6 ± 4.5

* Data are the mean ± SD (n = 3 independent formulations).

2.6. Determination of Acetone Residual in the Formulations

As acetone belongs to Class 3 solvents, its residual concentration should be less than 5000 ppm in the daily dose of the final product, a requirement of the International Conference for Harmonisation (ICH) Q3C (R5) guideline for residual solvents. The residual acetone content was determined in both coated and uncoated formulations using gas chromatography, shown in Table 4.

Table 4. Concentration of residual organic solvent in the optimized formulations.

Formulation	Acetone (ppm)	Maximum Residual Level * (ppm)
Uncoated liposomes	442 ppm	5000
Coated liposomes	47 ppm	

* Based on the International Conference for Harmonisation (ICH) Q3C (R5).

Both results were high under the standard criteria of maximum allowed residual level, supporting the applicability of the DPM for the preparation of liposomes.

2.7. Encapsulation Efficiency, Percentage Yield, and Drug-Loading Analysis

The encapsulation efficiency was found to be 90 ± 3.6% and showed very good results for PG-loaded liposomes. The percentage yield was 71.33 ± 1.52%, which also indicates that the results of PG-loaded liposomes were within the aimed criteria. The drug-loading capacity of the liposomes was 2.81%, which can be associated with a higher amount of lipid applied for the wall-forming agent. The measured encapsulation efficiency (EE) of the optimized formulation was higher, with the purpose of having a high amount of the drug at the site of action [32].

2.8. Fourier-Transform Infrared Spectroscopy (FTIR) Spectroscopy Analysis

The FTIR spectra of the components of coated and uncoated liposomes are presented in Figure 5a. Each spectrum includes two different regions. The high-wave-number part of the spectrum (3000–2800 1/cm) derives from C-H stretching vibrations only. In turn, it mainly originates from the hydrocarbon chains. The low-wave-number region of the spectrum (below 1800 1/cm) shows the fingerprint region. The ester ν (C=O) is usually the strongest peak, followed by the phosphate contributions near 1240 1/cm ($\nu_{as}(PO^{2-})$) and 1090 1/cm ($\nu_{s}(PO^{2-})$). The peaks at ~900–600 1/cm are essentially coherent to the polar head groups of the lipids. The hydrocarbon chains do contribute near 1465 1/cm, but all-trans conformations absorb near 1470 1/cm, where there is C–H deformation of CH_2. The contribution of the lipid hydrocarbon chains is present in various spectral regions (3000–2800 1/cm). This region contains C-H stretching bands from different vibrational modes: ν_{as} (CH_2) near 2920 1/cm, ν_{s} (CH_2) near 2850 1/cm, ν_{as} (CH_3) near 2960 1/cm, and $\nu_{s}(CH_3)$ near 2870 1/cm. Compatibility study results showed that there was no interaction between the formulation components. The spectra of coated liposomes showed peaks at ~1650 1/cm (amide I of the α-helical region) and 1050 1/cm (C-O-C stretching vibrations of the α-glucopyranose structure), that could not be observed in the spectra of uncoated liposomes, suggesting that the HA coating was successfully performed.

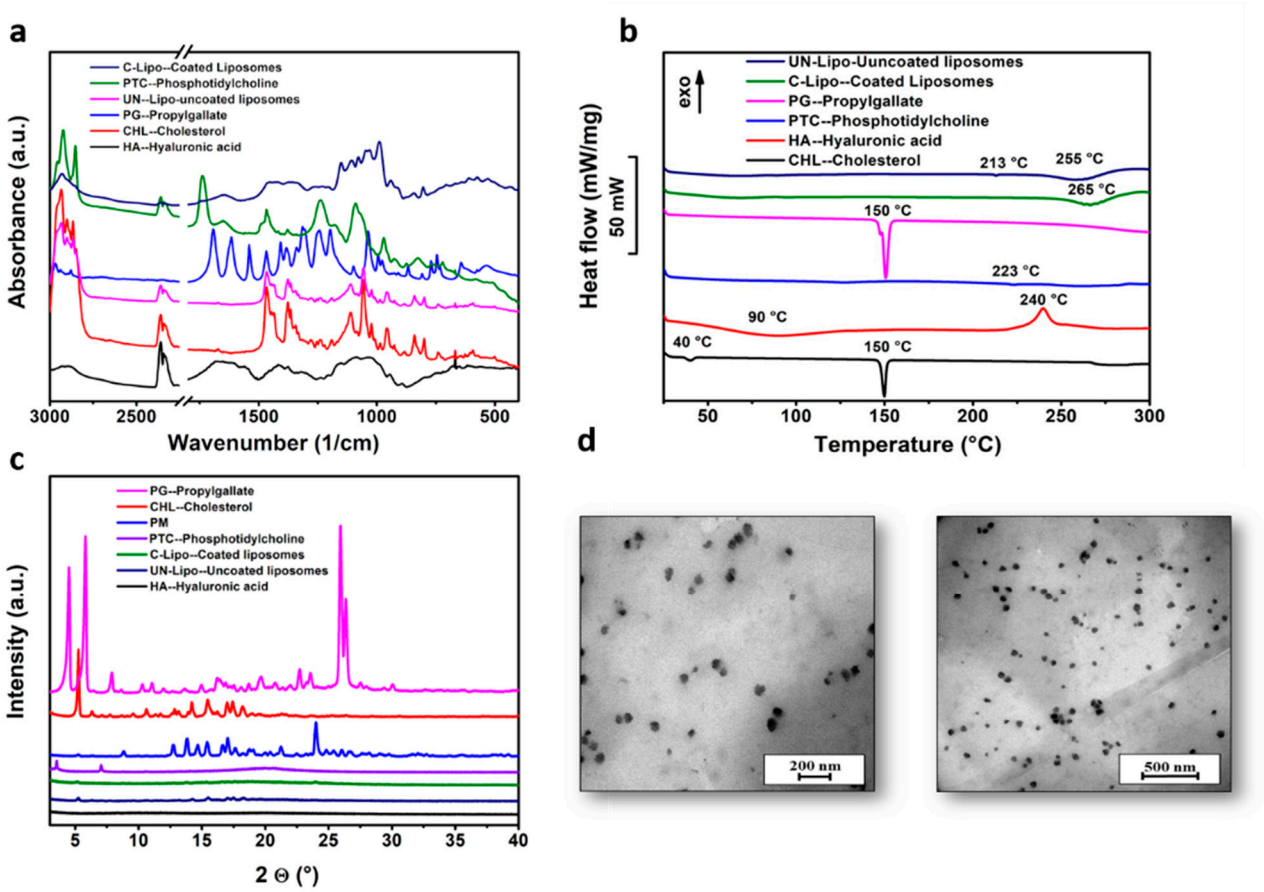

Figure 5. Fourier-transform infrared spectroscopy (FTIR) spectra (**a**), differential scanning calorimetry (DSC) thermograms (**b**), and X-ray powder diffraction (XRPD) diffractograms of coated and uncoated liposomes and components of liposomal formulation (**c**), and transmission electron microscopy (TEM) images of liposomes at different resolution scales (**d**).

2.9. Differential Scanning Calorimetry (DSC) Analysis Results

The thermal behavior of PG, cholesterol, PC, HA, and liposomes coated and uncoated with HA was investigated with DSC (Figure 5b). The endothermic peaks at 150 °C on the DSC curves of PG and cholesterol correspond to their melting points. PC and HA did not exhibit any distinct melting event, possibly due to their non-crystalline nature, while an endothermic peak at 223 °C (PC) and an exothermic peak at 240 °C (HA) was observed due to their degradation pattern. The decomposition of HA can also be observed on the DSC curves of liposomes at 255 °C (uncoated) and 265 °C (coated), but the decomposition of PC as a wall-forming agent was only detected in the case of uncoated liposomes at 213 °C. HA coating increased the thermal stability of liposomes and prevented them from degradation until 265 °C. Since the thermograms of PG-loaded liposomes did not display any endothermic peaks at 150 °C compared to the pure PG thermogram, the encapsulation of PG in the liposomes was indicated.

2.10. X-ray Powder Diffraction (XRPD) Analysis Results

XRPD studies showed the crystalline nature of PG and cholesterol and the amorphous nature of PC and HA as coating materials in accordance with the DSC results, as shown in Figure 5c. In the diffractograms of uncoated and coated liposomes, the characteristic peaks of cholesterol (at 5.18, 13.8, 15.34, 16.6, 17, and 17.6 2θ) as a wall-forming agent can be observed, but in the case of coated liposomes, these peaks disappeared. The characteristic peaks of PG could be detected in the liposomal formulations, which shows that the drug was encapsulated.

2.11. Morphology of Liposomes

The transmission electron microscopy (TEM) images of PG-loaded liposomes with coating and without coating showed the spherical shape and uniform distribution of liposomes, as shown in Figure 5d, showing a monodisperse distribution without any aggregation. The TEM images revealed that particle sizes were ~100–120 nm. The morphological study via TEM revealed that particle sizes were ~100–120 nm. The results of TEM images were comparable with the dynamic light scattering (DLS) results and were within the nano-range (the Z-average values were ~135 2 ± 5.2 and 167 ± 3.5 nm), underlining that the acquired Z-average results are suitable for explaining the effects of synthesis parameters on particle size.

2.12. In Vitro Release Studies

In vitro release studies of uncoated and HA-coated liposomes showed 75% and 60% drug release within 24 h, respectively, in simulated nasal electrolyte solution (SNES) (pH 5.6), as shown in Figure 6a, while 80% of the drug was released within 48 h from coated liposomes. The release of PG from solution was significantly lower (10% within 24 h) in comparison to other liposomal formulations. Drug release kinetics were determined by fitting kinetic models, and data were evaluated by the correlation coefficient (R^2) (Table 5). R^2 values were used as a standard to choose the best model to describe drug release from the liposomes and the drug solution. In the case of uncoated and HA-coated liposomes, the R^2 obtained for fitting the release data of PG to the Higuchi model indicated that drug release from the liposomes was diffusion controlled, as shown in Table 5. In vitro release study results have shown that the slower release from coated liposomes is due to the restriction of water diffusion into the carrier matrix, which subsequently slows down the drug release rate. Another possible reason is that coating adds a barrier against drug diffusion with regard to the electrostatic interaction between the positively charged PC and the negatively charged HA [33]. The kinetic model data evaluated the release of PG following the diffusion-controlled release, as shown in Table 5.

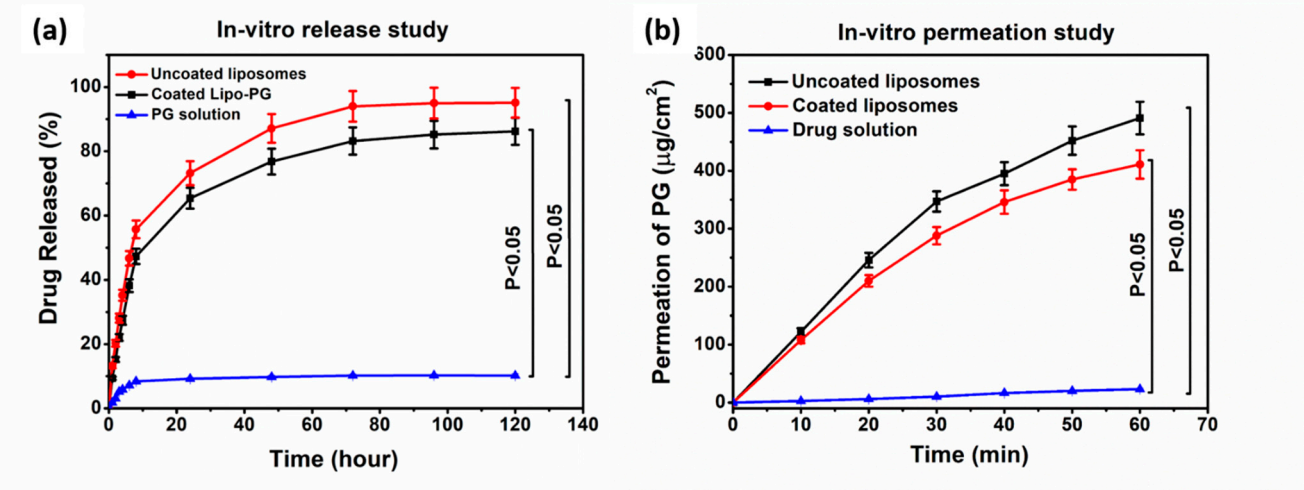

Figure 6. In vitro release study of PG in phosphate buffer (pH 5.6) (**a**) and in vitro permeability studies of uncoated-liposomes, coated liposomes, and PG solution (**b**).

Table 5. R^2 values of drug release from uncoated and HA-coated liposomes.

Kinetic Model	Zero Order	First Order	Korsmeyer–Peppas	Higuchi	Hixson–Crowel
R^2 value of uncoated liposomes	0.7211	0.8922	0.8656	0.9238	0.8691
R^2 value of coated liposomes	0.745	0.8935	0.8662	0.9073	0.8488

2.13. In Vitro Permeability Study

The modified side-by-side-type apparatus was used for the in vitro nasal permeation study of uncoated and coated PG-loaded liposomes and the PG solution. Figure 6b shows the rate of PG permeation from the donor to the acceptor phase. The maximum permeation of PG from coated liposomes that was measured after 60 min was 420 μg/cm^2. The PG-containing uncoated liposomes provided faster diffusion and higher drug concentration (>500 μg/cm^2 after 60 min) in comparison to the PG solution. In the case of the PG solution, permeation was negligible, about 5 μg/cm^2. However, when compared with coated liposomes, there was a difference of 80 μg/cm^2 between the permeation values. A slightly lower permeation rate of coated liposomes was observed due to the muco-adhesive nature of HA, which helps to increase the residence time of the coated formulation on the mucosa and protects it from premature mucocililary clearance. The in vitro permeation of the PG-containing coated liposomes provided faster diffusion and higher drug concentration in comparison to the PG solution [34].

2.14. Antioxidant Activity Measurement with Hydrogen Peroxide (H_2O_2)-Scavenging Assay

The antioxidant activity of PG was investigated in order to confirm whether the DPM is gentle enough to encapsulate the drug in liposomes and to preserve its stability. Preserving enzyme activity is essential in the pharmacological effect. It has been demonstrated that free radicals assume an important role in the pathogenesis of specific diseases and also in different types of cancer. Coated and uncoated liposomes containing PG in different concentrations were screened for in vitro scavenging activity using hydrogen peroxide. The scavenging activity of the formulations and the initial PG solution (as a control) are presented in Figure 7. It was revealed that the liposomal formulations preserved the antioxidant activity of PG based on the scavenging activity measurement against H_2O_2. The hydrogen-donating activity, measured using hydrogen peroxide radicals as the hydrogen acceptor, demonstrated a strong association between the concentration of PG and the rate of inhibition. Increasing the concentration of PG enhanced the inhibition. At a low concentration of 125 μg/mL, no significant difference in the antioxidant activity

was observed for both PG liposomes and the initial PG solution. In the case of higher PG concentrations (250 and 500 µg/mL), a significantly improved antioxidant activity of both coated and uncoated liposomes was reached, which can be explained by the stabilizing effect of the liposome carrier at a 95% confidence interval. The enzyme activity was remarkably higher in the case of coated liposomes, which proves that the HA coating enhances the stability of PG in comparison to uncoated liposomes.

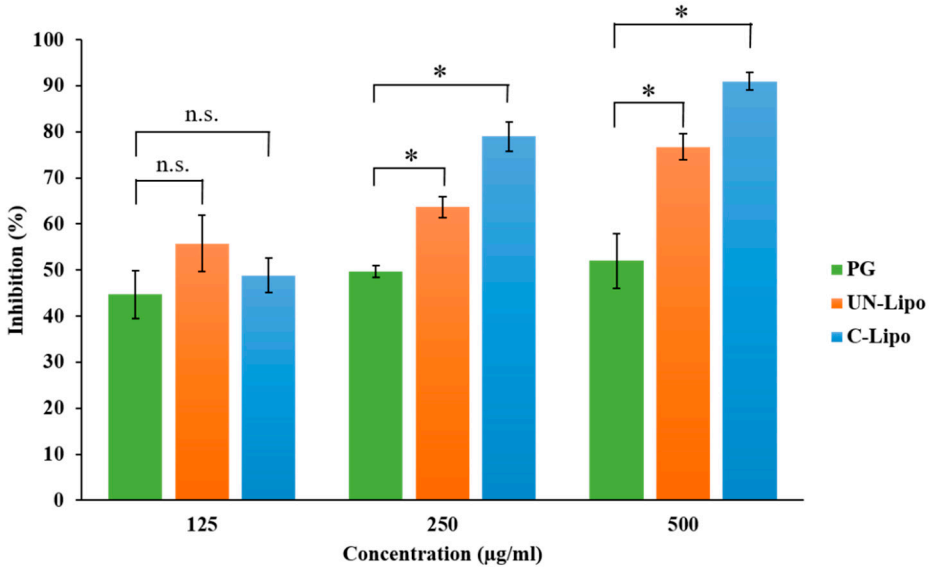

Figure 7. Percentage inhibition of hydrogen-peroxide-scavenging activity of different concentrations of PG-containing coated and uncoated liposomes in comparison to the initial PG solution. Statistical analysis: t-test. * $p < 0.05$; n.s. means not significant compared to the PG control.

2.15. Accelerated Stability Studies

An accelerated stability test was carried out to investigate the physical stability and shelf life of both coated and uncoated formulations. Data were evaluated for the Z-average, EE, PDI, and zeta potential and during 6 months of storage, as illustrated in Table 6. The liposomes showed enhanced physical stability under accelerated stability study conditions, and no significant difference was observed between all measured physical parameters after the sixth month of the study period. Accelerated stability studies revealed that coated liposomes were more stable than uncoated liposomes, which suggests applying the coated carrier for therapy. The physical stability study validated the method of preparation (DPM) of both formulations, strengthening the evidence. The chemical stability of the drug was investigated retrospectively, the drug content was determined after 2, 5, and 8 months of storage, and the shelf life ($t_{90\%}$) was extrapolated. Experimental data showed that the shelf life of both formulations was lower than 2 months at 40 °C and 75% (RH), which suggests cold place storage (2–8 °C) of formulations to protect PG from degradation.

Table 6. Accelerated stability studies of coated and uncoated liposomes.

Formulation	Time (Months)	Decrease in EE * (%)	Z-Average * (nm)	PDI *	Z.P. * (mV)	P.A.
Uncoated liposomes	0	N.C.	N.C.	0.094 ± 0.03	−29.9 ± 2.3	Milky dispersion
	3	10 ± 2.0	N.C.	0.095 ± 0.01	−27.7 ± 3.3	Milky dispersion
	6	30 ± 3.0	550 ± 10	0.511 ± 0.54	−15.6 ± 4.5	Milky dispersion
Coated liposomes	0	N.C.	N.C.	N.C.	−33.6 ± 3.5	Milky dispersion
	3	N.C.	~170.2 ± 5.5	0.130 ± 0.02	−29.9 ± 5.5	Milky dispersion
	6	5 ± 2	180 ± 7.6	0.222 ± 0.03	−27.7 ± 6.4	Milky dispersion

* Data are the mean ± SD (n = 3 independent formulations); * P.A., physical appearance; * Z.P., zeta potential; * EE, encapsulation efficiency; N.C., no change.

3. Discussion

Nose-to-brain delivery is among the most significant administration routes to target the brain. Lipid nanoparticles are a most suitable delivery system due to high biocompatibility, safety, stability, and sustained release [35]. In the present work, liposomes were prepared through the novel DPM and loaded with an antioxidant (n-propyl gallate). The QbD methodology and risk assessment strategy was used to develop optimized formulation via the DPM. Applying the novel DPM avoids the use of any additional size reduction or extrusion technique, which makes the preparation process more feasible and precise and less time consuming. Moreover, this method also provides a greater percentage yield of liposomes. This method has a profound similarity to the solvent injection method, but here, we also avoid slow injection using a syringe or another instrument to mix both aqueous and organic phases [36,37]. The authors recommend this technique for industrial scale-up for more optimum preparation of liposomes. The conventional techniques for liposome development and size are convenient to use with sophisticated equipment. However, problems related to scale-up and scale-down applications have motivated improvements to conventional processes that have also led to the development of novel methods for liposome formation. Based on the impact of process parameters, critical factors were determined. The critical factors with the highest severity scores were used in the three-factor BBD. After combining the selected critical factors, i.e., particle size, PDI, and zeta potential, the optimized formulation was obtained. Characterization studies showed that the Z-average of uncoated liposomes was 135.2 ± 5.2 nm, with a PDI of 0.094 ± 0.001 and a zeta potential of −29.9 ± 5.8 mV, and for coated liposomes was 167.9 ± 3.5 nm, with a PDI of 0.129 ± 0.002 and a zeta potential of −33.6 ± 4.5 mV, with a 90 ± 3.6% EE. Compatibility study results showed no interaction between formulation components. FTIR measurement confirmed in the case of coated liposomes peaks appeared at ~1650 1/cm (amide I of the α-helical region) and 1050 1/cm (C-O-C stretching vibrations of the α-glucopyranose structure), suggesting that the HA coating of liposome was successful [38]. The in vitro release study results showed differences between coated and uncoated liposomes. The reason for the slower release from coated liposomes is the restriction of water diffusion into the carrier matrix, which subsequently decreases the drug release rate. Another possible reason is that coating adds a barrier against drug diffusion with regard to the electrostatic interaction between the positively charged L-α PC and the negatively charged HA [39]. The kinetic models data evaluated the release of PG following the Highuchi model of release [33]. The in vitro permeation of the PG-containing coated liposomes provided faster diffusion and higher drug concentration in comparison to the PG solution. In the case of the PG solution, the permeation was negligible, about 5 μg/cm^2. However, when compared with uncoated liposomes, there was a clear difference between both permeation values. The lower permeation rate of coated liposomes is due to the muco-adhesive nature of HA, which helps to increase the residence time of the coated formulation in the nasal mucosa and protects it from premature mucociliary clearance. The anti-cancer activity of PG is based on the removal of free radicals. The most important mechanism to achieve this goal is the donation of hydrogen to free radicals to convert them to nonreactive species.

The donation of hydrogen would remove the odd electron that is responsible for radical reactivity. In this study, for the evaluation of antioxidant activity, a hydrogen peroxide (H_2O_2)-scavenging assay was performed. Results concluded a proportional antioxidant activity increase at higher concentrations of PG. The enzyme activity was remarkably higher in the case of coated liposomes, which proves the HA coating enhances the stability of PG in comparison to uncoated liposomes. The results ensure potential use of PG against brain tumor via the intranasal route. There are several studies in favor of in vivo outcomes regarding PG that have reported anti-cancer, antioxidant, and anti-angiogenic activity [40]. PG induces apoptosis in human leukemia cells and HeLa cells by increasing the reactive oxygen species (ROS) or glutathione depletion. PG also plays a significant role in autophagy, which, in turn, plays an important role in cellular physiological processes [41]. Autophagy is stimulated as a stress response to pathological conditions, including inflammation, starvation, and cancer. The literature suggests that the regulation of autophagy is complex, occurring via the Akt/mTOR and MAPK/Erk1/2 signaling pathways, and serves as a potential treatment against cancer [42]. Wei et al. studied the PG anti-cancer activity in hepatocellular carcinoma cell growth via the induction of reactive oxygen species and the activation of autophagy. The studies found that PG also enhances the intracelular levels of superoxide and reactive oxidative stress, which could result in autophagosomes and lysosomes [13,43]. The accelerated stability studies were performed over a period of 6 months. All the measured parameters for stability studies, including the particle size, EE, PDI, and zeta potential, revealed that coated liposomes are more stable than the uncoated liposomes.

4. Materials and Methods

4.1. Materials

PG purchased from Sigma-Aldrich (Budapest, Hungary) was applied as the antioxidant drug. The excipients HA (Mw = 1400 kDa) (Sigma-Aldrich, Budapest, Hungary), L-α-phosphatidylcholine (PC) from soybean (Sigma-Aldrich, Budapest, Hungary), cholesterol (Molar Chemicals Ltd., Budapest, Hungary), 96% ethanol (Molar Chemicals Ltd., Budapest, Hungary), and sodium chloride physiological solution (Molar Chemicals Ltd., Budapest, Hungary) were used in the formulation.

4.2. Initial Knowledge Space Development and Collection of Influencing Factors of PG-Lipo

The QTPP is defined as the potential quality attributes of a product that will be achieved to ensure the required characteristics, considering the safety and efficacy of the final product. It is the basis of structuring product design and development that could be achieved, which includes product performance that meets the regulatory-based professional need as well as patient and clinical application related to product performance. The screening of the QTPP from the previous literature was done with precise planning and contemplation based on the relevant International Conference for Harmonisation (ICH) guidelines [17,44]. The QTPP selection is the initial step of the QbD methodology used in this research, and to set up the criteria for this screening, a prospective summary of the literature and the experience from previous studies are required. This is called knowledge space development and includes materials, techniques, and other formulation components. The Ishikawa diagram as a quality management tool was applied for evaluating the cause-and-effect relationships for screening the CQAs that influence the final product profile [45]. This cause-and-effect diagram is also significant for the selection of the QTPP and CPPs in new QbD-guided design development [25,46]. The identification and selection of factors having critical effects on the product is the second step of the QbD approach. These factors are called CQAs, which have a critical influence on the final product quality and can be evaluated or controlled. These are basically biological or microbiological, physical, or chemical; CQAs should be in the appropriate range or limit to ensure the final product quality characteristics. The list of CQAs is always unique; it depends on the QTPP as defined initially. In this step of the QbD approach, critical process and/or material

parameters should be analyzed. These factors or parameters are particularly relevant to the method used for the development of liposomes; hence, they may influence the CQAs.

4.3. Risk Assessment (RA)

After determining the QTPP and selecting the critical factors (CQAs, CPPs), the next step is to perform the RA. The RA is the evaluation of interdependence between the QTPP elements and CQAs and between the CPPs and CQAs. The RA was implemented by using Lean QbD® software (QbDworks.com, QbDworksLLc., Fremont, CA, USA). The evaluation of connections between these screened factors was structured by using a 3-level scale. Each factor and parameter was thoroughly evaluated. The 3-grade scale reflected the impact of factor interactions with each other evaluated one by one in pairs, their interaction being low (L, green), medium (M, yellow), and high (H, red). This interdependence rating step was followed by an occurrence rating estimation of the CPPs using the same 3-grade scale. The determination of this risk occurrence is compulsory for analysis; hence it was performed using risk management protocols. As a result of the RA, the ranking of CQAs and CPPs was plotted on Pareto diagrams generated by the QbD software. The following Pareto chart ranked the impact of potential factors and highlighted the significant factors. This software application in the development of pharmaceutical formulation helps to select the items of the factorial design of experiments to obtain the optimized formulation strategy [46].

4.4. Design of Experiments by the Box–Behnken Design (BBD) for Optimizing the Composition of Coated Liposomes (C-Lipo)

Among the various methods of optimization, the BBD is the most broadly accepted and extrapolated in the design of the experimental phase of pharmaceutical formulation development. The significance of the BBD in the development of pharmaceutical formulations is based on screening and evaluating highly influential factors by applying the response surface methodology (RSM) with high precision and only a few experimental trials [46]. The 3-level BBD was exercised and carried out using TIBCO Statistica® 13.4 software (Statsoft Hungary, Budapest, Hungary), and analysis of variance (ANOVA) was applied to calculate the statistical significance of each model coefficient at a 95% confidence level. Differences were considered significant when $p < 0.05$. For the factorial design, the variables were selected based on the RA results. By exercising the response surface methodology, three different independent factors and dependent factors were assessed: the independent factors included the amount of phospholipids (X_1, 12 to 36 mg), the amount of cholesterol (X_2, 8 to 24 mg), and the effect of temperature (X_3, 40 to 80 °C), while the dependent factors included the Z-average (Y_1), zeta potential (Y_2), and polydispersity index (PDI) (Y_3). The type and ratio of the organic solvent were constant. Polynomial equations showing the correlation among the independent and dependent variables were generated in order to get the optimized particle size, PDI, and zeta potential (i.e., the minimum Z-average and PDI and the optimum zeta potential).

4.5. Preparation of Liposomes via the DPM and Coating of the Lyophilized NPs with HA Polymer Solution

Liposomes were prepared using a novel direct pouring method. This method is a simple bottom-up size reduction technique and results in a stabilized formulation using the optimized concentration of lipids. Different amounts of PG (12, 20, and 40 mg), PC (12, 24, and 32 mg), and cholesterol (8, 16, and 24 mg) were dissolved in 4 mL of an ethanol:acetone (3:1) mixture and directly added to the 10 mL aqueous phase. The organic phase was evaporated at 60 °C under constant stirring (400 rpm) using a hot-plate magnetic stirrer. The unentrapped drug was removed by dialysis at 4 °C for further analysis. The liposome formulations were centrifuged for 1.5 h at 13,500 rpm to collect and separate the pellets from impurities and then redispersed in 1 mL of purified water. HA coating solution (50 mg/mL) was prepared by soaking HA on the surface of purified water under constant stirring at 400 rpm for 30 min until complete swelling occurred. Then 1 mL of HA solution was added dropwise by a syringe to the liposomal solution for 30 min under constant

stirring at 700 rpm at room temperature. Thereafter, the mixture was stored at 5 ± 3 °C for 24 h. After the coating process, the liposomal formulation was centrifuged again at 4 °C at 25,000 rpm for 10 min to remove the free HA that did not go through the electrostatic coating of liposomes, and the pellet was redispersed in 10 mL of purified water. Then 1.5 mL of the coated formulation was transferred to vials and freeze-dried at −40 °C for 12 h under a 0.013 mbar pressure and kept at 25 °C for 3 h for secondary drying to obtain lyophilized powders using a Scanvac Cool safe laboratory freeze-dryer (Labogene, Lynge, Denmark). The powder vials were stored at 5 ± 3 °C for further investigations, including compatibility and morphological characterization.

4.6. Average Hydrodynamic Diameter, Surface Charge, and Polydispersity Index

In 5 mL of purified water, 5 mg of lyophilized liposomes was redispersed, and to reduce the inter-particle aggregation, the solution was sonicated for 5 min. The average hydrodynamic diameter (Z-average), surface charge (zeta potential), and polydispersity index (PDI) of the liposomes were analyzed in folded capillary cells using the Malvern nano ZS instrument (Malvern Instruments, Worcestershire, UK). The temperature and refractive index of the apparatus were set at 25 °C and 1.445, respectively, and the total number of scans was 17. The measurements were repeated in triplicate, and the average value of each was evaluated. The standard acceptable ranges for the Z-average, zeta potential, and PDI are 100–200 nm, ±30 to 40 (mV), and 0.0–0.03, respectively.

4.7. Residual Solvent Determination with Gas Chromatography-Mass Spectrometry (GC-MS)

For determination of acetone, Shimadzu GCMS-QP2010 SE (Shimadzu Europa GmbH, Duisburg, Germany) gas chromatography equipment with a 30 m long, 0.25-mm-diameter ZBWax-Plus column using He as the carrier gas was applied. The instrument was calibrated with a five-point series for acetone.

4.8. Encapsulation Efficiency, Percentage Yield, and Drug-Loading Determination

To measure the encapsulation, percentage yield, and drug loading of PG-loaded liposomes, the centrifuge method was used. The nanoparticles were first centrifuged for 1 h at 22,413 relative centrifugal force (RCF 16,500 rpm, 4 °C) in a Hermle Z323 laboratory centrifuge. The supernatant was collected and screened by using Agilent 1260 (Agent Technologies, Santa Clara, CA, USA) HPLC. A Gemini-NX® C18 column (5 µm, 150 mm × 4.6 mm; Phenomenex, Torrance, CA, USA) was used as a stationary phase. The mobile phase was purified water adjusted to pH = 3.0, with phosphoric acid and acetonitrile in an 80:20 ratio. Twenty microliters of each sample was injected. Separation was performed by 10 min isocratic elution at 25 °C. The eluent flow rate was 1 mL/min, and the chromatograms were detected at 254 nm using a UV-VIS diode-array detector. For evaluation of data, ChemStationB.04.03 software (Agilent Technologies, Santa Clara, CA, USA) was used. The retention time of PG was 4 min. The linear regression of the calibration line was 0.998. The limit of detection (LOD) and limit of quantification (LOQ) in the case of PG were 21 ppm and 63 ppm, respectively. Each sample was run in triplicate, and the percentage of drug encapsulated was calculated by using the following formula [47]:

$$\text{Encapsulation Efficiency } (\%) = \frac{w_1 - w_2}{w_1} \times 100 \quad (4)$$

where w_1 is the total PG in the liposomes and w_2 is the free PG in the supernatant.

The percentage yield was calculated by weighing the lyophilized liposomes and evaluated by using the following formula:

$$\text{Percentage Yield } (\%) = \frac{\text{Actual Yield}}{\text{Theoretical Yield}} \times 100 \quad (5)$$

Drug loading was calculated by weighing the lyophilized liposomes and evaluated by using the following formula:

$$\text{Drug loading } (\%) = \frac{w_1 - w_2}{w_{NP}} \times 100 \quad (6)$$

where w_1 is the amount total PG in the liposomes, w_2 is the free PG in the supernatant, and w_{NP} is the amount of formulation used for analysis.

4.9. Fourier-Transform Infrared Spectroscopy (FTIR)

The FTIR spectra of pure PG, cholesterol, phospholipids, and coating material were collected using a Thermo Nicolet AVATAR FTIR spectrometer (Thermo-Fisher, Waltham, USA) in the spectral range of 4000 and 400 1/cm, with an optical resolution of 4 1/cm. The sample was mixed with 150 mg of dry KBr and compressed to prepare the pellet.

4.10. Differential Scanning Calorimetry (DSC)

To investigate the physiochemical properties and changes to analyze the crystallinity of solid-state products, DSC measurements were carried out. In this evaluation, HA-coated liposomes were investigated to assess the possible intermolecular interactions between the drug, the HA-coated material, and lipids. DSC measurements were performed using a Mettler Toledo DSC 821e instrument (Mettler-Toledo GmbH, Greifensee, Switzerland). Approximately 3–5 mg of samples of physical mixtures, all components used in formulation development along with the coated material and product samples, were loaded into an aluminum pan and examined in the scanning temperature range of 25–300 °C, with an empty Al pan used as reference. The heating rate was 20 °C/min in the presence of argon as a carrier gas with a flow rate of 150 mL/min. The data analysis of the components was performed by using STARe software V9.0 (Mettler-Toledo GmbH, Greifensee, Switzerland). Each measurement was normalized to the sample size.

4.11. X-ray Powder Diffraction (XRPD)

The XRPD method was used for structural characterization to investigate the effect of the preparation procedure on the particle characteristics, to check the state of the API entrapped in the liposomes, as well as to confirm the lack of lipid–drug interaction. The diffractograms of pure PG, coated liposomes, and physical mixture were obtained by using a BRUKER D8 Advance X-ray powder diffractometer (Bruker AXS GmbH, Karlsruhe, Germany). All the results were obtained with a slit-detector Cu Kλ1 radiation (λ = 1.5406 Å) source. This study was also helpful in analyzing the amorphous and crystalline structure of the drug compound and to predict in vitro release behavior. All the components of the formulation and the coated formulation itself were analyzed and scanned at 40 kV and 40 mA in the angular range of 3°–40° 2θ at a step time of 0.1 s and a step size of 0.007°. The samples were analyzed in a quartz holder and measured at ambient temperature and humidity.

4.12. Surface Morphology

The liposome formulations were screened to check the surface properties via transmission electron microscopy (TEM) (FEI Tecnai G2 20 X Twin; FEI Corporate Headquarters, Hillsboro, OR, USA) operated at a 200 kV accelerating voltage. A few microliters of the liposome dispersion was put onto a carbon-coated copper grid; filter paper was used to remove the extra drops of the sample suspension from the grid, leaving a thin liquid film spread over the holes. The sample was negatively stained with sodium silicotung-state solution directly within 1 min of being deposited. Filter paper was used to remove excess sodium silicotung-state solution, and the stained samples were observed [48].

4.13. In Vitro Release Test

The release study was performed under nasal conditions at 35 °C by using the dialysis method under constant stirring at 50 rpm. In a dialysis sac, 5 mg of lyophilized formulation was placed, and this was placed in 50 mL of simulated nasal electrolyte solution (SNES), which combined 8.77 g of NaCl, 2.98 g of KCl, and 0.59 g of $CaCl_2$ anhydrous in 1000 mL of deionized water at pH 5.60 [37]. The samples were withdrawn at predetermined time intervals for up to 120 h. After filtration of the withdrawn volume, the drug concentration was determined by the HPLC method described above. All the measurements were repeated in triplicate. The in vitro release data of the samples were analyzed kinetically by fitting mathematical models (first order, zero order, Higuchi, and Korsmeyer–Peppas model). The results of the release study were evaluated.

4.14. In Vitro Permeability Study

In vitro permeability studies were performed on a modified horizontal side-by-side diffusion apparatus at 35 °C under 100 rpm continuous stirring (Thermo Haake C 10-P5, Sigma-Aldrich Co.). The two compartments were separated by an isopropyl-myristate-impregnated cellulose membrane (Pall Metricel cellulose membrane, 0.45 µm pore size). The volumes of the donor and acceptor phases were both 9 mL, with a 0.69 cm^2 diffusion surface. The donor phase was pH = 5.6 SNES, and the acceptor phase was pH = 7.4 phosphate buffer saline solution (PBS). In the donor phase, 12 mg of the PG-containing formulation was inserted, and 2 mL of samples were withdrawn from the acceptor phase and replaced with fresh acceptor medium at predetermined time intervals (5, 10, 15, and 60 min) during the investigation. The concentration of the drug diffused via the membrane was determined by the HPLC method described above; each sample was analyzed in triplicate.

4.15. Hydrogen Peroxide (H_2O_2)-Scavenging Assay

A solution of hydrogen peroxide (40 mM) was prepared in 0.05 M phosphate buffer (pH 7.4). PG liposomes with different drug concentrations (125, 250, and 500 µg/mL) were added to the hydrogen peroxide solution (0.6 mL, 40 mM). The absorbance of hydrogen peroxide at 230 nm was determined after 10 min against a blank solution containing phosphate buffer without hydrogen peroxide. The percentage hydrogen-peroxide-scavenging activity was then calculated using the following equation:

$$H_2O_2\ scavanging\ effect\ (\%) = A_0 - \frac{A}{A_0} \times 100 \quad (7)$$

where A_0 is the absorbance of the control reaction and A is the absorbance in the presence of the initial PG-containing sample.

4.16. Stability Studies of Coated and Uncoated Liposomes

Stability studies were carried out to ensure the efficacy of the formulations throughout the shelf life. Accelerated stability studies were performed in accordance with ICH guidelines (Q1A R2), and the effect of temperature (40 ± 2 °C) and relative humidity (75 ± 5%) on formulation stability was observed for both coated and uncoated liposomal formulations for a duration of 6 months (at 0, 1, 3, and 6 months). All formulations (coated and uncoated liposomes) were evaluated for physical appearance, Z-average, PDI, zeta potential, and EE. The chemical stability of the drug was investigated retrospectively. The drug content was determined with the HPLC method described above after 2, 5, and 8 months of storage, and the shelf life ($t_{90\%}$) was extrapolated.

4.17. Statistical Analysis

The statistical analysis of the results of this research data was performed using Microsoft® Excel (Microsoft Office Professional Plus 2013) and JMP® 13 software (SAS Institute, Cary, CA, USA). All the results were replicated in triplicate and presented with mean

and standard deviation. In vitro release and in vitro permeability data were processed by using one-way analysis of variance (ANOVA). For the in vitro scavenging assay, a *t*-test was performed. Differences were considered significant when $p < 0.05$.

5. Conclusions and Future Perspectives

The DPM as a novel liposome preparation method has not been previously applied for the preparation of liposomes. As a gentle formulation method, it is suitable for loading antioxidants into liposomes, preserving their stability. Regulatory authorities suggest the application of the QbD approach for designing an optimized product suitable for intranasal delivery. This study helped in the preparation of coated liposomes, and PG was used as the model compound that has proven anti-cancer efficacy. It is expected to be applied in co-encapsulation with other chemotherapeutic drugs in the future and will help to target glioblastoma multiforme via the intranasal route. The results demonstrated that the prepared liposomes were stable even under accelerated conditions. The in vitro scavenging, release and permeation study results showed significant potential of PG liposomes for intranasal delivery.

Author Contributions: Conceptualization, F.S., G.K., and I.C.; methodology, F.S., G.K., E.P., D.G.D., H.A., D.B., and I.C.; software, F.S., G.K., D.B., and D.G.D.; validation, I.C. and Z.K.; formal analysis, G.K., E.P., D.G.D., and I.C.; investigation, F.S., G.K., E.P., D.G.D., H.A., and D.B.; resources, I.C. and Z.K.; data curation, F.S.; G.K., D.G.D., and D.B.; writing—original draft preparation, F.S.; writing—review and editing, G.K., E.P., D.G.D., and I.C.; visualization F.S., G.K., and D.G.D.; supervision, G.K., E.P., D.G.D., and I.C.; project administration, E.P.; funding acquisition, I.C. All authors have read and agreed to the published version of the manuscript.

Funding: This research received no external funding.

Data Availability Statement: The data presented in this study are available on request from the corresponding author.

Acknowledgments: The authors want to express their acknowledgment to the supporters. This study was supported by the Ministry of Human Capacities, Hungary (Grant TKP-2020), and by the National Research, Development and Innovation Office, Hungary (GINOP 2.3.2-15-2016-00060), projects.

Conflicts of Interest: The authors declare no conflict of interest.

Sample Availability: Samples of the compounds are not available from the authors.

References

1. Musumeci, T.; Pellitteri, R.; Spatuzza, M.; Puglisi, G. Nose-to-brain delivery: Evaluation of polymeric nanoparticles on olfactory ensheathing cells uptake. *J. Pharm. Sci.* **2014**, *103*, 628–635. [CrossRef] [PubMed]
2. Westin, U.E.; Boström, E.; Gråsjö, J.; Hammarlund-Udenaes, M.; Björk, E. Direct nose-to-brain transfer of morphine after nasal administration to rats. *Pharm. Res.* **2006**, *23*, 565–572. [CrossRef] [PubMed]
3. Jain, R.; Nabar, S.; Dandekar, P.; Patravale, V. Micellar nanocarriers: Potential nose-to-brain delivery of zolmitriptan as novel migraine therapy. *Pharm. Res.* **2010**, *27*, 655–664. [CrossRef]
4. Ozsoy, Y.; Gungor, S.; Cevher, E. Nasal delivery of high molecular weight drugs. *Molecules* **2009**, *14*, 3754–3779. [CrossRef]
5. Zheng, X.; Shao, X.; Zhang, C.; Tan, Y.; Liu, Q.; Wan, X.; Zhang, Q.; Xu, S.; Jiang, X. Intranasal H102 peptide-loaded liposomes for brain delivery to treat Alzheimer's disease. *Pharm. Res.* **2015**, *32*, 3837–3849. [CrossRef] [PubMed]
6. Sabir, F.; Ismail, R.; Csoka, I. Nose-to-brain delivery of antiglioblastoma drugs embedded into lipid nanocarrier systems: Status quo and outlook. *Drug Discov. Today* **2020**, *25*, 185–194. [CrossRef]
7. Suthar, S.M.; Rathva, B.A. Development of Liposomal Formulation: From Formulation To Sterilization. *W. J. Pharm. Res.* **2019**, *8*, 1561–1571.
8. de Oliveira, E.R.; Nascimento, T.L.; Salomao, M.A.; da Silva, A.C.G.; Valadares, M.C.; Lima, E.M. Increased nose-to-brain delivery of melatonin mediated by polycaprolactone nanoparticles for the treatment of glioblastoma. *Pharm. Res* **2019**, *36*, 131. [CrossRef] [PubMed]
9. Salatin, S.; Barar, J.; Barzegar, J.; Mohammad, A.; Khosro, M.; Mitra Alami Jelvehgari, M. Hydrogel nanoparticles and nanocomposites for nasal drug/vaccine delivery. *Arch. Pharm. Res.* **2016**, *39*, 1181–1192. [CrossRef]
10. Ham, J.; Lim, W.; Park, S.; Bae, H.; You, S.; Song, G. Synthetic phenolic antioxidant propyl gallate induces male infertility through disruption of calcium homeostasis and mitochondrial function. *Environ. Pollut.* **2019**, *248*, 845–856. [CrossRef] [PubMed]

11. Becker, L. Final report on the amended safety assessment of Propyl Gallate. *Int. J. Toxicol.* **2007**, *26*, 89–118.
12. Eler, G.J.; Santos, I.S.; de Moraes, A.G.; Mito, M.S.; Comar, J.F.; Peralta, R.M.; Bracht, A. Kinetics of the transformation of n-propyl gallate and structural analogs in the perfused rat liver. *Toxicol. Appl. Pharm.* **2013**, *273*, 35–46. [CrossRef]
13. Wei, P.L.; Huang, C.Y.; Chang, Y.J. Propyl gallate inhibits hepatocellular carcinoma cell growth through the induction of ROS and the activation of autophagy. *PLoS ONE* **2019**, *14*, e0210513. [CrossRef]
14. Rajagopalan, R.; Jain, S.K.; Trivedi, P. Synergistic anti-cancer activity of combined 5-fuorouracil and gallic acid-stearylamine conjugate in A431 human squamous carcinoma cell line. *Trop. J. Pharm. Res.* **2019**, *18*, 471–477.
15. Pallagi, E.; Karimi, K.; Ambrus, R.; Szabó-Révész, P.; Csóka, I. New aspects of developing a dry powder inhalation formulation applying the quality-by-design approach. *Intern. J. Pharm.* **2016**, *511*, 151–160. [CrossRef]
16. Zidan, A.S.; Sammour, O.A.; Hammad, M.A.; Megrab, N.A.; Habib, M.J.; Khan, M.A. Quality by design: Understanding the formulation variables of a cyclosporine A self-nanoemulsified drug delivery systems by Box–Behnken design and desirability function. *Intern. J. Pharm.* **2007**, *332*, 55–63. [CrossRef] [PubMed]
17. Charoo, N.A.; Shamsher, A.A.A.; Zidan, A.S.; Rahman, Z. Quality by design approach for formulation development: A case study of dispersible tablets. *Intern. J. Pharm.* **2012**, *423*, 167–178. [CrossRef] [PubMed]
18. Kovács, A.; Erős, I.; Csóka, I. Optimization and development of stable w/o/w cosmetic multiple emulsions by means of the Quality by Design approach. *Intern. J. Cosmet. Sci.* **2016**, *38*, 128–138. [CrossRef]
19. Chatterjee, S. Role of models in the quality by design (QbD) paradigm: Regulatory perspective. In Proceedings of the AAPS Annu. Meeting, Washington, DC, USA, 24–27 October 2011.
20. ICH. *Quality Risk Management Q9, ICH Harmonised Tripartite Guideline*; ICH: Geneva, Switzerland, 2005.
21. ICH. *ICH Q10 Pharmaceutical Quality Systems*; ICH: Geneva, Switzerland, 2008.
22. ICH. *Pharmaceutical Development Q8, ICH Harmonised Tripartite Guideline*; ICH: Geneva, Switzerland, 2009.
23. Németh, Z.; Pallagi, E.; Dobó, D.G.; Csóka, I. A proposed methodology for a risk assessment-based liposome development. *Pharmaceutics* **2020**, *12*, 1164. [CrossRef]
24. Pallagi, E.; Jójárt-Laczkovich, O.; Németh, Z.; Szabó-Révész, P.; Csóka, I. Application of the QbD-based approach in the early development of liposomes for nasal administration. *Intern. J. Pharm.* **2019**, *562*, 11–22. [CrossRef]
25. Porfire, A.; Achim, M.; Barbalata, C.; Rus, I.; Tomuta, I.; Cristea, C. Pharmaceutical Development of Liposomes Using the QbD Approach, in Liposomes-Advances and Perspectives. *Liposomes Adv. Perspect.* **2019**, *2019*, 1–20.
26. Massoni, M.; Clavijo, J.C.T.; Colina-Vegas, L.; Villarreal, W.; Dias, J.S.; da Silva, G.A.; Guilherme, A.F.; Ionta, M.; Soares, M.; Ellena, J.; et al. Propyl gallate metal complexes: Circular dichroism, BSA-binding, antioxidant and cytotoxic activity. *Polyhedron* **2017**, *129*, 214–221. [CrossRef]
27. Battaglia, L.; Panciani, P.P.; Muntoni, E.; Capucchion, M.T.; Biasibetti, E.; De Bonis, P.; Mioletti, S.; Fontanella, M.; Swaminathan, S. Lipid nanoparticles for intranasal administration: Application to nose-to-brain delivery. *Exp. Op. Drug. Deliv.* **2018**, *15*, 369–378. [CrossRef]
28. Bourganis, V.; Kammona, O.; Alexopoulos, A.; Kiparissides, C. Recent advances in carrier mediated nose-to-brain delivery of pharmaceutics. *Eur. J. Pharm. Biopharm.* **2018**, *128*, 337–362. [CrossRef]
29. Zhou, M.; Hou, J.; Zhong, Z.; Hao, N.; Lin, Y.; Li, C. Targeted delivery of hyaluronic acid-coated solid lipid nanoparticles for rheumatoid arthritis therapy. *Drug. Deliv.* **2018**, *25*, 716–722. [CrossRef] [PubMed]
30. Xu, X.; Khan, M.A.; Burgess, D.J. A quality by design (QbD) case study on liposomes containing hydrophilic API: I. Formulation, processing design and risk assessment. *Intern. J. Pharm.* **2011**, *419*, 52–59. [CrossRef] [PubMed]
31. Li, Q.; Pu, H.; Tang, P.; Tang, B.; Sun, Q.; Li, H. Propyl gallate/cyclodextrin supramolecular complexes with enhanced solubility and radical scavenging capacity. *Food Chem.* **2018**, *245*, 1062–1069. [CrossRef]
32. Cruz, L.; Soares, L.U.; Costa, T.D.; Mezzalira, G.; da Silveria, N.P.; Gutteres, S.S.; Pohlman, A.R. Diffusion and mathematical modeling of release profiles from nanocarriers. *Intern. J. Pharm.* **2006**, *313*, 198–205. [CrossRef]
33. Qindeel, M.; Ahmed, N.; Sabir, F.; Khan, S.; Ur-Rehman, A. Development of novel pH-sensitive nanoparticles loaded hydrogel for transdermal drug delivery. *Drug. Dev. Ind. Pharm.* **2019**, *45*, 629–641. [CrossRef] [PubMed]
34. Hong, S.S.; Oh, K.T.; Choi, H.G.; Lim, S.J. Liposomal formulations for nose-to-brain delivery: Recent advances and future perspectives. *Pharmaceutics* **2019**, *11*, 540. [CrossRef]
35. Meure, L.A.; Foster, N.R.; Dehghani, F. Conventional and dense gas techniques for the production of liposomes: A review. *AAPS Pharm. Sci. Tech.* **2008**, *9*, 798–809. [CrossRef] [PubMed]
36. Yu, B.; Lee, R.J.; Lee, L.J. Microfluidic methods for production of liposomes. *Methods. Enzymol.* **2009**, *465*, 129–141.
37. Mishra, H.; Mishra, P.K.; Iqbal, Z.; Jaggi, M.; Madan, A.; Bhuyan, K.; Gupta, N.; Gupta, N.; Vats, K.; Verma, R.; et al. Co-delivery of eugenol and dacarbazine by hyaluronic acid-coated liposomes for targeted inhibition of survivin in treatment of resistant metastatic melanoma. *Pharmaceutics* **2019**, *11*, 163. [CrossRef]
38. Ravar, F.; Saadat, E.; Gholami, M.; Dehghankelishadi, P.; Mahdavi, M.; Azami, S.; Dorkoosh, F.A. Hyaluronic acid-coated liposomes for targeted delivery of paclitaxel, in-vitro characterization and in-vivo evaluation. *J. Contorol. Rel.* **2016**, *229*, 10–22. [CrossRef]
39. Wang, J.; Lu, Y.; Zheng, T.; Sang, S.; Lv, L. Scavenging of acrolein by food-grade antioxidant propyl gallate in a model reaction system and cakes. *J. Agric. Food Chem.* **2019**, *67*, 8520–8526. [CrossRef] [PubMed]

40. Chen, C.H.; Lin, W.C.; Kuo, C.N.; Lu, F.J. Role of redox signaling regulation in propyl gallate-induced apoptosis of human leukemia cells. *Food Chem. Toxi.* **2011**, *49*, 494–501. [CrossRef] [PubMed]
41. Jacobi, H.; Eicke, B.; Witte, I. DNA strand break induction and enhanced cytotoxicity of propyl gallate in the presence of copper (II). *Free Rad. Biolo. Med.* **1998**, *24*, 972–978. [CrossRef]
42. Jung, H.J.; Kim, S.J.; Jeon, W.K.; Kim, B.C.; Ahn, K.; Kim, K.; Kim, J.M.; Park, E.H.; Lim, C.J. Anti-inflammatory activity of n-propyl gallate through down-regulation of NF-κB and JNK pathways. *Inflammation* **2011**, *34*, 352–361. [CrossRef] [PubMed]
43. Tague, N. Fishbone (Ishikawa) Diagram. Learn About Quality: About 7 Basic Quality Tools. 2005. Available online: https://en.wikipedia.org/wiki/Seven_basic_tools_of_quality (accessed on 5 March 2021).
44. Trias, E.; Nijs, M.; Ragescu, I.A.; Lombardo, F.; Nikolov, G.; Provoost, V.; Tolpe, A.; Vermeulen, M.; Veleva, Z.; Piteira, R.; et al. Evaluating risk, safety and efficacy of novel reproductive techniques and therapies through the EuroGTP II risk assessment tool. *Hum. Reprod.* **2020**, *35*, 1821–1838. [CrossRef] [PubMed]
45. Stadnichenko, A.V.; Krasnopolskiy Yarnyikh, T.G.; Kotvitskaya, A.A.; Buryak, M. The Concept "Quality by Design" in development of Liposomal cytostatics. *Res. J. Pharm. Technol.* **2020**, *13*, 674–678. [CrossRef]
46. Mishra, H.; Kumar, K.; Kaur, G.; Teotia, D. Formulation and evaluation of liposomes of indomethacin. *J. Adv. Scient. Res.* **2019**, *10*, 180–185.
47. Li, T.; Noewell, C.J.; Rades, T.; Boyd, B.J. Direct comparison of standard transmission electron microscopy and cryogenic-TEM in imaging nanocrystals inside liposomes. *Mol. Pharm.* **2019**, *16*, 1775–1781. [CrossRef] [PubMed]
48. Al-Amiery, A.A.; Al-Majedy, Y.K.; Kadhum, A.A.H.; Mohamad, A.B. Hydrogen peroxide scavenging activity of novel coumarins synthesized using different approaches. *PLoS ONE* **2015**, *10*, e0132175. [CrossRef] [PubMed]

ANNEX-III

pharmaceuticals

MDPI

Article

Development and Characterization of *n*-Propyl Gallate Encapsulated Solid Lipid Nanoparticles-Loaded Hydrogel for Intranasal Delivery

Fakhara Sabir [1], Gábor Katona [1], Ruba Ismail [1,2], Bence Sipos [1], Rita Ambrus [1] and Ildikó Csóka [1,*]

[1] Institute of Pharmaceutical Technology and Regulatory Affairs, Faculty of Pharmacy, University of Szeged, Eötvös Str. 6, H-6720 Szeged, Hungary; fakhra.sabir@gmail.com (F.S.); katona.gabor@szte.hu (G.K.); ruba.ismail@szte.hu (R.I.); sipos.bence@szte.hu (B.S.); ambrus.rita@szte.hu (R.A.)

[2] Department of Applied & Environmental Chemistry, Faculty of Science and Informatics, University of Szeged, Rerrich Béla sqr. 1, H-6720 Szeged, Hungary

* Correspondence: csoka.ildiko@szte.hu; Tel.: +36-62-546-116

Abstract: The objective of the present study was to develop *n*-propyl gallate-loaded solid lipid nanoparticles (PG-SLNs) in a hydrogel (HG) formulation using Transcutol-P (TC-P) as a permeation enhancer. Modified solvent injection technique was applied to produce optimized PG-SLNs via the Quality by Design approach and central composite design. The in vitro mucoadhesion, scavenging activity, drug release, permeation studies of PG from PG-SLNs-loaded HG were evaluated under simulated nasal conditions. Compared with in vitro release behavior of PG from SLNs, the drug release from the PG-SLNs-loaded HG showed a lower burst effect and sustained release profile. The cumulative permeation of PG from PG-SLNs-loaded HG with TC-P was 600 μg/cm^2 within 60 min, which is 3–60-fold higher than PG-SLNs and native PG, respectively. Raman mapping showed that the distribution of PG-SLNs was more concentrated in HG having lower concentrations of hyaluronic acid. The scavenging assay demonstrated increased antioxidant activity at higher concentrations of HG. Due to enhanced stability and mucoadhesive properties, the developed HG-based SLNs can improve nasal absorption by increasing residence time on nasal mucosa. This study provides in vitro proof of the potential of combining the advantages of SLNs and HG for the intranasal delivery of antioxidants.

Keywords: hydrogel; SLNs; nose-to-brain delivery; mucoadhesion; quality by design; antioxidant activity

Citation: Sabir, F.; Katona, G.; Ismail, R.; Sipos, B.; Ambrus, R.; Csóka, I. Development and Characterization of *n*-Propyl Gallate Encapsulated Solid Lipid Nanoparticles-Loaded Hydrogel for Intranasal Delivery. *Pharmaceuticals* **2021**, *14*, 696. https://doi.org/10.3390/ph14070696

Academic Editors: Ana Catarina Silva, João Nuno Moreira and José Manuel Sousa Lobo

Received: 1 June 2021
Accepted: 15 July 2021
Published: 19 July 2021

1. Introduction

In the past few years, the intranasal administration route has gained considerable interest since it provides a non-invasive method to bypass the blood–brain barrier (BBB). Most regions in the central nervous system (CNS) can be directly reached along the olfactory and trigeminal nerves by intranasal administration of drugs. This intranasal administration route is broadly innervated by the olfactory nerve, which is localized in the epithelial tissue of the nasal olfactory mucosa and respiratory mucosa [1]. Various studies provide promising data for the potential of nose-to-brain delivery pathway in the treatment of CNS diseases such as brain tumors, Parkinson's disease and Alzheimer's disease [2,3].

Nose-to-brain delivery is considered very effective for many CNS active drugs that have limited administration because of low bioavailability through other delivery routes including paclitaxel, levetiracetam, cephalexin, dopamine, estrogen or even nerve growth factor-1 [4]. Limited brain uptake can be achieved in numerous intranasally applied compounds from conventional formulations, including chemotherapeutics and antineoplastic agents, due to their low permeability, enzymatic degradation and rapid elimination by mucociliary clearance from the nasal cavity [5–7]. To hurdle these obstacles, the application of nano drug delivery systems can be a suitable tool.

Lipid nanoparticles, including liposomes, niosomes, nanoemulsions and solid lipid nanoparticles (SLNs), are among the most promising drug delivery systems because of their biocompatible nature [8–10]. Moreover, these nanosystems can provide protection of the embedded active pharmaceutical ingredient (API) against efflux transporters (P-glycoprotein), enzymatic degradation or chemical destabilization at nasal conditions [11]. Compared with conventional lipid nanoparticulate drug delivery systems, active targeting has attracted significant attention due to enhanced therapeutic benefits and reduced undesirable side effects.

Hyaluronic acid (HA), a glycosaminoglycan, is a linear polysaccharide that is composed of β-1,4-D-glucoronic acid and 1,3-*N*-acetyl-D-glucosamine disaccharides via alternating glycosidic bonds [12–14]. Hydrogels (HG) containing HA have been successfully developed and evaluated for several promising biomedical applications as carrier systems in nasal, pulmonary, parenteral, topical and ophthalmic delivery [15,16]. Loading nanoparticles into low molecular weight HA-HG can improve nasal absorption by increasing residence time on nasal mucosa through enhanced viscosity and mucoadhesive properties. Improved mechanical stability against degradation and enhanced biochemical functionality of HA can be easily reached using cross-linkers such as glutaraldehyde (GA), divinyl sulfone, carbodiimide or bisepoxide [17,18]. In addition to the gel-forming properties, HA can also be applied in targeted drug delivery [19]. In our experiments, GA was applied due to having high potency to function as a proper cross-linker and because the nasal lining is fairly resistant to aldehyde toxicity below millimolar concentrations [20].

Propyl gallate (PG) (propyl 3,4,5-tri-hydroxybenzoate) is an ester form of gallic acid, and propanol functions as a synthetic antioxidant. Previous studies showed that PG has a high antioxidant capacity, which may contribute to decreasing mitochondrial impairment and to inhibiting cellular respiration. PG has demonstrated anticancer effects on various normal and tumor cells that may lead to DNA genotoxicity, cytotoxicity and fragmentation [21,22]. It has been revealed that PG used along with other anti-tumor agents such as probiotics was effective in mice for tumor treatment [23]. The PG anticancer activity can stop cell proliferation, reduce reactive oxygen species production and stimulate the autophagy of malignant cells [24].

This study aimed to optimize PG containing solid lipid nanoparticles (PG-SLNs) embedded into chemically linked HA-HG as a suitable delivery system for the intranasal route. Intranasal administration of PG can be a promising approach for targeted treatment of brain tumors, e.g., glioblastoma multiforme [25] bypassing the BBB; moreover, this non-invasive way of administration can be more favorable for patients. A further aim was to investigate the effect of excipients as a permeation enhancer for Transcutol-P (TC-P) due to its nontoxicity and biocompatibility and GA as cross-linker for intranasal route. For the formulation optimization, the Quality by Design (QbD) methodology was applied as a quality improvement principle that is able to take into account all critical parameters that have an impact on final product quality, safety and efficacy using a response surface quadratic model.

2. Results

2.1. Quality by Design Approach and Risk Assessment (RA)

Screening of the quality target product profile (QTPP) was based on previous experimental data and according to the relevant International Conference on Harmonization (ICH) guidelines (Q8,Q9,Q10,Q11) [26,27]. The QTPP elements in this study were the route of administration, indication, dissolution and permeability profiles, stability and brain distribution [28,29]. QTPPs contain the information required by the mentioned ICH guidelines on the one hand, and the basic assumptions that our product must meet on the other. Based on the QTPPs, the defined aim was to develop a monodisperse PG-containing SLN embedded in a HG formulation that is able to enter the central nervous system via the nose-to-brain pathway as a patient adherence improving drug delivery pathway offering direct transport to the CNS. Figure S1 shows the relations established between the QTPP-

CQA (QTPP-critical quality attribute) and the critical process parameters/critical materials attributes (CPPs/CMA-CQA) elements on a 3-grade scale. During the RA process, the particle characteristics of the nanoformulation were placed under thorough evaluation as they are the key elements during the incorporation to an HG formulation.

Based on the interdependence rating and using the software, quantification of these relations was performed, and severity scores were assigned for each CQA and CPP/CMA element, as presented in Figure 1.

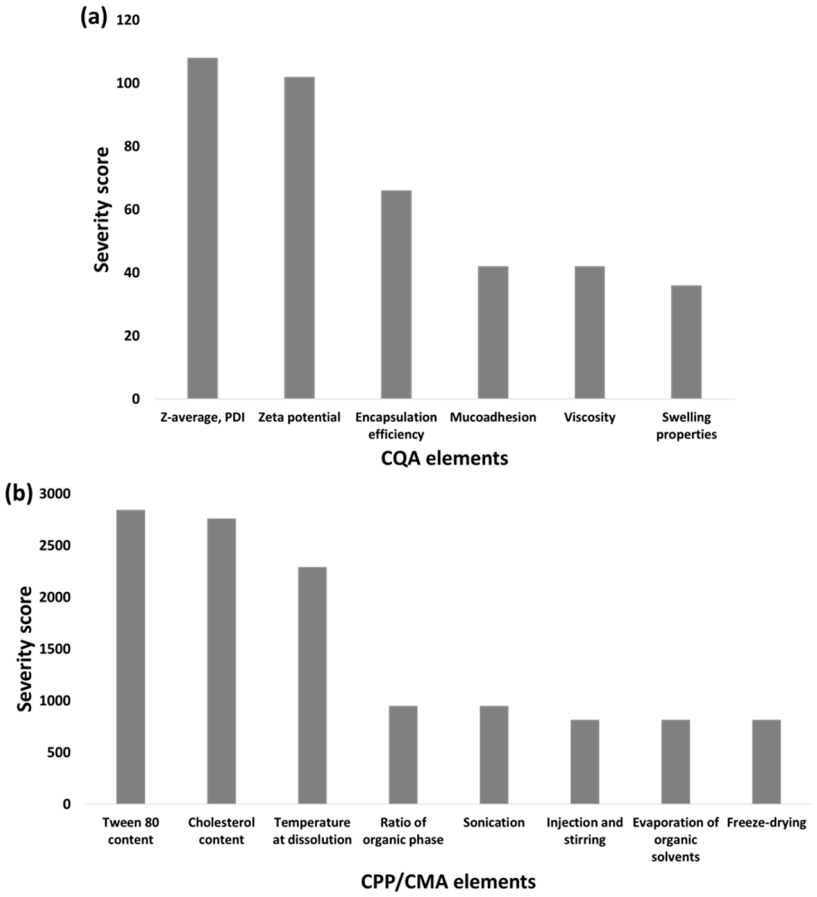

Figure 1. Probability rating of CQA (**a**) and CPP/CMA (**b**) elements. The Pareto charts are presented as the calculated severity scores assigned to the elements.

The interdependence rating (Figure S1) assigned mostly high-grade scores concerning the relations of particle characteristics (Z-average, PDI and zeta potential) which is supported by the higher severity scores in Figure 1a compared with the applicability affecting risk factors such as muco-adhesivity, viscosity and swelling properties. The key element in QbD-driven nanoparticle formulation is to establish the basis for proper particle size and distribution, as these are the main elements influencing the dissolution and permeability profile, which are the first crucial steps in the nasal administration in the nasal cavity and through the nasal mucosa. Based on the calculations, it can be claimed that material attributes such as the concentration of Tween 80 and cholesterol hold the highest risk severity, followed by the temperature at dissolution phase compared with the subprocesses, as seen on Figure 1b. The subprocesses might hold low severity due to the fact that these are either easily controllable processes or because their main function is to achieve the final dosage form, whilst without the appropriate ratios and proportions of the material attributes, the nanosystem cannot be formed.

2.2. Central Composite Design (CCD)

2.2.1. Optimization and Impact of Critical Parameters on Z-Average, Polydispersity Index (PDI), Zeta Potential

Based on the QbD methodology-based RA process, the design of the experiment was conducted according to severity scores. The effect of the characteristics with the highest severity score, i.e., the cholesterol content (A), the Tween 80 content (B) and temperature (°C), were investigated on the independent factors: Z-average, PDI and zeta potential in a 15-formulation experiment series presented in Table 1. We incorporated the results into the software, and as a result, a design expert selected a run (7) depending upon the smallest size, PDI and the characteristic with more negative zeta potential. The software screened the optimized trial with the desirability of 0.99 depending on the lowest Z-average, PDI and more negative zeta potential. The optimized PG-SLNs consisted of 1:6 of Tween 80 and cholesterol. The effects of each individual factor and the combined effect of factors on studied factors are shown in Figure S2a. It was revealed that at a low amount of cholesterol (20 mg), the Z-average was slightly higher than set trials where the maximum amount of it (60 mg) was used. With surfactant addition, the Z-average was less at low concentration of cholesterol due to lower lipid aggregation because of Tween 80 incorporation.

Table 1. Effect of independent variables (temperature, surfactant, cholesterol) on Z-average, PDI and Zeta potential of 15 runs on design of expert. * Data are presented as average ± SD (n = 3 independent measurements).

Number of Runs	Temperature (°C)	Amount of Surfactant (mg)	Amount of Cholesterol (mg)	Z-Average (nm)	PDI	Zeta Potential (mV)
1	45	25	40	150 ± 10	0.30 ± 0.01	−30 ± 8.4
2	20	25	40	220 ± 5.5	0.22 ± 0.02	−29 ± 6.5
3	45	25	40	140 ± 4.5	0.23 ± 0.02	−31 ± 8.4
4	80	10	40	155 ± 5.5	0.25 ± 0.05	−29 ± 8.4
5	45	40	40	500 ± 6.6	0.44 ± 0.07	−5 ± 7.5
6	70	40	20	400 ± 7.8	0.55 ± 0.01	−6 ± 8.5
7 *	70	10	60	120 ± 8.8	0.12 ± 0.08	−38 ± 10.2
8	45	25	40	155 ± 22	0.26 ± 0.09	−29 ± 12
9	45	10	40	200 ± 2.3	0.21 ± 0.08	−29 ± 5.5
10	20	10	20	230 ± 2.4	0.22 ± 0.06	−19 ± 6.5
11	45	25	40	160 ± 40	0.25 ± 0.08	−28 ± 10
12	45	25	40	145 ± 20	0.18 ± 0.05	−28 ± 10.2
13	20	40	60	600 ± 12	0.46 ± 0.01	−4 ± 3.3
14	45	25	20	222 ± 10	0.23 ± 0.02	−20 ± 5.5
15	45	25	60	190 ± 14	0.22 ± 0.02	−19 ± 6.2

* Parameters of optimized formulation.

Even though smaller particle size was obtained at a higher temperature, the temperature effect was not statistically significant. The interaction of individual factors, i.e., cholesterol, on particle size, PDI and zeta potential, are also presented in Figure S2b.

The significance of the applied model was evaluated by F-value and p-value. In the case of particle size analysis, the model F-value of 56.89 implies that the model is significant. The following equations describe the linear and quadratic relations of the individual parameters influencing the dependent factors:

$$\text{Particle size} = 160.57 - 23.74A + 144.53B - 60.62C + 16.88AB - 17.97AC - 50.11BC + 26.74A^2 + 176.21B^2 - 16.67C^2 \quad (1)$$

In the case of zeta potential, the model *F*-value of 10.31 implies that the model is significant. There is only a 0.97% chance that a "model *F*-value" this large could occur due to noise. Values of "Prob > *F*" less than 0.0500 indicate that model terms are significant.

$$\text{Zeta Potential} = -27.42 - 0.8A + 11.08B + 3.45C + 8.7AB - 0.67AC + 2.8BC + 4.78A^2 + 8.2B^2 - 0.73C^2 \quad (2)$$

In the case of PDI, the model *F*-value of 9.41 implies that the model is significant.

$$\text{PDI} = 0.24 - 0.01A + 0.0988B + 0.028C + 0.042AB - 0.057AC + 0.026BC - 0.012A^2 + 0.075B^2 + 0.019C^2 \quad (3)$$

Regarding the particle size, B, C, B^2 are significant model terms, while in the case of the Zeta potential and PDI, B, B^2 are significant models. In all three cases, the values were less than 0.1000, indicating the significance of the applied model. The optimized PG-SLNs were further evaluated for encapsulation efficiency (EE), percentage yield and loading capacity (LC). Optimized PG-SLNs resulted in 84 ± 0.47% EE and 60 ± 0.03% LC. The yield of the PG-SLNs was up to 80 ± 0.1%. Z-average, PDI and zeta potential were also measured for optimized PG-SLNs. The Z-average of PG-SLNs was reported as 103 ± 46 nm with PDI of 0.16 ± 0.001 and zeta potential of −36 ± 4.78 mV.

2.2.2. XRPD and FTIR Analysis

X-ray powder diffractograms (XRPD) of PG show sharp, characteristic peaks confirming its crystalline nature (Figure 2a). The results show that the characteristic peaks of PG (4.1°, 6.2°, 25.8° and 26.4° 2θ) could not be observed in the diffractogram of PG-SLNs, which shows that the crystalline structure of PG is converted into amorphous form and also supports the EE measurement data according to the high amount of PG that was successfully encapsulated into SLNs. In the diffractogram of PG-SLNs, only one peak can be detected at 5.2° 2θ, which corresponds to cholesterol as a carrier base material. These results of PG-SLNs are in agreement with similar experiments reported in the literature [30]. The FTIR spectra (Fourier-transformed infrared spectroscopy) of the components and the formulation are presented in Figure 2b. The characteristic peaks of PG including O–H stretching vibration at 3331 cm^{-1}, C=O stretching of ester at 1539 cm^{-1}, phenol O–H bending at 1246 cm^{-1} as well as C–O–C stretching of aromatic ester at 770 cm^{-1} and 745 cm^{-1} become unobvious in the spectrum of PG-SLNs, which also indicates the encapsulation of PG into SLNs. No other remarkable shift was observed in the other spectral regions, which supports that there is no interaction between SLNs and components.

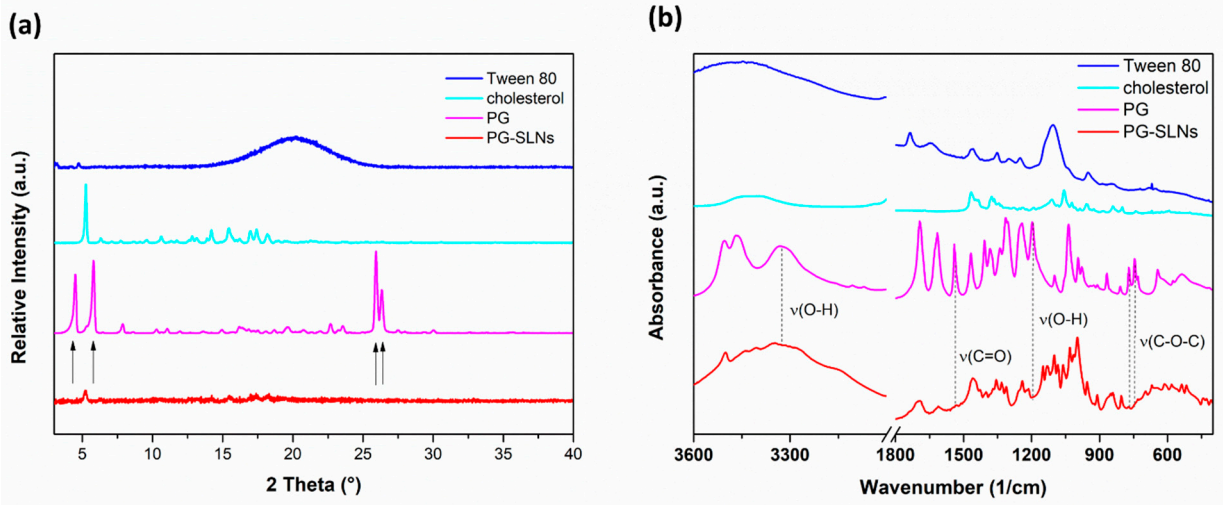

Figure 2. XRPD diffractogram (**a**) and FTIR spectra (**b**) of PG-SLNs and their components.

2.3. Characterization of Hydrogels

2.3.1. Evaluation of pH and Drug Contents of Hydrogels

It has been reported in several previous studies that lysozyme as a physiological nasal mucosa enzyme could inhibit specific types of microbes under slightly acidic conditions [31]. Therefore, the pH of an ideal nasal formulation should be in the range of 5.0 to 6.0 to preserve the physiological microbiological defense [32,33]. The pH of the HA-HGs was between 5.2 and 5.9, which is suitable for nasal administration. Drug content of HA-HGs was 78–82% *w*/*v* measured by HPLC, as shown in Table 2.

Table 2. Main physicochemical characteristics of hydrogels at various hyaluronic acid concentrations.

HA Content (% *w*/*v*)	pH Value	Drug Contents (%)	Spreadability (mm^2)	Mucoadhesion Displacement (mm) after 7 h	Viscosity Cross-Linked (Pas)	Viscosity Non-Cross-Linked (Pas)
0.5	5.3 ± 0.2	78 ± 2.5	222.45 ± 0.22	20 *	0.112	0.181
1	5.2 ± 0.3	82 ± 3.3	360 ± 0.33	20	1.88	2.11
2	5.5 ± 0.4	80 ± 1.4	320 ± 0.44	10	14.29	15.45
3	5.9 ± 0.6	79 ± 4.2	340 ± 0.012	1	66.34	157

* After 2 h maximum displacement on agar-mucin plate was already reached.

2.3.2. Raman Chemical Mapping

Raman mapping was carried out in order to examine the distribution of PG-SLNs in non-cross-linked HA-HGs (SLNs-HGnCL) of different concentrations. For localization of nanoparticles, the Raman spectrum of PG-SLNs were set as profile, whose frequency of occurrence is shown in the chemical maps (Figure 3). The different colors of the chemical map show the relative intensity change of PG-SLNs in the gel structure. Red color indicates strong existence of PG-SLNs, whereas blue color marks those regions of the map whose spectral resolution contains different spectra, characteristic for another component. The results reveal that the distribution of PG-SLNs is more concentrated in HGs containing HA in lower concentration (0.5% and 1% *w*/*v*), as shown by high relative intensity values of the Raman map, whereas in the case of higher HA concentration (2% and 3% *w*/*v*), PG-SLNs can be found in well-defined packages.

2.3.3. Spreadability and Swelling Studies of Hydrogel

The spreadability values of both cross-linked (SLNs-HGCL) and non-cross linked (SLNs-HGnCL) SLNs-HGs was investigated. No significant effect of cross-linking was observed in case of spreadability; SLNs-HGs with different concentrations of HA (0.5, 1, 2 and 3% *w*/*v*) showed 222.45 ± 0.22, 360.10 ± 0.33, 320.12 ± 0.44 and 340 ± 0.01 mm^2 spreading surface, respectively (Table 2). Values in this range ensure proper spreading of the hydrogel. The spreadability study showed that the optimized SLNs-HG (1% *w*/*v* HA) resulted in the highest spreading surface [34,35]. Swelling studies were performed both with cross-linked and non-cross-linked hydrogels. The results show that all the non-cross-linked formulations show a higher swelling index than the chemically cross-linked HG, which can be claimed with the hindered diffusion of water into the cross-linked HG network (Figure 4). The formulation's property to spread uniformly and easily on an applied surface is important to deliver a uniform dose of the active compound.

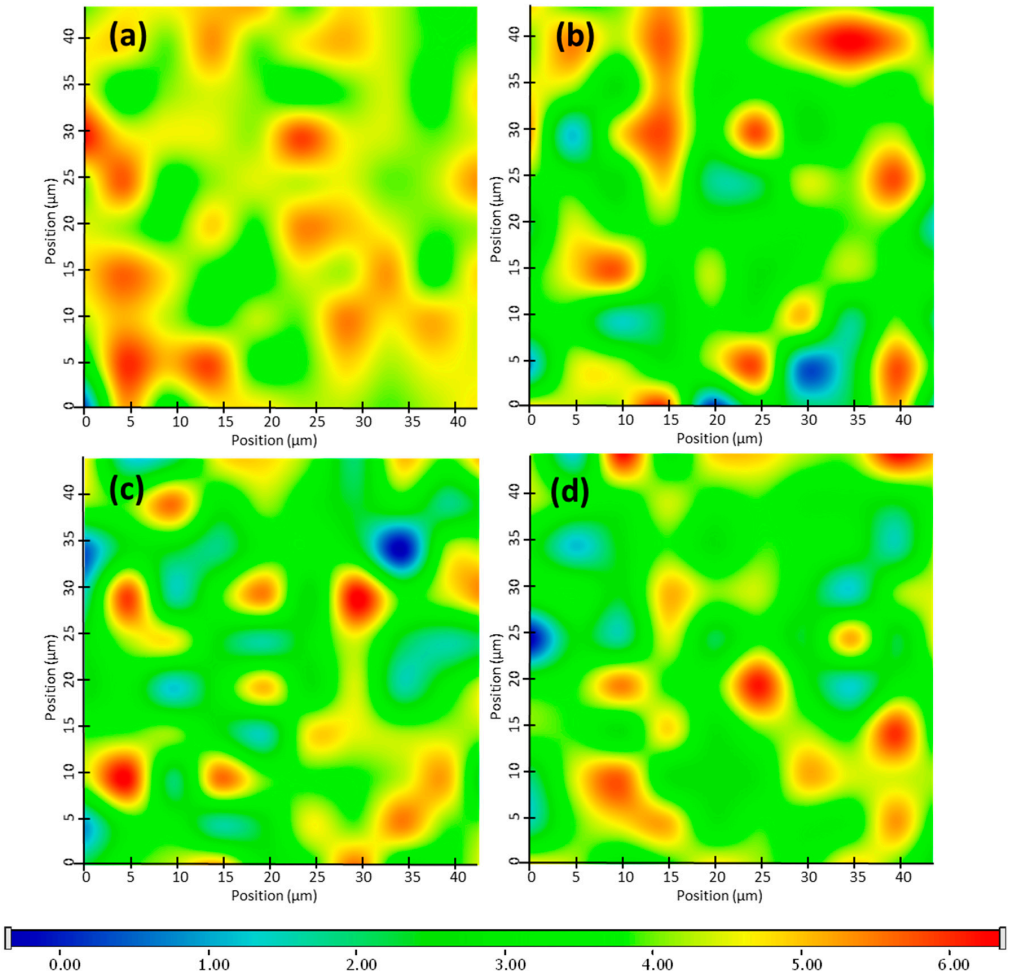

Figure 3. Raman chemical mapping of PG-SLNs in HGs with different concentration of HA: 0.5 (**a**), 1 (**b**), 2 (**c**) and 3% *w*/*v* (**d**).

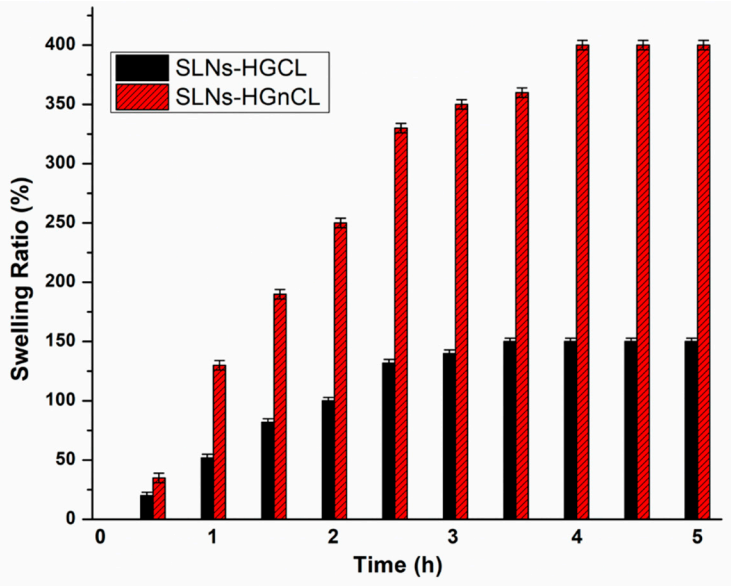

Figure 4. Swelling study of optimized cross-linked (SLNs-HGCL) and non-cross-linked (SLNs-HGnCL) HG (1% *w*/*v* HA). Data are means ± SD (*n* = 3 independent measurements).

2.3.4. Viscosity Measurement

Viscosity is of paramount importance in the case of the applicability of hydrogels to the intranasal administration route, which influences the mucoadhesive properties of the formulation and can prolong the residence in the nasal cavity. Proper polymer concentration must be set in order to achieve the desired high viscosity value, allowing increased residence time and making it possible to enhance the absorption through the nasal mucosa. However, too high viscosity can also be disadvantageous, resulting in hindered drug release of the formulation in the nasal cavity. The viscosity of both cross-linked and non-cross-linked HGs was measured (Table 2). The viscosity measurement of all formulations showed that there was an inverse relation between shear rate and viscosity of HG, which proves the thixotropic nature of HGs (Figure 5). No significant differences among viscosities of cross-linked and non-cross-linked HGs was observed. Furthermore, the non-cross linked SLNs-HGs were characterized due to the spreadability investigation, where SLNs-HGnCL formulations showed higher swelling ratio and spreadability, along with the non-significant difference experienced in the viscosity compared with cross-linked SLNs-HGs.

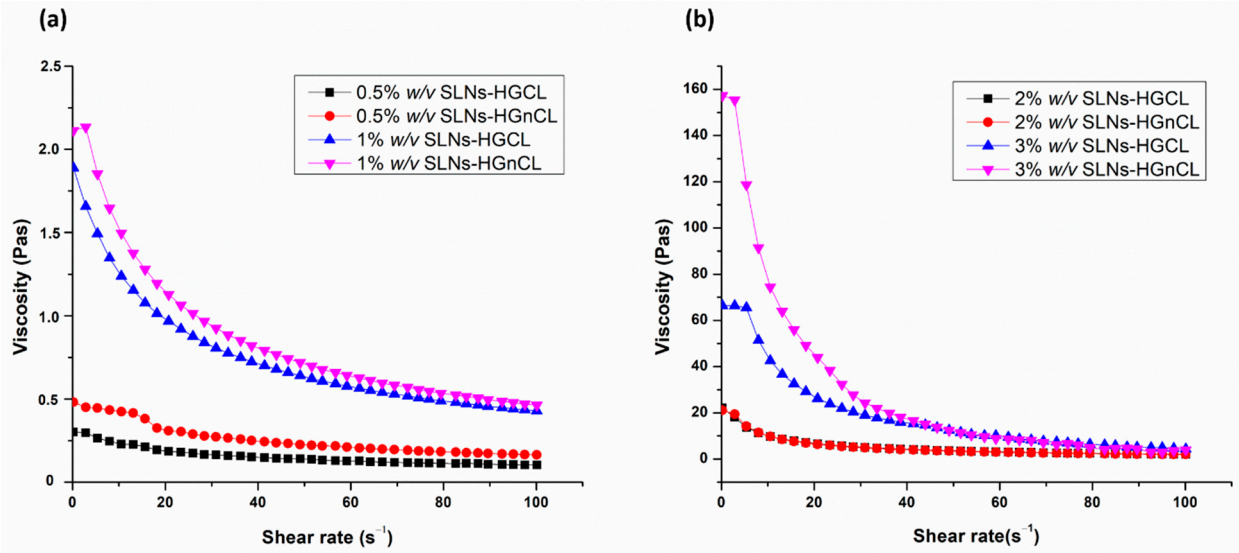

Figure 5. Viscosity profiles of cross-linked (SLNs-HGCL) and non-cross-linked (SLNs-HGnCL) containing HA in 0.5–1% w/v (**a**) and 2–3% w/v (**b**) concentration. Data are means ± SD (n = 3 independent measurements).

2.3.5. In Vitro Mucoadhesion Study

The in vitro mucoadhesion of HGs was investigated through their displacement on an agar-mucin plate. Figure 6 shows that the adhesion potential of HGs at different concentrations of HA is inversely related to the displacement of the HG. As the polymer (HA) concentration increased, lower displacement was observed on the surface of agar after 7 h, indicating higher mucoadhesive properties of formulation. This can be related to the increasing strength of chemical interactions (secondary bonding) between mucin and HA. At the highest concentration (3% w/v) of HA, hardly any displacement was observed during the studied time, indicating remarkable mucoadhesion of formulation. At a lower concentration (0.5% w/v) of HA, displacement was not adequate for nasal administration, and after 2 h it was totally displaced from the agar-mucin plate. Based on these results, the optimized concentration of HG (1% w/v) was screened out, as displacement measured at this concentration was adequate and also in accordance with the results of viscosity, spreadability and swelling ratio measured at this specific concentration, as shown in Table 2.

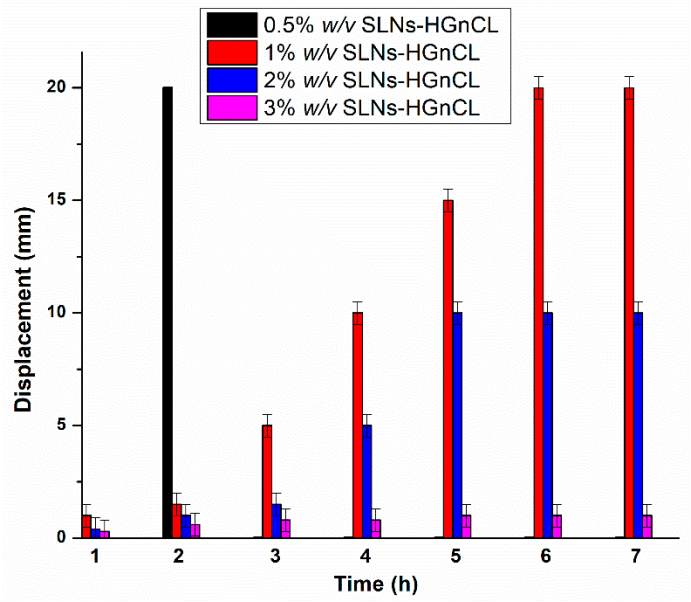

Figure 6. In vitro mucoadhesive studies of SLNs-HGs on agar-mucin gel. Data are means ± SD (n = 5 independent measurements).

2.3.6. Morphological Study of PG-SLNs and PG-SLNs-Loaded HG

SEM images of lyophilized PG-SLNs, shown in Figure 7, also proves that the nanoparticles have spherical morphology and are homogenously distributed in the gel structure. The SEM image of optimized freeze-dried 1% w/v SLNs-HGnCL shows porous structure with a dense cross-linking network.

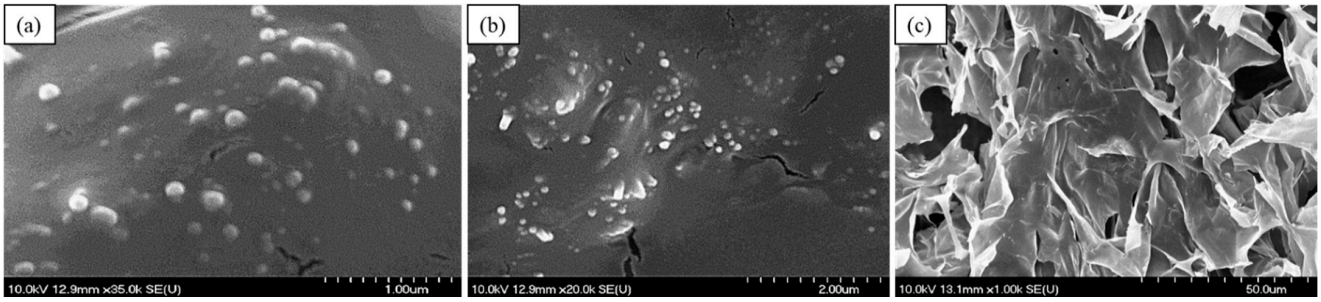

Figure 7. SEM images of optimized lyophilized PG-SLNs (**a**,**b**) and 1% w/v SLNs-HGnCL (**c**) at various resolution.

2.3.7. In Vitro Permeation

Modified Side-Bi-Side® apparatus was used for the in vitro nasal permeation study, whereas the diffusion of PG solution, PG-SLNs, as well as TC-P containing and TC-P-free 1% w/v SLNs-HGnCL was compared. The TC-P was used as permeation enhancer due to its nontoxic and biocompatible nature. Several studies reported its permeation-enhancing effect through a synthetic membrane and on excised skin, reported in previous studies with different drugs [31,36–38]. Figure 8a shows the cumulative PG permeation from donor to acceptor phase through a synthetic cellulose membrane impregnated with isopropyl myristate. The cumulative permeation of PG from PG-SLNs was ~190 µg/cm^2 after 60 min. The TC-P-free 1% w/v SLNs-HGnCL showed a lower permeation of about 180 µg/cm^2, which supports the advantage of application of permeation enhancer. In the case of pure PG dispersion, the permeation was lower than 10 µg/cm^2. The significantly highest permeability was achieved with the HG containing TC-P reaching, with a value around 600 µg/cm^2.

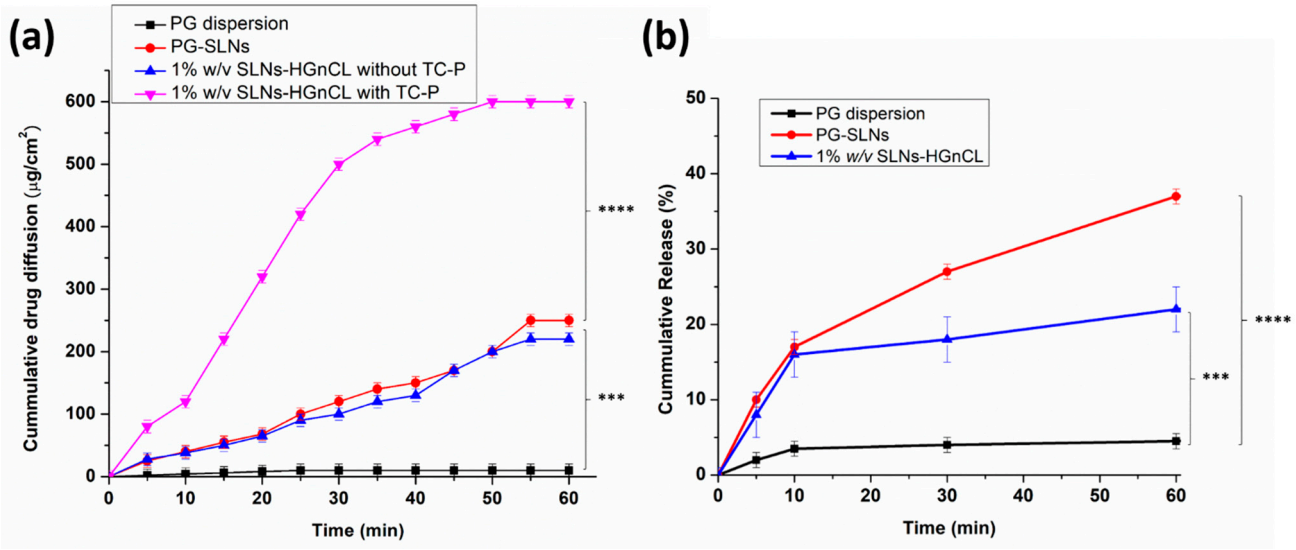

Figure 8. In vitro permeation of pure PG dispersion, PG-SLNs, 1% *w*/*v* SLNs-HGnCL with and without TC-P (**a**). In vitro release study of PG dispersion, PG-SLNs, 1% *w*/*v* SLNs-HGnCL (**b**). Data are means ± SD ($n = 3$ independent measurements). *** $p < 0.001$, **** $p < 0.0001$.

2.3.8. In Vitro Release Study

In vitro release studies of PG-SLNs showed burst release of drug in the first 60 min (~40% of drug) at pH 5.6. After that, the drug release rate decreased following a sustained release tendency, as shown in Figure 8b. In the case of the HG formulation, the initial burst effect was lower, which can be claimed with the controlled release effect of the gel matrix. After 60 min only 15% of PG was released from the HG. To determine the release kinetic of PG from SLNs as well as HG, various dissolution kinetic models including zero-order, first-order, Higuchi, Korsmeyer–Peppas and Hixon–Crowel were fitted to the release data, and kinetic parameters were calculated (Table S1). The drug release both from SLNs and HG followed Higuchi kinetics ($R^2 = 0.96$ and 0.9783 respectively), which can be claimed with the drug release controlling mechanism of lipid matrix and swelling ability of HA-PG matrix in the simulated nasal medium [39]. Fitting the Korsmeyer-Peppas model, the "*n*" value was lower than 0.5, which indicates that both formulations follow Fickian drug diffusion. The significant difference between SLNs and HG can be claimed with the presence of gel network surrounding the SLNs, which decreases the velocity of Fickian diffusion, resulting in sustained release of PG.

2.3.9. In Vitro Antioxidant Activity Evaluation with Hydrogen Peroxide Scavenging Assay

The antioxidant activity of PG was investigated, aiming to confirm that PG-SLNs embedded in HA-HG can preserve antioxidant activity, which is essential in their pharmacological effect. It has been demonstrated that free radicals have a pivotal role in the pathogenesis of different diseases, as well as in several types of cancer [40]. The in vitro scavenging activity of PG-SLN-loaded HA-HGs was investigated containing PG in different concentrations utilizing hydrogen peroxide (H_2O_2) as oxidative medium (Figure 9). It has been revealed that by increasing the polymer concentration in the HG, the antioxidant activity of PG against H_2O_2 was improved, which can be explained by the protective effect of the hydrogel network. The results also support that a strong correlation could be found between the concentration of PG and the rate of inhibition of scavenging activity of H_2O_2. By increasing the concentration of PG, the inhibition was enhanced. At 10 and 30 μg/mL PG containing HGs (containing 2% and 3% *w*/*v* HA), the antioxidant activity was significantly higher in comparison with low HA concentration HGs and PG-SLNs or PG control, which also supports the stabilizing effect of the polymer matrix. In the

case of 20 μg/mL, the same tendency of difference was also demonstrated, but it was not significant.

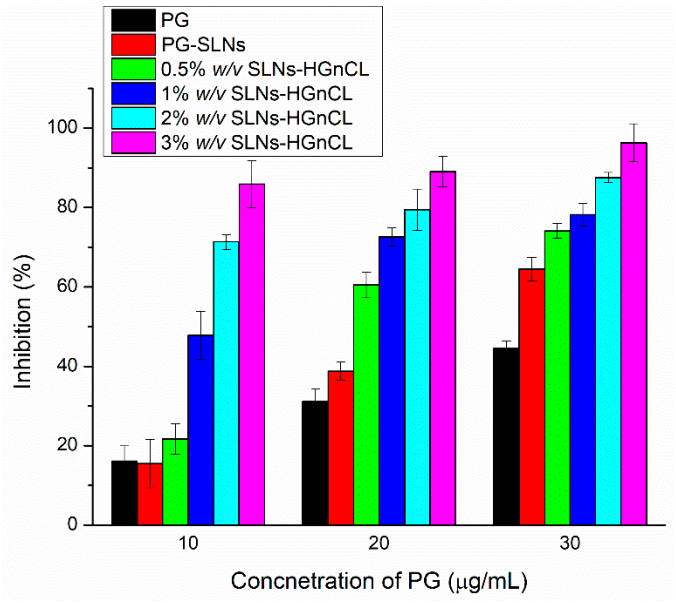

Figure 9. Percentage inhibition of the hydrogen-peroxide-scavenging activity of different concentrations of PG-containing SLNs and PG-SLNs-loaded HA-HG in comparison with the initial PG solution. Data are means ± SD (n = 3 independent measurements). Statistical analysis: t-Test.

3. Discussion

In our previous work we had already investigated the formulation possibilities of PG-loaded liposomes coated with HA [41], as PG has advantageous effects (anti-inflammatory, antioxidant and anticancer activity) in the treatment of brain tumors, e.g., glioblastoma multiforme. As PG is a water-insoluble compound, loading it into a nanocarrier can enhance its water solubility and drug release profile in different administration routes. The present study focused on the formulation of PG-SLNs and loading into HA-HG for brain targeting through intranasal administration. The novelty of our work lies in the fact that our research team explored the first-time application of the PG-SLNs-loaded HA-HG for intranasal delivery route.

SLNs were developed in our study due to their advantageous properties (biocompatibility, increased solubility, protection of drug and permeability enhancement) and loaded into HA-HG as a secondary carrier for facilitating drug transport via the intranasal route. Due to its mucoadhesive property, the role of HA is vital for intranasal drug delivery systems because the nasal cavity is subjected to mucociliary clearance [42,43]. TC-P was utilized as a permeation enhancer as it was previously successfully used as a surfactant or co-surfactant for intranasal application. TC-P has adequate solubilizing property, and it has the ability to enhance the drug's solubility by orders of magnitude compared with other penetration enhancers.

Aiming to develop novel PG-SLNs-loaded into the HA-HG system, the QbD approach was applied. After the determination of the QTPP elements, the relations between CQA and CMA/CPP elements were evaluated, and a risk order was set up based on the software-calculated severity scores. By optimizing the factors having the highest severity via central composite design, the optimized SLNs had a Z-average of 120 ± 8.8 nm, with a PDI of 0.12 ± 0.08 and a zeta potential that was a more negative −38 ± 10.2 mV. The indirect and direct co-effect of cholesterol and Tween 80 on Z-average can be clearly seen in both the single factor and 3D plot (Figure S2a,b). The results show weak repulsion forces between lipid nanoparticles and the surfactant at lower concentration of cholesterol. However, at higher lipid concentrations, prominent repulsion forces can be observed, which can be

explained by the presence of the surfactant phase between lipid nanoparticles and the decrease in van der Waals forces, all reducing the aggregation tendency of lipid droplets [44]. The surfactant concentration showed higher impact on the reduction of Z-average and PDI as compared with cholesterol. These results are in accordance with those reported by Azhar Shekoufeh Bahari et al. and Severino et al. [39,45]. The low Z-average and narrow PDI indicate improved nasal absorption, while the highly negative zeta potential due to surface properties of cholesterol supports high stability of formulation. The absolute value of zeta potential was higher than 30 mV, which ensures sufficient repulsive forces to attain better physical and colloidal stability of the nanosystem [46,47]. The morphological studies by SEM showed spherical shaped SLNs with homogenous distribution and nano-range particle size.

Raman mapping showed that the increasing concentration of polymer forms well-designed hydrogel matrix embedding PG-SLNs homogenously, indicating higher stability of nanoparticles avoiding aggregation [48–50]. The swelling study revealed that the polymeric chains were more flexible in cross-linker-free HG, ensuring water diffusion into the gel matrix.

In the case of chemically cross-linked HG, the free association of the polymer chain is hindered, resulting in a decreased swelling ratio. From these results, it can be concluded that by adding a cross-linker, the mechanical strength of the HG was enhanced. More precise controlled release of the nano-carrier from the gel matrix was reached as compared with simple HG, which is mechanically fragile; thus, larger pores may be created through which nano-carriers can easily liberate the active substance initiating a burst release. Previous studies already reported the similar effect of GA with chitosan HG [51–53]. Safety application of GA is based on previous studies, which showed the nose is very resistant to the aldehydes requiring the application of millimolar concentrations before toxic responses [30].

Our results indicate the significant potential of TC-P in enhancing the permeation of PG-SLNs across the artificial cellulose membrane from the HG matrix. TC-P has a greater influence on the thermodynamic driving force. The maximum thermodynamic driving force occurring at saturation is based on Fickian diffusion, according to which the concentration gradient is formed from a high concentration region to a region of lower concentration phase [36]. TC-P was previously used as a surfactant, co-surfactant and permeation enhancer for intranasal delivery in different micro- and nanoemulsions. Several studies demonstrated the influence of TC-P alone or in combination with propylene glycol on clonazepam permeation both in vitro and ex vivo via application of carbomer HGs. Mura et al. revealed that applying TC-P in the concentration range of 10–50% w/w increased skin penetration of the drug [42].

The anticancer activity of PG is based on its antioxidant property of removing free radicals [54]. The most important mechanism to achieve this goal is to donate hydrogen to free radicals and convert them into nonreactive species. PG can inhibit cellular damage mainly through their free radical scavenging property [40]. Therefore, we aimed to evaluate the antioxidant activity; the hydrogen peroxide (H_2O_2)-scavenging assay results showed enhanced antioxidant activity in case of applying PG as well as HA in higher concentrations. The developed PG-SLNs-loaded HA-HG with the TC-P system, by controlling the drug release, increasing the physical stability and enhancing the drug permeability via nasal mucosa while protecting its antioxidant activity, imparts a promising carrier system for the brain targeting of antioxidant drugs.

4. Materials and Methods

4.1. Materials

PG, the model antioxidant compound, HA (Mw = 14 kDa) and Tween 80 were purchased from Sigma-Aldrich (Budapest, Hungary). Cholesterol, acetone, ethanol (96% v/v), glutaraldehyde (25% w/v) and sodium chloride for physiological salt solution were pur-

chased from Molar Chemicals Ltd. (Budapest, Hungary). Transcutol-P (diethyl glycol monoethyl ether) was supplied by Gattefossé (saint-Priest, France).

4.2. Optimization of SLNs by Quality by Design (QbD) Approach and Risk Assessment Strategy

First, the quality target product profile (QTPP) was defined, followed by selecting the critical quality attributes (CQAs) and critical process parameters (CPPs). The next step was to perform the risk assessment (RA) [55–57]. At first, an interdependence rating was established between the QTPP and CQA elements as well as between CPPs and CQAs. The RA was conducted using Lean QbD®® software (QbDworks.com, QbD works LLc., Fremont. CA, USA). Each factor was thoroughly evaluated on a 3-grade scale using low ("L"), medium ("M") and high ("H") attributives reflecting the relations between the elements. Based on the interdependence rating, the next step was to quantify the severity of the risk factors via a probability rating. As a result of the RA, the severity scores of CQAs and CPPs were plotted on Pareto diagrams generated by the software.

4.3. Response Surface Quadratic Model

Stat-Ease Design Expert® version 10 (stat-Ease, INC.2021 East Hennepin Ave., Suite 480 software) was used to optimize the formulation process and product quality of PG encapsulated SLNs. The amount of cholesterol (20–60 mg), Tween 80 (10–40 mg) and temperature (20–70 °C) where chosen as independent factors based on the RA process, while the ratio of aqueous to organic phases (acetone:ethanol) was kept constant (1:4). Central composite design was applied where SLNs were prepared for each trial, and three responses were evaluated—namely, average hydrodynamic diameter (Z-average), polydispersity index (PDI) and zeta potential.

4.4. Development of PG-SLNs by Modified Injection Method

PG-SLNs were prepared through the modified injection method, where 10 mL of 0.2% *w*/*v* Tween 80 aqueous solution and 5 mL of the organic phase (ethanol:acetone 4:1) were added in different ratios. The PG (10 mg) and cholesterol (60 mg) was dissolved in a mixture of the organic phase and injected dropwise into surfactant solution under constant stirring at 700 rpm at 70 °C. After complete evaporation of the organic phase, the formulation was purified using a Hermle Z323K high performance refrigerated centrifuge (Hermle AG, Gossheim, Germany) for 2 h at 13,500 rpm to separate pellets from supernatant and residual solvent. The collected pellets were redispersed in 5 mL purified water and freeze-dried using a Scanvac CoolSafe laboratory freeze-dryer (Labogene, Lynge, Denmark) at −40 °C for 12 h under a 0.013 mbar pressure with additional 3 h secondary drying at 25 °C in presence of 5% *w*/*v* trehalose as cryoprotectant to obtain lyophilized powders. The lyophilized powder was stored at 5 ± 3 °C until further investigation.

4.5. Preparation of Mucoadhesive HA-Based Hydrogel Formulations with PG-SLNs

Different concentrations (0.5, 1, 2 and 3 *w/v*) of HA were used to prepare colloidal HA-HGs, dissolving them in water for half an hour at 400 rpm. After complete swelling of the HA, the freeze-dried SLNs and 0.1% *w*/*v* glutaraldehyde as cross-linker were added into the HA to form an acetal bond among the aldehyde and hydroxyl group by maintaining acidic conditions. After the reaction, 1 mL of TC-P, as permeation enhancer, was added to the HGs.

4.6. Characterization of PG-SLNs

4.6.1. X-ray Powder Diffraction (XRPD)

Structural characterization of PG-SLNs was performed using a BRUKER D8 Advance X-ray powder diffractometer (Bruker AXS GmbH, Karlsruhe, Germany). All the components and formulations were analyzed in a quartz sample holder and were scanned at 40 kV and 40 mA with Cu K λI radiation (λ = 1.5406 Å) using a VANTEC-1 slit detector in

the angular range of 3° to 40° 2θ, at a step time of 0.1 s and an increment of 0.007°. Each measurement was carried out at ambient humidity and temperature.

4.6.2. Fourier-Transformed Infrared Spectroscopy (FTIR)

The compatibility and interactions between PG and the components of the formulation were investigated using a Thermo Nicolet AVATAR FTIR instrument (Thermo-Fisher, Waltham, MA, USA). For the investigation, pellets were prepared by co-grinding 10 mg compound with 150 mg potassium bromide (KBr) and compressed with 10 tons using a hydraulic press. The FTIR spectra were measured over the range of 4000–400 cm^{-1} with a resolution of 4 cm^{-1} for 128 scans. The recorded spectra were reported as absorbance as a function of wavenumber.

4.6.3. Measurement of Z-Average, Surface Charge and Polydispersity Index

The measured amount (6 mg) of lyophilized SLNs was reconstituted in 6 mL of purified water and sonicated for 4 min to minimize the inter-particle aggregation. The Z-average, PDI and surface charge (zeta potential) of PG-SLNs were measured in folded capillary cells using a Malvern Zetasizer nano ZS instrument (Malvern Instrument, Worcestershire, UK) at 25 °C, with the refractive index 1.445. All the measurements were conducted in triplicate, and data are presented as average ± SD.

4.6.4. Encapsulation Efficiency (EE), Loading Capacity (LC) and Percentage Yield Determination

EE and LC of PG-SLNs were determined using an indirect method. PG-SLNs were first centrifuged for 1 h at 16,500 rpm at 4 °C in a Hermle laboratory centrifuge (Hermle AG, Gosheim, Germany). The supernatant was collected and diluted 10-fold with purified water. The concentration of PG was determined using HPLC. The EE, as the actual PG content in the optimized formulation, was measured according to the following equation:

$$\text{Encapsulation Efficiency } (\%) = \frac{w_1 - w_2}{w_1} \times 100 \quad (4)$$

where w_1 is the total amount of added PG, and w_2 is the amount of free PG in the supernatant.

The LC was calculated via the following equation:

$$\text{Loading capacity } (\%) = \frac{w_1 - w_2}{w_3} \times 100 \quad (5)$$

where w_1 is the total amount of added PG, and w_2 is the amount of free PG in the supernatant, while w_3 is the total amount of lipid added to the formulation.

The percentage yield was calculated by weighing the dried PG-SLNs and determined by using the following formula [58]:

$$\text{Percentage yield } (\%) = \frac{\text{weight of dried NPs}}{\text{theoretical weight of drug and components}} \times 100 \quad (6)$$

4.6.5. HPLC Method

The PG quantification was carried via HPLC (Agilent 1260, agent technologies, Santa Clara, CA, USA). The stationary phase was C18 column (Gemini-NX® 150 mm × 4.6 mm, 5 µm (Phenomenex, Torrance, CA, USA). Purified water and acetonitrile in 80:20 ratio adjusted pH = 3.0, with phosphoric acid used as mobile phase. A set of 20 µL samples were injected, whereas separation was performed by 10 min isocratic elution at 25 °C temperature with 1 mL/min eluent flow. The UV-Vis diode array detector was applied for the detection of chromatograms at 254 nm. ChemStation B.04.03 Software (Santa Clara, CA, USA) was used for evaluation of data. PG retention time was detected at 4 min. For the calibration line, the linear regression was 0.998. The quantification limit (LOQ) and detection (LOD) of PG were 63 ppm and 21 ppm, respectively [41,59].

4.7. Characterization of PG-SLNs Loaded Hydrogels

4.7.1. Physical Appearance, pH and Drug Contents of Hydrogels

PG-SLN HGs containing HA in different concentrations (0.5, 1, 2 and 3% *w*/*v*) were evaluated apparently for grittiness and uniformity. The pH of HGs was measured directly by dipping pH meter (WTW® inoLab® pH 7110 laboratory pH tester, Thermo Fisher Scientific, Budapest, Hungary). To determine the drug contents in the formulation, 1 g of HG was dispersed in 10 mL of phosphate buffer (pH 7.4). This diluted gel was filtered with a membrane filter (0.45 µm, polypropylene) and analyzed by HPLC. All measurements were carried out in triplicate. Drug content was evaluated by the following formula:

$$\text{Percent Drug contents} = \frac{\text{Actual amount of drug in the formulation}}{\text{Theoretical amount of drug in thr formualtion}} \times 100 \quad (7)$$

4.7.2. Raman Spectroscopy

A Thermo Fisher DXR Dispersive Raman instrument (Thermo Fisher Scientific Inc., Waltham, MA, USA) was used for investigation of SLNs. This instrument was equipped with a 780 nm wavelength diode laser and a CCD camera. The laser power of 12 mW at 50 µm slit aperture size was used for Raman measurements with 2 and 6 s of exposure and acquisition time, for a total of 32 scans per spectrum in the spectral range 3500–200 cm^{-1} with fluorescence and cosmic ray corrections. The PG-SLNs distribution in HGs was determined via Raman chemical mapping in the formulation. For the total of 16 scans, a 45 µm × 45 µm size surface was evaluated with a 10 µm step size. To eliminate the intensity deviation between the measured areas, the normalization of Raman spectra was ensured [60].

4.7.3. Swelling Index

To measure the swelling index of the HGs, the gravimetric method was applied. Lyophilized gel of both cross-linked and non-cross-linked HGs was soaked in phosphate buffer saline (PBS) (pH = 7.4). After swelling, HGs were taken out from the medium and weighed at different time intervals (after every 30 min) until the weight of the swelled HG became constant. Percentage swelling was calculated using the formula [58]:

$$\text{Swelling } (\%) = \frac{w_2 - w_1}{w_1} \times 100 \quad (8)$$

where w_1 is the initial weight of hydrogel, and w_2 is the weight of swollen HG after each sampling point.

4.7.4. Spreadability Test

Spreadability of HGs was measured using the glass slide method. The center of the glass slide was marked with a 1 cm diameter circle upon which 0.5 g of gel was placed. Another glass slide was placed over the HG, forming a sandwich arrangement. The load of the 500 g was placed on the upper plate and weighted for 5 min. After 5 min, the load was removed, and the increment in HG diameter was measured [61]. All the results were evaluated with respect to the spreading area and applied weight by using the following equation:

$$s_i = d^2 \times \frac{\pi}{4} \quad (9)$$

where S_i is the swelling index, d the diameter of the glass slide and π the shear stress.

4.7.5. Viscosity Measurement

Viscosity measurement was performed at 37 °C with a Haake Rheostress 1 instrument (Thermo Scientific, Karlsruhe, Germany). A cone-plate device was used where the cone

diameter was 6 cm with an angle of 1° and a 0.052 mm gap size. The apparent viscosity curves of the samples were plotted under the shear rate range of 0.01–100 s^{-1}.

4.8. In Vitro Characterization of Nanoparticles and Hydrogel

4.8.1. In Vitro Mucoadhesion Testing

In vitro mucoadhesion was performed using the displacement method. A specified weighted amount (5 mg) of HG for each respective HA concentration (0.5, 1, 2 and 3% *w*/*v*) was placed on the top of 1% *w*/*v* agar and 2% *w*/*v* mucin aqueous solution casted on a glass plate of 9 cm and was inclined at 60° in an incubator at 37 °C. The downward movement of the HG mass was measured in millimeters hourly up to 7 h. All the measurements were conducted in triplicate [61,62].

4.8.2. Surface Morphology

Scanning electron microscopy (SEM) (Hitachi S4700, Hitachi Scientific Ltd., Tokyo, Japan) was used to characterize the morphology and surface properties of both PG-SLNs-lyophilized formulation and PG-SLNs-loaded HG. A voltage of 10 kV and 10 mA amperage was applied at 1.3–13.1 mPa pressure. A greater vacuum evaporator and argon atmosphere were used to make the sputter-coated samples conductive with gold–palladium (Bio-Rad SC 502, VG Microtech, Uckfield, UK). The gold–palladium coating thickness was approximately 10 nm.

4.8.3. In Vitro Permeation Study

A modified horizontal side-by-side type diffusion apparatus was used for in vitro permeation studies at 37 °C and with 100 rpm constant stirring (Thermo Haake C10-P5, Sigma-Aldrich Co. LLC, St. Louis, MO, USA). The donor and receptor compartments were isolated with an isopropyl myristate impregnated artificial membrane (0.45 µm pore size, Pall Metri-cel cellulose membrane) with a 0.69 cm^2 diffusion surface. The donor compartment consisted of 9 mL simulated nasal electrolyte solution (SNES) with a pH of 5.6, which contained 0.59 g $CaCl_2$, 8.77 g NaCl, 2.98 g KCl anhydrous in 1000 mL of deionized water, where the acceptor compartment consisted of pH 7.4 PBS. The measured amount (5 mg) of formulation was placed in the donor phase 1 mL of each sample (PG, PG-SLNs, PG-SLNs-loaded HG with and without TC-P) and was withdrawn from the acceptor phase every 5 min and replaced with the same volume of fresh medium. The amount of the drug diffused through the membrane was quantified by using HPLC. Each formulation was analyzed in triplicate.

4.8.4. In Vitro Release Study

The in vitro dissolution study was performed under the nasal conditions at 37 °C by using the modified paddle method with a Hanson SR8 Plus apparatus (Teledyne Hanson Research, Chatsworth, CA, USA) at 50 rpm constant stirring. The PG (10 mg) containing formulation was placed into 50 mL SNES (pH 5.60) as dissolution medium, and samples were withdrawn in predetermined time intervals of 5, 15, 30, 60, 180, 360 and 720 min. After filtration (0.45 µm membrane filter), the PG concentration of the aliquots was analyzed using HPLC. All the measurements were performed in triplicate. The in vitro drug release kinetics of each sample were also evaluated, fitting various mathematical models—namely, zero-order, first-order, Higuchi, Korsmeyer–Peppas and Hixon–Crowel models.

4.8.5. Hydrogen Peroxide Scavenging (H_2O_2) Assay

A solution of hydrogen peroxide (40 mM) was prepared in 0.05 M phosphate buffer (pH 7.4). PG SLNs with different drug concentrations (10, 20 and 30 µg/mL) were incorporated in a 0.6 mL and 40 mM hydrogen peroxide solution. After 10 min of addition of hydrogen peroxide, the absorbance at wavelength of 230 nm was determined spec-

trophotometrically using phosphate buffer as reference [40,61,63]. The hydrogen peroxide percentage scavenging activity was then measured using the following formula:

$$H_2O_2 \text{ scavenging effect } (\%) = A_0 - \frac{A}{A_0} \times 100 \quad (10)$$

where A_o is the absorbance of the control reaction, and A is the absorbance in the presence of initial PG containing sample.

4.9. Statistical Analysis

The statistical analysis was applied to all the results using Microsoft® 13 software (SAS Institute, Cary, NC, USA). All the results were repeated in triplicate, and the means of data are expressed with standard deviation. In vitro permeation and release data were compared using the one-way analysis of variance (ANOVA); differences were considered significant when $p < 0.05$.

5. Conclusions

PG-SLNs were successfully prepared using a modified injection method. For the optimization of formulation and process parameters affecting the quality of the nanosystem, the initial risk assessment study and the design of experiment were applied following the QbD approach. The addition of PG endowed the HG with the ability to facilitate anticancer activity and with significant potential to be co-encapsulated with other anti-glioblastoma drugs. Our optimized platform provided in vitro proof of the potential of combining the advantages of lipid-based NPs with HG as a promising intranasal delivery system.

Supplementary Materials: The following are available online at https://www.mdpi.com/article/10.3390/ph14070696/s1, Figure S1: Interdependence rating amongst QTPP—CQA (a) and CPP/CMA—CQA (b) elements, Figure S2: 3D surface plot (a) and one-factor interaction (b) graph showing the effects of surfactant and cholesterol on Particle Size, PDI and Zeta potential, Table S1: Kinetic parameters of in vitro drug release.

Author Contributions: Conceptualization, F.S., G.K. and I.C.; methodology, F.S., G.K., B.S. and I.C.; software, F.S., G.K. and B.S.; validation, G.K. and I.C.; formal analysis, G.K., R.I. and I.C.; investigation, F.S., G.K. and R.A.; resources, I.C.; data curation, F.S., G.K. and B.S.; writing—original draft preparation, F.S.; writing—review and editing, G.K., R.I. and I.C.; visualization, F.S. and G.K.; supervision, I.C.; project administration, I.C.; funding acquisition, I.C. All authors have read and agreed to the published version of the manuscript.

Funding: The publication was funded by The University of Szeged Open Access Fund (FundRef, Grant No. 5349).

Institutional Review Board Statement: Not applicable.

Informed Consent Statement: Not applicable.

Data Availability Statement: Data is contained within the article and supplementary material.

Acknowledgments: The authors want to express their acknowledgment to the supporters. This study was supported by the Ministry of Human Capacities, Hungary (Grant TKP-2020), and by the National Research, Development and Innovation Office, Hungary (GINOP 2.3.2-15-2016-00060).

Conflicts of Interest: The authors declare no conflict of interest.

Abbreviations

ANOVA	one-way analysis of variance
BBB	blood–brain barrier
CNS	central nervous system

CPPs	critical process parameters
CMA	critical materials attributes
CQA	critical quality attributes
CCD	central composite design
°C	centigrade
EE	encapsulation efficiency
FTIR	Fourier-transformed infrared spectroscopy
GA	glutaraldehyde
HA	hyaluronic acid
HG	hydrogel
HA-HG	hyaluronic acid—hydrogel
HPLC	high proficiency liquid chromatography
H_2O_2	hydrogen peroxide
ICH	International Conference on Harmonization
KBr	potassium bromide
kDa	kilo Dalton
LC	loading capacity
LOQ	limit of quantification
LOD	limit of detection
mV	millivolt
mm	millimol
mA	milliampere
mPa	millipascal
mg	milligram
mm^2	square millimeter
Mw	molecular weight
nm	nanometer
ppm	parts per million
PBS	phosphate buffer saline
PG	propyl gallate
PG-SLNs	PG-solid lipid nanoparticles
PDI	polydispersity index
Pas	pascal
QbD	Quality by Design
QTPP	quality target product profile
RA	risk assessment
SLNs	solid lipid nanoparticles
SEM	scanning electron microscopy
SLNs-HGnCL	SLNs non-cross-linked HG
SLNs-HGCL	SLNs cross-linked HG
TC-P	Transcutol-P
μm	micrometer
w/v	weight/volume
XRPD	X-ray powder diffractograms

References

1. Chung, E.P.; Cotter, J.D.; Prakapenka, A.V.; Cook, R.L.; Diperna, D.M.; Sirianni, R.W. Targeting small molecule delivery to the brain and spinal cord via intranasal administration of rabies virus glycoprotein (RVG29)-modified PLGA nanoparticles. *Pharmaceutics* **2020**, *12*, 93. [CrossRef]
2. Gonçalves, J.; Bicker, J.; Gouveia, F.; Liberal, J.; Oliveira, R.C.; Alves, G.; Falcão, A.; Fortuna, A. Nose-to-brain delivery of levetiracetam after intranasal administration to mice. *Int. J. Pharm.* **2019**, *564*, 329–339. [CrossRef] [PubMed]
3. Kanazawa, T.; Kaneko, M.; Niide, T.; Akiyama, F.; Kakizaki, S.; Ibaraki, H.; Shiraishi, S.; Takashima, Y.; Suzuki, T.; Seta, Y. Enhancement of nose-to-brain delivery of hydrophilic macromolecules with stearate- or polyethylene glycol-modified arginine-rich peptide. *Int. J. Pharm.* **2017**, *530*, 195–200. [CrossRef] [PubMed]
4. Ullah, I.; Chung, K.; Bae, S.; Li, Y.; Kim, C.; Choi, B.; Nam, H.Y.; Kim, S.H.; Yun, C.O.; Lee, K.Y.; et al. Nose-to-Brain Delivery of Cancer-Targeting Paclitaxel-Loaded Nanoparticles Potentiates Antitumor Effects in Malignant Glioblastoma. *Mol. Pharm.* **2020**, *17*, 1193–1204. [CrossRef] [PubMed]

5. Ul Islam, S.; Shehzad, A.; Bilal Ahmed, M.; Lee, Y.S. Intranasal delivery of nanoformulations: A potential way of treatment for neurological disorders. *Molecules* **2020**, *25*, 1929. [CrossRef] [PubMed]
6. Sintov, A.C. AmyloLipid Nanovesicles: A self-assembled lipid-modified starch hybrid system constructed for direct nose-to-brain delivery of curcumin. *Int. J. Pharm.* **2020**, *588*, 119725. [CrossRef] [PubMed]
7. Sabir, F.; Ismail, R.; Csoka, I. Nose-to-brain delivery of antiglioblastoma drugs embedded into lipid nanocarrier systems: Status quo and outlook. *Drug Discov. Today* **2020**, *25*, 185–194. [CrossRef]
8. Agrawal, M.; Konwar, A.N.; Alexander, A.; Borse, V. Nose-to-brain delivery of biologics and stem cells. In *Direct Nose-To-brain Drug Delivery*; Elsevier: Amsterdam, The Netherlands, 2021; pp. 305–328. [CrossRef]
9. Madav, Y.; Wairkar, S. Strategies for enhanced direct nose-to-brain drug delivery. In *Direct Nose-to-Brain Drug Delivery*; Elsevier: Amsterdam, The Netherlands, 2021; pp. 169–184. [CrossRef]
10. Pardeshi, C.V.; Souto, E.B. Surface modification of nanocarriers as a strategy to enhance the direct nose-to-brain drug delivery. In *Direct Nose-to-Brain Drug Delivery*; Elsevier: Amsterdam, The Netherlands, 2021; pp. 93–114. [CrossRef]
11. Battaglia, L.; Panciani, P.P.; Muntoni, E.; Capucchio, M.T.; Biasibetti, E.; De Bonis, P.; Mioletti, S.; Fontanella, M.; Swaminathan, S. Lipid nanoparticles for intranasal administration: Application to nose-to-brain delivery. *Expert Opin. Drug Deliv.* **2018**, *15*, 369–378. [CrossRef]
12. Kadam, T.S.; Agrawal, A. Short Review on the Important Aspects Involved in Preparation, Characterization and Application of Nanostructured Lipid Carriers for Drug Delivery. *Curr. Nanomed.* **2020**, *10*, 188–207. [CrossRef]
13. Mahmood, H.S.; Alaayedi, M.; Ashoor, J.A.; Alghurabi, H. The enhancement effect of olive and almond oils on permeability of nimesulide as transdermal gel. *Int. J. Pharm. Res.* **2019**, *11*, 1200–1206.
14. Fytianos, G.; Rahdar, A.; Kyzas, G.Z. Nanomaterials in cosmetics: Recent updates. *Nanomaterials* **2020**, *10*, 979. [CrossRef]
15. Yasir, M.; Sara, U.V.S.; Chauhan, I.; Gaur, P.K.; Singh, A.P.; Puri, D.; Ameeduzzafar, A. Solid lipid nanoparticles for nose to brain delivery of donepezil: Formulation, optimization by Box–Behnken design, in vitro and in vivo evaluation. *Artif. Cells, Nanomed. Biotechnol.* **2018**, *46*, 1838–1851. [CrossRef]
16. Vasvani, S.; Kulkarni, P.; Rawtani, D. Hyaluronic acid: A review on its biology, aspects of drug delivery, route of administrations and a special emphasis on its approved marketed products and recent clinical studies. *Int. J. Biol. Macromol.* **2020**, *151*, 1012–1029. [CrossRef] [PubMed]
17. Taymouri, S.; Shahnamnia, S.; Mesripour, A.; Varshosaz, J. In vitro and in vivo evaluation of an ionic sensitive in situ gel containing nanotransfersomes for aripiprazole nasal delivery. *Pharm. Dev. and Tech.* **2021**. just-accepted. [CrossRef]
18. Zhang, H.; Fan, T.; Chen, W.; Li, Y.; Wang, B. Recent advances of two-dimensional materials in smart drug delivery nano-systems. *Bioact. Mater.* **2020**, *5*, 1071–1086. [CrossRef]
19. Thompson, C.M.; Gentry, R.; Fitch, S.; Lu, K.; Clewell, H.J. An updated mode of action and human relevance framework evaluation for Formaldehyde-Related nasal tumors. *Crit. Rev. Toxicol.* **2020**, *50*, 919–952. [CrossRef] [PubMed]
20. Huang, H.M.; Wu, P.H.; Chou, P.C.; Hsiao, W.T.; Wang, H.T.; Chiang, H.P.; Lee, C.M.; Wang, S.H.; Hsiao, Y.C. Enhancement of T2* weighted MRI imaging sensitivity of U87MG glioblastoma cells using γ-ray irradiated low molecular weight hyaluronic acid-conjugated iron nanoparticles. *Int. J. Nanomed.* **2021**, *16*, 3789–3802. [CrossRef] [PubMed]
21. Khorsandi, L.; Mansouri, E.; Rashno, M.; Karami, M.A.; Ashtari, A. Myricetin Loaded Solid Lipid Nanoparticles Upregulate MLKL and RIPK3 in Human Lung Adenocarcinoma. *Int. J. Pept. Res. Ther.* **2020**, *26*, 899–910. [CrossRef]
22. Hadavi, R.; Jafari, S.M.; Katouzian, I. Nanoliposomal encapsulation of saffron bioactive compounds; characterization and optimization. *Int. J. Biol. Macromol.* **2020**, *164*, 4046–4053. [CrossRef]
23. Salmanzadeh, R.; Eskandani, M.; Mokhtarzadeh, A.; Vandghanooni, S.; Ilghami, R.; Maleki, H.; Saeeidi, N.; Omidi, Y. Propyl gallate (PG) and tert-butylhydroquinone (TBHQ) may alter the potential anti-cancer behavior of probiotics. *Food Biosci.* **2018**, *24*, 37–45. [CrossRef]
24. Detsi, A.; Kavetsou, E.; Kostopoulou, I.; Pitterou, I.; Pontillo, A.R.N.; Tzani, A.; Christodoulou, P.; Siliachli, A.; Zoumpoulakis, P. Nanosystems for the encapsulation of natural products: The case of chitosan biopolymer as a matrix. *Pharmaceutics* **2020**, *12*, 669. [CrossRef]
25. Yang, J.T.; Lee, I.N.; Lu, F.J.; Chung, C.Y.; Lee, M.H.; Cheng, Y.C.; Chen, K.T.; Chen, C.H. Propyl Gallate Exerts an Antimigration Effect on Temozolomide-Treated Malignant Glioma Cells through Inhibition of ROS and the NF- κ B Pathway. *J. Immunol. Res.* **2017**, *2017*. [CrossRef]
26. Stocker, E.; Becker, K.; Hate, S.; Hohl, R.; Schiemenz, W.; Sacher, S.; Zimmer, A.; Salar-Behzadi, S. Application of ICH Q9 Quality Risk Management Tools for Advanced Development of Hot Melt Coated Multiparticulate Systems. *J. Pharm. Sci.* **2017**, *106*, 278–290. [CrossRef]
27. ICH. *Pharmaceutical Development Q8*; ICH Harmonised Tripartite Guideline; ICH: Geneva, Switzerland, 2009; pp. 1–28.
28. Németh, Z.; Pallagi, E.; Dobó, D.G.; Csóka, I. A proposed methodology for a risk assessment-based liposome development process. *Pharmaceutics* **2020**, *12*, 1164. [CrossRef]
29. Pallagi, E.; Jójárt-Laczkovich, O.; Németh, Z.; Szabó-Révész, P.; Csóka, I. Application of the QbD-based approach in the early development of liposomes for nasal administration. *Int. J. Pharm.* **2019**, *562*, 11–22. [CrossRef]
30. McGregor, D.; Bolt, H.; Cogliano, V.; Richter-Reichhelm, H.B. Formaldehyde and glutaraldehyde and nasal cytotoxicity: Case study within the context of the 2006 IPCS human framework for the analysis of a cancer mode of action for humans. *Crit. Rev. Toxicol.* **2006**, *36*, 821–835. [CrossRef]

31. Pillai, A.M.; Sivasankarapillai, V.S.; Rahdar, A.; Joseph, J.; Sadeghfar, F.; Anuf, A.R.; Rajesh, K.; Kyzas, G.Z. Green synthesis and characterization of zinc oxide nanoparticles with antibacterial and antifungal activity. *J. Mol. Struct.* **2020**, *1211*, 128107. [CrossRef]
32. Mertins, O.; Mathews, P.D.; Angelova, A. Advances in the design of ph-sensitive cubosome liquid crystalline nanocarriers for drug delivery applications. *Nanomaterials* **2020**, *10*, 963. [CrossRef] [PubMed]
33. Rajesh, S.; Zhai, J.; Drummond, C.J.; Tran, N. Synthetic ionizable aminolipids induce a pH dependent inverse hexagonal to bicontinuous cubic lyotropic liquid crystalline phase transition in monoolein nanoparticles. *J. Colloid Interface Sci.* **2021**, *589*, 85–95. [CrossRef]
34. Hao, J.; Zhao, J.; Zhang, S.; Tong, T.; Zhuang, Q.; Jin, K.; Chen, W.; Tang, H. Fabrication of an ionic-sensitive in situ gel loaded with resveratrol nanosuspensions intended for direct nose-to-brain delivery. *Colloids Surfaces B Biointerfaces* **2016**, *147*, 376–386. [CrossRef] [PubMed]
35. Khatoon, M.; Sohail, M.F.; Shahnaz, G.; ur Rehman, F.; Fakhar-ud-Din; ur Rehman, A.; Ullah, N.; Amin, U.; Khan, G.M.; Shah, K.U. Development and Evaluation of Optimized Thiolated Chitosan Proniosomal Gel Containing Duloxetine for Intranasal Delivery. *AAPS PharmSciTech* **2019**, *20*. [CrossRef] [PubMed]
36. Osborne, D.W.; Musakhanian, J. Skin Penetration and Permeation Properties of Transcutol®—Neat or Diluted Mixtures. *AAPS PharmSciTech* **2018**, *19*, 3512–3533. [CrossRef] [PubMed]
37. Chin, L.Y.; Tan, J.Y.P.; Choudhury, H.; Pandey, M.; Sisinthy, S.P.; Gorain, B. Development and optimization of chitosan coated nanoemulgel of telmisartan for intranasal delivery: A comparative study. *J. Drug Deliv. Sci. Technol.* **2021**, *62*, 102341. [CrossRef]
38. Sivasankarapillai, V.S.; Das, S.S.; Sabir, F.; Sundaramahalingam, M.A.; Colmenares, J.C.; Prasannakumar, S.; Rajan, M.; Rahdar, A.; Kyzas, G.Z. Progress in natural polymer engineered biomaterials for transdermal drug delivery systems. *Mater. Today Chem.* **2021**, *19*, 100382. [CrossRef]
39. Varma, L.T.; Singh, N.; Gorain, B.; Choudhury, H.; Tambuwala, M.M.; Kesharwani, P.; Shukla, R. Recent Advances in Self-Assembled Nanoparticles for Drug Delivery. *Curr. Drug Deliv.* **2020**, *17*, 279–291. [CrossRef]
40. Al-Amiery, A.A.; Al-Majedy, Y.K.; Kadhum, A.A.H.; Mohamad, A.B. Hydrogen peroxide scavenging activity of novel coumarins synthesized using different approaches. *PLoS ONE* **2015**, *10*, e0132175. [CrossRef]
41. Sabir, F.; Katona, G.; Pallagi, E.; Dobó, D.G.; Akel, H.; Berkesi, D.; Kónya, Z.; Csóka, I. Quality-by-Design-Based Development of n-Propyl-Gallate-Loaded Hyaluronic-Acid-Coated Liposomes for Intranasal Administration. *Molecules* **2021**, *26*, 1429. [CrossRef]
42. Javadzadeh, Y.; Adibkia, K.; Hamishekar, H. Transcutol® (Diethylene Glycol). In *Percutaneous Penetration Enhancers Chemical Methods in Penetration Enhancement: Modification of the Stratum Corneum*; Springer: Berlin/Heidelberg, Germany, 2015; pp. 195–205. [CrossRef]
43. Khan, A.; Aqil, M.; Imam, S.S.; Ahad, A.; Sultana, Y.; Ali, A.; Khan, K. Temozolomide loaded nano lipid based chitosan hydrogel for nose to brain delivery: Characterization, nasal absorption, histopathology and cell line study. *Int. J. Biol. Macromol.* **2018**, *116*, 1260–1267. [CrossRef] [PubMed]
44. Tapeinos, C.; Battaglini, M.; Ciofani, G. Advances in the design of solid lipid nanoparticles and nanostructured lipid carriers for targeting brain diseases. *J. Control. Release* **2017**, *264*, 306–332. [CrossRef]
45. Bahari, L.A.S.; Hamishehkar, H. The impact of variables on particle size of solid lipid nanoparticles and nanostructured lipid carriers; A comparative literature review. *Adv. Pharm. Bull.* **2016**, *6*, 143–151. [CrossRef]
46. Sarhadi, S.; Gholizadeh, M.; Moghadasian, T.; Golmohammadzadeh, S. Moisturizing effects of solid lipid nanoparticles (SLN) and nanostructured lipid carriers (NLC) using deionized and magnetized water by in vivo and in vitro methods. *Iran. J. Basic Med. Sci.* **2020**, *23*, 337–343. [CrossRef]
47. Naseri, M.; Golmohamadzadeh, S.; Arouiee, H.; Jaafari, M.R.; Nemati, S.H. Preparation and comparison of various formulations of solid lipid nanoparticles (SLNs) containing essential oil of Zataria multiflora. *J. Hortic. Postharvest Res.* **2020**, *3*, 73–84.
48. Zdaniauskienė, A.; Charkova, T.; Ignatjev, I.; Melvydas, V.; Garjonytė, R.; Matulaitienė, I.; Talaikis, M.; Niaura, G. Shell-isolated nanoparticle-enhanced Raman spectroscopy for characterization of living yeast cells. *Spectrochim. Acta Part A Mol. Biomol. Spectrosc.* **2020**, *240*, 118560. [CrossRef]
49. Shringarpure, M.; Gharat, S.; Momin, M.; Omri, A. Management of epileptic disorders using nanotechnology-based strategies for nose-to-brain drug delivery. *Expert Opin. Drug Deliv.* **2021**, *18*, 169–185. [CrossRef]
50. Affes, S.; Aranaz, I.; Acosta, N.; Heras, Á.; Nasri, M.; Maalej, H. Chitosan derivatives-based films as pH-sensitive drug delivery systems with enhanced antioxidant and antibacterial properties. *Int. J. Biol. Macromol.* **2021**, *182*, 730–742. [CrossRef]
51. Lee, H.; Song, C.; Baik, S.; Kim, D.; Hyeon, T.; Kim, D.H. Device-assisted transdermal drug delivery. *Adv. Drug Deliv. Rev.* **2018**, *127*, 35–45. [CrossRef]
52. Abhaihaidelmonem, R.; El Nabarawi, M.; Attia, A. Development of novel bioadhesive granisetron hydrochloride spanlastic gel and insert for brain targeting and study their effects on rats. *Drug Deliv.* **2018**, *25*, 70–77. [CrossRef] [PubMed]
53. Iglesias, N.; Galbis, E.; Valencia, C.; Díaz-Blanco, M.J.; Lacroix, B.; de-Paz, M.V. Biodegradable double cross-linked chitosan hydrogels for drug delivery: Impact of chemistry on rheological and pharmacological performance. *Int. J. Biol. Macromol.* **2020**, *165*, 2205–2218. [CrossRef]
54. Wei, P.L.; Huang, C.Y.; Chang, Y.J. Propyl gallate inhibits hepatocellular carcinoma cell growth through the induction of ROS and the activation of autophagy. *PLoS ONE* **2019**, *14*, e0210513. [CrossRef] [PubMed]

55. Bhise, K.; Kashaw, S.K.; Sau, S.; Iyer, A.K. Nanostructured lipid carriers employing polyphenols as promising anticancer agents: Quality by design (QbD) approach. *Int. J. Pharm.* **2017**, *526*, 506–515. [CrossRef] [PubMed]
56. Pallagi, E.; Ambrus, R.; Szabó-Révész, P.; Csóka, I. Adaptation of the quality by design concept in early pharmaceutical development of an intranasal nanosized formulation. *Int. J. Pharm.* **2015**, *491*, 384–392. [CrossRef] [PubMed]
57. Pallagi, E.; Ismail, R.; Paál, T.L.; Csóka, I. Initial Risk Assessment as part of the Quality by Design in peptide drug containing formulation development. *Eur. J. Pharm. Sci.* **2018**, *122*, 160–169. [CrossRef] [PubMed]
58. Qindeel, M.; Ahmed, N.; Sabir, F.; Khan, S.; Ur-Rehman, A. Development of novel pH-sensitive nanoparticles loaded hydrogel for transdermal drug delivery. *Drug Dev. Ind. Pharm.* **2019**, *45*, 629–641. [CrossRef] [PubMed]
59. Katona, G.; Balogh, G.T.; Dargó, G.; Gáspár, R.; Márki, Á.; Ducza, E.; Sztojkov-Ivanov, A.; Tömösi, F.; Kecskeméti, G.; Janáky, T.; et al. Development of meloxicam-human serum albumin nanoparticles for nose-to-brain delivery via application of a quality by design approach. *Pharmaceutics* **2020**, *12*, 97. [CrossRef]
60. Sipos, B.; Szabó-Révész, P.; Csóka, I.; Pallagi, E.; Dobó, D.G.; Bélteky, P.; Kónya, Z.; Deák, Á.; Janovák, L.; Katona, G. Quality by design based formulation study of meloxicam-loaded polymeric micelles for intranasal administration. *Pharmaceutics* **2020**, *12*, 697. [CrossRef] [PubMed]
61. Rajinikanth, P.S.; Chellian, J. Development and evaluation of nanostructured lipid carrier-based hydrogel for topical delivery of 5-fluorouracil. *Int. J. Nanomedicine* **2016**, *11*, 5067. [CrossRef]
62. Youssef, N.A.H.A.; Kassem, A.A.; Farid, R.M.; Ismail, F.A.; EL-Massik, M.A.E.; Boraie, N.A. A novel nasal almotriptan loaded solid lipid nanoparticles in mucoadhesive in situ gel formulation for brain targeting: Preparation, characterization and in vivo evaluation. *Int. J. Pharm.* **2018**, *548*, 609–624. [CrossRef] [PubMed]
63. Porfiryeva, N.N.; Semina, I.I.; Salakhov, I.A.; Moustafine, R.I.; Khutoryanskiy, V.V. Mucoadhesive and mucus-penetrating Interpolyelectrolyte complexes for nose-to-brain drug delivery. *Nanomed. Nanotechnol. Biol. Med.* **2021**, 102432. [CrossRef]

ANNEX-IV

pharmaceutics

MDPI

Article

Development of Lomustine and *n*-Propyl Gallate Co-Encapsulated Liposomes for Targeting Glioblastoma Multiforme via Intranasal Administration

Gábor Katona [1,*,†], Fakhara Sabir [1,†], Bence Sipos [1], Muhammad Naveed [2], Zsuzsanna Schelz [3], István Zupkó [3] and Ildikó Csóka [1]

[1] Institute of Pharmaceutical Technology and Regulatory Affairs, Faculty of Pharmacy, University of Szeged, Eötvös Str. 6, H-6720 Szeged, Hungary; fakhra.sabir@gmail.com (F.S.); sipos.bence@szte.hu (B.S.); csoka.ildiko@szte.hu (I.C.)

[2] Department of Pharmacology and Pharmacotherapy, Faculty of Medicine, University of Szeged, Dóm Sqr. 12, H-6720 Szeged, Hungary; naveed.muhammad@med.u-szeged.hu

[3] Department of Pharmacodynamics and Biopharmacy, Faculty of Pharmacy, University of Szeged, Eötvös Str. 6, H-6720 Szeged, Hungary; schelz.zsuzsanna@szte.hu (Z.S.); zupko@pharm.u-szeged.hu (I.Z.)

* Correspondence: katona.gabor@szte.hu; Tel.: +36-62-545-575

† These authors contribute equally to this work.

Abstract: This work aimed to develop lomustine (LOM) and *n*-propyl gallate (PG)-loaded liposomes suitable for targeting glioblastoma multiforme (GBM) via the auspicious nose-to-brain drug delivery pathway. The therapeutical effect of LOM, as a nitrosourea compound, can be potentiated by PG suitable for enhanced anti-cancer therapy. Nose-to-brain delivery of PG and LOM combined in liposomes can overcome the poor water solubility, absorption properties, and toxicity issues in the systemic circulation. Optimization and characterization of the liposomal carrier with binary drug contents were carried out in order to achieve adequate encapsulation efficiency, loading capacity, drug release, and ex vivo permeation. The optimized liposome co-encapsulated with both drugs showed suitable Z-average (127 ± 6.9 nm), size distribution (polydispersity index of 0.142 ± 0.009), zeta potential (−34 ± 1.7 mV), and high encapsulation efficacy (63.57 ± 1.3% of PG and 73.45 ± 2.2% of LOM, respectively) meeting the acceptance criteria of nose-to-brain transport for both drugs. MTT assays of PG-LOM formulations were also conducted on NIH/3T3 (murine embryonic fibroblast), U87 (glioblastoma), and A2780 (ovarian cancer) cell lines indicating reduced an antiproliferative effect on all types of cells. Our results supported the use of this novel combination of LOM and PG in a liposomal formulation as a promising carrier for glioblastoma targeting via the intranasal route.

Keywords: lomustine; *n*-propyl gallate; glioblastoma multiforme; liposome; nasal delivery; controlled release

Citation: Katona, G.; Sabir, F.; Sipos, B.; Naveed, M.; Schelz, Z.; Zupkó, I.; Csóka, I. Development of Lomustine and *n*-Propyl Gallate Co-Encapsulated Liposomes for Targeting Glioblastoma Multiforme via Intranasal Administration. *Pharmaceutics* **2022**, *14*, 631. https://doi.org/10.3390/pharmaceutics14030631

Academic Editor: Eliana Leo

Received: 12 February 2022
Accepted: 11 March 2022
Published: 12 March 2022

1. Introduction

Glioblastoma multiforme (GBM) is an aggressive and the most recurrent form of the central nervous system (CNS) tumors, which accounts for 65% of the cases of brain tissue-associated tumors. The poor prognosis, uncontrolled cell division, diffuse infiltration, and significant angiogenesis are associated with the main GBM characteristics [1,2]. The effective treatment for GBM belongs to unmet medical needs. The morphologically diffuse and heterogeneous nature of GBM makes it especially challenging for therapeutics to access the tumor site [3]. Besides the structural limitations, the blood–brain barrier (BBB) forms another obstacle limiting the successful delivery of antineoplastic agents to target GBM, which is the major drawback of therapy through conventional administration routes. To overcome these obstacles, novel strategies and drug carriers are required to enhance the successful localization of chemotherapeutics to the tumor site [4].

To deliver chemotherapeutics to the target site, the common treatment strategy is to apply them peripherally (parenteral or oral), however, these delivery routes reduce the potency of the drug molecule leading to low brain targeting efficacy [5]. Moreover, the first-pass effect, systemic clearance, enzymatic degradation, plasma protein binding, and the volume of distribution can reduce the bioavailability of drugs through conventional administration routes [6]. Intranasal administration (IN) can overcome the limitations of conventional drug delivery and allows a faster delivery process [7]. Nose-to-brain delivery is a simple, direct approach resulting in a shorter onset of action, improved targetability, low systemic toxicity, and clearance [8]. In addition to that, an increased concentration of the active pharmaceutical agent (API) can be achieved in the CNS through this pathway bypassing the BBB [9].

The following important features of the nasal epithelial should be considered while administering nanoparticles via IN route. The epithelial surface of the nasal mucosa is covered with a protective mucin layer as the primary non-aqueous component of mucus. Mucin is a polymer carrying a complex and heterogeneous structure with domains that undergo a variety of molecular interactions, such as primary hydrophilic/hydrophobic and secondary hydrogen bonds besides electrostatic interactions, which can additionally contribute to the limitation of sufficient nose-to-brain transport of particles due to filtration [10]. In the case of particles that can overcome these hurdles by passing through the mucin layer have a chance for efficient absorption through the nasal mucus. Nasal mucus is a selective barrier with a thickness of 5–15 µm and a pore size of 150 ± 50 nm, which regulates permeability by hindering the transport of particles (>200 nm) across the mucosal epithelia [11]. Those particles, which meet the particle size criterion are able to absorb through different pathways. Extracellular nasal transport can occur across the tight junctions; however, mainly free molecules are able to get over this narrow passage (3.9–8.4 Å). The application of absorption enhancers can facilitate this transport by opening the tight junctions; therefore, the particles with a diameter smaller than 20 nm are more likely to achieve this way of extracellular transport from the nasal cavity to the brain. In the case of intracellular transport, the expected size of the nanoparticles should be smaller than the diameter of the olfactory axons. Previous studies revealed the diameter of the olfactory axons in rabbits is around 200 nm and in humans between 10 and 700 nm. Therefore, the internalization of the nanoparticles is strongly dependent on their concentration, lipophilicity, and particle characteristics [12,13].

Liposomes are potential vehicles for nose-to-brain delivery as they consist of a water-soluble core surrounded by a phospholipid membrane, which is able to improve permeation through the nasal mucosa membrane. Therefore, this characteristic increases lipophilicity and facilitates lipophilic molecules crossing the BBB [14]. The encapsulation of the drug into liposomes can reduce its peripheral toxicity and increase bioavailability and CNS retention. Furthermore, it can also preserve the structural stability of the drug. Liposomes are capable of directly penetrating tumor cells by means of endocytosis and thereby release the drugs locally for highly targeted treatment [15]. Previous studies revealed co-encapsulation of antioxidant compounds with drug components into liposomes or niosomes can potentiate the therapeutic effect at the targeting site [16]. Several studies also revealed the synergic potential of nitrosoureas combined with PG, which contributes to reducing the dosage of required alkylating agents [17].

Lomustine (LOM) is an alkylating anticancer drug, which non-specifically mutates the cell cycle at the G1 stage, G2 stage, G2/S, and M stage. LOM is able to enhance the sensitivity of tumor cells and induce apoptotic cell death through TRC8-mediated degradation targeting heme oxygenase-1 [18]. Conventionally, LOM is orally administered although it has very low bioavailability and significant side effects. Recent studies revealed *n*-Propyl gallate (PG), an antioxidant compound, also has biological applications including antitumor, anti-angiogenic, and anti-inflammatory effects [19]. PG can induce apoptosis in human leukemia cells and HeLa cells by increasing the reactive oxygen species (ROS) levels or glutathione (GSH) depletion through the activation of caspase-3, 8, and 9 [20]. Therefore,

the combination of LOM and PG in a suitable drug carrier can be advantageous, especially through nose-to-brain. By exploiting this alternative route, an increased bioavailability of both LOM and PG is expected at low therapeutic doses reducing the occurrence of side effects [21,22]. Yasaswi et al. reported LOM, loaded nanoparticles, prepared with molecular envelope technology showed improved brain tumor therapy without major toxicity [23]. Yang et al. developed LOM and iohexol (a contrast medium for visualization via Computed Tomography) containing thermo-sensitive liposomes for site-specific delivery into the brain tumor showing increased half-life and bioavailability on the C6 glioma model [24]. Wang et al. also developed LOM-loaded thermo-sensitive liposomes with improved properties for targeted tumor therapy [25].

In this study, LOM and PG were co-encapsulated into liposomes with the aim of developing a suitable carrier system applicable in the treatment of GBM through the intranasal route. The nasal applicability of the novel liposomal formulation was characterized according to nanoparticulate properties (average hydrodynamic diameter, polydispersity index, surface charge, encapsulation efficacy), drug release, and ex vivo nasal diffusion. In vitro cellular uptake and the antiproliferative and cytotoxic effects of liposomes co-encapsulated with PG-LOM on normal cell lines (NIH/3T3 mouse embryonic) and different cancer cell lines (U-87 and U251 glioblastoma as well as A2780 ovarium cancer) were investigated.

2. Materials and Methods

2.1. Materials

LOM (≥98%), PG (≥98%), and phosphatidylcholine (PCL, ≥99%) from soybean were purchased from Sigma-Aldrich Co. Ltd. (Budapest, Hungary). Cholesterol (CHL, ≥99%), ethanol (96% *v/v*), and sodium chloride physiological solution (0.9% *w/w*) were obtained from Molar Chemicals Ltd., (Budapest, Hungary). All cell lines were purchased from the European Collection of Cell Cultures (Salisbury, UK). All reagents for cell line studies were purchased from Sigma–Aldrich Co. Ltd. (Budapest, Hungary) if not indicated otherwise.

2.2. Preparation of Liposomes

A novel direct pouring method (DPM) was used to develop liposomal formulations. This simple technique was based on a modified solvent evaporation method resulting in the stabilized formulation in the case of applying the optimal composition of lipids. In our previous study, the critical factors of the DPM method were determined by a risk assessment (RA)-based experimental design. The RA is the evaluation of the interdependence between the quality target product profile (QTPP) elements and critical quality attributes (CQAs) and between the critical process parameters (CPPs) and CQAs [26]. The RA was implemented by Lean QbD® software (QbDworks.com, QbDworks LLC., Fremont, CA, USA). Based on the RA, the quantity of PCL, the quantity of CHL, the temperature of evaporation showed the highest severity score, indicating a major influence on QTPP. The optimal ranges of these significant parameters, which were also applied in the present study, were determined using a Box–Behnken experimental design [27]. To reach the optimal lipid composition, CHL and PCL were used in different molar ratios (0.67, 1, 1.33, 1.5, 2, 2.67, 4, and 6 mol/mol for CHL). Lipids were dissolved in 4 mL of ethanol–acetone (3:1) mixture and directly added to 10 mL of purified water. After that, the organic solvents were evaporated at 60 °C under constant stirring (400 rpm) by using a hot-plate magnetic stirrer. Drug loaded liposomes were prepared with the same procedure, during which both PG and LOM were added in different mass ratios (1:1, 1:2, 1:3, 2:1, 3:1, 3:4, and 4:3 *w/w*) to the formulation to reach the optimal composition while dissolving lipids in the organic solvent mixture. Three types of liposomes were prepared containing PG and LOM separately and also combined, namely, PG-loaded liposomes (PG-Lipo), LOM-loaded liposomes (LOM-Lipo), and combined PG- and LOM-loaded Liposomes (PG-LOM-Lipo). After constructing the liposomes, the unencapsulated drug was removed via dialysis at 4 °C by using an 8 kDa MWCO dialysis membrane (Spectra/Por®, Spectrum Laboratories Inc., Rancho Dominguez, CA, USA). Liposomal formulations were poured into a dialysis bag

and sunk into a beaker containing 500 mL physiological saline solution in order to maintain consistent osmotic pressure. After 24 h dialysis, liposomes were centrifuged for 1.5 h at 13,500 rpm in two cycles, among which the pellet was collected and redispersed in 10 mL of purified water using a vortex mixer at 500 rpm (Biobase MX-S, Jinan, Shandong, China). For solid-state characterization, the redispersed pellet was freeze-dried after a purification process at −40 °C and 0.013 mbar for 12 h using ScanVac CoolSafe 100–9 (LaboGene, ApS, Lynge, Denmark) laboratory apparatus. Secondary drying was carried out at 25 °C and 0.013 mbar for 6 h.

2.3. Average Hydrodynamic Diameter, Polydispersity Index, and Surface Charge

Average hydrodynamic diameter (Z-average), polydispersity index (PDI), and zeta potential of liposomal formulations were analyzed in folded capillary cells using a Malvern Nano ZS instrument (Malvern Instruments, Worcestershire, UK). Measurements were carried out at room temperature (25 °C) with a refractive index of 1.445 in three parallel runs and the average value of runs was evaluated. Our standard acceptable criteria range meeting the requirements of IN delivery for the Z-average, PDI, and zeta potential was set to 100–200 nm, 0.0–0.5, and <−15 or >+15 (mV), respectively [28].

2.4. Determination of Encapsulation Efficiency, Loading Capacity, and Drug Content of Compared Formulations

To measure the encapsulation efficiency (EE) and drug loading capacity (LC), liposomal formulations were centrifuged for 1 h at 4 °C and 16,500 rpm (22,413 RCF) in a Hermle Z323 laboratory centrifuge (Hermle AG, Gossheim, Germany), then, the pellet was purified in two cycles, among which it was redispersed in 1.5 mL of purified water using a vortex mixer (Biobase MX-S, Jinan, Shandong, China). After the purification process, the pellet was collected and dissolved in 1 mL of acetonitrile. The quantification of the PG and LOM was performed by HPLC. Each formulation was measured in triplicate. The encapsulation efficacy of LOM and PG was calculated using the following equation [29]:

$$\text{Encapsulation efficiency } (\%) = \frac{w_1}{w_1 + w_2} \times 100 \quad (1)$$

where w_1 represents the amount of liposomal entrapped drug (i.e., recovered from the pellet) and w_2 represents the amount of freely un-entrapped drug (i.e., detected in the supernatant).

The LC was calculated via the following equation:

$$\text{Loading capacity } (\%) = \frac{w_1 - w_2}{w_3} \times 100 \quad (2)$$

where w_1 represents the initial amount of the drug used for the formulation, w_2 represents the entrapped drug in the pellet, and w_3 represents the total amount of lipids applied in the formulation. Drug content (DC) was measured by HPLC after a 10-fold dilution of 1.0 mL liposomal formulation with acetonitrile and filtering through a 0.1 µm membrane filter.

2.5. HPLC Method

The quantification of LOM and PG was carried out via HPLC (Agilent 1260, Agilent Technologies, Santa Clara, CA, USA). In the case of LOM, the stationary phase was a Kinetex® EVO C18 column (150 mm × 4.6 mm, 5 µm (Phenomenex, Torrance, CA, USA). The mobile phases used were Milli-Q® ultrapure water (A) and acetonitrile (B). Twenty microliter samples were analyzed. Separation was performed in two steps by gradient elution at 30 °C. The proportion of starting 50% A eluent was reduced to 25% by 10 min and then raised again to 50% by 11 min. For PG analysis as stationary phase a Gemini-NX® C18 column (150 mm × 4.6 mm, 5 µm (Phenomenex, Torrance, CA, USA) was applied. As the mobile phase, Milli-Q® ultrapure water and acetonitrile in an 80:20 ratio, with an adjusted pH = 3.0 using *ortho*-phosphoric acid. Twenty microliter samples were injected, whereas separation was performed by 10 min isocratic elution at 25 °C temperature with

1 mL/min eluent flow. In both measurements, the eluent flow rate was set to 1 mL/min and the chromatograms were detected at 254 nm using an UV-VIS diode array detector. ChemStation B.04.03 Software (Santa Clara, CA, USA) was used for the evaluation of the data. The linear regression of the calibration was 0.999 in the case of LOM, while it was 0.998 for PG. The quantification limit (LOQ) and detection (LOD) of LOM were 40 ppm and 13 ppm, while in the case of PG, 63 ppm and 21 ppm, respectively.

2.6. Differential Scanning Calorimetry (DSC)

DSC measurements were performed using a Mettler Toledo DSC 821e instrument (Mettler–Toledo GmbH, Greifensee, Switzerland) to investigate the thermal behavior of freeze-dried pellets (PG-Lipo, LOM-Lipo, and PG-LOM-Lipo) obtained by centrifugation. Approximately 3–5 mg of liposomal pellets was measured into a 40 µL aluminum pan. As a reference, an empty aluminum pan was used. Both pans were perforated, in order to allow the atmosphere above the sample to expand. Measurement was performed in the temperature range of 25 to 325 °C, at a 10 °C/min heating rate under a constant argon atmosphere with a flow rate of 150 mL/min. Data analysis was performed by using STARe software V9.0 (Mettler–Toledo GmbH, Greifensee, Switzerland). Each measurement was normalized to the sample size, according to the measured weight of each composition.

2.7. X-Ray Powder Diffractometry (XRPD)

The XRPD diffractogram of the initial PG, LOM, and freeze-dried pellets obtained by centrifugation (PG-Lipo, LOM-Lipo, and PG-LOM-Lipo) was measured by using a Bruker D8 ADVANCE X-ray powder diffractometer (Bruker AXS GmbH, Karlsruhe, Germany). All the results were obtained using a VANTEC slit detector with Cu K λI radiation (λ = 1.5406). The investigation of all components was carried out at 40 kV and 40 mA in the angular range of 3 to 40° 2θ with a step time of 0.1 s and a step size of 0.007°. The samples were measured on a quartz sample holder at room temperature. The crystallinity index (CI) of both PG and LOM was determined semi-quantitatively based on the total area under diffractograms of the starting compounds ($A_{crystalline}$) compared to the total area under diffractograms of the liposomal formulations ($A_{crystalline}$ + $A_{amorphous}$) [30]:

$$CI\ (\%) = \frac{A_{crystalline}}{A_{crystalline} + A_{amorphous}} \times 100 \quad (3)$$

2.8. In Vitro Release Studies

In vitro release study was performed at 35 °C using dialysis membrane method at 50 rpm constant stirring. 1 mL of liposomal formulations (PG-Lipo, LOM-Lipo, PG-LOM-Lipo, PG suspension, and LOM suspension containing 1-1 mg of PG and LOM, respectively) were poured into an 8 kDa dialysis bag (Spectra/Por®, Spectrum Laboratories Inc., Rancho Dominguez, CA, USA) and placed in 50 mL of 7.4 pH PBS. Aliquots were taken at predetermined time intervals for 120 min, then, both LOM and PG contents were determined via the HPLC method, as described above. Each measurement was carried out in triplicate, data were shown as mean ± SD. The in vitro drug release kinetics was evaluated by fitting mathematical models (First order, Zero-order, Korsmeyer–Peppas, Hixson–Crowell, and Higuchi-model) [31].

2.9. Stability Studies

The stability of freeze-dried liposomal formulations (PG-Lipo, LOM-Lipo, PG-LOM-Lipo) was evaluated over a period of 4 weeks. Briefly, the formulations were stored at 4 °C and 25 °C (ambient temperature), while samples were withdrawn at specific time intervals (1, 2, 3, and 4 weeks). The samples were analyzed for Z-average, zeta potential, and EE, as described above.

2.10. Ex-Vivo Studies

2.10.1. Isolation of Rabbit Nasal Mucosa

Nasal mucosa was isolated from male New Zealand rabbits (body mass 2–3 kg) Immediately after the animals (n = 4) were sacrificed by rapid cervical dislocation, nasal cavities of the rabbits were opened surgically, and the nasal mucosa was isolated [32]. The nasal septum was extracted, and the mucosa layers were carefully detached from the septum cartilage by using bone cutters or surgical scissors and cut into 400 ± 50 µm thick slices. This thickness is sufficient to represent the entire mucosal barrier of the nasal cavities, including the epithelial barrier (thickness around 100 µm) as well as part of the underlying connective tissue [33]. Total nasal mucosa was obtained and used for the experiment. To maintain the viability of the excised nasal tissue, it was immediately immersed in ice-cold phosphate buffer saline pH 7.4 for 15 min and aerated (95% O_2 and 5% CO_2) until further use [34]. All experiments conformed to the Directive 2010/63/EU of the European Parliament. The protocols have been approved by the Ethical Committee for the Protection of Animals in Research of the University of Szeged, Szeged, Hungary, and by the Department of Animal Health and Food Control of the Ministry of Agriculture and Rural Development (authority approval numbers XIII./4227/2016).

2.10.2. Ex Vivo Raman Chemical Mapping on Rabbit Nasal Mucosa

Five microliters of PG-Lipo, LOM-Lipo, PG-LOM-Lipo, PG suspension, and LOM suspension containing 1-1 mg of PG and LOM, respectively, were instilled at the epithelial surface of the nasal mucosa. After 60 min, the formulation was wiped off and washed two times with physiological saline solution, and the nasal mucosa was divided into cross-sections into the incision point, then inverted to the cross-sectional side and placed on an aluminum foil-coated glass slide. Ex vivo Raman chemical mapping was performed via a ThermoFisher XDR Dispersive Raman instrument (ThermoFisher Scientific Inc., Waltham, MA, USA) equipped with a CCD camera and a diode laser operating at a wavelength of 780 nm. A 500 µm × 500 µm size surface was analyzed with a step size of 50 µm with an exposure time of 4 s and acquisition time of 4 s, for a total of 4 scans per spectrum in the spectral range of 3500 to 200 cm^{-1} with cosmic-ray and fluorescence corrections. The Raman spectra were normalized, in order to eliminate the intensity deviation between the measured areas.

2.10.3. Ex Vivo Nasal Diffusion Study on Rabbit Nasal Mucosa

The ex vivo transmucosal passive diffusion study of the formulations under nasal conditions was performed in a modified Side-Bi-Side® type horizontal diffusion apparatus. The diffusion of PG-Lipo, LOM-Lipo, PG-LOM-Lipo, PG suspension, and LOM suspension containing 1-1 mg of PG and LOM, respectively, was tested. The freshly excised rabbit nasal mucosa was mounted between the donor and acceptor compartment (effective diffusion surface area of 0.785 cm^2). The donor phase consisted of 8.0 mL of Simulated Nasal Electrolyte Solution (SNES, containing 8.77 g/L sodium chloride (NaCl), 2.98 g/L potassium chloride (KCl), 0.59 g/L anhydrous calcium chloride ($CaCl_2$) dissolved in purified water, pH 5.6), while the acceptor phase contained 9.0 mL of pH 7.4 PBS. The temperature of both chambers was controlled at 35 ± 0.5 °C using a heating circulator (ThermoHaake C 10-P5, Sigma–Aldrich Co., Ltd., Budapest, Hungary). For the diffusion study, each formulation (1 mL) was placed in the donor compartment of the diffusion cell. Both donor and acceptor compartments were continuously stirred at 100 rpm using magnetic stirrers. Aliquots from the acceptor phase (150 µL) were taken at predetermined time points (1, 3, 5, 10, 15, 30, and 60 min) and replaced with fresh medium. LOM and PG concentrations were determined using HPLC. The flux (J) was calculated from the quantity of the drug permeated through the membrane, divided by the surface of the membrane insert (0.785 cm^2) and the duration of the experiment (µg/cm^2/h). The permeability coefficient

(K_p) was determined from J and the drug concentration in the donor phase (Cd (μg/cm^3)). as seen in the following equation:

$$K_p\left[\frac{cm}{h}\right] = \frac{J}{C_d} \quad (4)$$

Relative permeation at 60 min (RP_{60}) was calculated as a quotient of the liposomal formulations compared to the solutions. Statistical analysis was performed via one-way ANOVA with a posthoc Tukey's comparison test using TIBCO Statistica® 13.4 (Statsoft Hungary, Budapest, Hungary) software.

Change in Z-average and PDI of liposomes after diffusion through the nasal mucosa was also measured in the acceptor phase to predict the fate of the liposomal carrier after passing the nasal mucosa. At the predetermined time points mentioned above, aliquots were withdrawn from the acceptor phase (0.5 mL) and replaced with fresh medium. Z-average and PDI from the aliquots were determined with DLS.

2.11. Antiproliferative MTT Assay

The antiproliferative effect of LOM, PG, and their liposome complexes were determined via an in vitro experiment using NIH/3T3 mouse embryonic fibroblasts, A2780 human ovarian cancer, and U87 glioblastoma cells, by means of a MTT ([3-(4,5-dimethylthiazol-2-yl)-2,5-diphenyltetrazolium bromide]) assay. Glioblastoma cells were cultivated in Dulbecco's Modified Eagle's Medium supplemented with 1 mM sodium–pyruvate. NIH/3T3 and A2780 cells were cultured in Eagle's Minimal Essential Medium. Both culture media were supplemented with 10% fetal bovine serum, 1% non-essential amino acids, and an antibiotic–antimycotic mixture. A limited number of human cancer cells and murine fibroblasts (5000/well) were seeded into a 96-well micro-plate and became attached to the bottom of the well overnight. On the second day of the procedure, the test substances were added in serial dilution (applied in six different concentrations). After an incubation period of 72 h, the living cells were assayed by the addition of 20 μL of 5 mg/mL MTT solution. After a 4 h incubation, the medium was removed, and the precipitated formazan was dissolved in 100 μL/well of DMSO during a 60-min period of shaking. Finally, the reduced MTT was assayed at 545 nm, by reading the absorbance, using a Spectrostar Nano spectrophotometer (BMG Labtech, Ortenberg, Germany). Untreated cells were taken as the negative control. All in vitro experiments were carried out on two 96-well microplates with at least five parallel wells in two independent experiments [35].

2.12. In Vitro Cellular Uptake Study

In vitro cellular uptake of the liposomal carrier was investigated by propidium iodide (PI) labeled liposomes on U87 and a more resistant U251 glioblastoma cell line. PI-loaded liposomes were prepared with DPM, similarly to PG- and LOM-loaded liposomes using the optimized lipid composition of CHL and PCL, as described previously. The prepared PI-loaded liposomal formulation contained PI in a 50 μg/mL concentration. The cells were seeded into 96-well microplates with 5000 cell/well cell number. All culture media contained 10% fetal bovine serum, antibiotic/antimycotic complex, and non-essential amino acids. The plates were incubated at 37 °C at 5% CO_2 tension in a humidified atmosphere overnight and the liposomal nanoparticles were added to the wells in order to have 100 μM PI in each well. After a 24h incubation period, the cells were stained with cell track green (CTG) in a 5 μM concentration. The supernatant was removed and 100 μL medium was added to each well. The cells were examined by a Nikon Fluorescent Microscope (Nikon Instruments Inc., Amstelveen, The Netherlands) equipped with a Digital Sight Camera System, including appropriate filters for PI.

2.13. Statistical Analysis

The statistical analysis of the results of this research data was performed using TIBCO Statistica® 13.4 (Statsoft Hungary, Hungary). All the results were repeated in triplicate. All

data presented are means ± SD. In vitro release and ex-vivo permeability data were processed using one-way analysis of variance (ANOVA). Changes were considered statistically significant at $p < 0.05$. Calculations of the cell-based assay were performed by GraphPad Prism 5 (GraphPad Software; San Diego, CA, USA).

3. Results

3.1. Optimization of the Liposomal Carrier

The effect of different weight ratios of CHL and PCL were investigated on Z-average, PDI, and zeta potential (ZP), as shown in Figure 1. The particle size of IN administered nanoparticles is required to be reduced as low as possible, to ensure adequate absorption of the encapsulated drug. The Z-average of CHL:PCL 1.33 was found to be significantly lower in comparison to other investigated compositions, the only exception was detected in the case of CHL:PCL 6. From this point of view, these two compositions seemed to be optimal. However, investigating the PDI, it was clearly shown that CHL:PCL 6 had a significantly higher PDI, which predicts hyperdispersed particle size distribution, therefore, uncertain absorption properties and physical stability. The third important parameter was the ZP for defining the optimal composition. From a stability point of view, the higher the absolute value of ZP, the higher the chance to avoid aggregation of nanoparticles as a result of repulsion forces. However, as the mucosal membrane is also negatively charged, the absorption of highly negatively charged nanoparticles may be hindered. This fact also supports the selection of CHL:PCL 1.33 as the optimal composition, showing the least negative surface charge (−31 ± 2.9 mV), which indicates minimal electrostatic repulsion with mucosal membrane, therefore improved nasal absorption. CHL:PCL 1.33 also resulted in one of the lowest Z-average (118 ± 6.3 nm) and narrow PDI (0.13 ± 0.014).

After selecting the optimal lipid composition of the liposomal carrier (CHL:PCL 1.33), drug-loading in different mass ratios was performed. To reach the optimal PG-LOM composition, the effect of different drug ratios on nanoparticulate characteristics, such as Z-average, PDI, zeta potential, and EE, was evaluated (Figure 2).

PG and LOM tend to encapsulate both inside the phospholipid bilayer and precipitate in a crystalline form in the aqueous vesicle of the liposome, because of their lipophilic nature. This fact is also supported by the slight increase in Z-average while increasing the quantity of the drugs in the formulation. Based on the Z-average values, the applied drug concentrations should be minimized to avoid significant deviation in the vesicle size of the liposomal formulation. The PDI values were not clearly associated with these findings; at higher drug concentrations, similar narrow PDI was observed as in the case of the blank carrier. The ZP values were proportional with increasing drug concentrations, indicating inhibition of aggregation due to electrostatic repulsion. However, increased ZP had a negative effect on the absorption ability through the electrostatic interaction with the negatively charged mucosal membrane. The EE data showed appropriate results in the case of the PG-LOM 1:1 ratio. In the case of other compositions, the EE of one of the drugs was not optimum. All in all, it was revealed that the application of PG-LOM in a 1:1 ratio showed no significant effect on nanoparticle characteristics in comparison to the blank liposomal carrier; therefore, this drug mass ratio was selected for further characterization. The obtained Z-average (127 ± 6.9 nm), PDI (0.142 ± 0.009), ZP (−34 ± 1.7 mV), and high EE (59.87 ± 0.9% of PG, and 71.78 ± 1.5% of LOM, respectively), in the case of both drugs, were suitable for acceptance criteria of nose-to-brain transport [28]. Based on these results, the optimized co-encapsulated formulation (PG-LOM-Lipo) contained both PG and LOM in 1-1 mg/mL after re-dispersion of the pellet in 10 mL purified water, which was applied for further characterizations. For comparison, single drug-loaded liposomes, PG-Lipo, and LOM-Lipo (containing 1-1 mg/mL of PG and LOM, respectively) were also prepared and characterized. The EE, LC, and DC of the optimized and control formulations were determined and compared to each other (Table 1). Each composition resulted in a high EE, LC, and DC, which estimates encapsulated drug found both in the membrane and vesicle of liposomes, indicating controlled drug release from the liposomes mediated by

small lipid–drug aggregates or assemblies formed due to the lipophilic nature of drugs. The combined formulation (PG-LOM-Lipo) showed reduced EE and LC in comparison to corresponding single component-loaded liposomes, which can be claimed with the steric hindrance caused by the presence of two drug molecules. However, the relative value of EE and LC of both PG and LOM in PG-LOM-Lipo was quite similar. This effect can probably be explained primarily by the almost same molecular weight of two compounds.

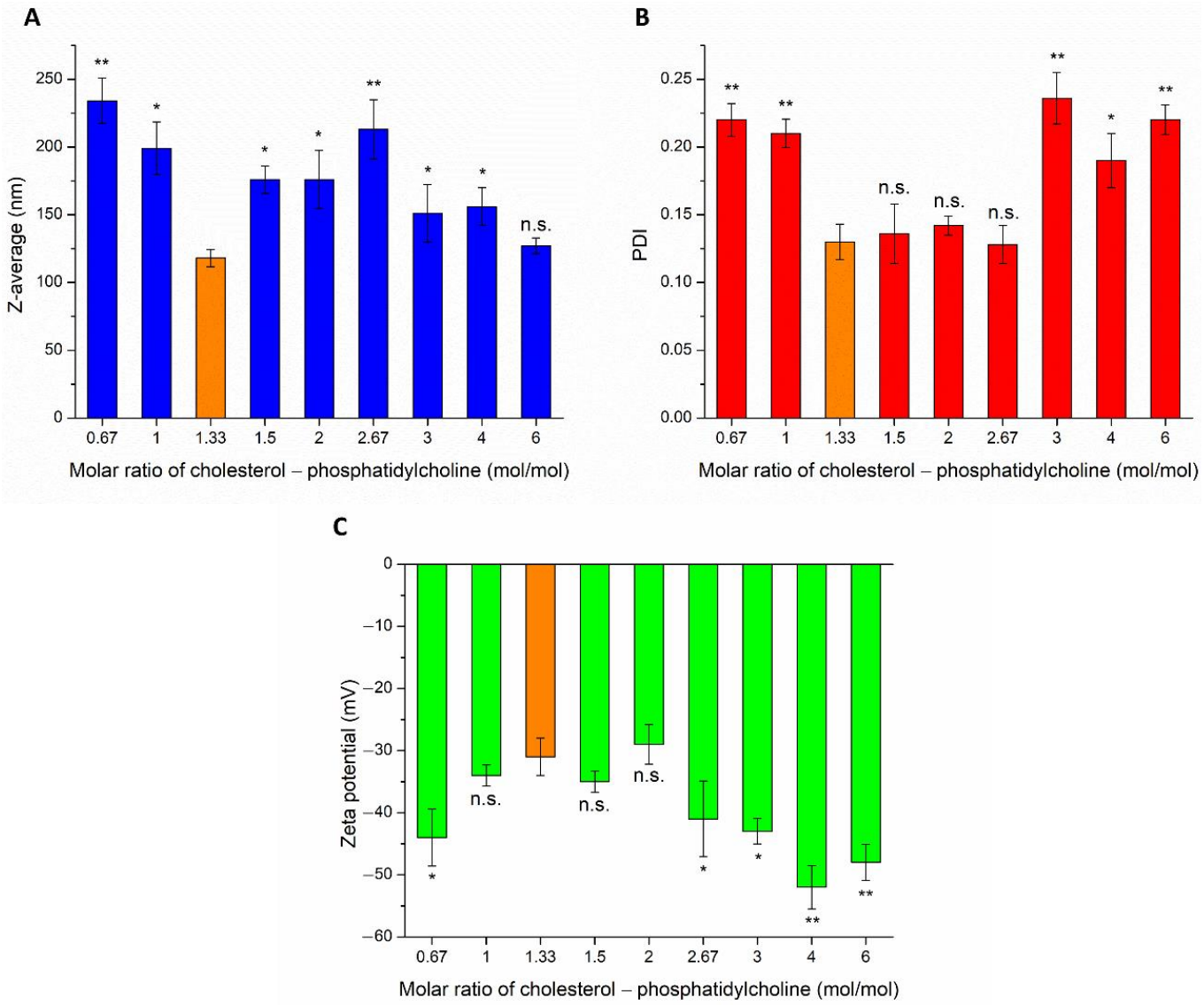

Figure 1. Effect of different molar ratios of cholesterol and phosphatidylcholine (CHL:PCL) for cholesterol on Z-average (**A**), polydispersity index (**B**), and zeta potential (**C**). An ANOVA test was performed to check the significance of the differences between CHL:PCL 1.3 and other compositions, * $p < 0.05$; ** $p < 0.01$; n.s. indicates no significant differences. Measurements were carried out in triplicate ($n = 3$ independent formulations), and data are represented as means ± SD.

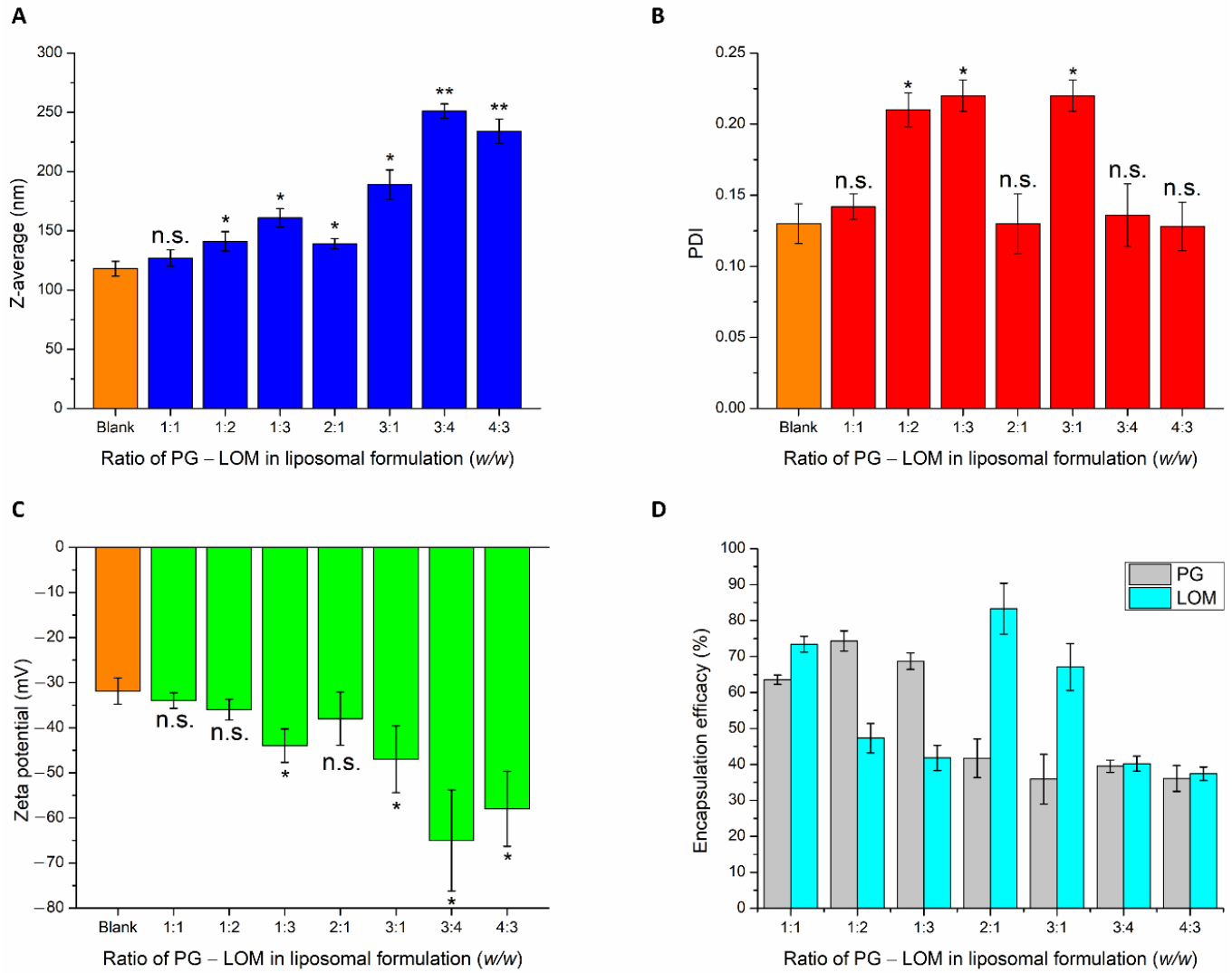

Figure 2. Effect of different PG-LOM ratios on Z-average (**A**), polydispersity index (**B**), zeta potential (**C**), and encapsulation efficacy (**D**) of the optimized liposomal carrier. An ANOVA test was performed to check the significance of the differences between optimized blank liposome and drug-loaded formulation. * $p < 0.05$; ** $p < 0.01$; n.s. indicates no significant differences. Measurements were carried out in triplicate ($n = 3$ independent formulations), and data are represented as means ± SD.

Table 1. Effect of drug components on encapsulation efficacy (EE), loading capacity (LC), and drug content (DC). Data is presented as mean ± SD ($n = 3$ independent formulations).

Liposomal Formulation	EE_{PG} (%)	EE_{LOM} (%)	LC_{PG} (%)	LC_{LOM} (%)	DC_{PG} (%)	DC_{LOM} (%)
PG-Lipo	78.46 ± 3.1	—	19.46 ± 1.1	—	98.56 ± 0.5	—
LOM-Lipo	—	83.48 ± 2.9	—	28.65 ± 1.9	—	97.47 ± 1.6
PG-LOM-Lipo	62.33 ± 1.7	74.11 ± 1.5	12.91 ± 1.8	17.11 ± 2.1	96.24 ± 2.2	96.71 ± 2.9

3.2. Differential Scanning Calorimetry (DSC) Analysis Results

The thermal behavior of pellets (PG-Lipo, LOM-Lipo, and PG-LOM-Lipo) was investigated with DSC (Figure 3). The calorimetric measurement brought supplementary evidence of successful encapsulation of both drugs into the liposomal carrier by the appearance of discrete melting points characteristic of the initial drug. The endothermic peak at 141 °C (PG-Lipo) and 140 °C (PG-LOM-Lipo) can be related to the melting point of PG, while at

88 °C (PG-Lipo) and 89 °C (PG-LOM-Lipo), related to the melting point of LOM. A slight shift in the melting points to lower temperatures can be observed in comparison to initial substances, which might be the effect of the lipids.

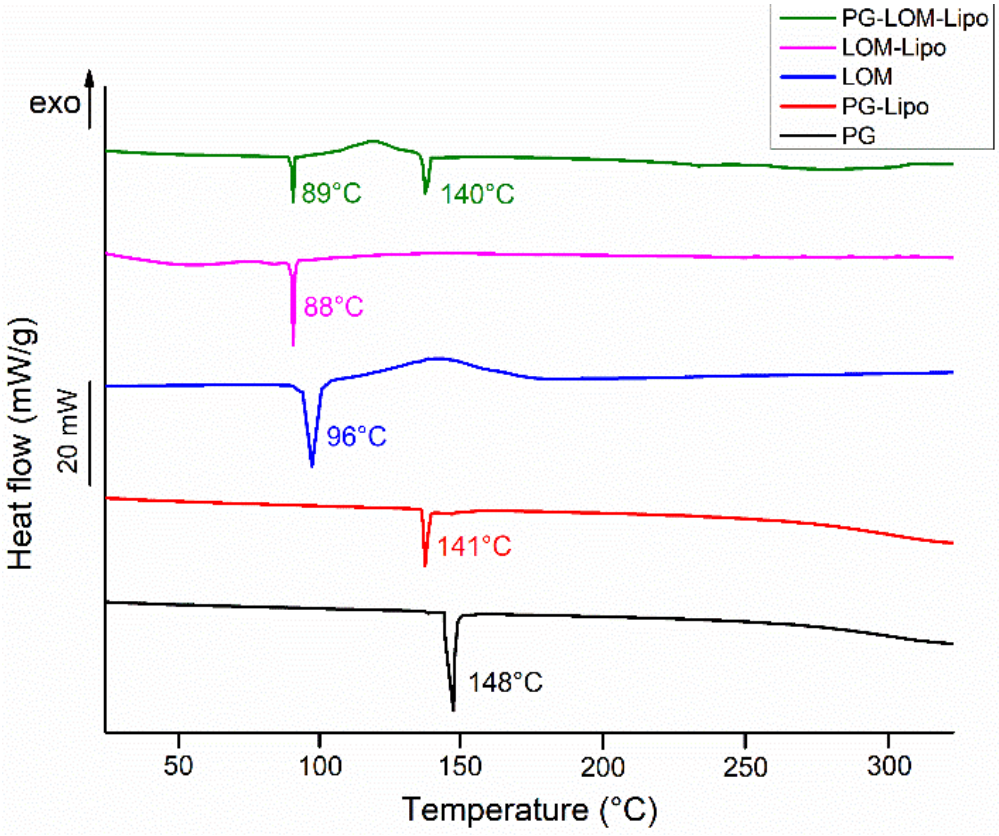

Figure 3. DSC thermogram of liposomal formulations (PG-Lipo, LOM-Lipo, and PG-LOM-Lipo) and initial active ingredients (PG and LOM).

Taking the melting enthalpy values ($_{\Delta}H$) of the thermograms of liposomal formulations into account, a similar tendency in the change in area under endothermic peak was observed in comparison to the DSC curve of initial PG and LOM, which corresponds to the amounts of encapsulated compounds (Table 2) [36]. These findings were in good agreement with the previous EE data (Table 1). No other heat effect was observed in the DSC curves, which indicates no degradation occurred during the liposome preparation process.

Table 2. Melting points (T_m) and melting enthalpies ($_{\Delta}H$) of encapsulated components.

Liposomal Formulation	$T_{m\mathrm{PG}}$ (°C)	$T_{m\mathrm{LOM}}$ (°C)	$_{\Delta}H_{\mathrm{PG}}$ (J/g) *	$_{\Delta}H_{\mathrm{LOM}}$ (J/g) *
PG	148.1	—	111.1	—
LOM	—	96.3	—	140.7
PG-Lipo	141.2	—	86.6	—
LOM-Lipo	—	88.1	—	117
PG-LOM-Lipo	140.2	89.2	59.9	94.4

* g indicates the calculated melting enthalpy values (J) were normalized to sample size.

3.3. XRPD Analysis

XRPD analysis was carried out to support DSC results. The XRPD diffractograms of liposomal formulations and initial compounds are presented in Figure 4.

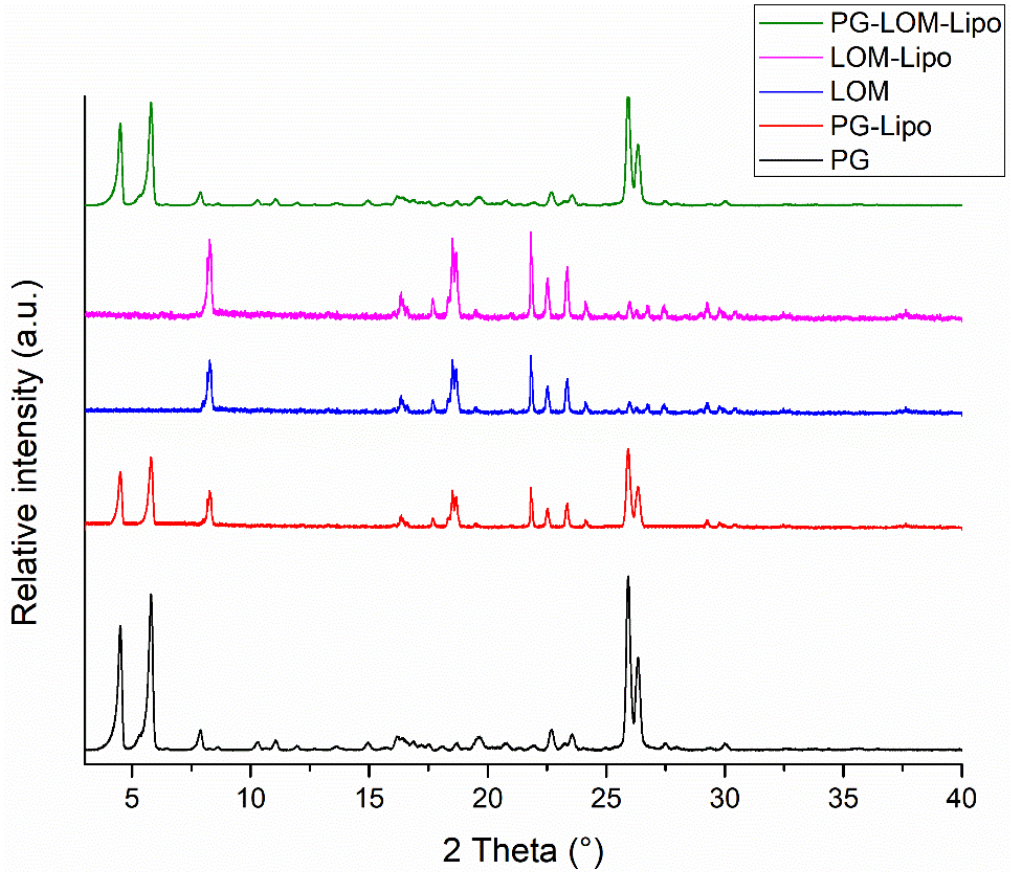

Figure 4. XRPD diffractograms of liposomal formulations and their constituents.

XRPD diffractograms of liposomal pellets supported DSC results. Characteristic peaks related to PG and LOM were present in the liposomal formulations, which supported the crystalline existence of both drugs in the liposomal formulation. The crystallinity index (CI) was calculated in each formulation to compare crystalline fractions of encapsulated drugs (Table 3).

Table 3. Crystallinity index of liposomal formulations.

Liposomal Formulation	CI_{PG} (%)	CI_{LOM} (%)
PG-Lipo	68.3	—
LOM-Lipo	—	72.4
PG-LOM-Lipo	43.7	49.1

The CI values clearly indicate that significant PG and LOM can be found in crystalline form in the liposomal formulation, which indicated supplementary evidence of successful co-encapsulation of both PG and LOM.

3.4. In Vitro Release Study

Drug release kinetic of liposomal formulations is a crucial part of the rational design, predicting the subsequent characteristics of a drug delivery system after administration. The in vitro release profile reveals important information on the structure and behavior of the formulation, possible interactions between the drug and lipid composition, and their influence on the rate and mechanism of drug release. The dialysis-based release method is a well-established and useful technique to study in vitro release from nano-particulate delivery systems. Applying a dialysis bag with an 8 kDa cutoff ensured the physical separation of liposomes and suspended particles of the initial control suspension from the

release medium and allowed only the passive diffusion of free LOM and PG. The time-dependent in vitro release profiles of LOM- and PG-loaded liposomes were determined with HPLC (Figure 5).

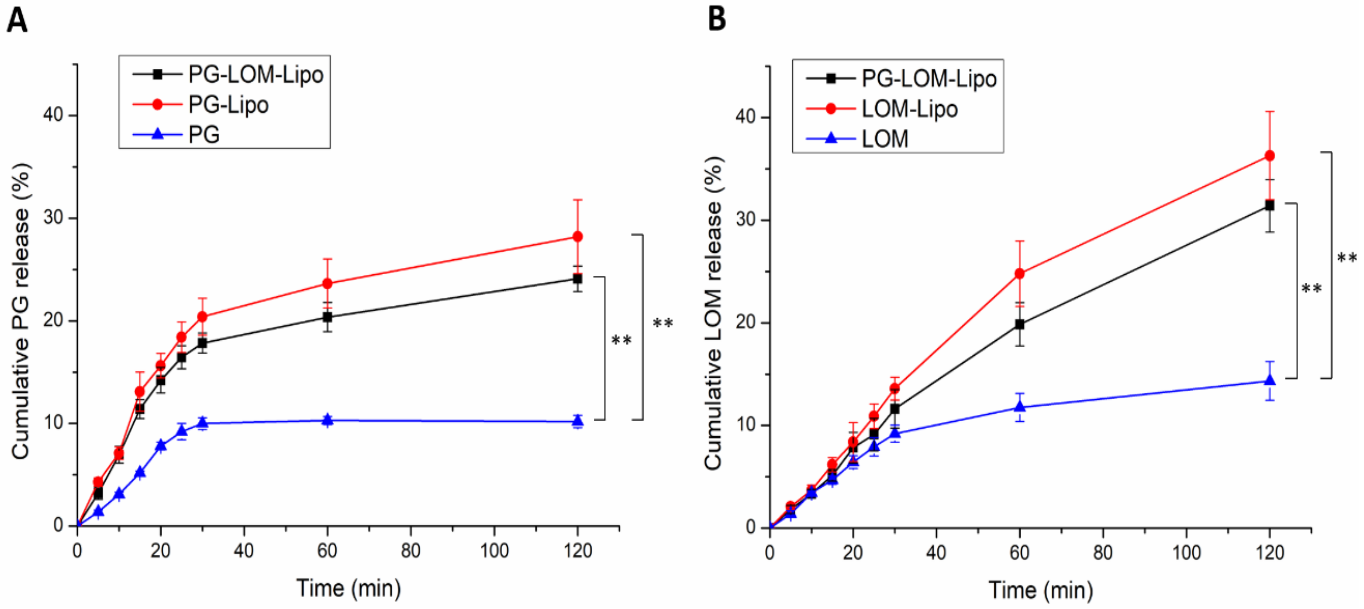

Figure 5. Cumulative drug release of PG- (**A**) and LOM-containing (**B**) formulations in comparison to initial LOM and PG suspension. An ANOVA test was performed to check the significance of the differences between liposomal formulations and initial drug suspension, ** $p < 0.01$. Measurements were performed in triplicate ($n = 3$ independent formulations), and data are represented as means ± SD.

The drug release profile of reference LOM and PG suspension showed only a slight increase; both drugs reached their equilibrium solubility in 60 min. However, in the case of liposomal formulations, a significant increase (~3-fold) in drug release was observed compared to both LOM and PG (**, $p < 0.01$), which can be explained by the tonicity difference in liposomal formulations and release medium. SNES forms a hypotonic environment in comparison to liposomal formulations, which results in swelling of the liposomes, reducing the thickness of the phospholipid bilayer, therefore, enhancing the drug release kinetics of both PG and LOM [29].

LOM release from PG-LOM-Lipo ($R^2 = 0.9971$) and LOM-Lipo ($R^2 = 0.9968$) followed Hixson–Crowell kinetics, as well as PG release from the PG-LOM-Lipo ($R^2 = 0.994$) and PG-Lipo ($R^2 = 0.9947$), which is presumably the result of specific surface area and Z-average changes due to drug release and the effect of ion strength on SNES and drug diffusion from liposomes.

3.5. Stability Studies

Liposomal formulations are known to suffer several stability issues. Therefore, the development of a stable liposomal formulation is a basic requirement for designing a suitable drug delivery system. The stability of the optimized liposomal formulation—PG-Lipo, PG-LOM-Lipo, and LOM-Lipo—was evaluated in terms of Z-average, surface charge, and EE as a function of the storage period at room temperature (25 °C) and at 4 °C. There was minimal impact on the Z-average and surface charge of liposomes, only a slight increase in particle size (~10 nm), and zeta potential (~7 mV) was found after 4 weeks of storage at 4 °C (Figure S1A,B). However, storing at room temperature (25 °C) for 4 weeks resulted in the aggregation of particles, leading to 199 ± 6.8 nm (PG-Lipo), 202 ± 9.1 nm (PG-LOM-Lipo), and 191 ± 14.2 nm (LOM-Lipo) particle size, which in turn impacted the surface charge, causing a reduction in zeta potential to −7.9 ± 2.6 mV (PG-Lipo), −8.3 ± 1.9 mV (PG-LOM-Lipo), and −11.9 ± 2.5 mV (LOM-Lipo), respectively

(Figure S1E,F). The entrapment efficiency of liposomal formulations was found to be stable at 4 °C, with only about a 5–5% drug entrapment reduction after 4 weeks detected for PG and LOM, as seen in Figure S1C,D. However, in the case of storage at 25 °C for 4 weeks, a 25–28% reduction in EE was detected for both PG and LOM (Figure S1G,H), which indicates that for liposomal formulations it is preferable to store them in a cool place to prolong stability.

3.6. Ex Vivo Raman Mapping

In order to investigate the passive trans-mucosal uptake of liposomal formulations, Raman mapping was applied. Isolated rabbit mucosa was treated with PG-Lipo, LOM-Lipo, PG-LOM-Lipo, PG suspension, and LOM suspension, and the penetration depth was analyzed and compared with non-treated nasal mucosa specimen using Raman correlation mapping. The mucosal distribution correlation maps showed a remarkable Raman intensity on the top of the nasal mucosa specimens in both cases (non-treated, treated), which corresponded to the high protein content of the epithelial layer. Figure 6. shows the Raman maps of treated and non-treated mucosa, profiling the individual spectrum of both LOM (Figure 6A) and PG (Figure 6B). The intensity changes in the Raman maps clearly indicate that both LOM and PG penetrated from the suspension through the nasal mucosa but with less extent in comparison to the encapsulated liposomal carrier. The findings were consistent with the ex vivo diffusion studies results. Based on these results, the improved penetration of both LOM and PG through the nasal mucosa can be supported by using liposomal carriers.

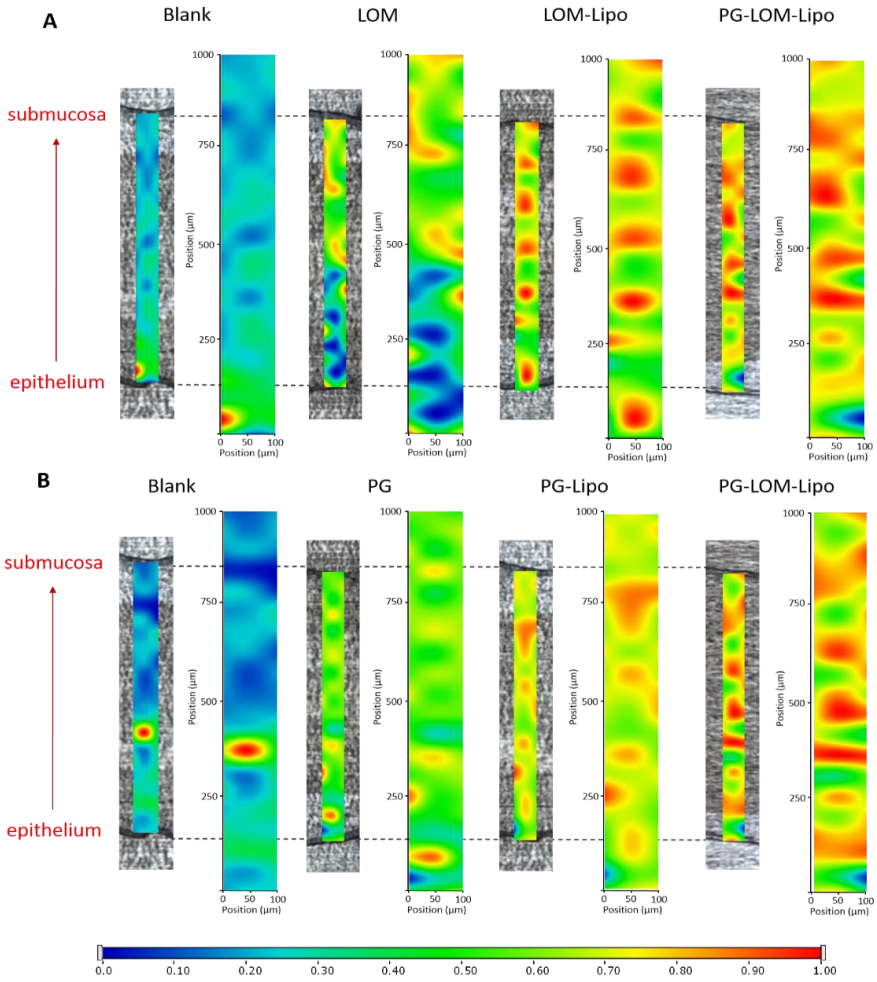

Figure 6. Raman correlation maps of the distribution of LOM (**A**) and PG (**B**) in the rabbit nasal mucosa compared to the non-treated nasal mucosa specimen.

3.7. Ex Vivo Permeation Studies

A modified Side-Bi-Side® type diffusion cell was used for the in vitro nasal permeation study, whereas the diffusion of PG-Lipo, LOM-Lipo, PG-LOM-Lipo was compared to a PG suspension and LOM suspension through rabbit nasal mucosa. Figure 7A shows the cumulative LOM permeation, while Figure 7B, the cumulative PG permeation from donor to acceptor phase through the isolated nasal mucosa. Both in the case of LOM and PG, the permeation was significantly higher in the case of liposomal formulations compared to suspensions.

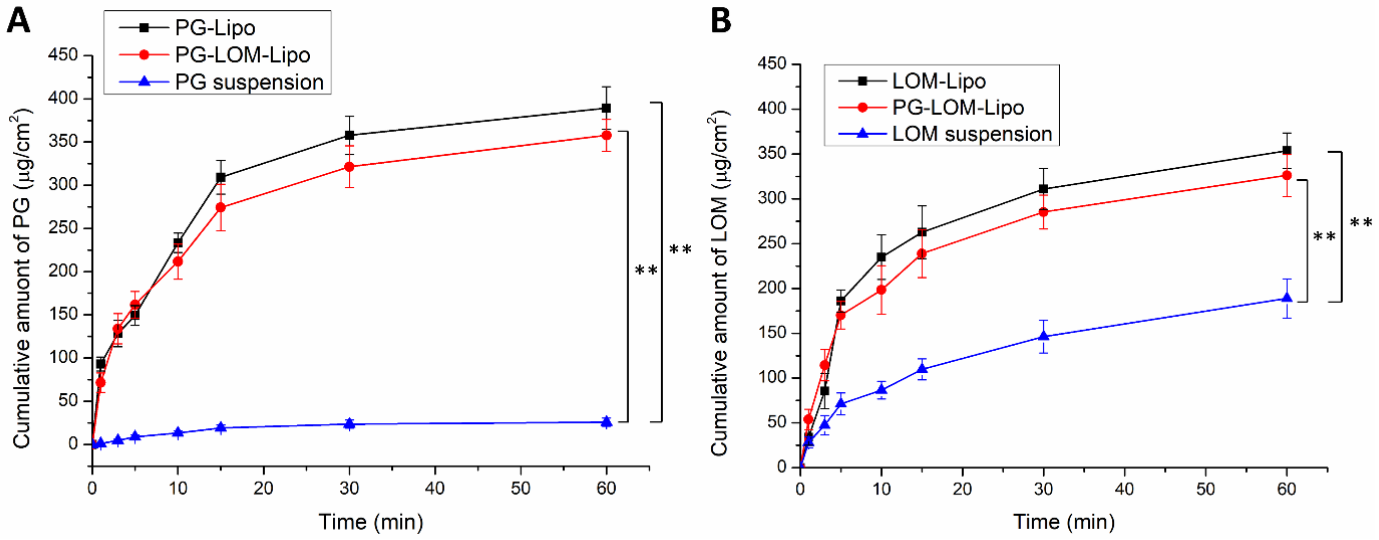

Figure 7. Ex vivo nasal permeability study of PG-containing (**A**) and LOM-containing (**B**) liposomal formulations in comparison to suspensions. An ANOVA test was performed to check the significance of the differences between liposomal formulations and initial drug suspension, ** $p < 0.01$. Measurements were performed in triplicate ($n = 3$ independent formulations), and data are represented as means ± SD.

Both in the case of PG and LOM liposomal formulations, the flux and permeability coefficient values were significantly higher (** $p < 0.01$) compared to the initial PG and LOM suspensions. Comparing the liposomal carriers, no significant difference in the cumulative permeation of LOM and PG was achieved between LOM-Lipo and PG-LOM-Lipo. The calculated flux, permeability coefficient values, and relative permeability values can be found in Table 4.

Table 4. Flux (J), permeability coefficient (K_p), and relative permeability at 60 min (RP_{60}) of the liposomal formulations and the reference raw suspensions. * Data are presented as average ± SD ($n = 3$).

Sample	Flux * (µg/cm²/h)	K_p (cm/h)	RP_{60}
LOM values			
LOM suspension	188.918 ± 21.7	0.850	1.00
LOM-Lipo	353.587 ± 19.8	1.591	1.87
PG-LOM-Lipo	326.172 ± 23.7	1.467	1.73
PG values			
PG suspension	25.9 ± 1.7	0.116	1.00
PG-Lipo	399.517 ± 16.7	1.796	15.38
PG-LOM-Lipo	291.236 ± 24.2	1.302	11.46

The change in vesicle size and PDI in the acceptor phase was also investigated during the ex vivo permeability study. By this measurement, the fate of the liposomal carrier was

predicted after nasal uptake. Figure 8 presents the obtained results at the submucosal site of the nasal mucosa.

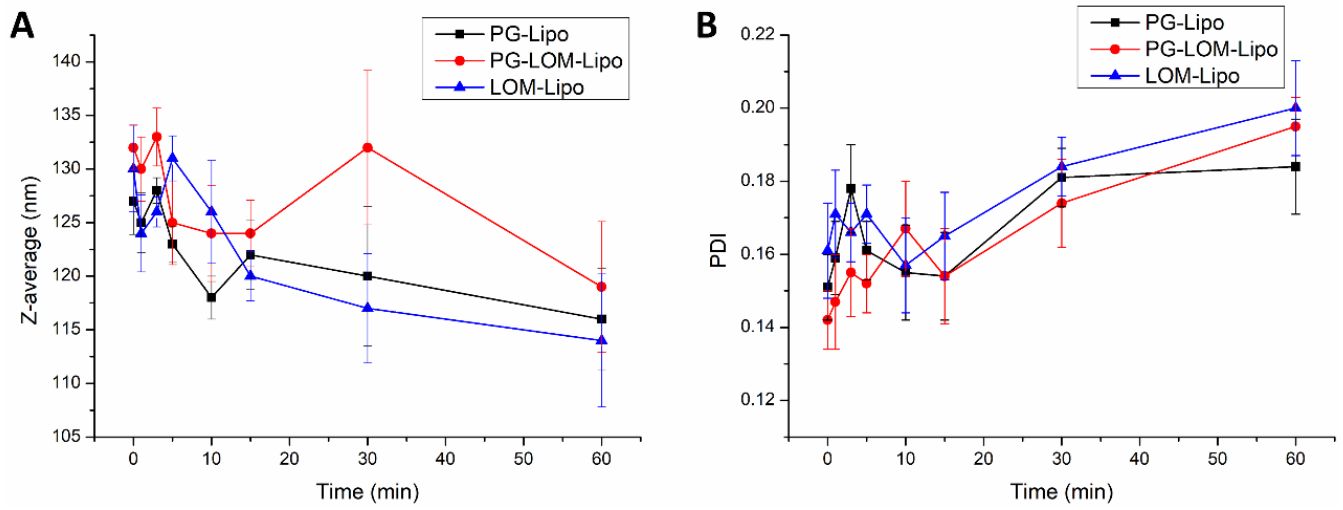

Figure 8. Change in Z-average (**A**) and PDI (**B**) of liposomes during ex vivo permeation study.

Each liposomal formulation shows no significant change in the Z-average and PDI in the acceptor compartment after permeation through the nasal mucosa in comparison to the initial Z-average and PDI measured at time point 0 in the donor compartment. These results indicated liposomes may penetrate through the nasal mucosa delivering the encapsulated drug.

3.8. Cellular Uptake of Propidium–Iodide Labelled Liposomes

As PI is not membrane permeable, it is a suitable indicator for investigating cellular uptake. By loading PI as a chemical marker in the liposomal carrier, the endocytosis of liposomes can be visualized. Figure 9 shows the fluorescent microscopic results of U87 and U251 cells treated with PI-loaded liposomes (PI-Lipo) for 24 h.

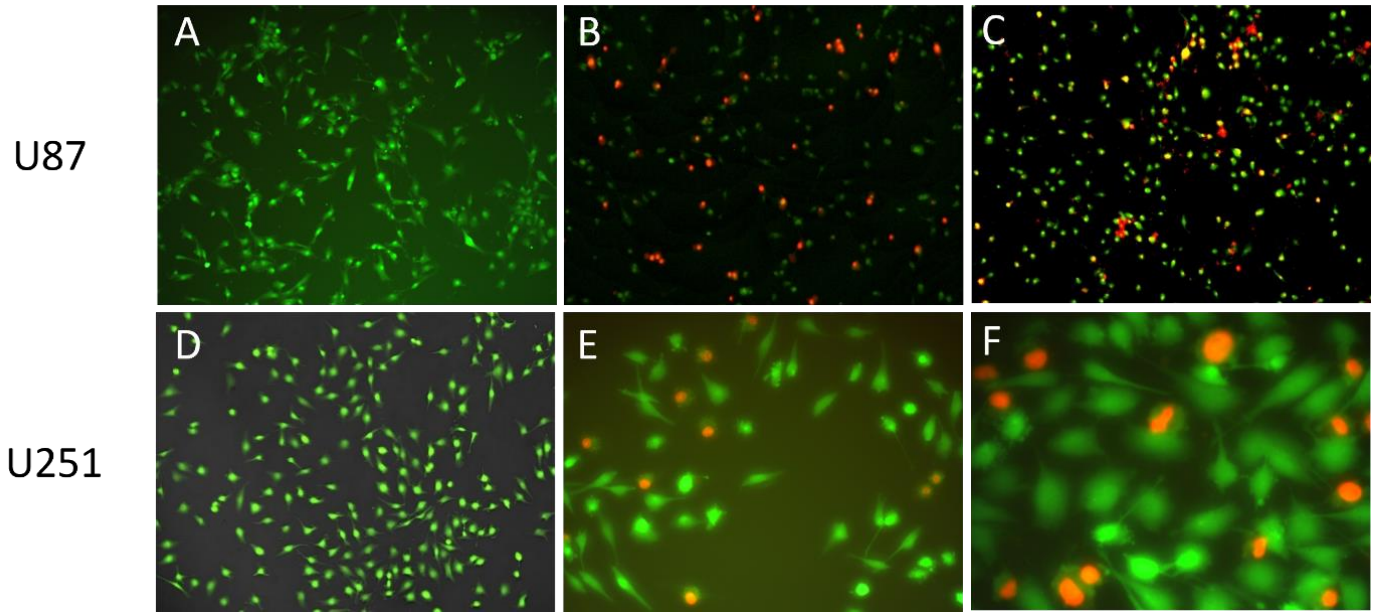

Figure 9. Fluorescence imaging of PI-Lipo cellular uptake on U87 (**B**,**C**) at 10× magnification and U251 cell line at 20× (**E**) and 40× magnification (**F**) after 24 h incubation compared to control group of U87 (**A**) and U251 (**D**) stained with cell track green.

On both U87 and the more resistant U251 cell lines, successful uptake of liposomes can be detected, as indicated by the red fluorescence inside the cells. These results support that the liposomal carrier was able to transport the encapsulated drug inside the tumor cell, triggering a targeted cytotoxic effect after drug release.

3.9. In Vitro Cell Line Studies (Antiproliferative Assay Results)

The antiproliferative effect of LOM-Lipo, PG-Lipo, PG-LOM-Lipo formulations was tested on murine fibroblast cells (NIH), human glioblastoma cell lines (U87), and human ovarian cancer cell lines (A2780) by MTT assays. IC_{50} values of the tested formulations and their 95% confidence intervals (CI) were calculated (Table 5).

Table 5. IC_{50} values of the tested formulations LOM-Lipo, PG-Lipo, PG-LOM-Lipo, and control solutions of LOM-DMSO and PG-DMSO.

Test Substance	IC_{50} Values (μM) [95% Confidence Interval]		
	NIH/3T3	**U87**	**A2780**
LOM-DMSO	264.8 [220.3–318.3]	35.09 [31.02–39.69]	41.88 [35.74–49.09]
PG-DMSO	29.14 [25.10–33.83]	59.42 [51.67–68.32]	14.64 [12.97–16.53]
LOM-Lipo	>500	>500	>100
PG-Lipo	62.93 [56.83–69.69]	275.3 [246.8–307.2]	49.00 [44.24–54.27]
PG-LOM-Lipo *	140.20 [125.3–156.8]	217.60 [190.6–248.4]	70.45 [63.55–78.10]

* IC_{50} values are given as LOM concentration. PG concentrations present at the IC_{50} values of LOM are NIH/3T3: 154.46 μM; U87: 239.74 μM; A2780: 77.62 μM. Blank liposomal samples did not show considerable inhibitory effects.

MTT assay results revealed the antioxidant PG can contribute to the anticancer effects by exerting antiproliferative action itself, which can be advantageous in combination with other anticancer drugs, such as LOM. However, in the given experimental environment, PG-Lipo and LOM-Lipo showed higher IC_{50} values on the NIH/3T3 cell line in comparison to PG-DMSO and LOM-DMSO solutions. This phenomenon can be related to the protective effect of the liposomal carrier. From the point of nose-to-brain administration of an anticancer drug, it is essential to reduce the cytotoxic effect on the nasal mucosa. For that reason, liposomes offer a suitable solution. PG-LOM-Lipo showed a lower IC_{50} related to LOM concentrations in comparison to LOM-DMSO, which can be explained by the additional antiproliferative effect of co-encapsulated PG beside LOM. MTT assay results on U87 glioblastoma cell lines showed remarkably higher IC_{50} values of liposomal formulations in comparison to PG-DMSO and LOM-DMSO, which can be attributed to the increased resistance of glioblastoma cells against nanocarrier-mediated drug therapy. However, it is stated that PG and LOM suspension showed poor dissolution and permeability properties both in vitro and ex vivo, which inhibits these formulations from reaching the optimal antiproliferative effect, which was observed in the case of PG-DMSO and LOM-DMSO solutions. To improve tumor targeting through the nasal mucosa, the application of a liposomal carrier is essential, however, due to high EE and LC, a sufficient amount of the drugs can be loaded to provide adequate antiproliferative effects. The cytotoxic effect of formulations was also tested on A2780 ovarium carcinoma cells, which are less resistant than the U87 cell line. It was revealed that the A2780 cell line showed higher sensitivity toward all liposomal formulations.

4. Discussion

Various studies support the in vivo evidence of anticancer and antiangiogenic properties of PG, which is primarily applied as an antioxidant compound [37–39]. It has been reported PG can cause apoptosis in human leukemia cells and HeLa cells by inducing

reactive oxygen species (ROS) and depleting glutathione [40]. PG also plays a significant role in autophagy and plays a crucial role in cellular physiological processes.

In our previous studies, the ability of PG loading into two types of lipid nano-carriers (liposomes and solid lipid nanoparticles) was reported. In addition to the high EE of PG-loaded lipid nano-formulation, it was also revealed lipid nano-carriers can preserve the stability of encapsulated drugs, as shown in antioxidant activity measurements. The above-mentioned literature data and our previous findings suggested that the incorporation of PG in combination with an antitumor drug (LOM) in a liposomal carrier can be advantageous in the treatment of GBM via the IN route. The combination of PG and LOM may have an additional benefit, as single compound therapy failed to show meaningful advantages for GBM patients due to poor drug delivery, tumor heterogeneity, and drug resistance mechanisms [41]. Drug combinations, in theory, should take advantage of each compound's strengths and limitations to improve efficacy and overcome drug resistance. It all begins with the administration method (systemic vs. local), which has a significant impact on these parameters and defines how each component is distributed [42].

Therefore, the present study aimed to optimize and investigate the IN applicability of PG-LOM co-encapsulated liposomes as a suitable formulation for brain tumor therapy. IN drug delivery is a favorable, noninvasive, safe, and effective drug transport method, with the aim of bypassing the BBB. It allows delivering a wide range of therapeutic agents to the brain, including small molecules, growth factors, viral vectors, and even stem cells. Encapsulation of LOM into liposomes provides an interesting idea to resolve the insufficient drug delivery issue to cancer cells and to reduce the side effects on healthy tissues [43,44]. The combination of PG and LOM is novel; their combined anti-proliferative effect has not been studied before.

First, the composition of the liposomal carrier was optimized. As an optimization criterion, the least negatively surface charge was set, which supports the reduction in electrostatic repulsion with the negatively charged nasal mucosa and also avoids the aggregation of nanoparticles. Based on this requirement, CHL:PCL 1.33 showed the minimal ZP (-31 ± 2.9 mV). This composition also resulted in one of the lowest Z-average (118 ± 6.3 nm) and narrow PDI (0.13 ± 0.014), which is essential to improve drug absorption. After selecting the optimal lipid composition of the liposomal carrier, the appropriate drug ratio was investigated. It was revealed that the application of PG-LOM in 1:1 ratio showed no significant effect on Z-average, PDI, and ZP. Moreover, a high EE was achieved in the case of both drugs, which may facilitate nasal drug absorption. The obtained Z-average (127 ± 6.9 nm), PDI (0.142 ± 0.009), ZP (-34 ± 1.7 mV), and high EE ($63.57 \pm 1.3\%$ of PG and $73.45 \pm 2.2\%$ of LOM, respectively) in the case of both drugs were suitable for acceptance criteria of nose-to-brain transport [28]. Similarly, the DLS and EE results were obtained with co-encapsulated drugs into nanoparticles reported by Yan et al. [45] and are in accordance with the standard acceptance criteria of brain targeted anticancer drug-loaded lipid nanoparticles reported by Khan et al. [46]. Based on these findings, the optimized co-encapsulated formulation PG-LOM-Lipo (CHL:PCL 1.33) contained both PG and LOM in 1 mg/mL. The successful co-encapsulation was further supported by DSC and XRPD measurements. In vitro drug release, permeability studies, and ex vivo Raman measurements showed that the application of liposomes significantly improved the intranasal applicability, predicting increased bioavailability of the co-encapsulated drug components.

In vitro cellular uptake studies with PI-loaded liposomes supported the drug transport by the liposomal carrier inside the tumor cell, triggering targeted cytotoxic effects after drug release. Antiproliferative studies on fibroblasts and human cancer cells revealed reduced cytotoxicity related to the liposomal carrier. The antiproliferative activity of liposomal formulation was also proved on A2780 ovarium cancer cell lines and U87 glioblastoma cells, however, U87 cells showed increased resistance against liposomal formulations.

The ex vivo study results conducted on both PG- and LOM-loaded liposomal formulations resulted in significantly higher (** $p < 0.01$) flux and permeability coefficients

compared to initial PG and LOM suspensions; however, no significant difference in cumulative permeation was obtained between the liposomal formulations. The liposomal formulation showed no significant change in Z-average and PDI after permeation through the nasal mucosa, which indicated that the liposomes may penetrate through the nasal mucosa transporting encapsulated drugs. Praveen et al. investigated the nasal permeability of rhodamine-loaded liposomes prepared similarly from CHL and PCL (Phospholipid90G) [47]. It was revealed that the mucosa treated with liposomes showed high fluorescence intensity due to deeper penetration, while rhodamine solution showed only low penetration. The higher penetration of liposomal formulations through nasal mucosa was explained by the composition, small particle size, and flexibility to change the shape of vesicles, which helped in deeper penetration of the mucosa.

The results obtained indicated the optimized liposomal drug delivery system can be suitable for nose-to-brain delivery of PG and LOM. Guo et al. reported that celecoxib-loaded liposomes consisting of CHL and PCL (Lipoid S100) similar to our composition, improved the brain transport of celecoxib either by penetrating or evading the BBB, upregulating neurogenesis, and targeting Alzheimer's disease [48].

5. Conclusions

In summary, we concluded that all three compared formulations (PG-Lipo, LOM-Lipo, PG-LOM-Lipo) met the acceptance criteria of nose-to-brain administration based on vesicle size, PDI, ZP (mV), and EE (%). In vitro and ex vivo characterizations supported the improved effect of the liposomal carrier on drug release and permeability. In addition to adequate nanoparticulate characteristics, the peripheral side effects of PG and LOM on the nasal mucosa can be reduced due to the application of liposomes by preserving antiproliferative potency at the site of action. The developed and optimized liposomal system provides a suitable tool to treat GBM via the intranasal route.

Supplementary Materials: The following supporting information can be downloaded at: https://www.mdpi.com/article/10.3390/pharmaceutics14030631/s1, Figure S1: Stability of liposomal formulations evaluated at different temperatures; 4 °C (A–D) and room temperature (25 °C) (E–H) expressed as Z-average (A and E), zeta potential (B and F), and EE regarding to PG (C and G) and LOM (D and H) over period of four weeks.

Author Contributions: Conceptualization, G.K., F.S., I.C.; methodology, G.K., F.S.; B.S., Z.S., M.N., and I.Z. software, G.K., F.S., B.S., and Z.S.; validation, I.C., and I.Z.; formal analysis, G.K., B.S., Z.S., I.Z., and I.C.; investigation, G.K., F.S., B.S., and Z.S.; resources, I.Z., and I.C.; data curation, G.K., F.S., Z.S., and I.Z.; writing—original draft preparation, G.K., and F.S.; writing—review and editing, B.S., Z.S., I.Z., and I.C.; visualization, G.K., and F.S.; supervision, I.Z., and I.C.; project administration, I.C.; funding acquisition, I.C. All authors have read and agreed to the published version of the manuscript.

Funding: The publication was funded by the University of Szeged Open Access Fund (FundRef, Grant No. 5523).

Institutional Review Board Statement: All experiments conformed to the Directive 2010/63/EU of the European Parliament. The protocols were approved by the Ethical Committee for the Protection of Animals in Research of the University of Szeged, Szeged, Hungary, and by the Department of Animal Health and Food Control of the Ministry of Agriculture and Rural Development (authority approval numbers XIII./4227/2016).

Informed Consent Statement: Not applicable.

Data Availability Statement: The data presented in this study are available on request from the corresponding author.

Acknowledgments: This work was supported by Project no. TKP2021-EGA-32 was implemented with support provided by the Ministry of Innovation and Technology of Hungary from the National Research, Development, and Innovation Fund, financed under the TKP2021-EGA funding scheme. This topic is respectfully dedicated to Piroska Szabó-Révész, Emerita for her scientific support and research motivation in the field of innovative drug formulation. Her scholarly work and intellectual advice play a vital role in the past and current scientific achievements of the Institute of Pharmaceutical Technology and Regulatory Affairs, University of Szeged.

Conflicts of Interest: The authors declare no conflict of interest.

References

1. De Paula, L.B.; Primo, F.L.; Tedesco, A.C. Nanomedicine associated with photodynamic therapy for glioblastoma treatment. *Biophys. Rev.* **2017**, *9*, 761–773. [CrossRef] [PubMed]
2. Carmo, A.; Crespo, I.; Lopes, M.C. Genetics and Biology of Glioblastoma Multiforme. In *Molecular Targets of CNS Tumors*; InTechOpen: Rijeka, Croatia, 2011; p. 289. [CrossRef]
3. Hanif, F.; Muzaffar, K.; Perveen, K.; Malhi, S.M.; Simjee, S.U. Glioblastoma Multiforme: A Review of its Epidemiology and Pathogenesis through Clinical Presentation and Treatment. *Asian Pac. J. Cancer Prev. APJCP* **2017**, *18*, 3–9.
4. Ahlawat, J.; Barroso, G.G.; Asil, S.M.; Alvarado, M.; Armendariz, I.; Bernal, J.; Carabaza, X.; Chavez, S.; Cruz, P.; Escalante, V.; et al. Nanocarriers as Potential Drug Delivery Candidates for Overcoming the Blood–Brain Barrier: Challenges and Possibilities. *ACS Omega* **2020**, *5*, 12583–12595. [CrossRef] [PubMed]
5. Keller, L.-A.; Merkel, O.; Popp, A. Intranasal drug delivery: Opportunities and toxicologic challenges during drug development. *Drug Deliv. Transl. Res.* **2021**, *12*, 735–757. [CrossRef]
6. Wen, H.; Jung, H.; Li, X. Drug Delivery Approaches in Addressing Clinical Pharmacology-Related Issues: Opportunities and Challenges. *AAPS J.* **2015**, *17*, 1327–1340. [CrossRef] [PubMed]
7. Erdő, F.; Bors, L.A.; Farkas, D.; Bajza, Á.; Gizurarson, S. Evaluation of intranasal delivery route of drug administration for brain targeting. *Brain Res. Bull.* **2018**, *143*, 155–170. [CrossRef]
8. Islam, S.U.; Shehzad, A.; Ahmed, M.B.; Lee, Y.S. Intranasal Delivery of Nanoformulations: A potential way of treatment for neurological disorders. *Molecules* **2020**, *25*, 1929. [CrossRef]
9. Upadhyay, R.K. Drug Delivery Systems, CNS Protection, and the Blood Brain Barrier. *BioMed Res. Int.* **2014**, *2014*, 869269. [CrossRef]
10. Leal, J.; Smyth, H.D.; Ghosh, D. Physicochemical properties of mucus and their impact on transmucosal drug delivery. *Int. J. Pharm.* **2017**, *532*, 555–572. [CrossRef]
11. Lai, S.K.; Suk, J.S.; Pace, A.; Wang, Y.-Y.; Yang, M.; Mert, O.; Chen, J.; Kim, J.; Hanes, J. Drug carrier nanoparticles that penetrate human chronic rhinosinusitis mucus. *Biomaterials* **2011**, *32*, 6285–6290. [CrossRef] [PubMed]
12. Madara, J.L. Modulation of tight junctional permeability. *Adv. Drug Deliv. Rev.* **2000**, *41*, 251–253. [CrossRef]
13. Illum, L. Nanoparticulate Systems for Nasal Delivery of Drugs: A Real Improvement over Simple Systems? *J. Pharm. Sci.* **2007**, *96*, 473–483. [CrossRef] [PubMed]
14. Hsu, J.-F.; Chu, S.-M.; Liao, C.-C.; Wang, C.-J.; Wang, Y.-S.; Lai, M.-Y.; Wang, H.-C.; Huang, H.-R.; Tsai, M.-H. Nanotechnology and Nanocarrier-Based Drug Delivery as the Potential Therapeutic Strategy for Glioblastoma Multiforme: An Update. *Cancers* **2021**, *13*, 195. [CrossRef] [PubMed]
15. Maurer, N.; Fenske, D.B.; Cullis, P.R. Developments in liposomal drug delivery systems. *Expert Opin. Biol. Ther.* **2001**, *1*, 923–947. [CrossRef]
16. Aguilar-Pérez, K.M.; Avilés-Castrillo, J.I.; Medina, D.I.; Parra-Saldivar, R.; Iqbal, H.M.N. Insight Into Nanoliposomes as Smart Nanocarriers for Greening the Twenty-First Century Biomedical Settings. *Front. Bioeng. Biotechnol.* **2020**, *8*, 579536. [CrossRef] [PubMed]
17. Asadi-Samani, M.; Farkhad, N.K.; Mahmoudian-Sani, M.R.; Shirzad, H. Antioxidants as a double-edged sword in the treat-ment of cancer. In *Antioxidants 2019*; InTechOpen: Rijeka, Croatia, 2019.
18. Tse, A.K.-W.; Chen, Y.-J.; Fu, X.-Q.; Su, T.; Li, T.; Guo, H.; Zhu, P.-L.; Kwan, H.Y.; Cheng, B.C.-Y.; Cao, H.-H.; et al. Sensitization of melanoma cells to alkylating agent-induced DNA damage and cell death via orchestrating oxidative stress and IKKβ inhibition. *Redox Biol.* **2017**, *11*, 562–576. [CrossRef] [PubMed]
19. Almatroodi, S.A.; Almatroudi, A.; Khan, A.A.; Alhumaydhi, F.A.; Alsahli, M.A.; Rahmani, A.H. Potential Therapeutic Targets of Epigallocatechin Gallate (EGCG), the Most Abundant Catechin in Green Tea, and its Role in the Therapy of Various Types of Cancer. *Molecules* **2020**, *25*, 3146. [CrossRef] [PubMed]
20. Wei, P.-L.; Huang, C.-Y.; Chang, Y.-J. Propyl gallate inhibits hepatocellular carcinoma cell growth through the induction of ROS and the activation of autophagy. *PLoS ONE* **2019**, *14*, e0210513. [CrossRef]
21. Mittal, D.; Ali, A.; Shadab; Baboota, S.; Sahni, J.K.; Ali, J. Insights into direct nose to brain delivery: Current status and future perspective. *Drug Deliv.* **2013**, *21*, 75–86. [CrossRef] [PubMed]
22. Mehrotra, A.; Pandit, J.K. Preparation and Characterization and Biodistribution Studies of Lomustine Loaded PLGA Nanoparticles by Interfacial Deposition Method. *J. Nanomed. Nanotechnol.* **2015**, *6*, 1–13. [CrossRef]

23. Meyers, J.D.; Doane, T.; Burda, C.; Basilion, J.P. Nanoparticles for imaging and treating brain cancer. *Nanomedicine* **2013**, *8*, 123–143. [CrossRef] [PubMed]
24. Yasaswi, P.S.; Shetty, K.; Yadav, K.S. Temozolomide nano enabled medicine: Promises made by the nanocarriers in glioblastoma therapy. *J. Control. Release* **2021**, *336*, 549–571. [CrossRef] [PubMed]
25. Wang, J.; Huang, G. Preparation of itraconazole-loaded liposomes coated by carboxymethyl chitosan and its pharmacokinetics and tissue distribution. *Drug Deliv.* **2011**, *18*, 631–638. [CrossRef] [PubMed]
26. Pallagi, E.; Jójárt-Laczkovich, O.; Németh, Z.; Szabó-Révész, P.; Csóka, I. Application of the QbD-based approach in the early development of liposomes for nasal administration. *Int. J. Pharm.* **2019**, *562*, 11–22. [CrossRef] [PubMed]
27. Sabir, F.; Katona, G.; Pallagi, E.; Dobó, D.; Akel, H.; Berkesi, D.; Kónya, Z.; Csóka, I. Quality-by-Design-Based Development of n-Propyl-Gallate-Loaded Hyaluronic-Acid-Coated Liposomes for Intranasal Administration. *Molecules* **2021**, *26*, 1429. [CrossRef] [PubMed]
28. Tzeyung, A.S.; Md, S.; Bhattamisra, S.K.; Madheswaran, T.; Alhakamy, N.A.; Aldawsari, H.M.; Radhakrishnan, A.K. Fabrication, Optimization, and Evaluation of Rotigotine-Loaded Chitosan Nanoparticles for Nose-To-Brain Delivery. *Pharmaceutics* **2019**, *11*, 26. [CrossRef] [PubMed]
29. Wu, I.Y.; Nikolaisen, T.E.; Skalko-Basnet, N.; di Cagno, M.P. The Hypotonic Environmental Changes Affect Liposomal Formulations for Nose-to-Brain Targeted Drug Delivery. *J. Pharm. Sci.* **2019**, *108*, 2570–2579. [CrossRef] [PubMed]
30. Bartos, C.; Szabó-Révész, P.; Bartos, C.; Katona, G.; Jójárt-Laczkovich, O.; Ambrus, R. The Effect of an Optimized Wet Milling Technology on the Crystallinity, Morphology and Dissolution Properties of Micro- and Nanonized Meloxicam. *Molecules* **2016**, *21*, 507. [CrossRef] [PubMed]
31. Jain, A.; Jain, S.K. In vitro release kinetics model fitting of liposomes: An insight. *Chem. Phys. Lipids* **2016**, *201*, 28–40. [CrossRef] [PubMed]
32. Pászti, B.J.; Prorok, J.; Magyar, T.; Árpádffy-Lovas, T.; Györe, B.; Topál, L.; Gazdag, P.; Szlovák, M.J.; Naveed, M.; Jost, N.; et al. Cardiac electrophysiological effects of ibuprofen in dog and rabbit ventricular preparations: Possible implication to enhanced proarrhythmic risk. *Can. J. Physiol. Pharmacol.* **2021**, *99*, 102–109. [CrossRef] [PubMed]
33. Richter, T.; Keipert, S. In vitro permeation studies comparing bovine nasal mucosa, porcine cornea and artificial membrane: Androstenedione in microemulsions and their components. *Eur. J. Pharm. Biopharm.* **2004**, *58*, 137–143. [CrossRef] [PubMed]
34. Pund, S.; Rasve, G.; Borade, G. Ex vivo permeation characteristics of venlafaxine through sheep nasal mucosa. *Eur. J. Pharm. Sci.* **2013**, *48*, 195–201. [CrossRef] [PubMed]
35. Mosmann, T. Rapid colorimetric assay for cellular growth and survival: Application to proliferation and cytotoxicity assays. *J. Immunol. Methods* **1983**, *65*, 55–63. [CrossRef]
36. Juhász, Á.; Ungor, D.; Várkonyi, E.Z.; Varga, N.; Csapó, E. The pH-Dependent Controlled Release of Encapsulated Vitamin B_1 from Liposomal Nanocarrier. *Int. J. Mol. Sci.* **2021**, *22*, 9851. [CrossRef] [PubMed]
37. Park, W.H. Propyl gallate reduces the growth of lung cancer cells through caspase-dependent apoptosis and G1 phase arrest of the cell cycle. *Oncol. Rep.* **2020**, *44*, 2783–2791. [CrossRef] [PubMed]
38. Sabir, F.; Katona, G.; Ismail, R.; Sipos, B.; Ambrus, R.; Csóka, I. Development and Characterization of *n*-Propyl Gallate Encapsulated Solid Lipid Nanoparticles-Loaded Hydrogel for Intranasal Delivery. *Pharmaceuticals* **2021**, *14*, 696. [CrossRef] [PubMed]
39. Park, W.H. Enhanced cell death effects of MAP kinase inhibitors in propyl gallate-treated lung cancer cells are related to increased ROS levels and GSH depletion. *Toxicol. Vitr.* **2021**, *74*, 105176. [CrossRef] [PubMed]
40. Chen, C.-H.; Lin, W.-C.; Kuo, C.-N.; Lu, F.-J. Role of redox signaling regulation in propyl gallate-induced apoptosis of human leukemia cells. *Food Chem. Toxicol.* **2011**, *49*, 494–501. [CrossRef] [PubMed]
41. Zhao, M.; Van Straten, D.; Broekman, M.L.; Préat, V.; Schiffelers, R.M. Nanocarrier-based drug combination therapy for glioblastoma. *Theranostics* **2020**, *10*, 1355–1372. [CrossRef] [PubMed]
42. Rahdar, A.; Hajinezhad, M.R.; Nasri, S.; Beyzaei, H.; Barani, M.; Trant, J.F. The synthesis of methotrexate-loaded F127 microemulsions and their in vivo toxicity in a rat model. *J. Mol. Liq.* **2020**, *313*, 113449. [CrossRef]
43. Allahou, L.W.; Madani, S.Y.; Seifalian, A. Investigating the Application of Liposomes as Drug Delivery Systems for the Diagnosis and Treatment of Cancer. *Int. J. Biomater.* **2021**, *2021*, 3041969. [CrossRef] [PubMed]
44. Zhong, L.; Li, Y.; Xiong, L.; Wang, W.; Wu, M.; Yuan, T.; Yang, W.; Tian, C.; Miao, Z.; Wang, T.; et al. Small molecules in targeted cancer therapy: Advances, challenges, and future perspectives. *Signal Transduct. Target. Ther.* **2021**, *6*, 201. [CrossRef] [PubMed]
45. Yan, J.; Wang, Y.; Zhang, X.; Liu, S.; Tian, C.; Wang, H. Targeted nanomedicine for prostate cancer therapy: Docetaxel and curcumin co-encapsulated lipid–polymer hybrid nanoparticles for the enhanced anti-tumor activity in vitro and in vivo. *Drug Deliv.* **2014**, *23*, 1757–1762. [CrossRef] [PubMed]
46. Khan, A.; Imam, S.S.; Aqil, M.; Ahad, A.; Sultana, Y.; Ali, A.; Khan, K. Brain Targeting of Temozolomide via the Intranasal Route Using Lipid-Based Nanoparticles: Brain Pharmacokinetic and Scintigraphic Analyses. *Mol. Pharm.* **2016**, *13*, 3773–3782. [CrossRef] [PubMed]

47. Praveen, A.; Aqil, M.; Imam, S.S.; Ahad, A.; Moolakkadath, T.; Ahmad, F. Lamotrigine encapsulated intra-nasal nanoliposome formulation for epilepsy treatment: Formulation design, characterization and nasal toxicity study. *Colloids Surfaces B Biointerfaces* **2018**, *174*, 553–562. [CrossRef] [PubMed]
48. Guo, J.-W.; Guan, P.-P.; Ding, W.-Y.; Wang, S.-L.; Huang, X.-S.; Wang, Z.-Y.; Wang, P. Erythrocyte membrane-encapsulated celecoxib improves the cognitive decline of Alzheimer's disease by concurrently inducing neurogenesis and reducing apoptosis in APP/PS1 transgenic mice. *Biomaterials* **2017**, *145*, 106–127. [CrossRef] [PubMed]